

# Heterogeneity design for stretchable electronics

Wang, Ting

2021

Wang, T. (2021). Heterogeneity design for stretchable electronics. Doctoral thesis, Nanyang Technological University, Singapore. <https://hdl.handle.net/10356/151917>

<https://hdl.handle.net/10356/151917>

<https://doi.org/10.32657/10356/151917>

---

This work is licensed under a Creative Commons Attribution-NonCommercial 4.0 International License (CC BY-NC 4.0).

*Downloaded on 13 Mar 2024 17:00:27 SGT*



**NANYANG  
TECHNOLOGICAL  
UNIVERSITY**  

---

**SINGAPORE**

**HETEROGENEITY DESIGN FOR STRETCHABLE  
ELECTRONICS**

**WANG TING**

**SCHOOL OF MATERIALS SCIENCE AND ENGINEERING**

**2021**



# **HETEROGENEITY DESIGN FOR STRETCHABLE ELECTRONICS**

**WANG TING**

**SCHOOL OF MATERIALS SCIENCE AND ENGINEERING**

A thesis submitted to the Nanyang Technological University  
in partial fulfilment of the requirement for the degree of  
Doctor of Philosophy

**2021**



## Statement of Originality

I hereby certify that the work embodied in this thesis is the result of original research, is free of plagiarised materials, and has not been submitted for a higher degree to any other University or Institution.

21 June 2021

.....

Date

Wang Ting

.....

Wang Ting



## Supervisor Declaration Statement

I have reviewed the content and presentation style of this thesis and declare it is free of plagiarism and of sufficient grammatical clarity to be examined. To the best of my knowledge, the research and writing are those of the candidate except as acknowledged in the Author Attribution Statement. I confirm that the investigations were conducted in accord with the ethics policies and integrity standards of Nanyang Technological University and that the research data are presented honestly and without prejudice.

21 June 2021

.....

Date



.....

Assoc Prof Alfred Tok ling Yoong



## Authorship Attribution Statement

This thesis **does not** contain any materials from papers published in peer-reviewed journals or from papers accepted at conferences in which I am listed as an author at this stage when I write the thesis.

The contributions of the co-authors for chapter 4 and 5 are as follows:

- Assoc Prof. Alfred Tok and Prof. Chen provided the initial project direction and edited the manuscript drafts.
- Prof. Liu instructed on experiment conduction, design, results discussion, and manuscript draft.
- Dr. Liu and Dr. Lu assisted in finite element simulation (CEL method) and revised the related result discussion.
- Dr. Cao conducted the focus ion beam.
- I prepared the manuscript drafts. The manuscript was revised by Dr. Wang, Dr. Wan and Dr. Leow.
- I performed materials synthesis, devices fabrication and characterization, carried out the mechanical test and scanning electron microscope.
- I collaborated with Dr. Wang in conducting mechanical simulation by using finite element analysis (Lagrangian method).

The contributions of the co-authors for chapter 6 are as follows:

- Prof. Chen provided the initial project direction.
- Dr. Liu and Dr. Pan assisted in experiment design, operation, and data analysis.
- Dr. Zhang contributed to the model for mechanism explanation.
- Dr. Cui guided me on using atomic force microscope.
- Dr. Jiang conducted the finite element simulation
- I conducted all experiment including sample preparation and characterization, atomic force microscope, scanning electron microscope, data collection and analysis.
- I wrote the manuscript draft.

21 June 2021

.....

Date

Wang Ting

.....

Wang Ting

## Abstract

Wearable electronics is a promising candidate for edging devices that can direct interact with users and collect data from them and process information locally close to users, which are the fundamental level for cyber-physical systems in the applications such as personalized healthcare, human-machine interfaces, and smart manufacturing. Conventional silicon-based electronics are rigid and fragile that are not comfortable with mechanical deformations from daily activities and are incompatible with human arbitrary body/skin/organs. This makes a huge demanded for developing stretchable electronics with good electrical performance under various mechanical forces.

Stretchable memristor, as a vital component in wearable electronics system, is accountable for data processing, information storage, neuromorphic and in-memory computing. Conventional memristor is a sandwich structure with a continuous bulk active layer between two electrodes. The insulative materials are metal oxide which is rigid and easily fracture under the forces from deformations or from accidently mechanical damages. The fracture of insulative materials threaten the electrical performance of memristor and cause the data loss. Thus, to develop a memristor with good mechanical adaptable to the various deformations and mechanical resistance against the damages is challenge. Although few papers have developed organic-based memristors with electrical performance under deformation and keep function under the mechanical damage, the organic materials are sensitive to the solvent and UV light that make it incompatible with CMOS techniques. The inorganic memristors that can work under mechanical deformations as well as mechanical damage have not been reported to the best of our knowledge. Herein, a flexible inorganic-based memristor with mechanical adaptability and mechanical damage endurance is developed via a novel structure in active layer by combining the discrete rigid structure with soft materials. The results demonstrate that the memristors based discrete structure possesses excellent stretchability (~40%) and flexibility (half-folded). Importantly, it performs an outstanding tolerance against the different level of mechanical damages such as puncture and tear, while remaining a good memory function. Meanwhile, even if undergoing serious mechanical damage, device can keep information from the lost

by some extent of self-healing property. This approach offers a new strategy for the next-generation stretchable memristor with mechanical damage resistance, which is promising and significant to wearable electronics in exploring more possibilities for applying flexible electronics in real-world environments.

Stretchable strain sensor is an essential component in wearable electronic system for data detection and collection, which transduces mechanical stimuli into electrical signals and is promising to apply for personal healthcare monitoring and motion detection system. The conventional crack-based stretchable strain sensors are fabricated through as homogenous thin layer on elastomer. The cracks are generated and propagated within the thin film when undergoing mechanical forces and cause the electrical conductivity change. However, the mechanical properties and electrical properties are a dilemma as large stretchability and high sensitivity cannot be obtained both. Inspired by biological materials from nature, the heterogenous structure with gradient change has a gradually force change rather than abrupt change, which reduce the strain concentration and can achieve a balance with two contradictory properties. Thus, we employ a heterogenous structure thin film with gradually change in thickness (thickness-gradient) on elastomer and investigate the electrical properties and mechanical properties of stretchable strain sensors. The results show that variation of the thickness-gradient affect the electromechanical properties of strain sensors. The anisotropic electrical property was discovered when force applied in a transverse and longitudinal manner corresponding to the thickness-gradient direction. A high sensitivity of strain sensor ( $GF \sim 1665$  at large strain  $\sim 30\%$ ) can be realized by this heterogenous structure.

This thesis has demonstrated how heterogenous structures being employed into stretchable memristors and strain sensors and endow them with a good electrical property and mechanical property, which provides promising and universal strategies for other stretchable electronics.

## Lay Summary

With development of information and communication technologies, the electronics have been transformed from immobile to mobile and to wearable. The transformation of electronics tends to be not only user-centric, but also be intelligent to deal with information between human and surrounding environment. Wearable electronics is the most promising platform that play a role in transforming information between users and virtual network that build up an intelligent environment for sustainable living, smart working, and manufacturing. Besides, due to the pandemic Covid-19, it has accelerated and prompted an explosion of interest of the wearable technology for health monitoring. For example, wearable sensors are used in textiles for clothing and efforts has been made to gear towards preventing the spread of virus and predicting the possible infection. Other wearable sensors can also potentially assist in providing real-time remote monitoring, symptom prediction and contact tracing for infected patients or self-quarantined individuals.

Among those wearable electronics, stretchable memristors is an important component for data processing and storage in wearable system. Currently, the memristors are fabricated based on rigid materials such as metal oxide and silicon. These materials are easily fracture and break into pieces when we bend or stretch. Besides, wearable electronics face the unexpected mechanical damages which comes from accidently puncture or cut in real applications. Those forces either from movement deformation or damages threaten the devices and will be a catastrophic damage for memristor if stored data is lost. Thus, to develop a stretchable memristor is demanded and necessary. This work is inspired by our human tissues such as bone and teeth, they can withstand impact force and keep biological function when we are running or chewing through a heterogenous structure that combine soft tissues and hard tissues. Borrowing concept from it, we develop a memristor with active materials which can be deems as a hard tissue and are surrounded by elastomer which is deems as soft tissue, the results show that memristor work properly under various deformation such as stretch, bend and twist. At the same time, device can tolerate mechanical damages from puncture and cut. This demonstrate that our design is effectively

endow the stretchable memristor with good mechanical adaptability and mechanical damage endurance.

Stretchable strain sensor is a vital component for information detection and collection. It transduces the mechanical deformation from our body movement or subtle face emotion and pulse to electrical signals and provide information for health monitoring and clinical diagnosis. One of challenge for stretchable strain sensor is that stretchability and sensitivity are difficult to achieve together. However, these two parameters are important to evaluate the performance of strain sensors for accurate data acquisition under the deformation. Inspired from nature, there are many paradigms such as bamboo and mussel, they can combine two contradictory properties via a gradient structure. We employed the same concept into stretchable strain sensors by using a thickness-gradient structure on elastomer and successful to develop a high sensitivity strain sensor.

The approaches used in in stretchable memristors and stretchable strain sensors in this thesis could be also applied for other stretchable electronics with similar structure, which pave a way for wearable electronics to gear towards practical applications

## Acknowledgements

Firstly, I am deeply indebted to my supervisors, Associate Professor Alfred Tok ling Yoong and Professor Chen Xiaodong for providing me PHD opportunity and continual support during last 4-year study journey. Especially, many thanks to Prof. Chen, who always provides constructive advice, constant guidance, and useful resources regarding the research project. Having been experienced stringent trainings by Prof. Chen, I have broadened my vision, sharpen my minds, and embolden to take up the challenges.

Secondly, special thanks are conveyed to my mentor Professor Liu Yaqing from Shandong University for his incisive recommendations concerning the scope of the research. During his time as a post doctor in NTU, he enlightened me on the ways of doing research, personally conducting me hand-on experience, and inspiring me of paper written. Without his patient guidance and unreserved instructions, I wouldn't have made a huge improvement on the research.

Thirdly, I would like to express heartfelt gratitude towards my excellent seniors. Dr. Wang Ming, who gives me valuable suggestions on my project and heuristic teaching to help me understand my work better; Dr. Pan Liang, who motivates me when I am depressed and generous shares his thoughts to improve my critical thinking; Dr. Cui Zequn, who teaches me AFM without reservation and always encourage me when I felt confused; Dr. Wan Changjin, who likes questioning me with stringent criticisms and giving useful suggestions to improve my ways of thinking; Dr. Wang Changxian, who teaches me Abaqus and clarifies my doubts patiently; Dr. He Ke, who helps me familiarize with group and equipment when I join this group.

In addition, I would like to appreciate the collaborators, Dr. Liu Zhuangjian and Dr. Lu Dingjie from Institute of High-Performance Computing, Agency of Science Technology and Research, Singapore, who assist me with the finite element analysis simulation. Dr. Leow Wan Ru, from Institute of Materials Research and Engineering, Agency for Science

Technology and Research, Singapore, who patiently review my paper and improve the quality of the English expression.

I am most grateful to MSE Staffs Dr. Wang Bochuan Victor, Dr. Derrick Ang, and Alan Lim, Lai Chee Hoong Patrick, Gan Zi Li and other MSE technicians for their kindly help and necessary equipment trainings and suggestions in developing the project. Besides, I would also like to give sincere appreciation to all my group members who provide me kind helps, bring me happy and shining my research life.

Lastly, I would like thanks to my family and good friends for their support, encourage and accompany!

## Table of Contents

<b>Abstract .....</b>	<b>i</b>
<b>Lay Summary .....</b>	<b>iii</b>
<b>Acknowledgements.....</b>	<b>v</b>
<b>Table of Contents .....</b>	<b>vii</b>
<b>Figure Captions .....</b>	<b>xiii</b>
<b>Abbreviations.....</b>	<b>xvii</b>
<b>Chapter 1 Introduction.....</b>	<b>1</b>
1.1 Hypothesis/Problem Statement .....	2
1.2 Objective and Scope.....	4
1.3 Dissertation Overview .....	5
1.4 Findings and Outcomes .....	6
References .....	7
<b>Chapter 2 Literature Review .....</b>	<b>9</b>
2.1 Introduction .....	10
2.2 Strategies to achieve mechanical adaptation .....	11
2.2.1 Stretchability.....	12
2.2.2 Materials development .....	13
2.2.3 Structure design .....	16

2.2.4	Flexibility.....	22
2.2.5	Mixed deformations.....	25
2.3	Strategies to tolerate mechanical damages .....	27
2.3.1	Tough materials/ Electronics-free .....	27
2.3.2	Self-healing.....	31
2.4	Heterogeneity .....	34
2.4.1	Learning heterogeneity design from nature .....	34
2.4.2	Heterogeneity design in stretchable electronics .....	37
2.5	Challenges for stretchable/flexible devices .....	44
2.5.1	Stretchable memristors .....	44
2.5.2	Stretchable strain sensors.....	47
2.6	Ph.D. in context of literature .....	50
	References .....	51
<b>Chapter 3</b>	<b>Experimental Methodology.....</b>	<b>65</b>
3.1	Synthesis techniques.....	66
3.1.1	Physical vapor deposition (PVD) .....	66
3.1.2	Electrochemical deposition.....	67
3.1.3	Photolithography .....	69
3.1.4	Electromechanical characterization .....	71

3.2 Rational selection for thickness measurement and simulation.....	73
3.2.1 Thickness measurement.....	73
3.2.2 Finite Element Analysis (FEA) simulation .....	75
References .....	77
 <b>Chapter 4* Mechanical Adaptation of Discrete Structure Based Memristors .....</b>	<b>79</b>
4.1 Introduction .....	80
4.2 Experimental methods .....	83
4.2.1 Fabrication of stretchable memristors .....	83
4.2.2 Electrical characterization of DS-memristor .....	85
4.2.3 Electrical characterization of electrode Au/SEBS .....	86
4.3 Principle Outcomes .....	88
4.3.1 Memristor flexibility.....	88
4.3.2 Memristor stretchability .....	91
4.4 Conclusion.....	95
References .....	96
 <b>Chapter 5* Mechanical Damages Endurance of Discrete Structure Based</b>	
<b>Memristors.....</b>	<b>99</b>
5.1 Introduction .....	100
5.2 Principle outcomes .....	101

5.2.1 Mechanical damages endurance of elastic substrate .....	101
5.2.2 Puncture endurance of stretchable memristors.....	103
5.2.3 Tear endurance of stretchable memristors.....	112
5.3 Conclusion.....	115
References .....	115

## **Chapter 6\* Electromechanical Property of Thickness-gradient Structure**

<b>Based Thin Film on Elastomers.....</b>	<b>119</b>
6.1 Introduction .....	120
6.2 Experimental methods.....	121
6.2.1 Fabrication of thickness-gradient thin film on elastic substrate .....	121
6.2.2 Thickness-gradient quantification .....	122
6.3 Principle Outcomes .....	124
6.3.1 Mechanical direction effect on electrical properties.....	124
6.3.2 Electrically anisotropic property of thickness-gradient Au / PDMS.....	126
6.4 Conclusion.....	133
References .....	134

<b>Chapter 7 Conclusions and Recommendations.....</b>	<b>137</b>
7.1 Conclusions .....	138
7.2 Future work recommendations .....	140

7.2.1	Theoretical study of anisotropic electrical property .....	140
7.2.2	Applications of stretchable strain sensors .....	141
7.3.3	Wearable system.....	146
References .....		148



## Figure Captions

**Figure 2.1** Schematic of biomedical and therapeutic applications of wearable electronics for monitoring electrophysiological activity and drug delivery

**Figure 2.2** The Young's modulus of biological and electronic substrate materials. Reproduced with permission.

**Figure 2.3** Stretchability strategies for developing intrinsic properties of materials.

**Figure 2.4** Stretchability strategies based on out-of-plane structure design.

**Figure 2.5** Stretchability strategies based on in-plane structure design.

**Figure 2.6** Strategies of flexibility in wearable electronics.

**Figure 2.7** Strategies for adapting to a mix of deformations.

**Figure 2.8** Strategies for tolerating mechanical damages while retaining the electronics functionalities.

**Figure 2.9** Illustration of self-healing strategies for resisting to mechanical damages.

**Figure 2.10** Local property and various forms of gradient in biological materials.

**Figure 2.11** Paradigms of biological materials with heterogeneity design.

**Figure 2.12** Heterogeneity design in elastomers and stretchable electrodes.

**Figure 2.13** Heterogeneity design in stretchable devices and wearable strain sensors.

**Figure 2.14** Stretchable strain sensors based on heterogeneity design in active material.

**Figure 2.15** The schematic diagram of RRAM structure, switching mechanism and its sweeping cycles of I-V characteristics of cation-type RRAM.

**Figure 2.16** Challenge of stretchable strain sensors.

**Figure 2.17** Linearity of capacitive-type strain sensor v.s resistive-type strain sensor.

**Figure 3.1** Schematic of physical vapor deposition techniques configuration

**Figure 3.2** Schematic illustration of three-electrode electrochemical cell system.

**Figure 3.3** Schematic illustration of photolithography configuration.

**Figure 3.4** photolithography procedures and steps (a) Experimental procedures, SU-8 is an epoxy-based negative photoresist. (b) photolithographic steps.

**Figure 3.5** The setup of electrochemical test. (a) configuration (b) Equipment for each component.

**Figure 3.6** The electrical connection for electromechanical test. (a) Manual mechanical tester (b) Automatic mechanical tester.

**Figure 3.7** Comparison of methods for measuring the thickness of thin film on elastomer.

**Figure 3.8** Cross-section of Au thin film on PDMS under (a-b) SEM and (c-d) FIB-SEM.

**Figure 3.9** Measuring the thickness of Au thin film on (a) wafer, and (b) PDMS

**Figure 3.10** Illustration of difference between (a) Eulerian and (b) Lagrangian.

**Figure 4.1** Continuous structure (CS) v.s Discrete structure (DS) during mechanical deformation.

**Figure 4.2** The configuration of a flexible discrete-structure memristor (DS-memristor) with crossbar.

**Figure 4.3** Fabrication process of discrete structure based stretchable memristors.

**Figure 4.4** The optical microscope images of discrete units with different sizes.

**Figure 4.5** A typical  $I$ - $V$  characterization of DS-memristor under a voltage sweeping mode at room temperature.

**Figure 4.6** Electrical and mechanical properties of top and bottom electrodes (Au/SEBS) with crossbar configuration.

**Figure 4.7** The behavior of Au strip on SEBS under cycling stretching and crack morphology in Au electrode.

**Figure 4.8** Comparison of CS and DS based on flexibility.

**Figure 4.9** Electrical performance of DS-memristor under flexion.

**Figure 4.10** Electrical performance of DS-memristor under tension.

**Figure 4.11** The comparison of resistance at LRS in CS memristor and DS-memristor against applied strain.

**Figure 4.12** Finite element simulations of strain distribution for continuous structure and discrete structure on elastic substrate under 30% strains, respectively.

**Figure 4.13** HRS and LRS of DS-memristor under various mechanical deformations such as standby, stretching, half-folding, twisting, and isotropic stretching.

**Figure 4.14** Real-time reading of HRS and LRS in a DS-memristor under the twisting and bending deformations. Some fluctuation in LRS come from the Au electrode resistance during the twist and bend.

**Figure 5.1** Comparison of mechanical behaviors of PDMS and SEBS under cut damage.

**Figure 5.2** Mechanical property of SEBS and electromechanical properties of Au/SEBS electrode without fully cut and fully cut with self-healing.

**Figure 5.3** Schematic of continuous structure and discrete structure under puncture damage.

**Figure 5.4** Comparison of I-V characteristics for discrete structure based memristor and continuous structure based memristor before and after pin puncture.

**Figure 5.5** Electrical performance of DS-memristor with pin puncture at static and dynamic conditions.

**Figure 5.6** Electrical performance of DS-memristor at extreme puncture damage condition.

**Figure 5.7** Schematic of the model setup for the FEA simulation.

**Figure 5.8** Finite element analysis simulations of displacement of discrete structure units during the whole pin puncture process.

**Figure 5.9** Optical image of pin and discrete units after puncture.

**Figure 5.10** Demonstration of DS-memristor performance in real application.

**Figure 5.11** Electrical performance of DS-memristor under tear damage.

**Figure 5.12** Electrical performance of DS-memristor after self-healing under extreme tear damage.

**Figure 5.13** Information storage for self-healed 3 x 2 array DS-memristor after 4 working cells with fully diagonal cut.

**Figure 6.1** Set-up configuration of thermal evaporation and location of sample template holders. (Schematic on the left and photograph on the right)

**Figure 6.2** Thickness gradient variation quantification.

**Figure 6.3** Electrical and mechanical properties of thickness-gradient gold film on elastic.

**Figure 6.4** Anisotropic property of gradient-thickness Au/PDMS versus strain at transverse and longitudinal direction.

**Figure 6.5** Confocal microscopic images of crack morphologies of thickness-gradient Au/PDMS at transverse and longitudinal direction.

**Figure 6.6** Schematic illustration of effect of crack propagation on relative resistance

change.

**Figure 6.7** Spring models involved into thickness-gradient thin film on elastomers.

**Figure 6.8** Illustration of electrically anisotropic property of thickness-gradient Au/PDMS based on spring models.

**Figure 6.9** Crack morphologies and electrical performance of stretchable strain sensors with thickness-gradient variation of 20.1%.

**Figure 7.1** The frame of this thesis.

**Figure 7.2** Recommendation for theoretical study of thickness-gradient stretchable strain sensors.

**Figure 7.3** Applications of stretchable strain sensors in healthcare monitoring.

**Figure 7.4** Stretchable strain sensor adhesive to kinesiology tape and mount on the knees for sport monitoring.

**Figure 7.5** HMI application.

**Figure 7.6** A wearable motion memory system with detection unit (stretchable strain sensor) and storage unit (stretchable memristor) for human motion monitoring.

**Figure 7.7** Schematic illustration of wearable device play a role in leveraging big data in health management.

## Abbreviations

AFM	Atomic Force Microscope
BEI	Backscatter Electron Images
BSE	Backscattered Electron
CNT	Carbon Nanotube
CB	Carbon Black
CS	Continuous Structure
CVD	Chemical Vapor Deposition
CMOS	Complementary Metal-Oxide Semiconductor
CEL	Combination of Eulerian and Lagrangian
CPS	Cyber Physical System
DOF	Degree of Freedom
DS	Discrete Structure
DI	Deionized
E	Young's modulus
EDS	Energy Dispersive X-ray Spectroscopy
eV	Electron Volt
FIB	Focus Ion Beam
FEA	Finite Element Analysis
FET	Field-Effect Transistor
GF	Gauge Factor
HR	Heart Rate
HRV	Heart Rate Variability
HMI	Human Machine Interface
HRS	High Resistance State
IoTs	Internet-of-Things
IC	Integrated Circuits
LRS	Low Resistance State
LCL	Lateral Collateral Ligament
MIM	Metal/Insulator/Metal

PVD	Physical Vapor Deposition
PDMS	Polydimethylsiloxane
PAA	Poly (Acrylic Acid)
PET	Polyethylene Terephthalate
PU	Polyurethane
PC	Polycarbonate
PEDOT:PSS	Poly(3,4-ethylenedioxythiophene):polystyrene sulfonate
PEN	Polyethylene Naphthalate
PI	Polyimide
RRAM	Resistive Random-Access Memory
SEBS	Poly[styrene- <i>b</i> -(ethylene-co-butylene)- <i>b</i> -styrene]
SEM	Scanning Electron Microscope
SEI	Secondary Electron Images
SHE	Standard Hydrogen Electrode
TEM	Transmission Electron Microscopy
TEG	Thermoelectric Generator
UV	Ultraviolet
1D	1 Dimensional
2D	2 Dimensional
3D	3 Dimensional

## **Chapter 1 Introduction**

### **Introduction**

*This chapter begins with motivation of stretchable electronics, followed by research challenges in development of stretchable electronics, next is inspiration of the heterogeneity design from biological materials and the statement of hypothesis, then presents the objective and work scope of this thesis and finally show the dissertation overview and outcomes.*

## 1.1 Hypothesis/Problem Statement

With the rise of the electronics, the size of devices has been transformed from immobile, mobile, and wearable to gear towards to human-centric smart system. Human, as a vital role in data generation, is a dynamic living system with arbitrary shapes that is continuously exchanging information internally and externally through biophysiological signal to maintain a good body condition and living function. Electronics, as powerful tools for signal detection, collection, and processing, are based on the silicon that are rigid, brittle, and susceptible to deformations and forces, which is compatible with human due to their inflexibility and large  $E$  (Young's modulus) between device ( $\sim E$  of GPa) and human skin ( $\sim E$  of kPa).<sup>[1-2]</sup> Therefore, in order to overcome the shortcomings of conventional Si-based electronics and a better and accurate data acquisition from human, stretchable electronics with good mechanical adaptability have been booming development to accommodate to the arbitrary body/organ shape and tolerate with forces from dynamic movements.

Currently, numerous researches focus on developing stretchable/flexible electronics through materials or structural designs to make electronics either intrinsically stretchable or strain accommodation to the external forces. Although the development of intrinsically organic materials can reduce mismatch of  $E$  and has achieved a high stretchability and a good electrical performance,<sup>[3-7]</sup> the process is incompatible with current existing photolithography microfabrication as they are sensitive to the organic solvents and ultraviolet (UV) light. New fabrication process requests new techniques and are costly that obstacle them in the scale up for industry application. On the other hands, the structural design has been alternative strategies to make electronics stretchable and functional under forces, which is in virtue of engineering strain on materials to make electronics accommodating to the deformations. This approach is compatible with current complementary metal-oxide semiconductor (CMOS) techniques and cost-effective that has been widely acceptable and employed in research. However, the challenge of this approach is the trade-off between electrical properties of devices and mechanical properties under external forces. This thesis emphases on dealing with this challenge by using two

heterogeneity designs to achieve stretchable electronics with high electrical performance and mechanical properties.

Biological materials in nature have been attracting scientists' attention. They are omnipresent in plant and animal bodies with diversity of biological function while providing mechanical protection and support. These biological materials function and sustain within the plants and animals in an environment consisting of dynamic movements and various forces, which is in the similar scenario for wearable electronics on human body. Thus, learning from biological materials from the viewpoint of materials science and discovering the process of nature structure may give some inspiration from it to develop new materials.

For example, tendon/ligament-to-bone insertion site (also called enthesis) is a transitional region to link two very different materials that wraps around the humeral head, which effectively facilitate the force transferring from soft tissues (tendon, ligament, cartilage with  $E$  of  $\sim$ kPa) to hard tissues (bone with  $E$  of  $\sim$ GPa), which ameliorates interfacial stress concentration.<sup>[8-9]</sup> Similarly, teeth can withstand mastication loads by dentin-with a heterogeneous structure of various  $E$ , such as periodontal ligament (with  $E$  of  $\sim$ 5 kPa to 9 MPa) between alveolar bone (with  $E$  of  $\sim$ 15 GPa to 20 GPa) and cementum (with  $E$  of  $\sim$ 15 GPa).<sup>[10-11]</sup> Besides, mussel attached to hard rock at a dynamic environment from sea waves without delamination through producing numerous extensible and shock-absorbing byssal threads with a step gradually change of  $E$ .<sup>[12]</sup> Bamboo (*Bambusa*) has a graded structure in longitudinal profile that can withstand extreme wind loads without fracture.<sup>[13]</sup> All these paradigms show that heterogenous structures have advantage in stress transmissions and hence achieve material properties that cannot be obtain by homogenous materials. For teeth and bone with heterogenous structure of abrupt  $E$ , the soft tissues surrounding the hard tissue facilitate force transmission and reduce stress concentration between hard tissues.<sup>[10, 14-15]</sup> Meanwhile, soft tissues can also act as cushion to protect the hard tissues from damages. Bamboo and mussel with gradient structure give a gradually force transition rather than abrupt change which enhance the both mechanical and functional performance of material.

Therefore, inspired by the biological materials above, a heterogeneous structure with combination of hardness and softness is employed into inorganic-based memristors to make it mechanically deformable and mechanically damage-endurable. The conventional inorganic memristor is a continuous bulky insulative layer (metal oxide) in between two electrodes, which is fragile under the mechanical deformation and mechanical damages. This thesis changes the rigid insulative layer (high  $E$ ) from continuous structure to discrete structure and filling in elastomer (low  $E$ ) in between the space, and verifies the hypothesis that the rigid active layers of memristor can be protected by the elastomer under mechanical damage forces; meanwhile, the elastomer can facilitate the force transmission and reduce the strain concentration under the deformation, which ensures the memristor electrical performance under the mechanical forces from motions and damages.

Another heterogeneous structure with a thickness that changes gradually (thickness-gradient) is employed into active layer in crack-based stretchable strain sensors. The conventional crack-based stretchable strain sensors employ a homogeneous thin film on elastomer. The strain energy is released by crack generating and propagating directly when stretching the strain sensors. There is a counter-part dilemma, that is a trade-off between large stretchability and high sensitivity.<sup>[16-17]</sup> To achieve a stretchable strain sensor with good mechanical property and electrical performance is a challenge. Thus, this thesis employs a thickness-gradient thin film instead of uniform thin film onto the elastomer and investigates the hypothesis that the strain energy within the thin film releases in a gradual manner which induces the strain distribution and regulates crack propagation, as a result, affecting the mechanical and electrical properties of stretchable strain sensors.

## 1.2 Objective and Scope

The objective of this thesis is to use heterogeneous structures to develop stretchable memristors and stretchable strain sensors with good mechanical properties and electrical performance under the mechanical forces. To fulfill this objective, the working scope includes:

- To develop inorganic-based memristors on elastomer with good electrical performance (in terms of writing, erasing and data storage) under various

mechanical deformations (stretch and flexion)

- To develop inorganic-based memristors on elastomer that can keep electrical performance (in terms of writing, erasing and data storage) under the mechanical damages (puncture and tear)
- To investigate the mechanical and electrical properties of stretchable strain sensors with a thickness-gradient thin film structure

### 1.3 Dissertation Overview

The thesis can be attributed to seven chapters as follows:

*Chapter 1* provides motivation and current challenges of stretchable electronics, states the inspiration of rationale design for the research and outlines the goals and scope.

*Chapter 2* reviews the literature concerning on conventional electronics and the state-of-art strategies for achieving stretchable electronics to overcome limitation of conventional electronics, as well as the strategies for stretchable electronics resist to mechanical damages that encounter in applications. It also presents some paradigms of heterogenous structure from biological materials and how it being apply in stretchable electronics to solve the existing challenges. The current challenges for development of stretchable memristor and stain sensors are discussed and the thesis in the context of literature is illustrated in this chapter.

*Chapter 3* discusses the working principles of techniques that are used to synthesis, fabrication, and characterization of devices. The selection of techniques for measurement and simulation are also illustrated.

*Chapter 4* elaborates how to fabricate stretchable inorganic-based memristor with an active layer consisted of discrete rigid materials and soft materials. The results show memristor with a heterogenous active layer possesses a good mechanical adaptability in terms of stretchability (~40%) and flexibility (bending radius of 0.1mm). In contrast, conventional memristor with a homogenous active layer can only remain electrical performance at ~10%

stretchability and rupture in bending condition. Demonstrating the advantage of this heterogenous structure prior to the conventional memristor homogenous active layer with continuous bulk of rigid material. Meanwhile, FEA manifest underlying reason is due to effectively alleviate the strain concentration by using combination of discrete hardness and softness.

*Chapter 5* mainly focus on demonstrating the mechanical damage endurance of stretchable memristor with heterogenous active layer in the two damage conditions, puncture and cut. At an extreme puncture and cut condition, this memristors can keep function in terms of data writing, erasing and storage when being punctured consecutively up to 100 times or undergoing a fully complete cut. Using FEA to elaborate the underlying reason why it can tolerate puncture damages. As a proof of concept in real application, the memristor was punctured with a spine of cactus and after that involving a dynamic movement by pulling up and down along the thorn of the cactus, proving data was robustly stored in memristor without loss. Finally, in the virtue of the self-healing property of SEBS, data in a memristor array with 4 fully complete cuts being able to restore after healing was demonstrated in this chapter.

*Chapter 6* mainly investigates the electrical and mechanical properties of a thickness-gradient thin film on elastomer. An anisotropic electrical property is discovered when applied force is parallel or perpendicular to the direction of thickness-gradient change. Discuss the mechanism behind it and establish a model for this property. Besides, a high sensitivity stretchable strain sensor is achieved by using this fabrication methods.

*Chapter 7* summarized the works that have been done and give a frame of this thesis. Meanwhile, the direction of future work is proposed including either theoretical study or practical applications. At last, an outlook of future and contribution of my work in this field are presented in this chapter.

## **1.4 Findings and Outcomes**

This research led to several novel outcomes by:

1. Developing a stretchable inorganic-based memristor with both outstanding mechanical adaptability and mechanical damage endurance by employing a heterogeneous design in active layer, which consist of discrete rigid materials and combining it with soft materials.
2. Investigating the mechanisms of how this heterogeneity design can impart outstanding mechanical adaptative properties and damage endurance with memristor and demonstrated feasibility of this stretchable memristor in real-world application.
3. Investigating the electrical and mechanical properties of a heterogenous metallic thin film on elastomer. Discovered the anisotropic electrical property, analyzed the mechanism, and proposed models for it. Fabricated a highly sensitivity stretchable strain sensors by using this thickness-gradient structure.

## References

- [1] H. W. a. C. J. B. Wei-Chen Huang, "Materials and microfabrication processes for next-generation brain-machine devices", can be found under <https://spie.org/news/6638-materials-and-microfabrication-processes-for-next-generation-brain-machine-devices?SSO=1#B5>, **2016**.
- [2] T. Wang, M. Wang, L. Yang, Z. Li, X. J. Loh, X. Chen, *Adv. Mater.* **2020**, *32*, e1905522.
- [3] J. Y. Oh, S. Rondeau-Gagné, Y.-C. Chiu, A. Chortos, F. Lissel, G.-J. N. Wang, B. C. Schroeder, T. Kurosawa, J. Lopez, T. Katsumata, J. Xu, C. Zhu, X. Gu, W.-G. Bae, Y. Kim, L. Jin, J. W. Chung, J. B. H. Tok, Z. Bao, *Nature* **2016**, *539*, 411.
- [4] J. Y. Oh, D. Son, T. Katsumata, Y. Lee, Y. Kim, J. Lopez, H.-C. Wu, J. Kang, J. Park, X. Gu, J. Mun, N. G.-J. Wang, Y. Yin, W. Cai, Y. Yun, J. B. H. Tok, Z. Bao, *Sci. Adv.* **2019**, *5*, eaav3097.
- [5] J. Xu, S. Wang, G.-J. N. Wang, C. Zhu, S. Luo, L. Jin, X. Gu, S. Chen, V. R. Feig, J. W. F. To, S. Rondeau-Gagné, J. Park, B. C. Schroeder, C. Lu, J. Y. Oh, Y. Wang, Y.-H. Kim, H. Yan, R. Sinclair, D. Zhou, G. Xue, B. Murmann, C. Linder, W. Cai, J. B. H. Tok, J. W. Chung, Z. Bao, *Science* **2017**, *355*, 59.

- [6] S. Wang, J. Xu, W. Wang, G. N. Wang, R. Rastak, F. Molina-Lopez, J. W. Chung, S. Niu, V. R. Feig, J. Lopez, T. Lei, S. K. Kwon, Y. Kim, A. M. Foudeh, A. Ehrlich, A. Gasperini, Y. Yun, B. Murmann, J. B. Tok, Z. Bao, *Nature* **2018**, 555, 83.
- [7] G.-J. N. Wang, A. Gasperini, Z. Bao, *Adv. Electron. Mater.* **2018**, 4, 1700429.
- [8] L. Smith, Y. Xia, L. M. Galatz, G. M. Genin, S. Thomopoulos, *Connect Tissue Res* **2012**, 53, 95.
- [9] S. Thomopoulos, G. R. Williams, J. A. Gimbel, M. Favata, L. J. Soslowsky, *J. Orthop. Res.* **2003**, 21, 413.
- [10] V. Imbeni, J. J. Kruzic, G. W. Marshall, S. J. Marshall, R. O. Ritchie, *Nat. Mater.* **2005**, 4, 229.
- [11] G. W. Marshall, Jr., M. Balooch, R. R. Gallagher, S. A. Gansky, S. J. Marshall, *J. Biomed. Mater. Res.* **2001**, 54, 87.
- [12] J. H. Waite, H. C. Lichtenegger, G. D. Stucky, P. Hansma, *Biochemistry* **2004**, 43, 7653.
- [13] S. Sutnaun, S. Srisuwan, P. Jindasai, B. Cherdchim, N. Matan, B. Kyokong, *WJST* **2011**, 2, 81.
- [14] Y. L. Chan, A. H. W. Ngan, N. M. King, *J. Mech. Behav. Biomed. Mater.* **2011**, 4, 785.
- [15] S. P. Ho, S. J. Marshall, M. I. Ryder, G. W. Marshall, *Biomaterials* **2007**, 28, 5238.
- [16] Y. Jiang, Z. Liu, C. Wang, X. Chen, *Acc. Chem. Res.* **2019**, 52, 82.
- [17] Z. Liu, D. Qi, P. Guo, Y. Liu, B. Zhu, H. Yang, Y. Liu, B. Li, C. Zhang, J. Yu, B. Liedberg, X. Chen, *Adv. Mater.* **2015**, 27, 6230.

## Chapter 2

### Literature Review

*This chapter reviews the state-of-art strategies to confer stretchability, flexibility, and mixed deformations on stretchable electronics, which include intrinsic materials development and structural designs. The state-of-art strategies for imparting stretchable electronics with mechanical damage endurance are discussed including developing tough materials, electronic-free, and self-healing. Besides, some of heterogenous structures from nature and the heterogeneity designs involved into the stretchable electronics are presented. Finally, the challenges of developing stretchable memristor and stretchable strain sensors are summarized and this thesis work in context of literature review is illustrated at the end of this chapter.*

## 2.1 Introduction

Conventional silicon-based CMOS electronics has been ubiquitous in every aspect of our life in past decades, including communication, transportation, city management, entertainment, and healthcare. Because of the planar and nature brittle of Si, which make electronics difficult incompatible with curvilinear surface and deformations, they are commonly fixed installed in rigid objects, in service statically without physical deformations, and widely well-accepted in transportation system, firms, buildings and equipment. In the applications of entertainment and healthcare which is human-centered system, wearable electronics such as iWatch, Google Glass and smart contact lenses, and Xiaomi smart bracelet are emerging and rapidly developing in recent years and able to monitor heart rate, track steps and sleep quality. However, they are only considered as wearable devices rather than go above and beyond for the flexibility and stretchability. Because human consists of soft tissues and arbitrarily curved surface and is living in activities, which requests electronics to be soft, deformable, and biocompatible to be compliant with body shapes and movements while keep electrical functions. Those requirements are challenging the conventional wearable electronics. Therefore, stretchable/flexible electronics underlie the solutions for those challenges and offer bio-physical interface for the fusion of virtual, physical, and biological world.

Biophysical signals (**Figure 2.1**) from human include electrophysiological signals (EEG, ECG, EMG, EOG, ECoG), biophysical signals (body temperature, strain, movement, skin hydration), biochemical signals (blood glucose, sweat composition) and photoelectric signals (blood oxygen and pressure).<sup>[1]</sup> All those signals are requested to be accurately monitoring and collecting for diagnosis and therapy. For example, ultrathin electrodes are intimate contact with human skin can improve the weak signal of SNG (signal noise ratio) like EEG and surface EMG <sup>[2-3]</sup> to ensure the fidelity. The stretchable/flexible sensors mounted on the human can provide the continuous track of electrophysiological activity for athletic performance and rehabilitation, and offer the long-term motoring of health status for highly vulnerable people like elderly or premature infants throughout the day.<sup>[4-5]</sup> Besides signal collection, the components for data processing and storage, computing

and transmission are also indispensable for a mature wearable system to achieve a higher level of multifunctionality, self-sustainability and intelligence in the era of AI and IoT.

Apart from physical deformations, wearable electronics in skin-mounted or textile form are facing a complex environment in practical, which consist of temperature change, moisture attacks and accidentally mechanical damages which also cause the electronics electrical functions failure.<sup>[6-7]</sup> Thus, to protect the stretchable/flexible electronics from uncertainties is also vital and worthy to put effort on it.

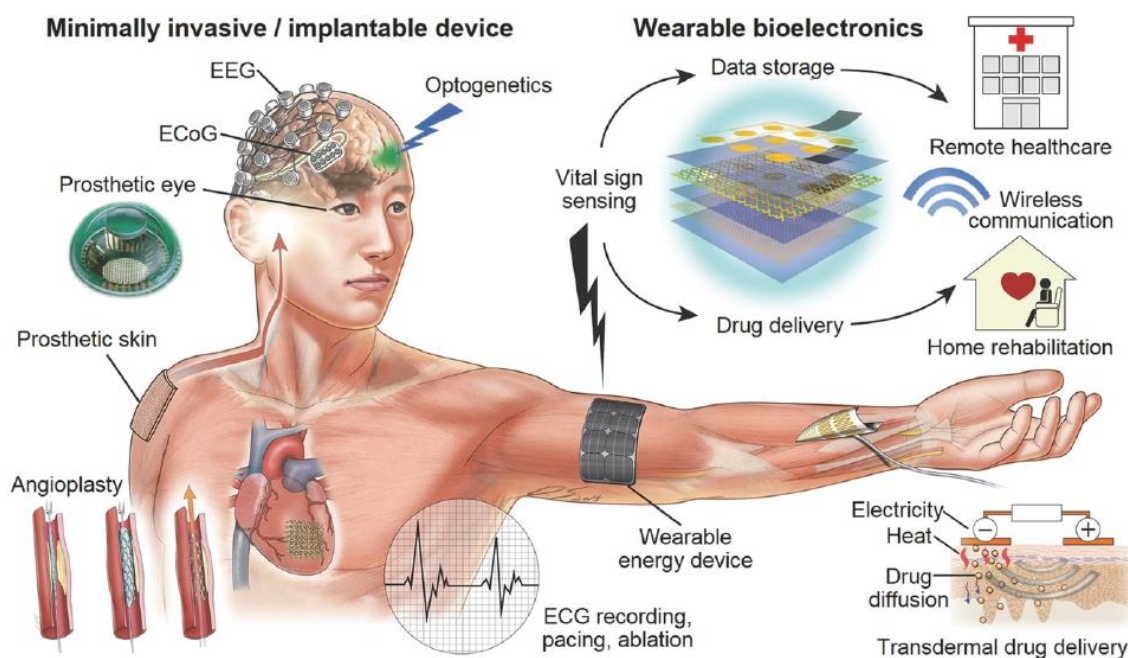


**Figure 2.1** Schematic of biomedical and therapeutic applications of wearable electronics for monitoring electrophysiological activity and drug delivery. Reproduced with permission.<sup>[1, 8-9]</sup> Copyright 2016, Wiley-VCH; Copyright 2008, Copyright 2014, Nature Publishing Group.

In this chapter, current strategies in wearable electronics to obtain mechanical adaptative properties such as stretchable, flexible, and shearing are reviewed. Then the methods of resistant to mechanical damages such as puncture, cut, scratch, tear, impact in stretchable electronics are discussed. Lastly, the heterogeneity designs for active material and substrate in stretchable electronics are presented.

## 2.2 Strategies to achieve mechanical adaptation

### 2.2.1 Stretchability

Human in daily life involve various movements and deformations. Our skin will stretch when we smile and speak, our wrists and knees will bend when we walk and run. Our inner organs such as the lung, heart, stomach, bladder, are also stretchable in nature. For example, strain on epidermal is 30%~70%, strain on heart is 20-35%, strain on moving brain is 10%.<sup>[10-14]</sup> So, stretchability is one of the most basic mechanical properties for wearable electronics and important for both vivo and vitro applications. For wearable electronics, it consists of two major parts. One is elastic substrates that provide the mechanical deformation like elongation and flexion, another part is active layer that gives the electrical functions. Hence, stretchability of wearable electronics refers to the critical strain that electronic devices can be tolerated without losing their original functions where electrical signals have no abrupt change. The examples of electrical failure like resistance in stretchable electrodes are changing from conductive to non-conductive or change of resistance in stretchable strain sensors is no more in step with deformations.

The large Young's modulus mismatch between conventional electronics (several GPa) and human skin and organs (~kPa) hinder conventional devices to be directly applied in wearable applications (**Figure 2.2**). To ensure electronics be in harmony with physical deformations and shape of human body, the materials with compatible Young's modulus of kPa are chosen as substrate to provide mechanical deformations. Depend on the target tissues, for example, hydrogels are used for implant tissue like brain, heart, and elastomers like polydimethylsiloxane (PDMS), copolymer styrene ethylene butadiene styrene (SEBS), Ecoflex, PVA, polyurethanes (PU) are commonly used for skin-mounted electronics and wearable devices.

Apart from substrates, the materials in active layer that is responsible for offering electrical functions, also need to elaborate design. Because the active layers are normally metallic or semiconductive materials that is rigid and not as stretchable as elastomer. If they are coupled with elastomer at the large elongation (>30%), the active materials either tend to break or peel-off from substrate and cause the device system breakdown. Therefore, to integrate the active materials with elastomers stably and durably so that functional layers

maintain their electrical performance under deformations is challenging for wearable electronics. In recent years, enormous research works have been done on engineering the active materials in molecular level or geometry way.

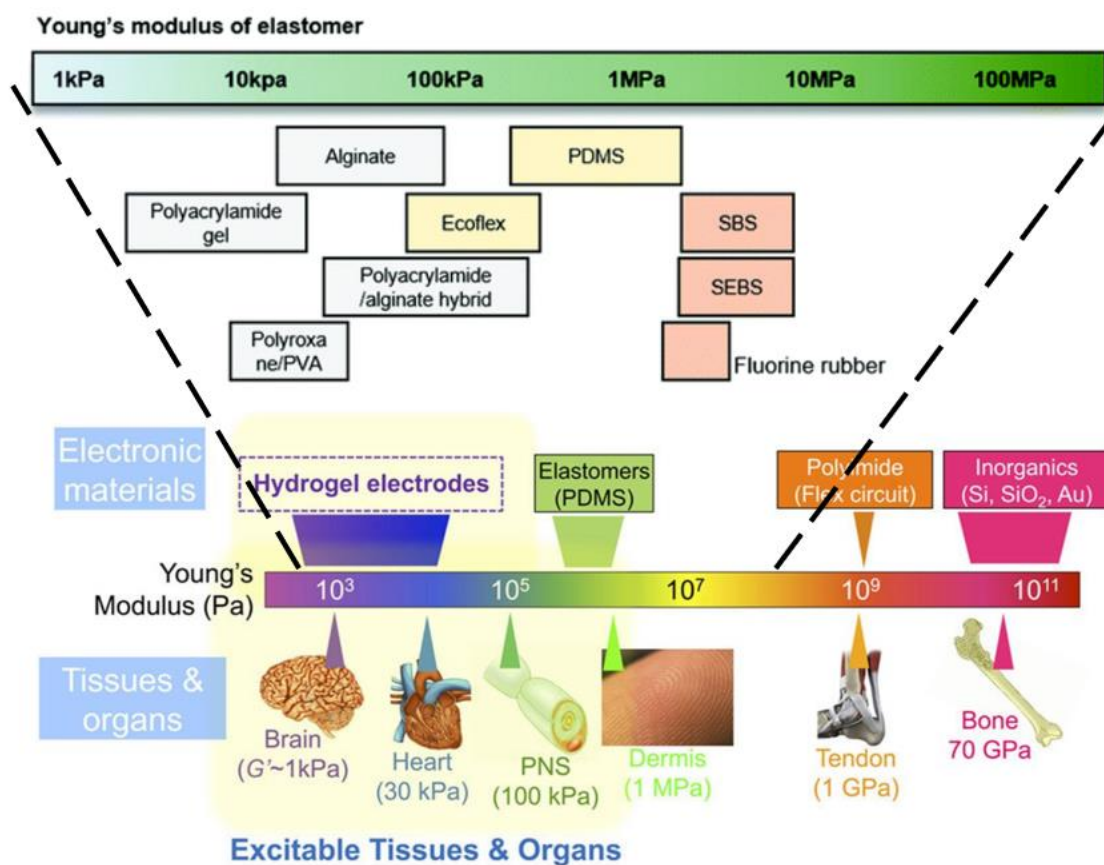


**Figure 2.2** The Young's modulus of biological and electronic substrate materials. Reproduced with permission.<sup>[15-16]</sup> Copyright 2019, RSC; Copyright 2016, SPIE.

The strategies of designing the active materials will be mainly discussed in the following sections. Those approaches are universally used and combined apply in stretchable electrode, stretchable strain sensors, devices, and integrated system.

## 2.2.2 Materials development

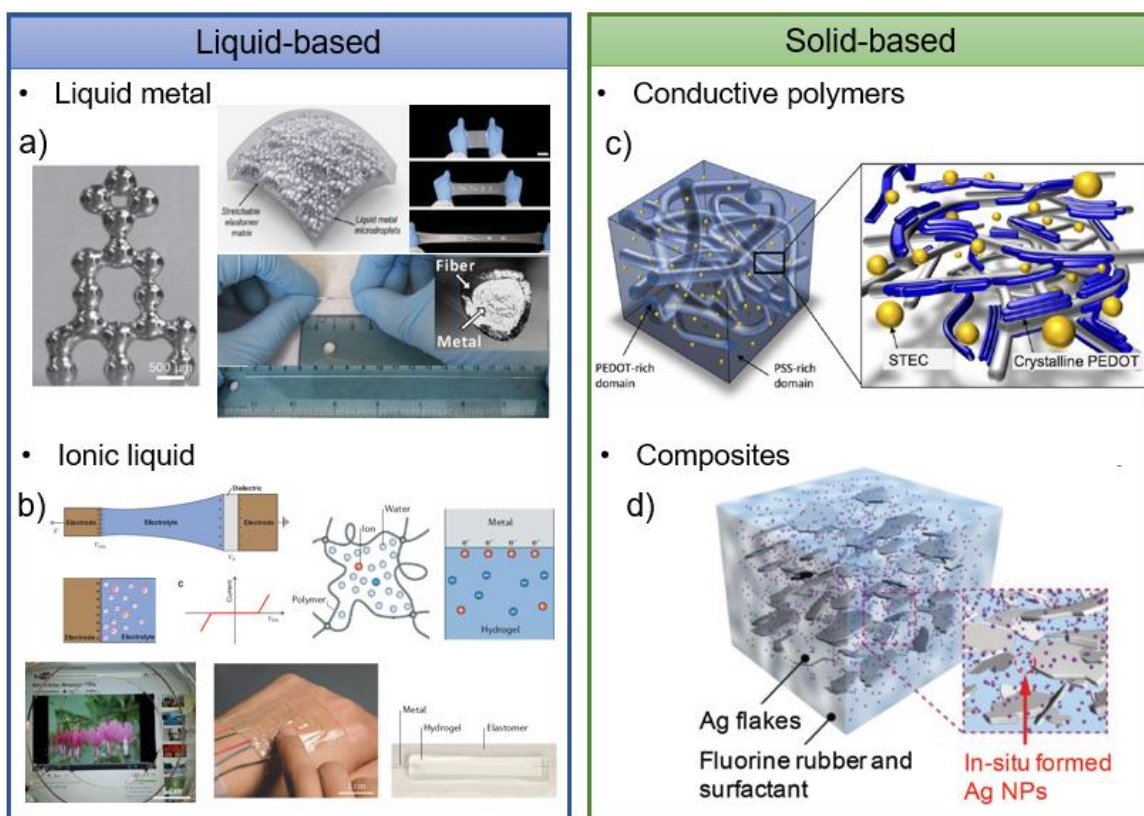


**Figure 2.3** Stretchability strategies for developing intrinsic properties of materials. (a) A photo mechanical stability of freestanding liquid metal droplets due to oxide forms on the metal outside. Reproduced with permission.<sup>[17]</sup> Copyright 2013, Wiley-VCH. Schematic diagram of liquid metal droplets dispersed in elastomer matrix and photos under stretching of 0%, 250% and 500%. Reproduced with permission.<sup>[18]</sup> Copyright 2016, Wiley-VCH. Liquid metal is injected into hollow thermoplastic fibers. Reproduced with permission.<sup>[19]</sup> Copyright 2013, Wiley-VCH. (b) Ionic conductive Hydrogels combine with metallic electrodes and dielectric elastic membrane can be formed artificial muscle, artificial skin and artificial axon under applied voltage. Reproduced with permission.<sup>[20-21]</sup> Copyright 2018, Springer Nature; Copyright 20013, AAAS. (c) Schematic diagram of PEDOT : PSS film with enhancers. Reproduced with permission.<sup>[22]</sup> Copyright 2017, AAAS. (d) Schematics diagram of micrometer-sized Ag flakes with in-situ formed Ag nanoparticles uniformly disperse in the elastomer. Reproduced with permission.<sup>[23]</sup> Copyright 2017, Springer Nature.

Liquid metals are deformable and conductive in nature. The metallic elements Fr, Cs, Rb, Hg, and Ga in liquid at room temperature are. Fr is radioactive, Rb and Cs are unstable in air, Hg is toxic and high surface tension, so they are not good choice to be used for wearable electronics. The commonly used liquid metals are Ga and its alloy such as EGaIn (75% Ga

and 25% In) and Galinstan (68.5% Ga, 21.5% In and 10% Tin), which are much less toxic.<sup>[24-25]</sup> Besides, a thin layer formation of  $\text{Ga}_2\text{O}_3$  in Ga based alloys in air that is mechanical stable and ease of patterning by existing techniques such as 3D printing and fluidic injection.<sup>[26-28]</sup> Generally, liquid metals are embedded in the channel of elastomers. One example as shown in **Figure 2.3 (a)**, the liquid metal droplets (eutectic EGaIn alloy) are dispersed in elastomer Ecoflex and achieving 600% strain.<sup>[18]</sup> The liquid metals can also inject into a polymer shell in the form of fibers, which can be stretched to 700% strain and woven into textile and clothes or made of stretchable cable for earphone.<sup>[19]</sup>

Another type of liquid based conductive material is ionic electrolyte based on ionic conduction (**Figure 2.3 b**). This type of mechanism is prevailing in living organs and cells to use ions exchange the information and nutrition and maintain balance of body environment. So artificial materials like hydrogels also adopt same mechanism which is naturally biocompatible and can be used for implant applications, human-machine interface, and artificial soft electronics.<sup>[29]</sup> A hydrogel is a network polymer with water molecules inside. If hydrogel contains electrolyte and cooperate with metallic electrode, the ions in hydrogel and electrons in metal will form an electrical double layer.<sup>[30]</sup> By adding a dielectric membrane sandwiched between two hydrogels-electrodes, the volume and shape of elastomer membrane can be changed under the applied time-varying voltage, which can be used for artificial skin, artificial muscle, and artificial axon.<sup>[20]</sup>

In addition to liquid-based intrinsic conductors, the solid-based conductors are made from modifying the molecule of conjugated polymers and adding the conductive fillers such as CNT and AgNPs into elastomer matrix.<sup>[31-33]</sup> Metal flakes like Ag flakes are commonly selected as conductive filler because they are able to self-organized upon stretching.<sup>[34]</sup> One example as shown in **Figure 2.3 d**, researcher found that a proper amount of surfactant and heating process can trigger the formation of AgNPs from Ag flake and promote the conductivity of polymer as high as  $935 \text{ S cm}^{-1}$  at 400% strain.<sup>[23]</sup> Polymer composite based on metal fillers has problem of cycling stability. Bao's group has achieved both highly conductivity (4100 S/cm) and stretchability (100%) polymer film (PEDOT:PSS) with highly cycling stability by incorporating ionic additive-assisted enhancers<sup>[22]</sup> (**Figure 2.3 c**).

No matter liquid-based or solid-based methods, they are all viable for conductors and be employed as stretchable electrodes in wearable electronics. However, using liquid-based intrinsic properties of materials as stretchable electrodes request a good encapsulation to prevent liquid metals from leakage in usage. Hydrogel ionic conductors are suitable for being used in aqueous environment as they are easily dehydrated in air, and another drawback is they are lacking mechanical toughness in some applications. For the solid-based intrinsic conductors, it may face problem of incompatible with current semiconductor devices and the conductivity of electrodes are sensitive to temperature.

### **2.2.3 Structure design**

Another strategy of achieving stretchability is to engineer the structure of inelastic metallic materials so that it can be elongated with underneath elastomers. It has been proven effective to enable tradition materials like silicon, metals, or graphene to be stretchable. There are two structural configurations under this strategy: out-of-plane and in-plane designs.

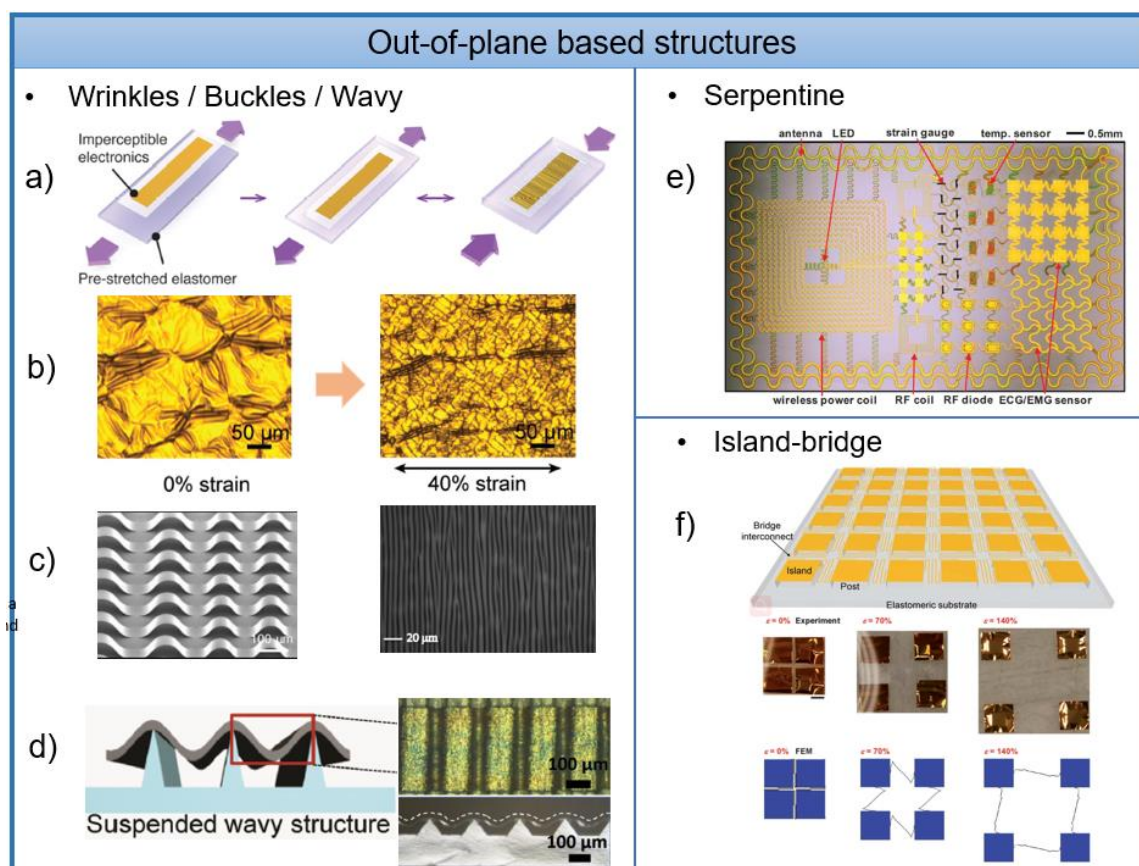


**Figure 2.4** Stretchability strategies based on out-of-plane structure design (a) Schematic diagram show wrinkle formation upon release by transferring electronics film to a pre-stretched elastomer. Reproduced with permission.<sup>[35]</sup> Copyright 2014, Wiley-VCH. (b) Optical images of Au thin film on silk substrate forms wrinkles by the ambient hydration of silk substrate at 0% and 40% strain. Reproduced with permission.<sup>[36]</sup> Copyright 2018, Wiley-VCH. (c) Optical image of 3D buckled semiconductor ribbon on PDMS substrate (left) and buckled PEDOT:PSS film. Reproduced with permission.<sup>[37-38]</sup> Copyright 2006, Nature Publishing Group; Copyright 2012, Wiley-VCH. (d) Gold nanobelts suspend on tripod PDMS. Reproduced with permission.<sup>[39]</sup> Copyright 2015, Wiley-VCH. (e) Image of demonstrative platform shows a collective of sensors, LED, circuit elements and devices for RF communication. Reproduced with permission.<sup>[40]</sup> Copyright 2011, AAAS. (f) Schematic of the island-bridge structure with serpentine interconnection. Reproduced with permission.<sup>[41]</sup> Copyright 2013, The Royal Society of Chemistry.

The common out-of-plane design involve a spring-like structure. They are in the form of wrinkles, buckles, and waves (**Figure 2.4 a-d**). During stretching, the induced strain is mostly absorbed by structural changes like spring and accordion bellows. The formation of wrinkles/buckles/waves structure are very common in deposition of thin film on elastomer

through pre-strain method, induced residual stress by thermal, hydrated, and mismatch of Young's modulus <sup>[42-51]</sup>, which are triggered by physical manner. The wave structure can also form manually through chemical treatment on the elastic substrate. For instance, PDMS exposed to UV light through a patterned mask, the area that exposed to UV has active bonds of  $-\text{O}_n\text{Si}(\text{OH})_{4-n}$  that can bond with inorganic materials with  $-\text{Si}-\text{OH}$  group to form siloxane linkage ( $-\text{O}-\text{Si}-\text{O}-$ ) via condensation reaction. The area unexposed to UV light remains inactive and reacts with other material through weak van der Waals interaction. When transferring Si nanoribbon to pre-stretched PDMS with patterned UV treatment, the exposed area has strong bond with nanoribbon while unexposed area has weak bond. Upon release the PDMS, the wave formation is contributed by the weak bond at unexposed region.<sup>[37, 52]</sup> The wave pattern does not need to be in contact with substrate, but can be in a suspended way. Chen's group fabricates stretchable electrode by suspending gold nanobelts on a wedge-shaped PDMS. This design reduces and provides sufficient space for gold nanobelts to bend during stretching and releasing process, hence further reduces strain concentration on the active material and enhances stretchability and mechanical stability.<sup>[39, 53]</sup>

In addition, serpentine and island-bridge structures are also widely used in stretchable electronics, especially for integrated electronics systems (**Figure 2.4 e-f**).<sup>[52, 54-55]</sup> Many existing components such as LEDs, chips, communication devices are still based on the rigid complementary metal-oxide semiconductor (CMOS) technology; island-bridge is able to bridge those traditional rigid electronics and flexible substrate to generate a stretchable/flexible hybrid electronics. The rigid devices are spatially separated and residue as islands across the elastomer with wavy/serpentine conductive interconnection as bridge.<sup>[55-61]</sup> The region between rigid devices are used to tolerate strain and the stretchability of the whole system highly depends on interconnection. The downsides of this approach are the delamination between rigid components and soft elastomers, and the out-of-plane interconnection is susceptible to external mechanical damages such as puncture and cut.

The in-plane design involves nanomaterials such as metal nanowires, nanomeshes, thin films, and CNT. The resistance response to exerted external strain with different mechanisms such as disconnection between adjacent sensing elements, tunneling effect,

and cracks open and close in the thin film. The conductivity depends on the entangled percolation networks of nanomaterials which maintain the conductive pathway under stretching.

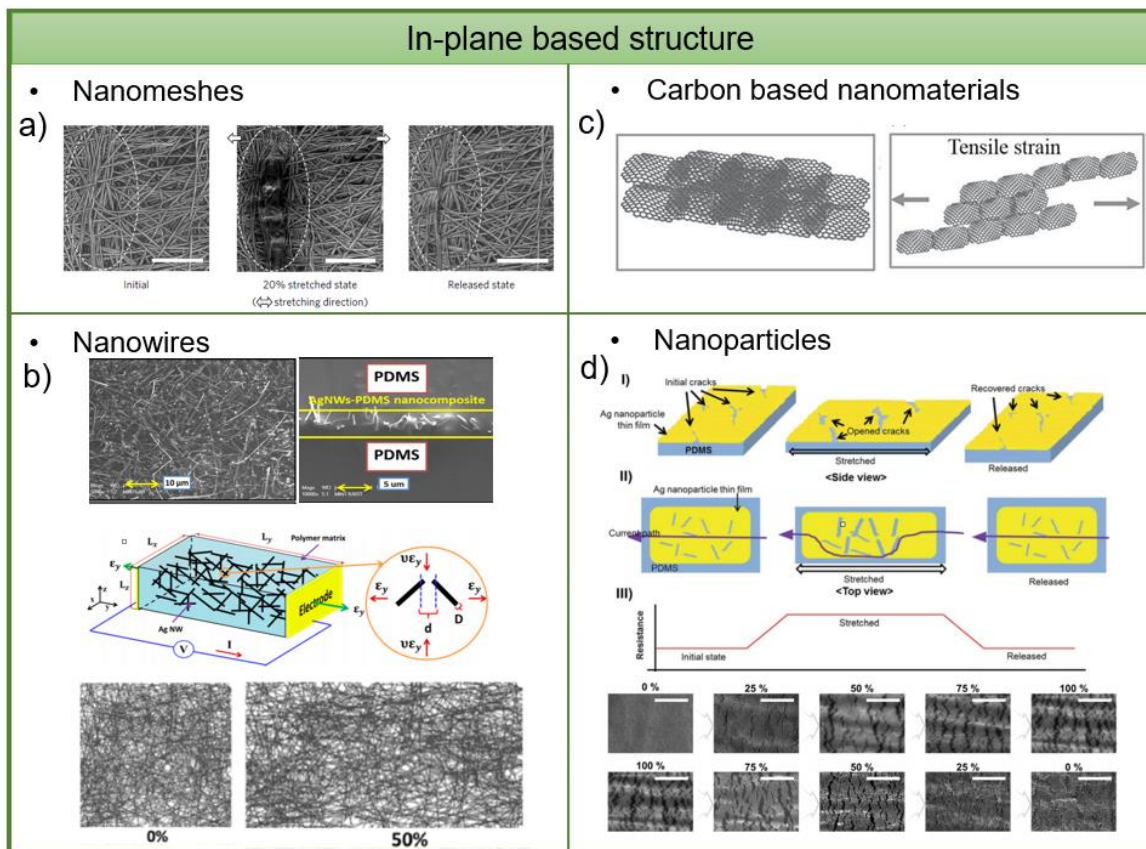


**Figure 2.5** Stretchability strategies based on in-plane structure design. (a) SEM images of Au nanomeshes in a stretching-releasing process with crack open at strain 20% and close at initial state. Reproduced with permission.<sup>[62]</sup> Copyright 2017, Springer Nature. (b) Top view SEM image of Ag NWs nanowires embedded at PDMS and cross-sectional SEM image. Computational model of Ag NWs randomly orientated in the PDMS and two neighboring NWs under the strain. Top projected view of Ag NWs network at initial state and stretching to 50%. Reproduced with permission.<sup>[63]</sup> Copyright 2014, American Chemical Society. (c) Schematic show overlap and connections of graphene platelet without /with tensile stress. Reproduced with permission.<sup>[64]</sup> Copyright 2016, Wiley-VCH. (d) (i-ii) Schematic show Ag NPs thin film on PDMS during stretching/releasing state. (iii) The resistance changes along with elongation based on crack open and close. Reproduced with permission.<sup>[65]</sup> Copyright 2014, The Royal Society of Chemistry. SEM of cracks morphologies during elongation/relaxation state. Reproduced with permission.<sup>[66]</sup> Copyright 2017, American Chemical Society.

For long-term physiological monitoring on human body, wearable electronics is not only requested to be intimately in contact with body shape, but also need to be inflammation-free, gas-permeable to attach to human skin. Nanomesh is a perfect structure to provide a highly precision and irritation-free platform for long-term continuously monitoring of vital signal and EMG recording.<sup>[62, 67]</sup> In **Figure 2.5 a**, Au nanomeshes were prepared by nanofibers with diameter of 300-500nm by electrospinning and were intertwined to form mesh-like sheet. When stretching, it has an open space under 20% tensile strain because of slipping of nanomesh bundle. When removing tensile strain, the nanomeshes recover to initial state indicating the reproducible process and robustness of nanomeshes under stretching.

Metal nanowires also have been studied extensively due to their good conductivity and mechanical ductility. They are entangled to form percolating network through diverse techniques like spin coating, spray coating and drop casting.<sup>[68-71]</sup> Among various nanowire materials, Ag NWs is the most widely explored in research as it has highest electrical conductivity compared to the rest metal NWs.<sup>[72-73]</sup> Besides, NWs at low density of the NW network is transparent and it is suitable for transparent stretchable electrodes.<sup>[74-75]</sup> The NW-NW junctions play a dominating role for conductivity.<sup>[76]</sup> Ligands used during synthesis and solution dispersion induce nanometer gap between nanowires and decrease conductivity of nanowire junction. By light-induced welding annealing such as thermal annealing,<sup>[77-78]</sup> mechanical pressing,<sup>[79-80]</sup> soldering by other materials,<sup>[81-82]</sup> can weld NW junction and increase conductivity at junction site through reduce NW contact resistance. Not only transparent electrode can be made by Ag NWs, but also the stretchable strain sensors. Ag NWs were embedded between two layers of PDMS can be used as stretchable strain sensors for motion detection of fingers (**Figure 2.5 b**). From computational model, the resistance of nanowires network depends on the junction of all pairs of NWs. The change of resistance under stretching are determine by the distance of two NWs which is classified into three stage. (i) At initial, they are complete in contact with each other and no contact resistance. (ii) Stretching to a certain level where shortest distance between the centerlines of two neighbor NW is larger diameter of NW but smaller than a cutoff distance, where electrons can tunnel through the polymer matrix and form tunneling current between two noncontact NWs. (iii) Further stretching causes the distance of two neighbor NWs

exceeds the cutoff distance, no electrons can pass through and electrical path is disconnected.<sup>[63]</sup> This is the critical point where stretchable strain loss electrical function from conductive to nonconductive. The stretchability of strain sensors is defined by this critical point.

Carbon based nanomaterials such as CNT<sup>[83-85]</sup> and graphene<sup>[86-90]</sup> are also developed as an active material in wearable electronics as their superior mechanical and electrical properties. They are popularly employed in stretchable strain sensors which consist of a thin layer of conductive materials on top with conductive NWs network<sup>[86, 91-93]</sup> or graphene flake,<sup>[91, 94-95]</sup> and a flexible elastomer substrate on bottom to support it. Imposed by force or pressure, overlapped NWs lost contact area or graphene flake were slid with the elongation of substrate because of the weak interfacial binding and large Young's modulus mismatch between carbon nanomaterials and the substrate or due to apart substrate under the stretching.<sup>[63-64, 96-98]</sup> The more stretching is, the more disconnection between the junction of graphene flakes, and thus the electrical resistance increases because of decreasing number of conductive pathways (**Figure 2.5 c**), where sensitivity comes from disconnection and tunneling effect that is similar to NWs based mechanism.

Metal nanoparticles deposited on the soft elastomer as a thin film is another commonly employed and universal strategies for stretchable electrodes<sup>[36, 99-100]</sup> or stretchable strain sensors.<sup>[66, 101-102]</sup> Cracks will be generated and propagate within the film to release the strain energy. The morphologies of cracks such as size,<sup>[101-102]</sup> density,<sup>[65]</sup> length,<sup>[103]</sup> width<sup>[104]</sup> determine the electrical property of thin film. **Figure 2.5 d** shows Ag NPs forms thin film on PDMS. The initial microcracks are enlarged under tensile strain. As further stretching, crack density increases and initial microcrack open hinder the electrical current path, hence resistance increase under stretching process. After remove the strain, microcracks close and recover to initial state, so does resistance.<sup>[65]</sup> The mechanism of stretchability are due to elastic deformation of thin film on elastomer under elongation. The metal ligament networks can twist and deflect out of plane, which minimize the energy release at the crack tip and inhibit the crack growth cross the metal film, thus reproducible electrical conduction is maintain.<sup>[105]</sup>

To sum up, to impart stretchability to the wearable electronics can be classified into two groups. One is developing intrinsically stretchable materials; another is structural design. For structural design, it consists of out-of-plane and in-plane design. Generally, the intrinsically stretchable materials and out-of-plane design is suitable for stretchable electrodes, the in-plane design can be applied for both stretchable electrodes and stretchable strain sensors in wearable electronics.

#### 2.2.4 Flexibility

In addition to stretchability, flexibility is another vital trait for wearable electronics, especially apply to the joint level of human body such as fingers, wrist, knees, and elbows.<sup>[66, 89]</sup> From the material standpoint, either elastomers such as PDMS, SEBS, Ecoflex and PU or the plastic films like polyethylene terephthalate (PET), polyimide (PI), polyethylene naphthalate (PEN), polycarbonate (PC) and even papers<sup>[106-109]</sup> can be used as flexible substrates.

Flexibility is defined as the wearable electronics tolerate a certain curvature in bending whilst maintaining the electronics performance. The maximum strain induced by bending can be calculated as  $\epsilon = \frac{h}{2r}$ , where  $h$  is the thickness of sheet or devices,  $r$  is the bending radius of the curvature.<sup>[110-112]</sup> For inorganic semiconductors, the relationship between bending stiffness and thickness can be expressed as  $EI = \frac{Ebh^3}{12}$ , where  $EI$  is bending stiffness,  $E$  is Young's modulus,  $b$  is width,  $h$  is thickness of semiconductors.<sup>[113]</sup> So, reducing the thickness of materials/substrates lessen bending-induced strain and bending stiffness at a giving bending radius, which can be one strategy to effectively improve the flexibility. For example, bulk semiconductor materials such as Si (~150 GPa), GaAs (~85GPa) are rigid and undergo fracture at strain <1%.<sup>[114]</sup> However, with extreme thinning, these materials show certain flexible because the bending stiffness and bending-induced strains reduce with the thickness decrease (**Figure 2.6 a**).<sup>[114-116]</sup> For example, silicon ribbons with 100 nm thickness experience peak strain of 0.0005% when bending at the radius of curvature of 1 cm, and even it mounts on plastic sheet with thickness of 20  $\mu$ m, the peak strain of silicon ribbon is around 0.1% at similar bend radius of 1 cm that is far below Si fracture limit of 1%.<sup>[117]</sup> Besides, nanomaterials that are employed in

stretchability such as 1D and 2D materials, graphene, CNT and inorganic materials can also be adopted in flexibility (Figure 2.5 b-d).

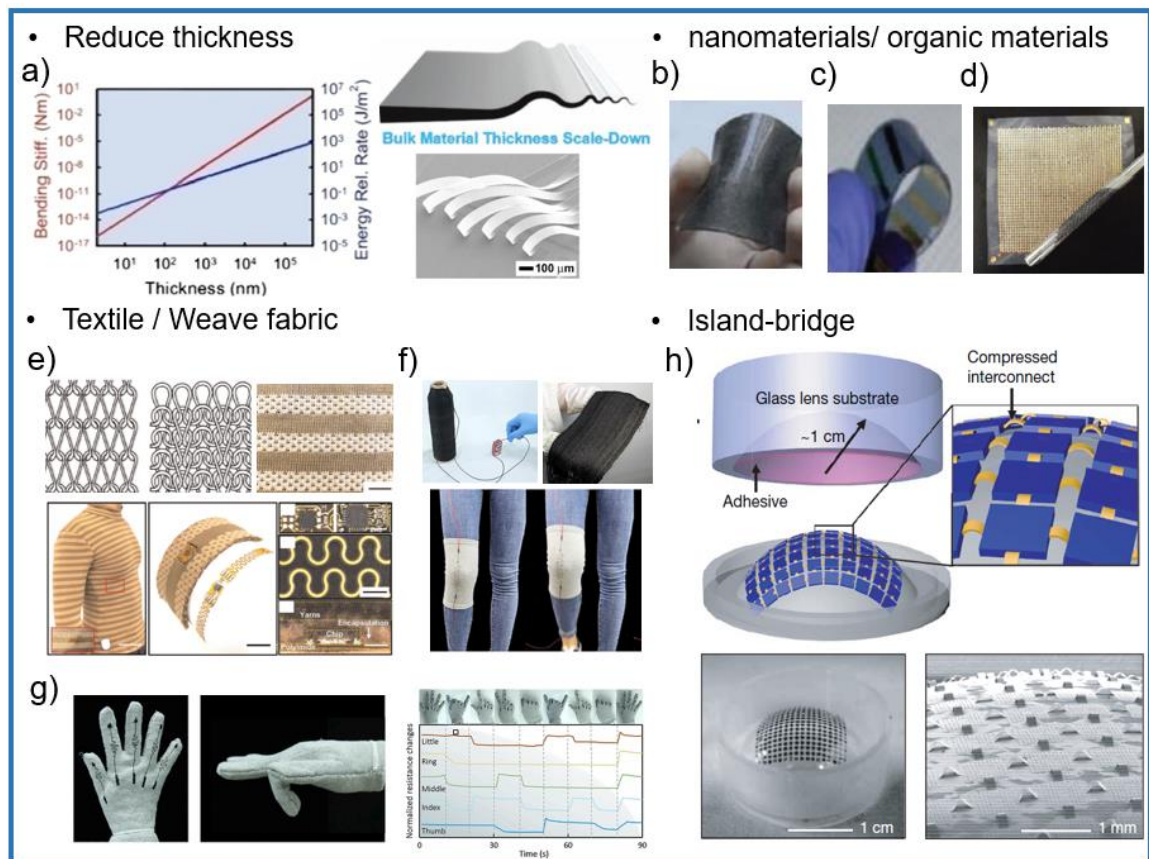


**Figure 2.6** Strategies of flexibility in wearable electronics. (a) silicon membrane bending stiffness (red) and energy release rate (blue) for delamination in a function of thickness between 2 nm and 200  $\mu\text{m}$ . Reproduced with permission.<sup>[118]</sup> Copyright 2011, Macmillan Publishers Limited. The plot shows that 2 nm thickness nanomembrane are  $10^{15}$  times less flexural rigidity and  $10^5$  times more adherent to substrate compared to 200  $\mu\text{m}$  thickness nanomembrane. SEM image of silicon nanoribbons with flexibility at a thickness around 300 nm. Reproduced with permission.<sup>[114]</sup> Copyright 2014, Materials Research Society. (b) photograph of bendable graphene foam. Reproduced with permission.<sup>[119]</sup> Copyright 2011, Macmillan Publishers Limited. (c) Photo of the flexible PP-PEDOT thermoelectric film at bending state. Reproduced with permission.<sup>[120]</sup> Copyright 2013, The Royal Society of Chemistry. (d) A photo of a flexible thermoelectric generator based on CNT/polystyrene composite roll around a tube. Reproduced with permission.<sup>[121]</sup> Copyright 2013, AIP Publishing LLC. (e) Sketch of two kinds of loop structure, single jersey knit loop structure (top left) and interlocking loop structure (top middle). A photograph of electronic textile conformable suit fabric channels with scale bar 1 cm (top right). Electronic strip with

temperature, accelerometer (scale bar: 3 mm) and interconnection wire (scale bar: 2 mm), and woven in knit textile (scale bar: 1 cm). Reproduced with permission.<sup>[122]</sup> Copyright 2020, The Author(s), licensed under a Creative Commons Attribution 4.0 International License (<http://creativecommons.org/licenses/by/4.0/>). (f-g) Photos of yarns of natural silk functionated with CNTs were used to light a bulb and weave into e-textile cloth. Photos of yarns (silk functionated with CNTs) were sewn into an e-kneepad and e-glove and can be used for detecting knee-bending angles during walk and hand gestures through the resistance change. Reproduced with permission.<sup>[123]</sup> Copyright 2019, Elsevier Inc. (h) Top: Illustration of focal plane arrays comprising of silicon devices (photodetector and p-n diodes) as islands and interconnection as bridges. Bottom left: photograph of island-bridge focal plane array on a hemispherical PDMS surface. Bottom right: SEM image of a portion of the focal plane array. Reproduced with permission.<sup>[8]</sup> Copyright 2008, Macmillan Publishers Limited.

Graphene is a two-dimensional monolayer of carbon atoms that exhibit extraordinary electrical, intrinsically strong and flexible.<sup>[124]</sup> Graphene sheets have high mobility and mechanical elasticity and strength due to the covalent carbon bonds packed in a honeycomb lattice.<sup>[125-126]</sup> Cheng et al. develop a 3D graphene foam (GF) and infiltrate it with PDMS (**Figure 2.6 b**). The GF/PDMS composites show a very high conductivity of  $\sim 10 \text{ Scm}^{-1}$  at an extremely low graphene loading of  $\sim 0.5 \text{ wt\%}$  ( $\sim 0.22 \text{ vol\%}$ ). The resistance increases only  $\sim 2.7\%$  after 10,000 cycles of bending radius of 2.5 mm. Even at small bending radius of  $\sim 0.8 \text{ mm}$ , the resistance increase remains constant at only  $\sim 7\%$  compared to flat state, showing an excellent electromechanical stability in flexional state. Conductive organic materials such as polypyrrole, polyaniline, PEDOT, PEDOT:PSS have been extensively studied. By controlling the oxidants and mediators for the polymerization, a large power factor of PP-PEDOT films ( $1270 \text{ uW m}^{-1} \text{ K}^{-2}$ ) were prepared and made into a flexible thermoelectric generator (TEG) by coating it on polymeric substrates (**Figure 2.6 c**).<sup>[120]</sup> Another flexible and lightweight TEG was fabricated by printing thermoelectric material which is comprised of CNT and polystyrene on a polyethylene naphthalate film and can tolerate bending radius of less than 6 mm (**Figure 2.6 d**).<sup>[121]</sup>

In addition, electronics comprised of temperature, accelerometer and interconnection on plastic substrates can be fabricated to knitted textile (**Figure 2.6 e**).<sup>[127]</sup> The knitted textile allows electronics to be in intimate contact with skin which provides a platform for large-scale

physiological sensing such as temperature monitoring, heart-rate detection, respiration monitoring during exercise.<sup>[122]</sup> Besides, natural silk fibers were functionalized by CNTs to fabricate electronics yarns and weave into e-textiles through yarn-spinning and automatic weaving techniques, which can be used to sense force, temperature and solvents (**Figure 2.6 f-g**).<sup>[123]</sup>

Island-bridge architecture is not only suitable for employing in stretchability, but also in flexibility. Rogers' group fabricated electronic eye camera with hemispherical shape based on Si materials and planar processing approaches through transfer printing. The single-crystalline silicon photodiodes, current-blocking p-n junction diodes and metal interconnection form a focal plane array on wafer using conventional planer processing, and then transfer focal plane array to a stretched, planar drumhead shape of PDMS substrate. After relaxing PDMS, the compressive force brings the island elements closer and the metal connection between island elements form an arc shape to accommodate the strains via delamination locally from PDMS substrate surface. This transfer printing approach and island-bridge structure enable the rigid silicon devices to be assembled on the non-planer surface and is compatible with existing planer silicon manufacturing facilities (**Figure 2.6 h**).<sup>[8]</sup>

### 2.2.5 Mixed deformations

Although stretchability and flexibility are important traits for wearable electronics, a complex of deformations are involved in motions and our daily activities. In human anatomy, there are six basic joint-level movements, namely, flexion, extension, abduction, adduction, medial rotation, and lateral rotation<sup>[128]</sup>. In addition, small deformations in skin-level motions include pulsation, blinking and breathing<sup>[66]</sup>. To deal with mixed deformations, some structure strategies can be used such as micro/nano fibers, origami and kirigami as shown in **Figure 2.7**.

Micro/nano fibers are one example to show highly flexible in a mixed deformation (**Figure 2.7 a**). A strain sensor was fabricated by coating  $\text{Fe}_3\text{O}_4$  nanoparticles with PAA polymer (poly acrylic acid) and mixing with monomer (acrylic acid), cross-linker, and thermal initiator to form ionogel through gelation process at  $60^\circ\text{C}$  one-pot method.<sup>[129]</sup> This ionogel

nanocomposite can be cut into strip and show high level flexibility in knotting, twisting, and stretching. Meantime, it shows an excellent self-healing efficiency (>95%).

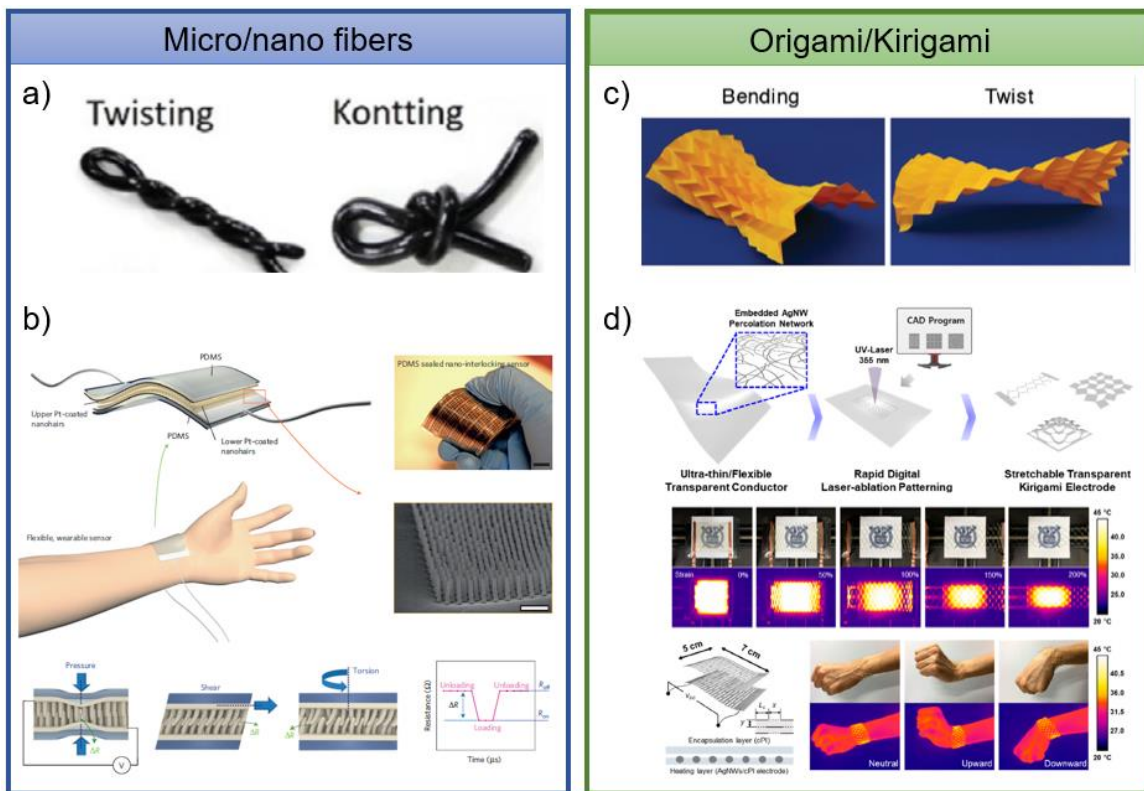


**Figure 2.7** Strategies for adapting to a mix of deformations. (a) A strain sensor was made of  $\text{Fe}_3\text{O}_4$  and PAA composites can be knotted and twisted in a strip form. Reproduced with permission.<sup>[129]</sup> Copyright 2019, Wiley-VCH. (b) Flexible strain-gauge sensor with interlocking Pt-coated polymer nanofibers can detect pressure, shear, and torsion through the electrical resistance which is affected by the displacement between hairs under different mechanical forces. Reproduced with permission.<sup>[130]</sup> Copyright 2012, Macmillan Publishers Limited. (c) Photographs of the Miura-ori paper model can bend and twist. Reproduced with permission.<sup>[131]</sup> Copyright 2017, Elsevier Ltd. Under the CC BY-NC-ND license (<http://creativecommons.org/licenses/by-nc-nd/4.0/>). (d) Illustration of fabrication process of a transparent kirigami electrode and its electrothermal performance under stretching condition from 0% to 200% when it was used as heater. The photos of transparent kirigami heater was mounted on the wrist and performs under dynamic upward and downward movement. Reproduced with permission.<sup>[132]</sup> Copyright 2019, American Chemical Society.

Inspired by hair-to-hair interlocking structure in nature, a strain sensor was fabricated by integration of two layers of metal-coated polyurethane-based nanofibers interlocked with each other, which can detect multiple mechanical forces such as pressure, shear, and torsion (**Figure 2.7 b**).<sup>[130]</sup> The displacement of hair-to-hair interlocking under different loadings cause the change of electrical resistance signal, and different physical inputs can be distinguished by gauge factor (GF~11.5 for pressure, 0.75 for shear, ~8.53 for torsion) of strain sensors due to the contact area of fibers and number of contact areas involved are different in each scenario.

Origami is an ancient paper art folding that can transform a planar sheet into 3D structure through the hinge crease patterns. The crease patterns consist of a periodic array of mountain and valley folds so that functional devices in facets can be avoid from large strain. By designing crease pattern, the desired 3D origami structure can be achieved.<sup>[133-135]</sup> As shown in **Figure 2.7 c**, Origami with the Miura-ori crease pattern can bend and twist.<sup>[131]</sup> Kirigami is combine paper folding and cutting that has been popular in stretchable electronics as it allows the formation of 3D objects from 2D sheets.<sup>[136-138]</sup> A stretchable transparent kirigami electrode were made by laser ablation technique, and the electrode elongation can be tuned by varying the cutting parameter (**Figure 2.7 d**).<sup>[132]</sup> The conductive material in this kirigami electrode consists of silver nanowires and an ultrathin colorless polyimide layer (<5 um) to make sure high optical, thermal, electrical properties and biocompatibility. This transparent electrode is able to conformally cover the irregular curved surface of human body and can be mounted on skin such as wrist and face for measuring electrophysiology signals in human-machine interface application, or used as wearable heater for thermal haptic, personal thermal treatment.

## 2.3 Strategies to tolerate mechanical damages

### 2.3.1 Tough materials/ Electronics-free

Numerous researches have been emphasizing on ensuring electronic units mechanically accommodate with physical deformations, however, the real world is dynamic and chaotic that is full of unforeseen accidents or damages from environments. For example, extreme temperatures or humidity that impair electrical functionalities, or mechanical attacks such

bumps, scratch, abrasion, puncture and cut which also destroy the device. Therefore, it requests the stretchable electronics not only mechanically adaptive but also damage tolerance. Among those damages, mechanical damages are the most happened and unforeseen in wearable applications. Currently, there are two antidotes to mechanical damage. One is to retain the electronics functionalities during or after mechanical damages. Another is to recover the original functionalities from damages, which is inspired by human skin recovery capability from wound. To retain the electrical functionality as shown in Figure 2.8, one approach is developing tough materials that resistant to some kinds of mechanical damages, another approach is sacrificing the electronic-free parts.

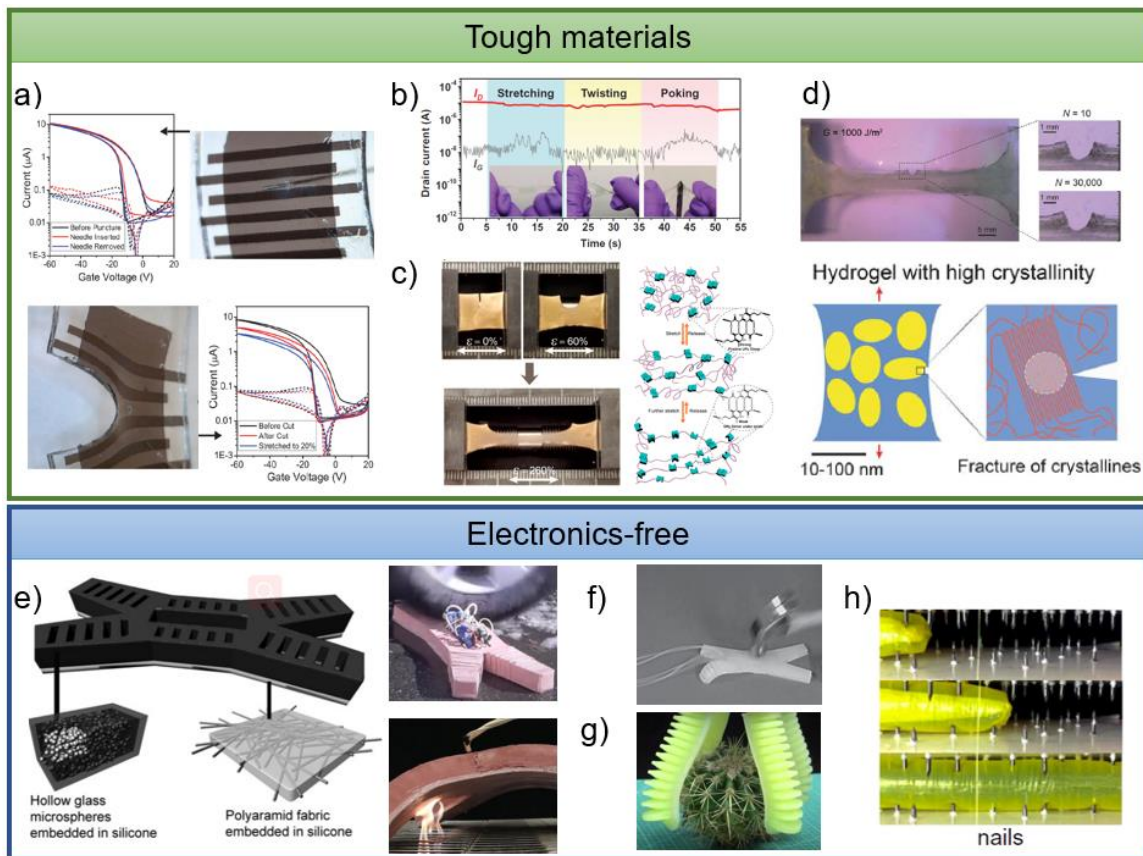


**Figure 2.8** Strategies for tolerating mechanical damages while retaining the electronics functionalities. (a) Transfer curve and photo of a stretchable transistor punctured with 200  $\mu\text{m}$  needle in the active channel, and transfer curve and photo of a stretchable transistor with a half-cut and stretched to 20% strain. Reproduced with permission.<sup>[139]</sup> Copyright 2015, Wiley-VCH. (b) Drain current and gate current of a stretchable thin-film transistor under different conditions. Reproduced with permission.<sup>[140]</sup> Copyright 2017, AAAS. (c) Optical image of stretchable gold thin

film on a supramolecular polymeric materials with a 20% UPy motif and was induced a notch in a stretching state. Illustration represents the proposed mechanism of highly stretchable supramolecular polymeric materials. Reproduced with permission.<sup>[141]</sup> Copyright 2018, American Chemistry Society. (d) Validation of fatigue threshold for a dry-annealed hydrogel as high as 1000 J/m<sup>2</sup> using the single-notch test. Illustration of fatigue crack propagation in the hydrogel with high crystallinity under cyclic loads. Reproduced with permission.<sup>[142]</sup> Copyright 2019, the Authors, some rights reserved; exclusive licensee American Association for the Advancement of Science. Distributed under a Creative Commons Attribution NonCommercial License 4.0(CC BY-NC). (e) Two composites materials are used in soft robot, top layer material is a blend of hollow glass sphere in silicone and bottom layer material is polyaramid fabric embedded in silicone. The material can withstand crushing force of being run over by a car and fire condition. Reproduced with permission.<sup>[143]</sup> Copyright 2014, Mary Ann Liebert, Inc. (f) Soft pneumatic actuator with composite structure consisting of Ecoflex and Nylon mesh strain-limiting layer resist impact from hammer striking. Reproduced with permission.<sup>[144]</sup> Copyright 2014, Wiley-VCH. (g) Photo of a soft gripper grasp a cactus. Reproduced with permission.<sup>[145]</sup> Copyright 2016, IEEE. (h) Photos of a soft robot lengthens through challenging environment by moving its tip. Reproduced with permission.<sup>[146]</sup> Copyright 2017, the Authors, some rights reserved; exclusive licensee American Association for the Advancement of Science

Bao's group have some research work on mechanical damage resistance. One work is using CNTs and tough high-modulus thermoplastic polyurethane to fabricate mechanical durable stretchable transistor (**Figure 2.8 a**). The large tear strength of polyurethane allow transistor to retain functionality under mechanical damages. When puncturing the active channel of the transistor with a 200  $\mu\text{m}$  needle or impact with hammer, the electrical performance exhibited little or temporarily change. Meanwhile, the transistor remained functional at 20% strain when inducing a propagation site for tearing by cutting half through the active channel. The transistor can operate under unstructured environment and resilience of device performance show device has robust mechanical properties against impact, puncture and tear.<sup>[139]</sup> Another work from her group is developing a stretchable polymer semiconductor films via nanoconfinement effect by conjugated-polymer and elastomer phase separation induced elasticity method. They used DPPT-TT as high mobility semiconducting polymer and SEBS as the soft elastomer<sup>[140]</sup>. This polymer semiconductor film was employed in TFT by soft contact lamination on a bottom-gate-

bottom-contact stack, the drain current of TFT keep stable under mechanical deformations (stretching and twisting) and mechanical damage that poked by a sharp object (**Figure 2.8 b**). Besides, Bao et al designed a supramolecular polymer materials (SPMs) with stronger quadruple H-bonding UPy (20%) and weaker urethane crosslink, which has high toughness (fracture energy  $\sim 30000 \text{ J/m}^2$ ) and autonomous self-healing ability.<sup>[141]</sup> They used SMPs to fabricate a high-performance thin film gold electrode with  $\sim 400\%$  stretchability and achieve  $\sim 250\%$  stretchability when inducing a notch in the film. The autonomous self-healing capability allow electrode after cutting into two segments to heal and recover the stretchability up to  $\sim 90\%$  (**Figure 2.8 c**). Suo and co-workers reported a tough hydrogel ( $\sim 9000 \text{ J/m}^2$ ) by combining ionically and covalently cross-linked networks.<sup>[147]</sup> Zhao et al also reported an anti-fatigue hydrogel by controlling crystallinity in it, because to fracture a crystalline domain of polymer request much higher energy per unit area than an amorphous chain of the same polymer.<sup>[142]</sup> The fatigue threshold  $\sim 1000 \text{ J/m}^2$  can be achieved by dry-annealing hydrogel for 90 mins using a single-notch test (**Figure 2.8 d**). All the mentioned works above are based on developing intrinsic tough materials to resist kinds of mechanical damages and adopt them in the stretchable electronics to retain the electrical functions under mechanical damages.

In addition to develop tough materials, another strategy is sacrificing the electronics-free parts which is commonly employed in soft robots and actuators. They used damage-resistant materials and control movement of soft robot/actuator pneumatically so that they can perform work under mechanical damages. Whitesides' group have done some research on this field. His team developed a flexible robot from silicon rubbers that is tough and can withstand extremely high temperature ( $\sim 3000 \text{ Kelvin}$ ) when exposing to flames from a Bunsen burner for 50 s and resistant to acid. Two composite materials are involved in this soft robot. The top layer is silicone with embedded hollow glass sphere to reduce the weight of robot body, while the bottom layer is silicone with embedded polyaramid fabric in order to prevent tears and bursting because of internal pressure from compressive air (**Figure 2.8 e**). Those materials and pneumatic operation enable the soft robot resilience to harsh conditions such as high/low temperature ( $-20^\circ\text{C}$  to  $300^\circ\text{C}$ ) and crushing force of being run over by a car.<sup>[143]</sup> Another work from his group is a soft pneumatic actuator comprising of Ecoflex and Nylon mesh embedded Ecoflex as strain-limiting layer, which can achieve

high toughness of  $\sim 400 \text{ kJ/m}^3$  and withstand the repeatedly struck from hammer as shown in **Figure 2.8 f**.<sup>[144]</sup> Similarly, a four-finger pneumatic soft gripper is made of silicon elastomeric materials that can offer infinite degree of freedom to grasp various objects with size, weight and shapes and be controlled by deflating and inflating(**Figure 2.8 g**). Because no electric part in the gripper, it can be used to catch sharp object such as cactus without worrying about damage the electronic units.<sup>[145]</sup> The last example for soft pneumatic robot is using pressurization of an inverted thin-wall vessel to lengthen the robot body and controlling the direction through asymmetric lengthening of tip. This movement of this tendril-like soft pneumatic robot is inspired by root growth through length increasement instead of locomotion. The electronics-free body and pneumatic controlling make it insensitive to surface condition such as sticky and glue surface or nail surface (**Figure 2.8 h**).<sup>[146]</sup>

### 2.3.2 Self-healing

No matter which types of strategies, either to develop tough materials or to scarify non-electronics parts, they remain the originally functional performance when encounter the mechanical damages. Alternatively, self-healing which is inspired by human skin that has capability to recover after injury is another antinode to mechanical damage.

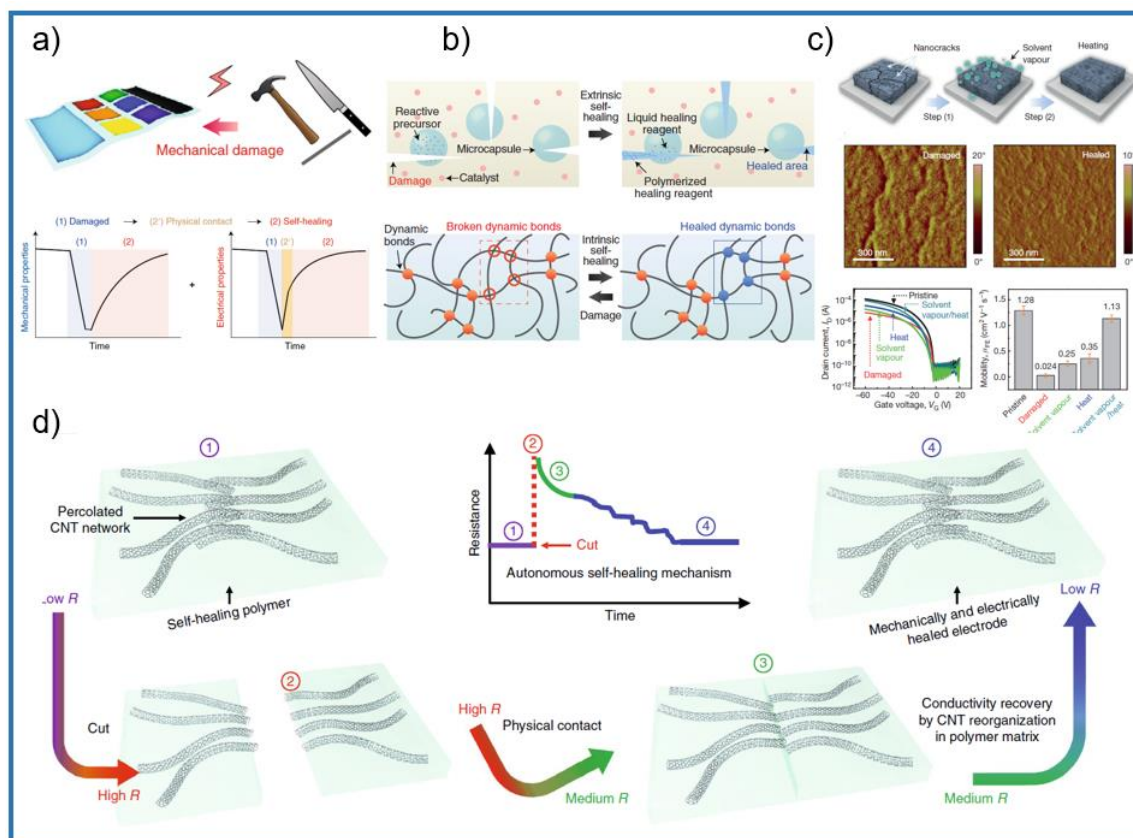


**Figure 2.9** Illustration of self-healing strategies for resisting to mechanical damages. (a) Self-repairable electronics not only need to restore their mechanical properties but also the electrical performance when damaged by scratching, poking, rubbing and tear. Reproduced with permission.<sup>[148]</sup> Copyright 2019, the Author(s), under exclusive license to Springer Nature Limited. (b) Schematic of two types of self-healing systems. Namely, the intrinsic and extrinsic self-healing system and their mechanism. Reproduced with permission.<sup>[148]</sup> Copyright 2019, the Author(s), under exclusive license to Springer Nature Limited. (c) Treatment for healing conjugated polymer film for an intrinsic self-healable organic transistor. AFM image for damaged and healed. The transfer curve for damaged and healed transistor, and the field-effect mobility for undamaged transistor and damaged transistors under different healing conditions. Reproduced with permission.<sup>[149]</sup> Copyright 2016, Macmillan Publishers Limited, part of Springer Nature. (d) The healing process after completely cut for electrodes which are made from CNTs within a self-healing polymeric matrix. CNT network reconstruct with the aid of naturally movement self-healing polymer chain and restore the electrical properties. Reproduced with permission.<sup>[150]</sup> Copyright 2018, Springer Nature.

Self-healing properties in electronics contains two parameters. One is mechanical properties restore and another is the electrical performance recovered from damages (**Figure 2.9 a**). For the restore of mechanical property as shown in **Figure 2.9 b**, the polymers can be healed intrinsically or extrinsically. The healing process of intrinsic self-healing polymers depends on the regeneration of broken dynamic covalent or non-covalent bonds and entanglement of polymer chains by diffusion at the damaged interfaces. The healing rate relies on the mobility of polymer chains, activation energy for exchange of dynamics bonds, and concentration of available broken dynamic site for reaction, which can be hydrogen bonding, metal-ligand interaction,  $\pi$ - $\pi$  stacking, imine bonding, and disulfide bonding.<sup>[129, 151-154]</sup> Extrinsic self-healing polymers need healing agents, normally reactive precursors inside the polymer matrix. These healing agents will release when incurring damage and repair the wounds through polymerization reaction and crosslink reconstruction.<sup>[148]</sup>

For electrical function recovery, since the conductive materials such CNTs and 1D metal nanowires or nanoparticles are unable to recover their original connectivity after electrodes being completely cut, the cut break the conducting network and resistance has a sharp increase to infinite. By bringing two cut pieces in contact physically at the bisected interface, the conducting network can rebuild and the resistance is gradually decrease over the time, indicating that conducting network is reconstructed and electrical performance is recovered with the assist of dynamic movement of polymer(**Figure 2.9 d**).<sup>[150]</sup> Besides electrodes, a stretchable organic transistor with self-healable property is fabricated by an intrinsically healable conjugated polymer. Post-treatments such solvent annealing and thermal annealing facilitate the healing efficient of polymer due to accelerate polymer chain movement. The nanocracks in damaged films disappeared after healed and the field-effect mobility was recovered to  $1.13 \text{ cm}^2\text{V}^{-1}\text{s}^{-1}$  (**Figure 2.9 c**).<sup>[149]</sup>

As compare to stretchable electrodes that consist of conductive materials and substrate, self-healing in devices are more challenging as device has multilayers that make it difficult for each layer to align correctly after mechanical cut. Thus, self-healing materials with high toughness are suitable to for devices, because high toughness materials give a cleaner and less plastic deformation bisected surfaces that facilitate each layer align in multilayer

structured devices. Besides, although self-healing is an effective way to recover the electrical function of device, it requests time to recover or external stimuli promote the self-healing process which is time-consuming and not instantaneously. Therefore, to develop wearable devices with mechanical damage endurance that can keep original electrical performance under damage is necessary.

## 2.4 Heterogeneity

### 2.4.1 Learning heterogeneity design from nature

Heterogeneity is ubiquitously existing in nature from plants to living organisms to adapt to heterogenous states of stress, strain, and temperature in applications. A lot of biological materials are evolved into heterogeneous forms in terms of microstructure, chemical composition, physical properties and geometrical arrangement, which possess unprecedented combination of properties and functionality.<sup>[155]</sup> For example, enhancing the mechanical properties by alleviating stress concentration or improving interfacial bonding through a gradient transition region. One famous paradigm is Bamboo (*Bambusa*) that has a graded structure in longitudinal profile that can survival from extreme load from wind.<sup>[156]</sup> The other well-known paradigms of heterogeneous biological materials are bone, teeth, seashells, nacre and so forth.<sup>[157-161]</sup>

The gradient can be described in terms of their changes in chemical/constituents and Micro/nanostructures including arrangement, distribution, dimensions and orientation of building units(**Figure 2.10 c-g**). The change manner can be either gradually or stepwise mode throughout the material volume. Or an abrupt change in a limit zone, normally happened close to the interface of two dissimilar components (**Figure 2.10 a-b, h**).<sup>[155]</sup> The heterogeneities have been employed to develop of high-performance materials or devices, which not only can endow materials/devices with combination of several properties that cannot be achieved by homogeneity, but also facilitate distribution and transmission of loads, and alleviate stress concentration between two dissimilar materials, improving interfacial bonding and maintaining the structure integrity.

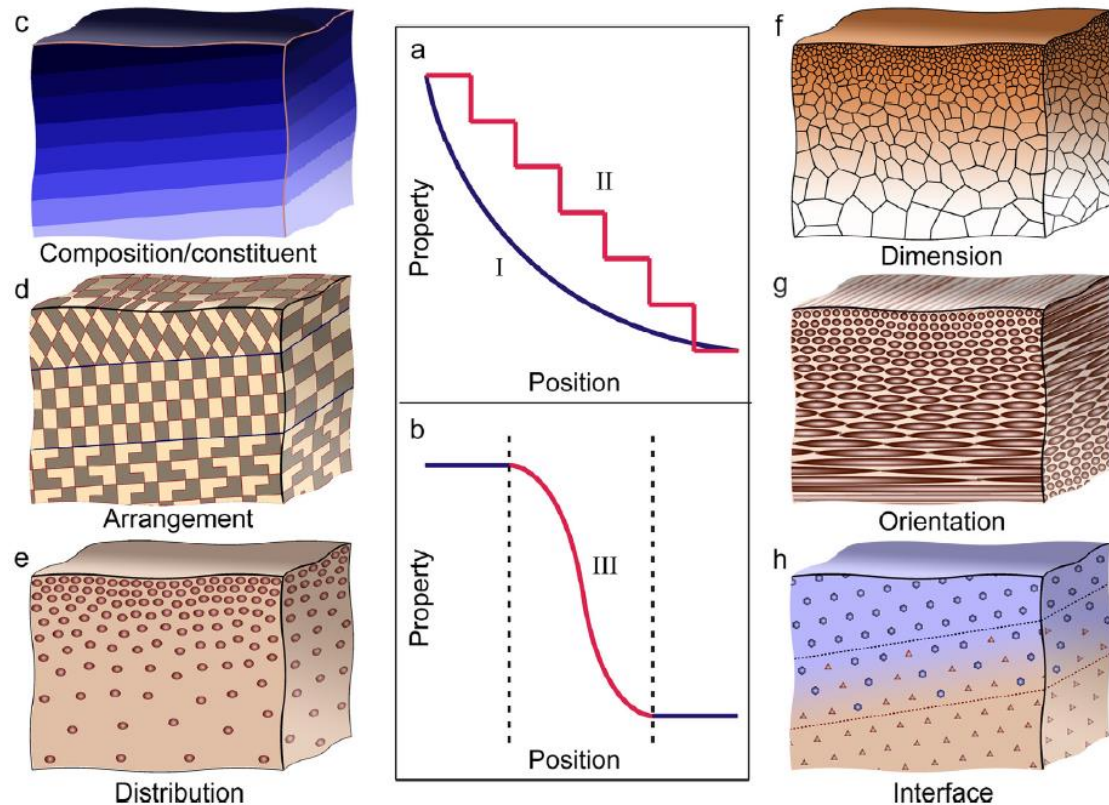


**Figure 2.10** Local property and various forms of gradient in biological materials. (a-b) Biological materials property change either in a gradually manner (I), in a stepwise mode (II) or an abrupt manner across the interface between two dissimilar components (III). (c) Gradient-changed in chemical/constituents, (d-g) Different characteristic of gradient-changed in micro/nano structure, (h) Gradient interface. Reproduced with permission.<sup>[155]</sup> Copyright 2017 Elsevier Ltd.

As shown in **Figure 2.11 (a-b)**, the marine mussel is attached to the rocks and pilings through numerous byssal threads as a mediator between a very hard surface and soft living tissue. The byssal thread has various stiffness (Young's modulus) of proteins along the length. The stiff silk-fibroin-like domains in distal portion and elastin-like domains in proximal portion. The distribution of these different stiffness proteins along the thread play a role in compensating mismatch between rocks and retractor muscles so that the two mismatch materials can be intimate contact. The Young's modulus of thread at the distal end is 500 Mpa, and 50 Mpa at the proximal end. Besides, the byssal thread possess of both high hardness and extraordinary extensibility due to the heterogeneous chemical structure

from higher density of cross-links complexes in granules and the less cross-linked matrix.<sup>[155, 162-163]</sup>

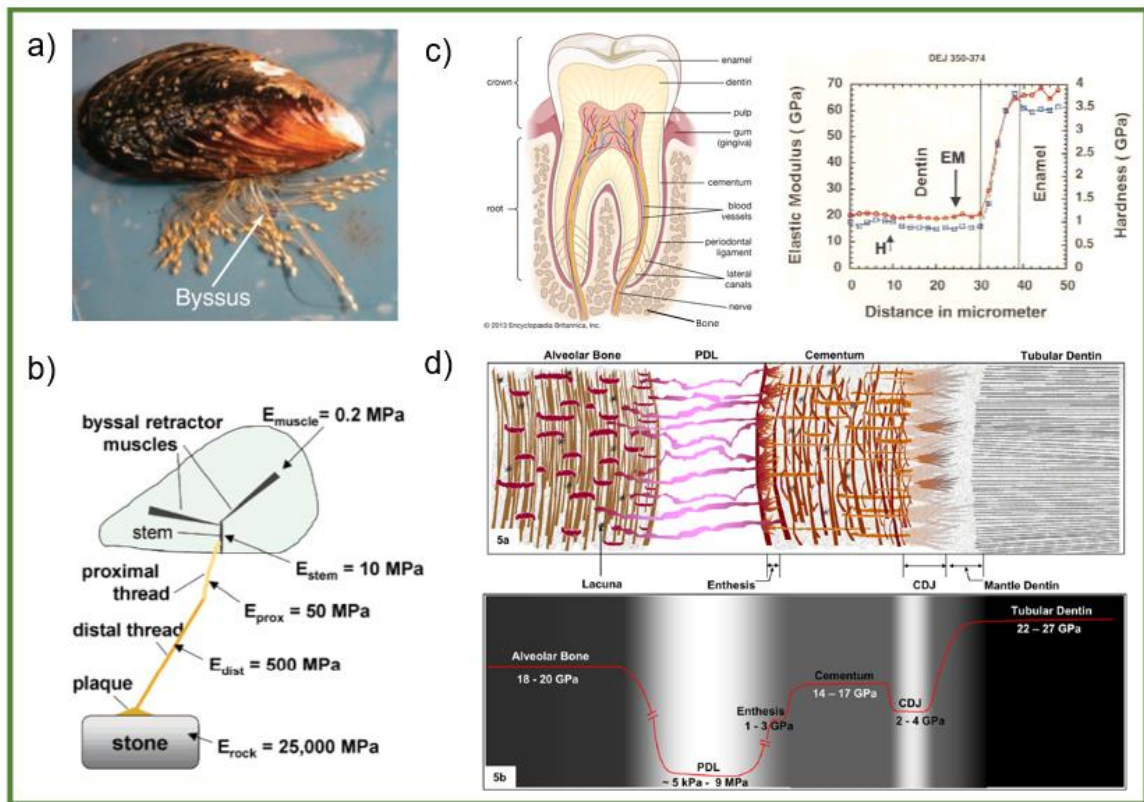


**Figure 2.11** Paradigms of biological materials with heterogeneity design (a) The photo of marine mussel attached to hard rock through numerous byssus threads. Reproduced with permission.<sup>[162]</sup> Copyright 2010, AAAS. (b) Schematic of one mussel byssal thread with different stiffness from byssal retractor muscles to the rock. Reproduced with permission.<sup>[163]</sup> Copyright 2004, American Chemical Society. (c) Schematics illustrate the structure of human teeth on the left and curve shows the Young's modulus and hardness of dentin, enamel, and gradient interface of the dentin-enamel junction (DEJ). Reproduced with permission.<sup>[164-166]</sup> Image: Encyclopædia Britannica, Inc; Copyright 2000, John Wiley & Sons, Inc; Copyright 2010, Elsevier Ltd. (d) Schematic of collagen fibers structure in periodontium and their variation in Young's modulus across alveolar bone, PDL, cementum and root dentin. Reproduced with permission.<sup>[167-168]</sup> Copyright 2007 Elsevier Ltd.

Human teeth crown consists of two calcified tissues which are dentin and enamel. Enamel is brittle and hard with a Young's modulus of  $\sim 70 \text{ GPa}$  and hardness of  $\sim 4 \text{ GPa}$ , which is the hardest tissue of human body on the outer surface and protect underlying dentine and responsible for cutting and grinding food during mastication. Dentin has a Young's

modulus of ~20GPa and hardness of ~1 GPa, which is distributing throughout the crown and root as shown in **Figure 2.11 c** and play a role in absorbing and distributing stresses within the tooth.<sup>[166]</sup> Normally, the mismatched materials with large Young's modulus difference will subject to stress concentration and cause delamination. However, the dissimilar properties of the dentin and the enamel has no such problem because of an interfacial region called dentin-enamel junction (DEJ) between them in crown of the teeth so that the teeth can persists millions cycles of mastication force during the whole working life. The DEJ act as a crack-retard barrier to prevent flaws forming in the brittle enamel. DEJ has mediate Young's modulus which is higher than dentin but lower than enamel so that the force can be transferred gradually throughout these two dissimilar tissues and shielding from catastrophic tooth fracture from the abrupt stress concentration.<sup>[165, 169]</sup> **Figure 2.11 d** is schematic collagen fibers structure of tissue and interface for tooth attachment and they possess different Young's modulus from alveolar bone, PDL, cementum and to too detin. The wide range of Young's modulus from the district region with different structure and heterogeneous properties ensure the tooth attachment and load bearing.

#### 2.4.2 Heterogeneity design in stretchable electronics

After billion years of evolution, nature has created abundant paradigms of heterogeneity designs in biological materials to provide both mechanical protection and biological functions in such a dynamic environment, which inspire scientists to develop new materials by using those strategies to circumvent complex of mechanical issues in applications. Especially in stretchable electronics. Many research works employ heterogeneity motif to reduce mechanical stress concentration and circumvent delamination issue due to mismatch properties in elastic substrates, stretchable electrodes, stretchable devices, and stretchable strain sensors.

Strain engineering of elastomer enable to transfer a 2D structure to 3D architecture with spatially varying amplitudes and periodicities through the heterogeneous integration of different moduli of materials from soft, medium and hard as shown in **Figure 2.12 a**. The heterogenous substrate with tailed material moduli is effectively control strain distribution such as strain isolation and magnification under external stretching. Laminating 2D

structure on a pre-stretched heterogeneous substrate and releasing it can produce compressive bulking with various degree at different locations and hence forming the spatially 3D architecture.<sup>[170]</sup>

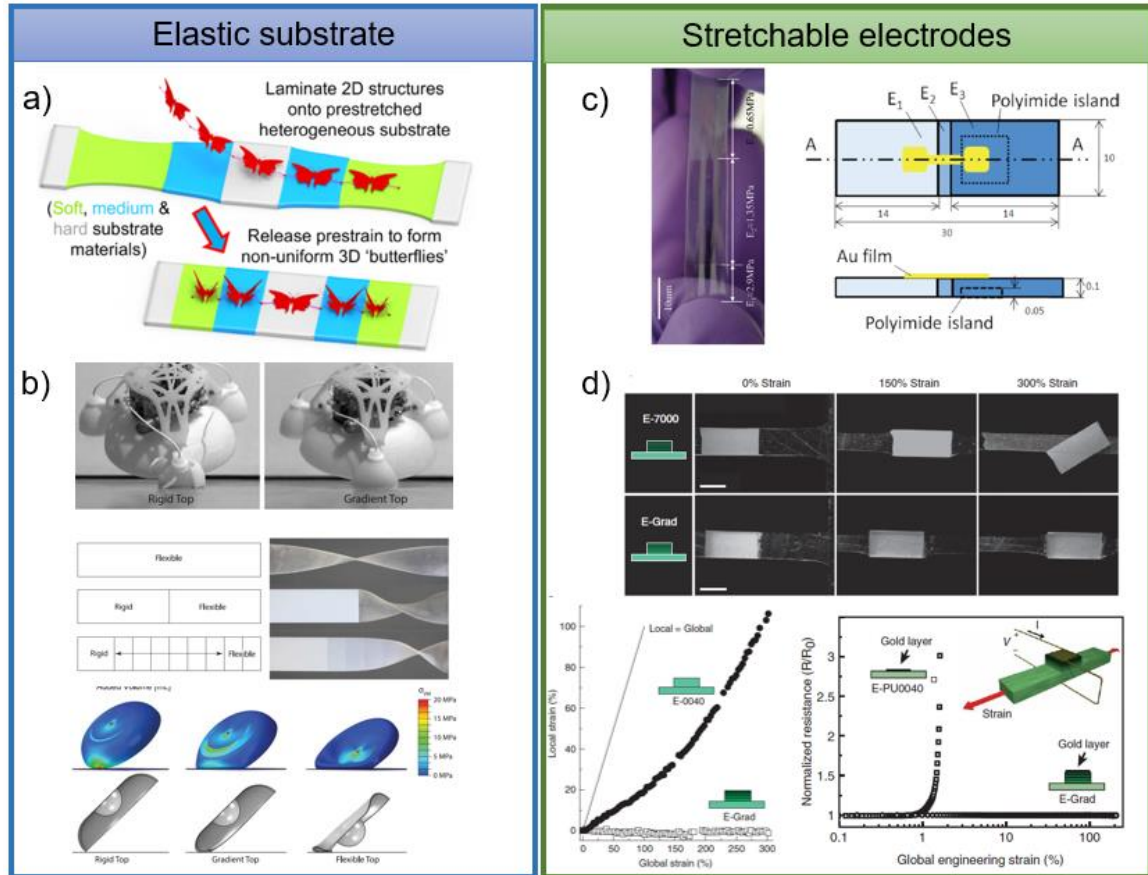


**Figure 2.12** Heterogeneity design in elastomers and stretchable electrodes. (a) Heterogeneous deformable substrate with variation of Young's modulus and realized transform the 2D structure into 3D structure with spatially varying amplitudes and periodicities due to the non-uniform strain field in substrate. Reproduced with permission.<sup>[170]</sup> Copyright 2018, American Chemical Society. (b) A combustion-powered soft robot with rigid body (left) and with a body of transition from rigid to soft exterior (right) perform untethered jumping. Photo of beams under different conditions, and simulation result shows a gradual transition from rigid to flexible in twist condition. Impact simulation of robot landing the ground by 45°. The FEA shows the comparison results of robot body with rigid, gradient modulus (from rigid to soft), and soft materials at 50N, respectively. Reproduced with permission.<sup>[171]</sup> Copyright 2015, AAAS. (c) Photo of a stretchable electrode with Au deposited on the mechanically graded elastomer of photopatterned PDMS at 20% strain. The diagram of Au thin film on PP-PDMS substrate with graded modulus of 0.65 MPa, 1.35 MPa, and 2.9 MPa. Reproduced with permission.<sup>[172]</sup> Copyright 2011, American Institute of Physics. (d)

Photos of graded and non-graded composites on stretchable substrate under stretching and compare their resistance to interfacial failure. The local strain increases much slower in graded patches than in non-graded patches under increasing global strains. Electrical performance of Au thin film on graded patch and non-graded patch under increasing global strains. Reproduced with permission.<sup>[173]</sup> Copyright 2012, Macmillan Publishers Limited.

Another work of heterogenous design in substrate is employing in a combustion-powered robot whose body is fabricated by a gradient transition in material stiffness from rigid core to soft exterior (**Figure 2.12 b**). A gradient moduli interface is the optimum choice to achieve both sufficient reaction force for robot to jump and dissipate the energy of landing impact for a stable landing with the least violent, which cannot be obtained by either homogenous flexible or rigid materials.<sup>[171]</sup>

A stretchable conductor was fabricated by a graded PDMS substrate with 3 different modulus of ~2.9 MPa, ~1.35 MPa, and ~0.65 MPa (**Figure 2.12 c**). Gold thin film was deposited in such substrate with polyimide platform embedded in the stiffest region. The cyclic electrical performance was performed under 20% strain for electrodes with plain PDMS and graded PDMS, showing that electrode made from plain PDMS has less durable and more fatigue than electrode with graded PDMS after 1000 cycles.<sup>[172]</sup> Integration of dissimilar materials has delamination problem due to poor bonding interface caused by stress localization. Local reinforcement weak site with heterogeneous components is an effective approach to obtain desired mechanical performance. A heterogeneous composite with a gradient in moduli spanning over 5 orders of magnitude from ~100 GPa to 1-5 MPa vertically (**Figure 2.12 d**), which was fabricated by tuning the levels of reinforcement element in the polymer matrix. The patch of such a heterogeneous structure with modulus gradually increases from the bottom to the top deposited on a polymer substrate shows a more resistance against local delamination during stretch as compared to non-graded patch. FEA indicate graded architecture help to reduce the mechanical mismatch by modulating strain distribution through the structure, namely less abrupt change in local elastic modulus and minimize the surface strain on the patch, hence preventing the structural failure. The stretchability of graded patch can be extended to 350% without delamination. In contrast, homogenous patch deposited on the elastomer delaminated completely at the strain of ~200%. The surface local strain of graded patch increase <1% at global strain of 300%

while a large increase for non-graded patch (**Figure 2.12 d**). Au was deposited to this 3D heterogeneous structure (graded moduli) and be tested as a stretchable electrode, it can be stretched to 200% without detectable resistance increase and structural failure. In contrast, Au in homogenous (non-graded moduli) structure has a sharp resistance increase at strain of  $\sim 2\%$ , indicating the effective protection of heterogeneous composite in brittle metallic film prior to homogenous composite.<sup>[173]</sup>

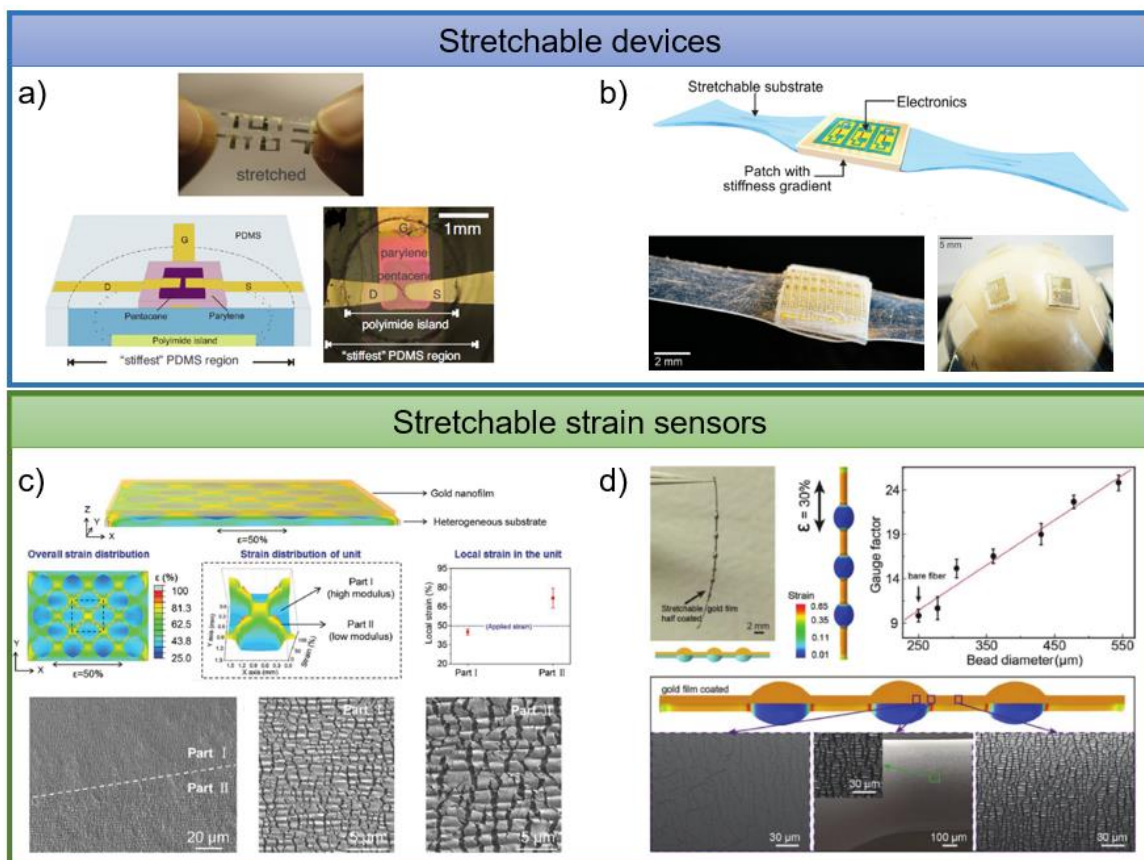


**Figure 2.13** Heterogeneity design in stretchable devices and wearable strain sensors. (a) Schematic and optical top view of Thin-film transistor on heterogeneous substrate with stiff photopatterned PDMS (2.88 MPa) region surrounded by soft photopatterned PDMS (1.35 MPa) and with the stiffest region centered on the PI island. Reproduced with permission.<sup>[174]</sup> Copyright 2011, American Institute of Physics. (b) Schematic and photograph of an amorphous indium-gallium-zinc-oxide (IGZO) based thin-film device on a graded patch with stiffness gradient, which is conformable to wrap around a curved artificial hip joint. Reproduced with permission.<sup>[175]</sup> Copyright 2015, Wiley-VCH. (c) Stretchable strain sensor under strain of 50%, which was fabricated by gold thin film deposited on a heterogeneous elastic substrate. FEA simulation shows

the overall strain distribution, strain distribution of one unit, and local strain in hard and low modulus region. SEM images of crack morphology in gold film at high and low modulus region. Reproduced with permission.<sup>[176]</sup> Copyright 2019, Wiley-VCH. (d) Photo of fiber with microbeads and half-coated gold thin film. The diameter of beads affects the sensitivity (gauge factor) of stretchable strain sensors. FEM simulation of strain distribution along the fiber with microbeads and corresponding crack morphologies at bead region, fiber region and interface between beads and fibers. Reproduced with permission.<sup>[177]</sup> Copyright 2017, Wiley-VCH.

Inorganic devices are brittle and fracture at very low strain ( $\ll 1\%$ ), the stretchable devices that are made from conventional inorganic devices should fulfill two conditions, that is, 1) conventional devices on stretchable devices must keep strain below fracture strain ( $< 1\%$ ), 2) the stiffness difference at the interface between rigid device and soft substrate should be as small as possible. So, the stretchable substrate is engineered with localized and graded mechanical compliance to relief strain concentration. Directly integrating a robust thin-film transistor with elastic modulus of gigapascal on soft elastomer ( $\sim \text{KPa}$ ) will cause structural and electrical failure under stretching. To solve the issue of large strain concentration at the interface of hard and soft materials, thin-film transistor was patterned on mechanically graded PDMS elastomer with stiff region (2.88 MPa) surrounded by a soft region (1.35 MPa) and centered on a stiffness PI island as shown in **Figure 2.13 a**. Thin-film transistor on a elastomer with heterogeneous structure can be stretched up to 13% without delamination and electrical failure. Further study of this work suggested that more compliance gradient moduli involved in the substrate can further reduce strain at the surface and rigid-to-soft interface for better locating rigid active device on it.<sup>[174]</sup> Similarly, an stretchable TFT based on inorganic material (In-Ga-Zn oxide) was fabricated on PDMS patterned with stiff island of mechanically graded multilayers ranging from 40 to 5150 MPa and achieve 20% stretchability (**Figure 2.13 b**). This strategy is using stiff island to minimize the surface strain of region where device is located and using gradual transition provided by graded heterogenous structure to prevent the delamination at the interfaces between rigid device and soft substrate. This structure also offers thin-film transistor a good conformability that can be wrap around a curved artificial hip joint.<sup>[175]</sup>

In addition to stretchable elastomer, conductor and devices, heterogeneity design is also popular to be employed in stretchable sensors, especially for crack-based strain sensors.

Because heterogenous substrate can modulate the strain distribution locally under global strain, and thereby affect the crack morphology and enhance the sensitivity of stretchable strain sensors. Chen' s group has systematical and statistical studied how the crack-based strain sensor sensitivity can be affected by heterogeneous substrate through strain distribution in terms of the low/high modulus ratio and structure (shape of high modulus units and their pitch, the center-to-center distance between two adjacent high modulus unit) as shown in **Figure 2.13 c**. FEA result shows that local strain in low modulus region was enhanced and higher than global strain which give rise to a longer and wider crack in length and compared to those in high modulus part, hence increasing the electrical resistance change under stretching. In contrast, the cracks appeared in homogenous film with uniform strain distribution are uniform distributed under the same strain, showing that strain distribution induced by heterogeneity design affect the resistance-strain property of strain sensors.<sup>[176]</sup> A high sensitivity strain sensor was made from a fiber with microbeads, which can tune the strain distribution along the fiber through the change of section area. The strain concentration is enhanced locally at edge of beads where sectional area increase dramatically that induce longer and wider microcracks in active film material (**Figure 2.13 d**). Consequently, longer and wider crack cause larger resistance change which impvoe the strain sensor sensitivity compared to homogeneity based strain sensors <sup>[177]</sup>.

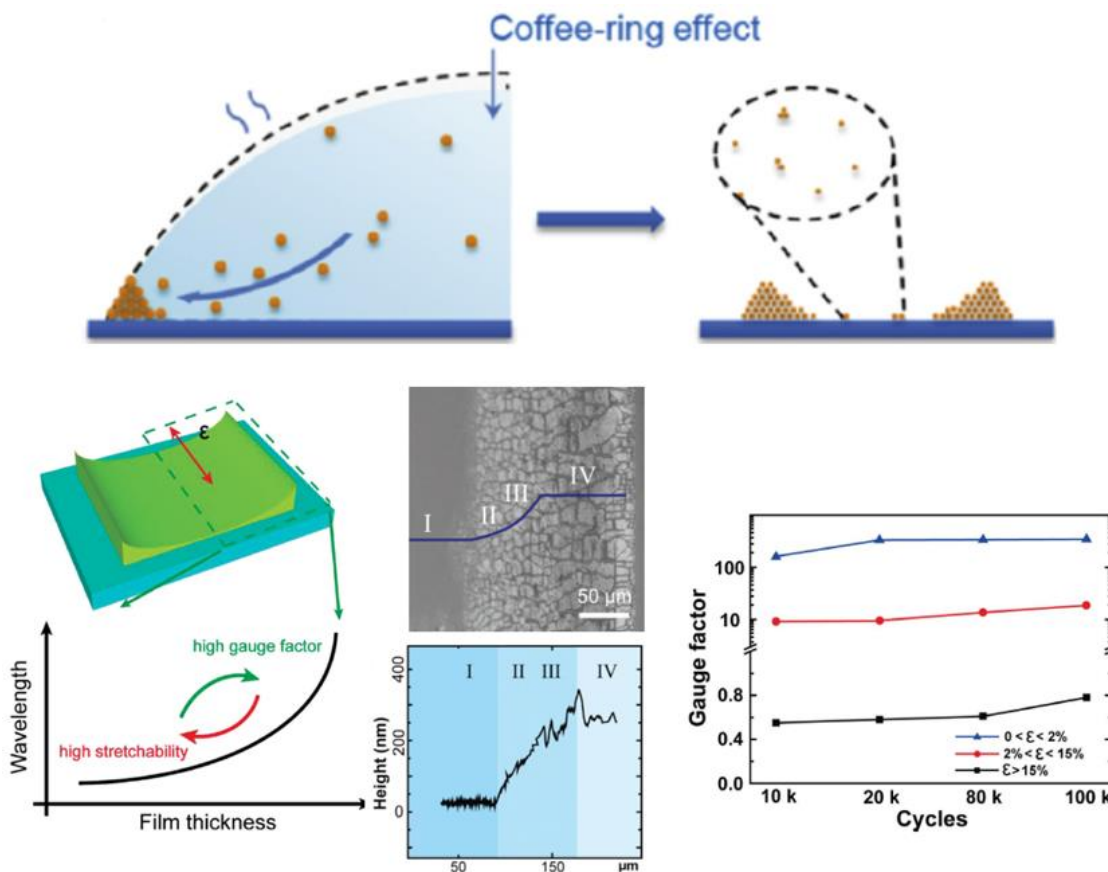


**Figure 2.14** Stretchable strain sensors based on heterogeneity design in active material. Schematic of formation of thickness-gradient structure by coffee ring effect. Reproduced with permission.<sup>[178]</sup> Copyright 2018, Elsevier B.V. Left: Schematic diagram to show the concept of thickness-gradient structure to combine high sensitivity with high stretchability. Middle: Thickness change in thickness-gradient structure. Right: Cycling performance and sensitivity drop at different strain range. Reproduced with permission.<sup>[179]</sup> Copyright 2015, Wiley-VCH.

Different from the foregoing heterogeneity design in elastic substrates, the last example of strain sensor is related to heterogeneity design in active material. A stretchable strain sensor was fabricated by a thickness-gradient structure in active conductive materials. The thickness-gradient was prepared by a self-assemble process, namely, coffee ring effect. During evaporation of solvent with CNTs suspended in it, capillary force drives the CNTs from the middle to the side and form the thickness-gradient ring (**Figure 2.14**). The thickness of CNT ranges from thin ( $\sim 25$  nm) in the inner region to thick ( $\sim 250$  nm) in the outside of rim. This thickness-gradient structure combines the rigid thick part outside with stretchable inner part inside, which can be reflected by the crack morphology in thick and

thin region. The big crack started from thick region, branched into gradient region, and then merge with microcracks in thin region. The wavelength of wrinkle gradually increased from inner to outer. This heterogeneity thin film endows strain sensor with both high sensitivity ( $\sim 161$  at strain of 2%) under and large stretchability (150%).<sup>[179]</sup>

## **2.5 Challenges for stretchable/flexible devices**

### **2.5.1 Stretchable memristors**

With the development of information and communication, the growth of data is explosive that require faster information processing and massive storage capacity. Current mature semiconductor technology faces the limit of the gate oxide and physical challenges such as fabrication cost, high-dense stacking, low power consumption and high-speed operation as the feature size is continuous scale down to around 10 nm. Besides, the classical computing architecture causes von Neumann bottleneck, which is related with data movement between memory and the CPU. Therefore, the further improvement of data storage and processing speed cannot achieve by scaling down strategy, but to seek for new generation technology.<sup>[180]</sup>

As the current charge-based memory such as DRAM (dynamic random access memory) and flash memory have problem in performance degradation as the scaling down, the non-charged-based memory such as resistive random access memory (RRAM),<sup>[181]</sup> phase-change random access memory (PCRAM),<sup>[182-183]</sup> ferroelectric random access memory (FeRAM)<sup>[184]</sup> and magneto-resistive random access memory (MRAM)<sup>[185-186]</sup> have drawn tremendous attention for their potentials in reducing the current bottleneck and improving the energy efficiency and speed of the system.<sup>[187]</sup> Memristors have a capacitor-like structure with an active layer (dielectric or semiconductive materials) sandwiched between two electrodes (conductor/insulator/conductor structure). Amongst them, RRAM---owning to the simple architecture, are a promising candidate for next generation memory as it could offer ultra-fast speed, and possible to fabricate in a vertically 3D-stacking for high-density data storage, and they are in good compatible with the existing CMOS process and able to integrate on the processor chip for commercialization and productions.<sup>[181]</sup>

Based on the resistive switching mechanisms, the RRAM can be classified into 3 types. That is, 1) Anion-type RRAM is dominated by oxygen ions. 2) Cation-type RRAM is also called conductive bridge RAM (CBRAM), is dominated by the redox reaction and migration of metal ions. 3) Carbon-based RRAM is using carbon-based materials as a switching active layer. The electrochemical process of resistive switching in cation-type RRAM is shown in **Figure 2.15**. the active metal such as Ag, Cu, are oxidized to  $\text{Ag}^+$  or  $\text{Cu}^+$  and injected into dielectric layer (active layer). The metal ions are attracted to bottom electrode where negative bias is applied and form filament between top and bottom electrodes during electroforming process. The filament is the conductive path that lead the whole memristor in a low resistance state (LRS) from original high resistance state (HRS). This filament can keep even remove electrical stimuli unless the bias is reversed, the filament is fused as a result of Joule heating and the electric field.<sup>[180]</sup>

The challenge of cation-type RRAM is the reliability such as device-to-device variability due to the fabrication non-uniformity and cycle-to-cycle variability due to the stochastic switching process.<sup>[188]</sup> The another issue is in crossbar array configuration, the memristor suffers from sneak path current during the writing operation or reading process, which cause inaccurate reading, reduce computation speed, and consume more power during storage and computing processes.<sup>[189]</sup>

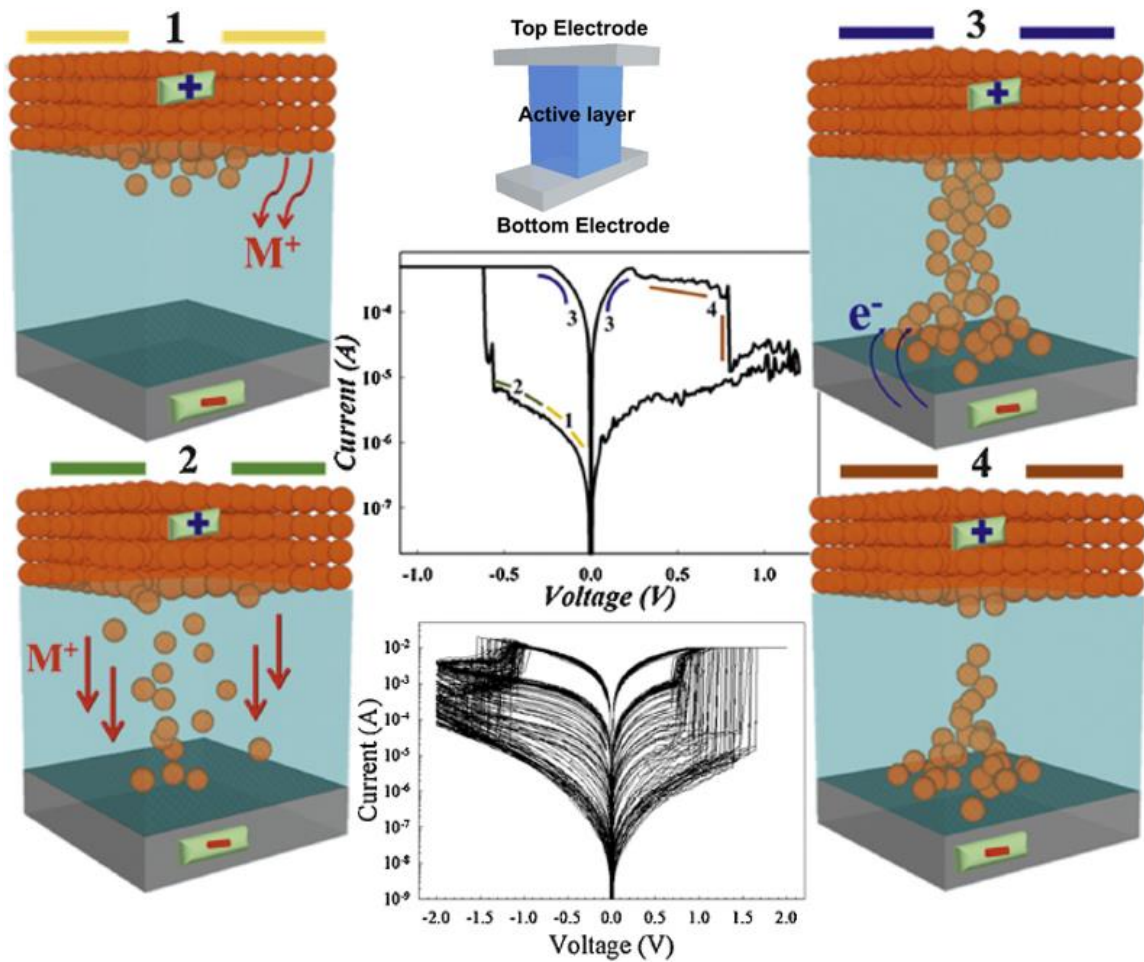


**Figure 2.15** The schematic diagram of RRAM structure and its switching mechanism of cation-type RRAM, and sweeping cycles of I-V characteristics of cation-type RRAM for 100 times. Reproduced with permission.<sup>[181, 190]</sup> Copyright 2015, the Authors, published by Elsevier Ltd. Under the CC BY-NC-ND license (<http://creativecommons.org/licenses/by-nc-nd/4.0/>); Copyright 2014, IEEE.

In addition, more issues are involved into stretchable memristors when fabricating on stretchable substrates. One challenge is selection of materials for fabricating stretchable memristors that are both mechanical adaptable and ensure a good electrical performance. Although memristor based on organic materials have good mechanical properties of flexibility and stretchability, the organic-based electronics are susceptible to environment conditions such as temperature, moisture, UV light, chemical solvents and the fabrication process is incompatible with current CMOS technology that necessitate a new fabrication process and increase cost. For inorganic-based electronics, it has mature fabrication

technology. However, the traditional Si-based information storage device is the complex and rigid metal-oxide-semiconductor structure that is highly susceptible to deformation and easily fracture under forces. The structure rupture is a critical problem that cause inorganic-based electronics electrical failure. Thus, to ensure the structure integrity of inorganic-based memristor accommodate to various deformation while maintaining a good electrical performance is huge challenge. Besides, stretchable electronics in wearable application may also be attacked by accidently mechanical damages such as cut, puncture, scratch, impact, or experienced long-term mechanical damage in usage such as repeated wear and abrasion. Those unexpected mechanical damages may also cause the device failure.

### 2.5.2 Stretchable strain sensors

Several parameters have been used to characterize the performance of stretchable strain sensors, such as stretchability, sensitivity (or gauge factor), linearity, durability, response time, hysteresis and so forth. They are the crucial parameters to be evaluated for real applications

- **Stretchability**

Stretchability of strain sensors depend on the type of strain sensors, substrates, active materials, structure, and fabrication process. The carbon black, nanoparticles and graphene thin film-based strain sensor normally have low stretchability ( $<10\%$ ) due to the lack of robust percolating networks of nanomaterials. However, stretchability can be improved by using 1D nanomaterials as an active material on polymer substrate because 1D nanomaterials have high aspect ratio that can easily form effective percolation networks to sustain a stable electro-mechanical characteristic at high strain levels. Besides, high stretchable strain sensors can be achieved by homogeneously microcrack propagation in thin film, special 3D fibrous structures<sup>[91, 191]</sup> and lateral interconnection between aligned CNTs<sup>[192]</sup> [87, 193-195]. The stretchability can be improved by mirco/nanostructure design, such as special 3D fibrous structure, crumpled graphene-nanocellulose nanopaper, fragmentized graphene foam<sup>[91, 191, 196]</sup>.

- **Sensitivity (or Gauge Factor)**

The sensitivity of strain sensors is defined by gauge factor (GF), which is expressed as relative change ratio of electrical signal (resistance or capacitance) to applied strain. The formula of GF is given by

For resistive-type strain sensors:

$$GF = \frac{\frac{R(\varepsilon) - R_0}{R_0}}{\varepsilon}$$

Where  $\varepsilon$  is applied uniaxial strain,  $R(\varepsilon)$  is electrical resistance at strain  $\varepsilon$ ,  $R_0$  is initial electrical resistance without strain (0%),

For capacitive-type strain sensor:

$$GF = \frac{\frac{C(\varepsilon) - C_0}{C_0}}{\varepsilon}$$

Where  $\varepsilon$  is applied uniaxial strain,  $C(\varepsilon)$  is electrical capacitance at strain  $\varepsilon$ ,  $C_0$  is initial electrical capacitance without strain (0%),

GF not only depends on the mechanism, nanomaterials, and structure, but also depends on applied strain. Generally, crack-based and disconnection-based strain sensors showed higher sensitivity than other mechanisms but established low stretchability ( $\leq 30\%$ )<sup>[102, 197-198]</sup>. The GF is importance factor to indicate the performance of stretchable strain sensors as it shows the relative change of output (electrical signals) with the applied strain. If the output is too small with applied force, the signals are so negligible that are difficult to be detected if strain sensitivity is not high. Thus, high sensitivity is important for stretchable strain sensors so that the any unusual or tidy changes from external stimulus like body movement or heartbeat and pulse can be captured and reflected by the strain sensors for a better signal fidelity (**Figure 2.16**). Although numerous research works have focused on this sensitivity either through the materials development or structure design, there is trade-off between high sensitivity and stretchability and linearity. To develop strain sensor that can achieve both large stretchability ( $>100\%$ ) and sensitivity ( $GF > 50$ ) is still a big challenge.<sup>[96]</sup>

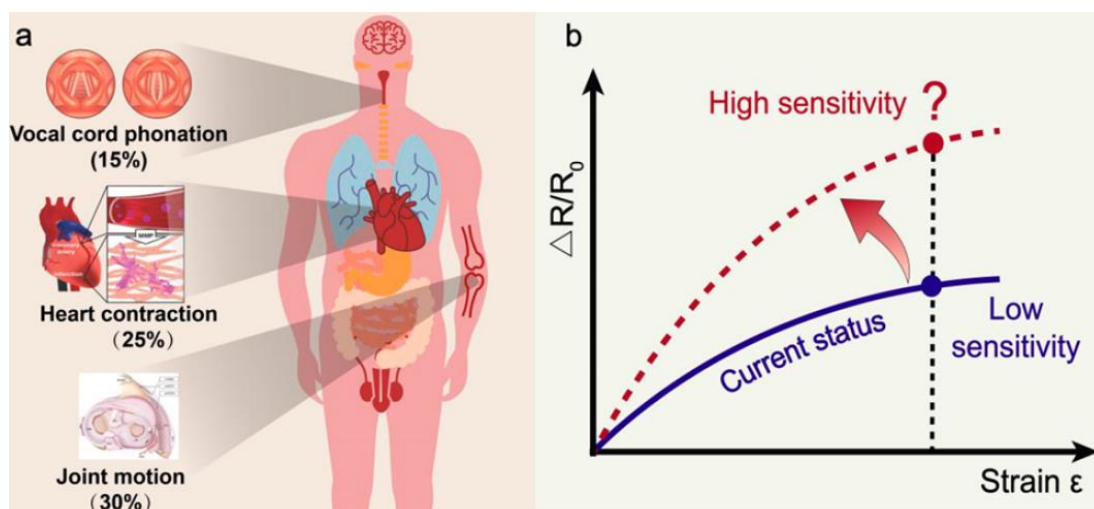


**Figure 2.16** Challenge of stretchable strain sensors. (a) Stretchable strain sensors can collect biological signals caused by strains in human body. (b) To obtain both large stretchability and high sensitivity is a challenge for stretchable strain sensors. Reproduced with permission.<sup>[199]</sup> Copyright 2018, American Chemical Society.

### • Linearity

Stretchable strain sensor with good linearity can make calibration process simple and easy. Normally, the resistive-type strain sensor has poor linearity as compared to the capacitive-type strain sensor. In resistive-type strain sensor, the linearity is poor because the GF cannot keep stable increasing when excessing a certain strain<sup>[197-198, 200-202]</sup>.

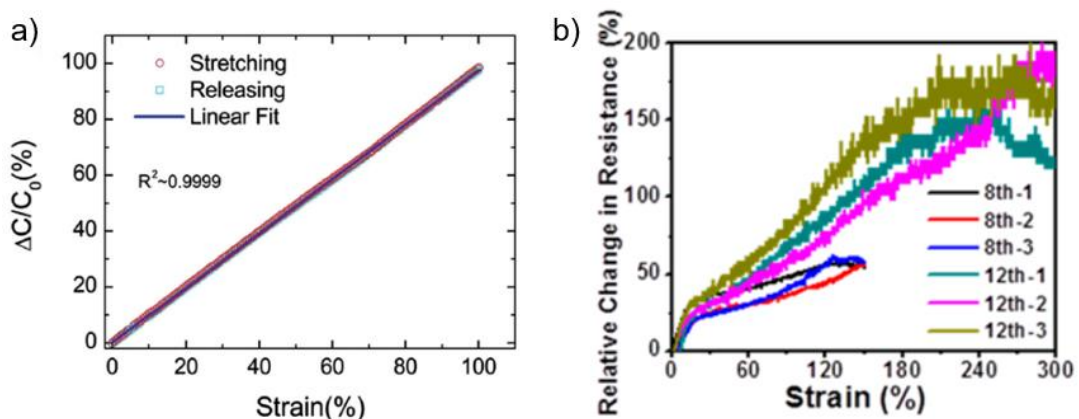


**Figure 2.17** Linearity of capacitive-type strain sensor v.s resistive-type strain sensor. (a) Capacitive-type strain sensor has a constant gauge factor that shows a good linearity. Reproduced with permission.<sup>[203]</sup> Licensed under a Creative Commons Attribution-NonCommercial-ShareAlike

3.0 Unported license (<http://creativecommons.org/licenses/by-nc-sa/3.0>). (b) Gauge factor decrease as stretching in resistive-type strain sensor which shows a poor linearity decrease. Reproduced with permission.<sup>[204]</sup> Copyright 2016 American Chemical Society.

This may due to the limitation from property of elastic substrate or inhomogeneously change in active materials (sensing materials), such as nonhomogeneous crack generation and propagation in NPs thin film or graphene flakes.

- **Durability**

Durability is an important parameter for skin-mounted or wearable strain sensors as they must be endured large and dynamic strains when applying in the human body. Durability represents the degree of tolerance of strain sensors to keep a stable electrical functionality and mechanical integrity under stretching-releasing cycles. The main reasons that causes durability degradation are fatigue and plastic deformation of polymer substrate, or due to the fracture and buckling of active materials (sensing materials).

## **2.6 Ph.D. in context of literature**

Inspired by the biological materials that heterogeneity designs have advantages on facilitating the force transition and improving materials mechanical properties. In this thesis, two heterogeneity designs are involved into stretchable electronics. Conventional silicon-based memristors are rigid and not mechanical conformable that makes it easily fracture under deformations and is susceptible to mechanical damages. One heterogeneity design is combination of discrete rigid active switching materials and soft material and employing it in the active layer of memristor to make device mechanical adaptable and mechanical damage endurable. This memristor is fabricated by commercial inorganic materials with CMOS compatible techniques. The mechanical adaptable properties come from the discrete structure of active layer that not only gives more freedom of movements for the memristor to deform but also alleviate the strain concentration when stretching. Besides, due to the large difference between discrete rigid active materials and soft materials, the soft materials act as a cushion by dissipating the large strain energy through deformation when there is puncture damage, which protect the rigid active materials from

the puncture. Meanwhile, the rigid active materials can ‘flow’ with soft materials under the influence of deformation and show an evasive behavior that allow the discrete active units to move away or self-spin when encounter sharp object. This evasive behavior confers protection on switching layer of memristor to resist to puncture and tear damages, which has been demonstrated by both experiment and finite element analysis.

Another heterogeneity design is a thickness-gradient structure with gradual change in thickness and employ it in active sensing material for stretchable strain sensors. The thickness-gradient based stretchable strain sensors show anisotropic electrical properties under stretching at the large variation of thickness-gradient. A stretchable strain sensor with highly sensitivity and large stretchability is probably achieved by this thickness-gradient structure when applying forces is perpendicular to the variation direction of thickness-gradient.

The contributions of this works are employing heterogeneity designs to bring out the best of electrical performance of stretchable electronics (stretchable memristors and stretchable strain sensors) under various mechanical deformation, which is promising for wearable application. Besides, to equip stretchable electronics with mechanical damages endurance enable it to work in an adverse environment, which is significantly to explore the stretchable electronics for extreme applications.

## References

- [1] S. Choi, H. Lee, R. Ghaffari, T. Hyeon, D. H. Kim, *Adv. Mater.* **2016**, 28, 4203.
- [2] D. H. Kim, J. Viventi, J. J. Amsden, J. Xiao, L. Vigeland, Y. S. Kim, J. A. Blanco, B. Panilaitis, E. S. Frechette, D. Contreras, D. L. Kaplan, F. G. Omenetto, Y. Huang, K. C. Hwang, M. R. Zakin, B. Litt, J. A. Rogers, *Nat Mater* **2010**, 9, 511.
- [3] L. Pan, P. Cai, L. Mei, Y. Cheng, Y. Zeng, M. Wang, T. Wang, Y. Jiang, B. Ji, D. Li, X. Chen, *Adv. Mater.* **2020**, e2003723.
- [4] H. U. Chung, B. H. Kim, J. Y. Lee, J. Lee, Z. Xie, E. M. Ibler, K. Lee, A. Banks, J. Y. Jeong, J. Kim, C. Ogle, D. Grande, Y. Yu, H. Jang, P. Assem, D. Ryu, J. W. Kwak, M. Namkoong, J. B. Park, Y. Lee, D. H. Kim, A. Ryu, J. Jeong, K. You, B. Ji, Z. Liu, Q. Huo, X. Feng, Y. Deng, Y. Xu, K. I. Jang, J. Kim, Y. Zhang, R. Ghaffari, C. M. Rand, M. Schau,

- A. Hamvas, D. E. Weese-Mayer, Y. Huang, S. M. Lee, C. H. Lee, N. R. Shanbhag, A. S. Paller, S. Xu, J. A. Rogers, *Science* **2019**, 363.
- [5] K. Lee, X. Ni, J. Y. Lee, H. Arafa, D. J. Pe, S. Xu, R. Avila, M. Irie, J. H. Lee, R. L. Easterlin, D. H. Kim, H. U. Chung, O. O. Olabisi, S. Getaneh, E. Chung, M. Hill, J. Bell, H. Jang, C. Liu, J. B. Park, J. Kim, S. B. Kim, S. Mehta, M. Pharr, A. Tzavelis, J. T. Reeder, I. Huang, Y. Deng, Z. Xie, C. R. Davies, Y. Huang, J. A. Rogers, *Nat. Biomed. Eng.* **2020**, 4, 148.
- [6] M. Kaltenbrunner, T. Sekitani, J. Reeder, T. Yokota, K. Kuribara, T. Tokuhara, M. Drack, R. Schwodiauer, I. Graz, S. Bauer-Gogonea, S. Bauer, T. Someya, *Nature* **2013**, 499, 458.
- [7] D. H. Kim, N. Lu, R. Ma, Y. S. Kim, R. H. Kim, S. Wang, J. Wu, S. M. Won, H. Tao, A. Islam, K. J. Yu, T. I. Kim, R. Chowdhury, M. Ying, L. Xu, M. Li, H. J. Chung, H. Keum, M. McCormick, P. Liu, Y. W. Zhang, F. G. Omenetto, Y. Huang, T. Coleman, J. A. Rogers, *Science* **2011**, 333, 838.
- [8] H. C. Ko, M. P. Stoykovich, J. Song, V. Malyarchuk, W. M. Choi, C. J. Yu, J. B. Geddes, 3rd, J. Xiao, S. Wang, Y. Huang, J. A. Rogers, *Nature* **2008**, 454, 748.
- [9] J. Kim, M. Lee, H. J. Shim, R. Ghaffari, H. R. Cho, D. Son, Y. H. Jung, M. Soh, C. Choi, S. Jung, K. Chu, D. Jeon, S.-T. Lee, J. H. Kim, S. H. Choi, T. Hyeon, D.-H. Kim, *Nat. Commun.* **2014**, 5, 5747.
- [10] D. H. Kim, R. Ghaffari, N. Lu, S. Wang, S. P. Lee, H. Keum, R. D'Angelo, L. Klinker, Y. Su, C. Lu, Y. S. Kim, A. Ameen, Y. Li, Y. Zhang, B. de Graff, Y. Y. Hsu, Z. Liu, J. Ruskin, L. Xu, C. Lu, F. G. Omenetto, Y. Huang, M. Mansour, M. J. Slepian, J. A. Rogers, *Proc. Natl. Acad. Sci. U S A* **2012**, 109, 19910.
- [11] D. Qi, Z. Liu, Y. Liu, Y. Jiang, W. R. Leow, M. Pal, S. Pan, H. Yang, Y. Wang, X. Zhang, J. Yu, B. Li, Z. Yu, W. Wang, X. Chen, *Adv. Mater.* **2017**, 29, 1702800.
- [12] D. Qi, K. Zhang, G. Tian, B. Jiang, Y. Huang, *Adv. Mater.* **2020**, e2003155.
- [13] S. Budday, R. Nay, R. de Rooij, P. Steinmann, T. Wyrobek, T. C. Ovaert, E. Kuhl, *J. Mech. Behav. Biomed. Mater.* **2015**, 46, 318.
- [14] T. Sekitani, T. Someya, *MRS Bull.* **2012**, 37, 236.
- [15] S. Choi, S. I. Han, D. Kim, T. Hyeon, D.-H. Kim, *Chem. Soc. Rev.* **2019**, 48, 1566.

- [16] H. W. a. C. J. B. Wei-Chen Huang, "Materials and microfabrication processes for next-generation brain-machine devices", can be found under <https://spie.org/news/6638-materials-and-microfabrication-processes-for-next-generation-brain-machine-devices#B5>, **2016**.
- [17] C. Ladd, J.-H. So, J. Muth, M. D. Dickey, *Adv. Mater.* **2013**, 25, 5081.
- [18] M. D. Bartlett, A. Fassler, N. Kazem, E. J. Markvicka, P. Mandal, C. Majidi, *Adv. Mater.* **2016**, 28, 3726.
- [19] S. Zhu, J.-H. So, R. Mays, S. Desai, W. R. Barnes, B. Pourdeyhi, M. D. Dickey, *Adv. Funct. Mater.* **2013**, 23, 2308.
- [20] C. Yang, Z. Suo, *Nat. Rev. Mater.* **2018**, 3, 125.
- [21] C. Keplinger, J.-Y. Sun, C. C. Foo, P. Rothmund, G. M. Whitesides, Z. Suo, *Science* **2013**, 341, 984.
- [22] Y. Wang, C. Zhu, R. Pfattner, H. Yan, L. Jin, S. Chen, F. Molina-Lopez, F. Lissel, J. Liu, N. I. Rabiah, Z. Chen, J. W. Chung, C. Linder, M. F. Toney, B. Murmann, Z. Bao, *Sci. Adv.* **2017**, 3, e1602076.
- [23] N. Matsuhisa, D. Inoue, P. Zalar, H. Jin, Y. Matsuba, A. Itoh, T. Yokota, D. Hashizume, T. Someya, *Nat. Mater.* **2017**, 16, 834.
- [24] Y. Lu, Q. Hu, Y. Lin, D. B. Pacardo, C. Wang, W. Sun, F. S. Ligler, M. D. Dickey, Z. Gu, *Nat. Commun.* **2015**, 6, 10066.
- [25] J. E. Chandler, H. H. Messer, G. Ellender, *J.Dent. Res.* **1994**, 73, 1554.
- [26] I. D. Joshipura, H. R. Ayers, C. Majidi, M. D. Dickey, *J. Mater. Chem. C* **2015**, 3, 3834.
- [27] Y. Lu, Q. Hu, Y. Lin, D. B. Pacardo, C. Wang, W. Sun, F. S. Ligler, M. D. Dickey, Z. Gu, *Nat. Commun.* **2015**, 6, 10066.
- [28] M. D. Dickey, *ACS Appl. Mater. Interfaces* **2014**, 6, 18369.
- [29] Y. Zhou, C. Wan, Y. Yang, H. Yang, S. Wang, Z. Dai, K. Ji, H. Jiang, X. Chen, Y. Long, *Adv. Funct. Mater.* **2019**, 29.
- [30] C. Keplinger, J.-Y. Sun, C. C. Foo, P. Rothmund, G. M. Whitesides, Z. Suo, *Science* **2013**, 341, 984.
- [31] K. Tybrandt, J. Voros, *Small* **2016**, 12, 180.

- [32] N. Matsuhisa, M. Kaltenbrunner, T. Yokota, H. Jinno, K. Kuribara, T. Sekitani, T. Someya, *Nat. Commun.* **2015**, 6, 7461.
- [33] K. Y. Chun, Y. Oh, J. Rho, J. H. Ahn, Y. J. Kim, H. R. Choi, S. Baik, *Nat. Nanotechnol.* **2010**, 5, 853.
- [34] Y. Kim, J. Zhu, B. Yeom, M. Di Prima, X. Su, J.-G. Kim, S. J. Yoo, C. Uher, N. A. Kotov, *Nature* **2013**, 500, 59.
- [35] M. Drack, I. Graz, T. Sekitani, T. Someya, M. Kaltenbrunner, S. Bauer, *Adv. Mater.* **2015**, 27, 34.
- [36] G. Chen, N. Matsuhisa, Z. Liu, D. Qi, P. Cai, Y. Jiang, C. Wan, Y. Cui, W. R. Leow, Z. Liu, S. Gong, K. Q. Zhang, Y. Cheng, X. Chen, *Adv. Mater.* **2018**, 30, e1800129.
- [37] Y. Sun, W. M. Choi, H. Jiang, Y. Y. Huang, J. A. Rogers, *Nat. Nanotechnol.* **2006**, 1, 201.
- [38] M. Vosgueritchian, D. J. Lipomi, Z. Bao, *Adv. Funct. Mater.* **2012**, 22, 421.
- [39] D. Qi, Z. Liu, M. Yu, Y. Liu, Y. Tang, J. Lv, Y. Li, J. Wei, B. Liedberg, Z. Yu, X. Chen, *Adv. Mater.* **2015**, 27, 3145.
- [40] D.-H. Kim, N. Lu, R. Ma, Y.-S. Kim, R.-H. Kim, S. Wang, J. Wu, S. M. Won, H. Tao, A. Islam, K. J. Yu, T.-i. Kim, R. Chowdhury, M. Ying, L. Xu, M. Li, H.-J. Chung, H. Keum, M. McCormick, P. Liu, Y.-W. Zhang, F. G. Omenetto, Y. Huang, T. Coleman, J. A. Rogers, *Science* **2011**, 333, 838.
- [41] Y. Zhang, S. Xu, H. Fu, J. Lee, J. Su, K. C. Hwang, J. A. Rogers, Y. Huang, *Soft Matter* **2013**, 9, 8062.
- [42] T. Chen, Y. Xue, A. K. Roy, L. Dai, *ACS Nano* **2014**, 8, 1039.
- [43] J. Y. Chung, T. Q. Chastek, M. J. Fasolka, H. W. Ro, C. M. Stafford, *ACS Nano* **2009**, 3, 844.
- [44] S. Deng, V. Berry, *Mater. Today* **2016**, 19, 197.
- [45] T. Ibru, K. Kalaitzidou, J. K. Baldwin, A. Antoniou, *Soft Matter* **2017**, 13, 4035.
- [46] S. S. Pandurangi, S. S. Kulkarni, *Int. J. Solids Struct.* **2015**, 62, 124.
- [47] D.-H. Kim, J. A. Rogers, *Adv. Mater.* **2008**, 20, 4887.
- [48] D.-Y. Khang, J. A. Rogers, H. H. Lee, *Adv. Funct. Mater.* **2009**, 19, 1526.
- [49] M. Watanabe, H. Shirai, T. Hirai, *J. Appl. Phys.* **2002**, 92, 4631.
- [50] M. Watanabe, *Soft Matter* **2012**, 8, 1563.

- [51] O. K. Oyewole, D. Yu, J. Du, J. Asare, D. O. Oyewole, V. C. Anye, A. Fashina, M. G. Z. Kana, W. O. Soboyejo, *J. Appl. Phys.* **2015**, *117*, 235501.
- [52] D. H. Kim, J. Xiao, J. Song, Y. Huang, J. A. Rogers, *Adv. Mater.* **2010**, *22*, 2108.
- [53] D. Qi, Z. Liu, W. R. Leow, X. Chen, *MRS Bull.* **2017**, *42*, 103.
- [54] R. C. Webb, A. P. Bonifas, A. Behnaz, Y. Zhang, K. J. Yu, H. Cheng, M. Shi, Z. Bian, Z. Liu, Y. S. Kim, W. H. Yeo, J. S. Park, J. Song, Y. Li, Y. Huang, A. M. Gorbach, J. A. Rogers, *Nat. Mater.* **2013**, *12*, 938.
- [55] S. Xu, Y. Zhang, L. Jia, K. E. Mathewson, K.-I. Jang, J. Kim, H. Fu, X. Huang, P. Chava, R. Wang, S. Bhole, L. Wang, Y. J. Na, Y. Guan, M. Flavin, Z. Han, Y. Huang, J. A. Rogers, *Science* **2014**, *344*, 70.
- [56] S. Emaminejad, W. Gao, E. Wu, Z. A. Davies, H. Yin Yin Nyein, S. Challa, S. P. Ryan, H. M. Fahad, K. Chen, Z. Shahpar, S. Talebi, C. Milla, A. Javey, R. W. Davis, *PNAS* **2017**, *114*, 4625.
- [57] W. Gao, S. Emaminejad, H. Y. Y. Nyein, S. Challa, K. Chen, A. Peck, H. M. Fahad, H. Ota, H. Shiraki, D. Kiriya, D.-H. Lien, G. A. Brooks, R. W. Davis, A. Javey, *Nature* **2016**, *529*, 509.
- [58] Z. Huang, Y. Hao, Y. Li, H. Hu, C. Wang, A. Nomoto, T. Pan, Y. Gu, Y. Chen, T. Zhang, W. Li, Y. Lei, N. Kim, C. Wang, L. Zhang, J. W. Ward, A. Maralani, X. Li, M. F. Durstock, A. Pisano, Y. Lin, S. Xu, *Nat. Electron.* **2018**, *1*, 473.
- [59] S. Imani, A. J. Bandodkar, A. M. V. Mohan, R. Kumar, S. Yu, J. Wang, P. P. Mercier, *Nat. Commun.* **2016**, *7*, 11650.
- [60] Y. Khan, M. Garg, Q. Gui, M. Schadt, A. Gaikwad, D. Han, N. A. D. Yamamoto, P. Hart, R. Welte, W. Wilson, S. Czarnecki, M. Poliks, Z. Jin, K. Ghose, F. Egitto, J. Turner, A. C. Arias, *Adv. Funct. Mater.* **2016**, *26*, 8764.
- [61] D.-H. Kim, J. Song, W. M. Choi, H.-S. Kim, R.-H. Kim, Z. Liu, Y. Y. Huang, K.-C. Hwang, Y.-w. Zhang, J. A. Rogers, *PNAS* **2008**, *105*, 18675.
- [62] A. Miyamoto, S. Lee, N. F. Cooray, S. Lee, M. Mori, N. Matsuhisa, H. Jin, L. Yoda, T. Yokota, A. Itoh, M. Sekino, H. Kawasaki, T. Ebihara, M. Amagai, T. Someya, *Nat. Nanotechnol.* **2017**, *12*, 907.
- [63] M. Amjadi, A. Pichitpajongkit, S. Lee, S. Ryu, I. Park, *ACS Nano* **2014**, *8*, 5154.

- [64] G. Shi, Z. Zhao, J.-H. Pai, I. Lee, L. Zhang, C. Stevenson, K. Ishara, R. Zhang, H. Zhu, J. Ma, *Adv. Funct. Mater.* **2016**, 26, 7614.
- [65] J. Lee, S. Kim, J. Lee, D. Yang, B. C. Park, S. Ryu, I. Park, *Nanoscale* **2014**, 6, 11932.
- [66] H. Jeon, S. K. Hong, M. S. Kim, S. J. Cho, G. Lim, *ACS Appl. Mater. Interfaces* **2017**, 9, 41712.
- [67] J. A. Rogers, *Nat. Nanotechnol.* **2017**, 12, 839.
- [68] M. S. Lee, K. Lee, S. Y. Kim, H. Lee, J. Park, K. H. Choi, H. K. Kim, D. G. Kim, D. Y. Lee, S. Nam, J. U. Park, *Nano Lett.* **2013**, 13, 2814.
- [69] A. R. Madaria, A. Kumar, C. Zhou, *Nanotechnology* **2011**, 22, 245201.
- [70] V. Scardaci, R. Coull, P. E. Lyons, D. Rickard, J. N. Coleman, *Small* **2011**, 7, 2621.
- [71] C. Yang, H. Gu, W. Lin, M. M. Yuen, C. P. Wong, M. Xiong, B. Gao, *Adv. Mater.* **2011**, 23, 3052.
- [72] F. Xu, Y. Zhu, *Adv. Mater.* **2012**, 24, 5117.
- [73] Y. Wang, J. Wang, S. Cao, D. Kong, *J. Mater. Chem. C* **2019**, 7, 9748.
- [74] J. Liang, L. Li, X. Niu, Z. Yu, Q. Pei, *Nat. Photon.* **2013**, 7, 817.
- [75] H. Guo, N. Lin, Y. Chen, Z. Wang, Q. Xie, T. Zheng, N. Gao, S. Li, J. Kang, D. Cai, D.-L. Peng, *Sci. Rep.* **2013**, 3, 2323.
- [76] E. C. Garnett, W. Cai, J. J. Cha, F. Mahmood, S. T. Connor, M. Greyson Christoforo, Y. Cui, M. D. McGehee, M. L. Brongersma, *Nat. Mater.* **2012**, 11, 241.
- [77] J. Lee, P. Lee, H. Lee, D. Lee, S. S. Lee, S. H. Ko, *Nanoscale* **2012**, 4, 6408.
- [78] A. R. Madaria, A. Kumar, F. N. Ishikawa, C. Zhou, *Nano Res.* **2010**, 3, 564.
- [79] T. Tokuno, M. Nogi, M. Karakawa, J. Jiu, T. T. Nge, Y. Aso, K. Suganuma, *Nano Res.* **2011**, 4, 1215.
- [80] L. Yang, T. Zhang, H. Zhou, S. C. Price, B. J. Wiley, W. You, *ACS Appl. Mater. Interfaces* **2011**, 3, 4075.
- [81] S. Dai, Q. Li, G. Liu, H. Yang, Y. Yang, D. Zhao, W. Wang, M. Qiu, *Appl. Phys. Lett.* **2016**, 108, 121103.
- [82] I. K. Moon, J. I. Kim, H. Lee, K. Hur, W. C. Kim, H. Lee, *Sci. Rep.* **2013**, 3, 1112.
- [83] R. Rahimi, M. Ochoa, W. Yu, B. Ziaie, *ACS Appl. Mater. Interfaces* **2015**, 7, 4463.

- [84] T. Yamada, Y. Hayamizu, Y. Yamamoto, Y. Yomogida, A. Izadi-Najafabadi, D. N. Futaba, K. Hata, *Nat. Nanotechnol.* **2011**, 6, 296.
- [85] J. Park, Y. Lee, J. Hong, M. Ha, Y.-D. Jung, H. Lim, S. Y. Kim, H. Ko, *ACS Nano* **2014**, 8, 4689.
- [86] M. Hempel, D. Nezich, J. Kong, M. Hofmann, *Nano Lett.* **2012**, 12, 5714.
- [87] X. Li, R. Zhang, W. Yu, K. Wang, J. Wei, D. Wu, A. Cao, Z. Li, Y. Cheng, Q. Zheng, R. S. Ruoff, H. Zhu, *Sci. Rep.* **2012**, 2, 870.
- [88] A. P. A. Raju, A. Lewis, B. Derby, R. J. Young, I. A. Kinloch, R. Zan, K. S. Novoselov, *Adv. Funct. Mater.* **2014**, 24, 2865.
- [89] Z. Yang, Y. Pang, X.-l. Han, Y. Yang, J. Ling, M. Jian, Y. Zhang, Y. Yang, T.-L. Ren, *ACS Nano* **2018**, 12, 9134.
- [90] G. Shi, S. Araby, C. T. Gibson, Q. Meng, S. Zhu, J. Ma, *Adv. Funct. Mater.* **2018**, 28.
- [91] C. S. Boland, U. Khan, C. Backes, A. O'Neill, J. McCauley, S. Duane, R. Shanker, Y. Liu, I. Jurewicz, A. B. Dalton, J. N. Coleman, *ACS Nano* **2014**, 8, 8819.
- [92] B.-U. Hwang, J.-H. Lee, T. Q. Trung, E. Roh, D.-I. Kim, S.-W. Kim, N.-E. Lee, *ACS Nano* **2015**, 9, 8801.
- [93] X. Xiao, L. Yuan, J. Zhong, T. Ding, Y. Liu, Z. Cai, Y. Rong, H. Han, J. Zhou, Z. L. Wang, *Adv. Mater.* **2011**, 23, 5440.
- [94] J. J. Park, W. J. Hyun, S. C. Mun, Y. T. Park, O. O. Park, *ACS Appl. Mater. Interfaces* **2015**, 7, 6317.
- [95] J. Zhao, G.-Y. Zhang, D.-X. Shi, *Chin. Phys. B* **2013**, 22, 057701.
- [96] M. Amjadi, K.-U. Kyung, I. Park, M. Sitti, *Adv. Funct. Mater.* **2016**, 26, 1678.
- [97] J. Ren, W. Zhang, Y. Wang, Y. Wang, J. Zhou, L. Dai, M. Xu, *InfoMat.* **2019**, 1, 396.
- [98] G. Shi, A. Michelfiore, J. Jin, L. H. Li, Y. Chen, L. Wang, H. Yu, G. Wallace, S. Gambhir, S. Zhu, P. Hojati-Talemi, J. Ma, *J. Mater. Chem. A* **2014**, 2, 20382.
- [99] Y. Liu, Z. Liu, B. Zhu, J. Yu, K. He, W. R. Leow, M. Wang, B. K. Chandran, D. Qi, H. Wang, G. Chen, C. Xu, X. Chen, *Adv. Mater.* **2017**, 29.
- [100] N. Matsuhisa, Y. Jiang, Z. Liu, G. Chen, C. Wan, Y. Kim, J. Kang, H. Tran, H.-C. Wu, I. You, Z. Bao, X. Chen, *Adv. Electron. Mater.* **2019**, 5, 1900347.

- [101] T. Lee, Y. W. Choi, G. Lee, S. M. Kim, D. Kang, M. Choi, *RSC Adv.* **2017**, 7, 34810.
- [102] D. Kang, P. V. Pikhitsa, Y. W. Choi, C. Lee, S. S. Shin, L. Piao, B. Park, K. Y. Suh, T. I. Kim, M. Choi, *Nature* **2014**, 516, 222.
- [103] Y. Jiang, Z. Liu, N. Matsuhisa, D. Qi, W. R. Leow, H. Yang, J. Yu, G. Chen, Y. Liu, C. Wan, Z. Liu, X. Chen, *Adv. Mater.* **2018**, 30, e1706589.
- [104] T. Sakorikar, M. K. Kavitha, P. Vayalamkuzhi, M. Jaiswal, *Sci Rep* **2017**, 7, 2598.
- [105] S. P. Lacour, D. Chan, S. Wagner, T. Li, Z. Suo, *Appl. Phys. Lett.* **2006**, 88.
- [106] Q. Zhong, J. Zhong, B. Hu, Q. Hu, J. Zhou, Z. L. Wang, *Energy Environ. Sci.* **2013**, 6, 1779.
- [107] D. Tobjörk, R. Österbacka, *Adv. Mater.* **2011**, 23, 1935.
- [108] L. Nyholm, G. Nyström, A. Mihranyan, M. Strømme, *Adv. Mater.* **2011**, 23, 3751.
- [109] J. P. Rojas, D. Conchouso, A. Arevalo, D. Singh, I. G. Foulds, M. M. Hussain, *Nano. Energy* **2017**, 31, 296.
- [110] L. Mao, Q. Meng, A. Ahmad, Z. Wei, *Adv. Energy Mater.* **2017**, 7.
- [111] Z. Suo, E. Y. Ma, H. Gleskova, S. Wagner, *Appl. Phys. Lett.* **1999**, 74, 1177.
- [112] S. Gupta, W. T. Navaraj, L. Lorenzelli, R. Dahiya, *npj Flex. Electron.* **2018**, 2.
- [113] H. Li, Y. Cao, Z. Wang, X. Feng, *Opt. Mater. Express* **2019**, 9.
- [114] J. A. Rogers, *MRS Bull.* **2014**, 39, 549.
- [115] X. Li, *J. Phys. D: Appl. Phys.* **2008**, 41, 193001.
- [116] O. G. Schmidt, K. Eberl, *Nature* **2001**, 410, 168.
- [117] S.-I. Park, J.-H. Ahn, X. Feng, S. Wang, Y. Huang, J. A. Rogers, *Adv. Funct. Mater.* **2008**, 18, 2673.
- [118] J. A. Rogers, M. G. Lagally, R. G. Nuzzo, *Nature* **2011**, 477, 45.
- [119] Z. Chen, W. Ren, L. Gao, B. Liu, S. Pei, H.-M. Cheng, *Nat. Mater.* **2011**, 10, 424.
- [120] T. Park, C. Park, B. Kim, H. Shin, E. Kim, *Energy Environ. Sci.* **2013**, 6, 788.
- [121] K. Suemori, S. Hoshino, T. Kamata, *Appl. Phys. Lett.* **2013**, 103, 153902.
- [122] I. Wicaksono, C. I. Tucker, T. Sun, C. A. Guerrero, C. Liu, W. M. Woo, E. J. Pence, C. Dagdeviren, *npj Flex. Electron.* **2020**, 4.
- [123] C. Ye, J. Ren, Y. Wang, W. Zhang, C. Qian, J. Han, C. Zhang, K. Jin, M. J. Buehler, D. L. Kaplan, S. Ling, *Matter* **2019**, 1, 1411.
- [124] C. Lee, X. Wei, J. W. Kysar, J. Hone, *Science* **2008**, 321, 385.

- [125] M. Orlita, C. Faugeras, P. Plochocka, P. Neugebauer, G. Martinez, D. K. Maude, A. L. Barra, M. Sprinkle, C. Berger, W. A. de Heer, M. Potemski, *Phys. Rev. Lett.* **2008**, *101*, 267601.
- [126] H. Wu, Y. Huang, F. Xu, Y. Duan, Z. Yin, *Adv. Mater.* **2016**, *28*, 9881.
- [127] X. Tao, T.-H. Huang, C.-L. Shen, Y.-C. Ko, G.-T. Jou, V. Koncar, *Adv. Mater. Technol.* **2018**, *3*, 1700309.
- [128] K. M. K. Hamill Joseph, Timothy R. Derrick, *Biomechanical-Basis-of-Human-Movement, 4th edition*, Lippincott Williams & Wilkins: Philadelphia, 2015.
- [129] L. M. Zhang, Y. He, S. Cheng, H. Sheng, K. Dai, W. J. Zheng, M. X. Wang, Z. S. Chen, Y. M. Chen, Z. Suo, *Small* **2019**, *15*, 1804651.
- [130] C. Pang, G.-Y. Lee, T.-i. Kim, S. M. Kim, H. N. Kim, S.-H. Ahn, K.-Y. Suh, *Nat. Mater.* **2012**, *11*, 795.
- [131] S. J. P. Callens, A. A. Zadpoor, *Mater. Today* **2018**, *21*, 241.
- [132] P. Won, J. J. Park, T. Lee, I. Ha, S. Han, M. Choi, J. Lee, S. Hong, K.-J. Cho, S. H. Ko, *Nano Lett.* **2019**, *19*, 6087.
- [133] L. Mahadevan, S. Rica, *Science* **2005**, *307*, 1740.
- [134] M. Schenk, S. D. Guest, *PNAS* **2013**, *110*, 3276.
- [135] K. Bertoldi, V. Vitelli, J. Christensen, M. van Hecke, *Nat. Rev. Mater.* **2017**, *2*, 17066.
- [136] Y. Tang, G. Lin, S. Yang, Y. K. Yi, R. D. Kamien, J. Yin, *Adv. Mater.* **2017**, *29*, 1604262.
- [137] Y. Zhang, Z. Yan, K. Nan, D. Xiao, Y. Liu, H. Luan, H. Fu, X. Wang, Q. Yang, J. Wang, W. Ren, H. Si, F. Liu, L. Yang, H. Li, J. Wang, X. Guo, H. Luo, L. Wang, Y. Huang, J. A. Rogers, *PNAS* **2015**, *112*, 11757.
- [138] C. Wang, C. Wang, Z. Huang, S. Xu, *Adv. Mater.* **2018**, *30*, 1801368.
- [139] A. Chortos, G. I. Koleilat, R. Pfattner, D. Kong, P. Lin, R. Nur, T. Lei, H. Wang, N. Liu, Y.-C. Lai, M.-G. Kim, J. W. Chung, S. Lee, Z. Bao, *Adv. Mater.* **2016**, *28*, 4441.
- [140] J. Xu, S. Wang, G.-J. N. Wang, C. Zhu, S. Luo, L. Jin, X. Gu, S. Chen, V. R. Feig, J. W. F. To, S. Rondeau-Gagné, J. Park, B. C. Schroeder, C. Lu, J. Y. Oh, Y. Wang, Y.-H. Kim, H. Yan, R. Sinclair, D. Zhou, G. Xue, B. Murmann, C. Linder, W. Cai, J. B. H. Tok, J. W. Chung, Z. Bao, *Science* **2017**, *355*, 59.

- [141] X. Yan, Z. Liu, Q. Zhang, J. Lopez, H. Wang, H. C. Wu, S. Niu, H. Yan, S. Wang, T. Lei, J. Li, D. Qi, P. Huang, J. Huang, Y. Zhang, Y. Wang, G. Li, J. B. Tok, X. Chen, Z. Bao, *J. Am. Chem. Soc.* **2018**, *140*, 5280.
- [142] S. Lin, X. Liu, J. Liu, H. Yuk, H.-C. Loh, G. A. Parada, C. Settens, J. Song, A. Masic, G. H. McKinley, X. Zhao, *Sci. Adv.* **2019**, *5*, eaau8528.
- [143] R. F. S. Michael T. Tolley, Bobak Mosadegh, Kevin C. Galloway, Michael Wehner, Michael Karpelson, Robert J. Wood, and George M. Whitesides, *Soft Robotics* **2014**, *1*, 213.
- [144] R. V. Martinez, A. C. Glavan, C. Keplinger, A. I. Oyetibo, G. M. Whitesides, *Adv. Funct. Mater.* **2014**, *24*, 3003.
- [145] Y. Hao, Z. Gong, Z. Xie, S. Guan, X. Yang, Z. Ren, T. Wang, L. Wen, "Universal soft pneumatic robotic gripper with variable effective length", presented at *2016 35th CCC*, 27-29 July **2016**, 2016.
- [146] E. W. Hawkes, L. H. Blumenschein, J. D. Greer, A. M. Okamura, *Sci. Robot.* **2017**, *2*, eaan3028.
- [147] J.-Y. Sun, X. Zhao, W. R. K. Illeperuma, O. Chaudhuri, K. H. Oh, D. J. Mooney, J. J. Vlassak, Z. Suo, *Nature* **2012**, *489*, 133.
- [148] J. Kang, J. B. H. Tok, Z. Bao, *Nat. Electron.* **2019**, *2*, 144.
- [149] J. Y. Oh, S. Rondeau-Gagné, Y.-C. Chiu, A. Chortos, F. Lissel, G.-J. N. Wang, B. C. Schroeder, T. Kurosawa, J. Lopez, T. Katsumata, J. Xu, C. Zhu, X. Gu, W.-G. Bae, Y. Kim, L. Jin, J. W. Chung, J. B. H. Tok, Z. Bao, *Nature* **2016**, *539*, 411.
- [150] D. Son, J. Kang, O. Vardoulis, Y. Kim, N. Matsuhisa, J. Y. Oh, J. W. F. To, J. Mun, T. Katsumata, Y. Liu, A. F. McGuire, M. Krason, F. Molina-Lopez, J. Ham, U. Kraft, Y. Lee, Y. Yun, J. B. H. Tok, Z. Bao, *Nat. Nanotechnol.* **2018**, *13*, 1057.
- [151] M. Burnworth, L. Tang, J. R. Kumpfer, A. J. Duncan, F. L. Beyer, G. L. Fiore, S. J. Rowan, C. Weder, *Nature* **2011**, *472*, 334.
- [152] P. Cordier, F. Tournilhac, C. Soulié-Ziakovic, L. Leibler, *Nature* **2008**, *451*, 977.
- [153] M. W. Urban, D. Davydovich, Y. Yang, T. Demir, Y. Zhang, L. Casabianca, *Science* **2018**, *362*, 220.
- [154] S. Xia, S. Song, F. Jia, G. Gao, *J. Mater. Chem. B* **2019**, *7*, 4638.
- [155] Z. Liu, M. A. Meyers, Z. Zhang, R. O. Ritchie, *Prog. Mater. Sci.* **2017**, *88*, 467.

- [156] A. K. Ray, S. K. Das, S. Mondal, P. Ramachandrarao, *J. Mat. Sci.* **2004**, 39, 1055.
- [157] P. Fratzl, R. Weinkamer, *Prog. Mater. Sci.* **2007**, 52, 1263.
- [158] B. Ji, H. Gao, *Annu. Rev. Mater. Res.* **2010**, 40, 77.
- [159] M. A. Meyers, J. McKittrick, P.-Y. Chen, *Science* **2013**, 339, 773.
- [160] J. Wang, Q. Cheng, Z. Tang, *Chem. Soc. Rev.* **2012**, 41, 1111.
- [161] A. Miserez, T. Schneberk, C. Sun, F. W. Zok, J. H. Waite, *Science* **2008**, 319, 1816.
- [162] M. J. Harrington, A. Masic, N. Holten-Andersen, J. H. Waite, P. Fratzl, *Science* **2010**, 328, 216.
- [163] J. H. Waite, H. C. Lichtenegger, G. D. Stucky, P. Hansma, *Biochemistry* **2004**, 43, 7653.
- [164] "Tooth anatomy", can be found under <https://www.britannica.com/science/tooth-anatomy>.
- [165] G. W. Marshall, Jr., M. Balooch, R. R. Gallagher, S. A. Gansky, S. J. Marshall, *J. Biomed. Mater. Res.* **2001**, 54, 87.
- [166] Y. L. Chan, A. H. W. Ngan, N. M. King, *J. Mech. Behav. Biomed. Mater.* **2011**, 4, 785.
- [167] P. M. Cattaneo, M. Dalstra, B. Melsen, *J. Dent. Res.* **2005**, 84, 428.
- [168] S. P. Ho, S. J. Marshall, M. I. Ryder, G. W. Marshall, *Biomaterials* **2007**, 28, 5238.
- [169] V. Imbeni, J. J. Kruzic, G. W. Marshall, S. J. Marshall, R. O. Ritchie, *Nat. Mater.* **2005**, 4, 229.
- [170] H. Luan, X. Cheng, A. Wang, S. Zhao, K. Bai, H. Wang, W. Pang, Z. Xie, K. Li, F. Zhang, Y. Xue, Y. Huang, Y. Zhang, *ACS Appl. Mater. Inter.* **2019**, 11, 3482.
- [171] N. W. Bartlett, M. T. Tolley, J. T. B. Overvelde, J. C. Weaver, B. Mosadegh, K. Bertoldi, G. M. Whitesides, R. J. Wood, *Science* **2015**, 349, 161.
- [172] D. P. J. Cotton, A. Popel, I. M. Graz, S. P. Lacour, *J. Appl. Phys.* **2011**, 109, 054905.
- [173] R. Libanori, R. M. Erb, A. Reiser, H. Le Ferrand, M. J. Süess, R. Spolenak, A. R. Studart, *Nat. Commun.* **2012**, 3, 1265.
- [174] I. M. Graz, D. P. J. Cotton, A. Robinson, S. P. Lacour, *Appl. Phys. Lett.* **2011**, 98, 124101.

- [175] N. Münzenrieder, G. Cantarella, C. Vogt, L. Petti, L. Bütthe, G. A. Salvatore, Y. Fang, R. Andri, Y. Lam, R. Libanori, D. Widner, A. R. Studart, G. Tröster, *Adv. Electron. Mater.* **2015**, *1*, 1400038.
- [176] S. Pan, Z. Liu, M. Wang, Y. Jiang, Y. Luo, C. Wan, D. Qi, C. Wang, X. Ge, X. Chen, *Adv. Mater.* **2019**, *31*, e1903130.
- [177] Z. Liu, D. Qi, G. Hu, H. Wang, Y. Jiang, G. Chen, Y. Luo, X. J. Loh, B. Liedberg, X. Chen, *Adv. Mater.* **2018**, *30*.
- [178] D. Mampallil, H. B. Eral, *Adv. Colloid Interface Sci.* **2018**, *252*, 38.
- [179] Z. Liu, D. Qi, P. Guo, Y. Liu, B. Zhu, H. Yang, Y. Liu, B. Li, C. Zhang, J. Yu, B. Liedberg, X. Chen, *Adv. Mater.* **2015**, *27*, 6230.
- [180] D.-H. Kwon, K. M. Kim, J. H. Jang, J. M. Jeon, M. H. Lee, G. H. Kim, X.-S. Li, G.-S. Park, B. Lee, S. Han, M. Kim, C. S. Hwang, *Nat. Nanotechnol.* **2010**, *5*, 148.
- [181] T.-C. Chang, K.-C. Chang, T.-M. Tsai, T.-J. Chu, S. M. Sze, *Mater. Today* **2016**, *19*, 254.
- [182] D. Loke, T. H. Lee, W. J. Wang, L. P. Shi, R. Zhao, Y. C. Yeo, T. C. Chong, S. R. Elliott, *Science* **2012**, *336*, 1566.
- [183] F. Rao, K. Ding, Y. Zhou, Y. Zheng, M. Xia, S. Lv, Z. Song, S. Feng, I. Ronneberger, R. Mazzarello, W. Zhang, E. Ma, *Science* **2017**, *358*, 1423.
- [184] C. Ma, Z. Luo, W. Huang, L. Zhao, Q. Chen, Y. Lin, X. Liu, Z. Chen, C. Liu, H. Sun, X. Jin, Y. Yin, X. Li, *Nat Commun* **2020**, *11*, 1439.
- [185] D. Apalkov, B. Dieny, J. M. Slaughter, *Proceedings of the IEEE* **2016**, *104*, 1796.
- [186] J.-M. Hu, Z. Li, L.-Q. Chen, C.-W. Nan, *Nat. Commun.* **2011**, *2*, 553.
- [187] M. A. Zidan, J. P. Strachan, W. D. Lu, *Nat. Electron.* **2018**, *1*, 22.
- [188] J. J. Yang, D. B. Strukov, D. R. Stewart, *Nat. Nanotechnol.* **2013**, *8*, 13.
- [189] Y. Cassuto, S. Kvatinsky, E. Yaakobi, *IEEE Trans. Inf. Theory* **2016**, *62*, 4801.
- [190] K. Chang, T. Tsai, T. Chang, K. Chen, R. Zhang, Z. Wang, J. Chen, T. Young, M. Chen, T. Chu, S. Huang, Y. Syu, D. Bao, S. M. Sze, *IEEE Electron Device Lett.* **2014**, *35*, 530.
- [191] Y. R. Jeong, H. Park, S. W. Jin, S. Y. Hong, S.-S. Lee, J. S. Ha, *Adv. Funct. Mater.* **2015**, *25*, 4228.

- [192] Y. Wang, R. Yang, Z. Shi, L. Zhang, D. Shi, E. Wang, G. Zhang, *ACS Nano* **2011**, 5, 3645.
- [193] J.-H. Kong, N.-S. Jang, S.-H. Kim, J.-M. Kim, *Carbon* **2014**, 77, 199.
- [194] M. Hempel, D. Nezich, J. Kong, M. Hofmann, *Nano Lett.* **2012**, 12, 5714.
- [195] S. Gong, D. T. H. Lai, Y. Wang, L. W. Yap, K. J. Si, Q. Shi, N. N. Jason, T. Sridhar, H. Uddin, W. Cheng, *ACS Appl. Mater. Interfaces* **2015**, 7, 19700.
- [196] C. Yan, J. Wang, W. Kang, M. Cui, X. Wang, C. Y. Foo, K. J. Chee, P. S. Lee, *Adv. Mater.* **2013**, 26, 2022.
- [197] Y. Wang, L. Wang, T. Yang, X. Li, X. Zang, M. Zhu, K. Wang, D. Wu, H. Zhu, *Adv. Funct. Mater.* **2014**, 24, 4666.
- [198] X. Li, R. Zhang, W. Yu, K. Wang, J. Wei, D. Wu, A. Cao, Z. Li, Y. Cheng, Q. Zheng, R. S. Ruoff, H. Zhu, *Sci. Rep.* **2012**, 2, 870.
- [199] Y. Jiang, Z. Liu, C. Wang, X. Chen, *Acc. Chem. Res.* **2019**, 52, 82.
- [200] J. Lee, S. Kim, J. Lee, D. Yang, B. C. Park, S. Ryu, I. Park, *Nanoscale* **2014**, 6, 11932.
- [201] M. Zheng, W. Li, M. Xu, N. Xu, P. Chen, M. Han, B. Xie, *Nanoscale* **2014**, 6, 3930.
- [202] H. Tian, Y. Shu, Y.-L. Cui, W.-T. Mi, Y. Yang, D. Xie, T.-L. Ren, *Nanoscale* **2014**, 6, 699.
- [203] L. Cai, L. Song, P. Luan, Q. Zhang, N. Zhang, Q. Gao, D. Zhao, X. Zhang, M. Tu, F. Yang, W. Zhou, Q. Fan, J. Luo, W. Zhou, P. M. Ajayan, S. Xie, *Sci. Rep.* **2013**, 3, 3048.
- [204] Z. Wang, Y. Huang, J. Sun, Y. Huang, H. Hu, R. Jiang, W. Gai, G. Li, C. Zhi, *ACS Appl. Mater. Interfaces* **2016**, 8, 24837.



## Chapter 3

### Experimental Methodology

*The chapter mainly introduce techniques that are used in this thesis including synthesis, optimization, simulation, characterization. Firstly, the synthesis techniques for fabrication of stretchable memristors and stretchable strain sensors were presented, followed by working principle for each technique. Secondly, rational selection for measuring the thickness on elastomer and simulation were discussed. Lastly, characterization techniques for material morphology, electrical and mechanical performance of stretchable electronics were described in this chapter.*

### 3.1 Synthesis techniques

#### 3.1.1 Physical vapor deposition (PVD)

Thin films have been widely used in microelectronics and usually deposited on the surface via physical vapor deposition (PVD) or chemical vapor deposition (CVD). PVD relies on evaporation of atoms from solid or liquid through the high temperature at vacuum condition and deposit those atoms on the surface of substrate through the condensation. PVD techniques include thermal evaporation, physical sputtering, laser ablation and cathode arc deposition. PVD techniques in this thesis are thermal evaporation and physical sputtering.

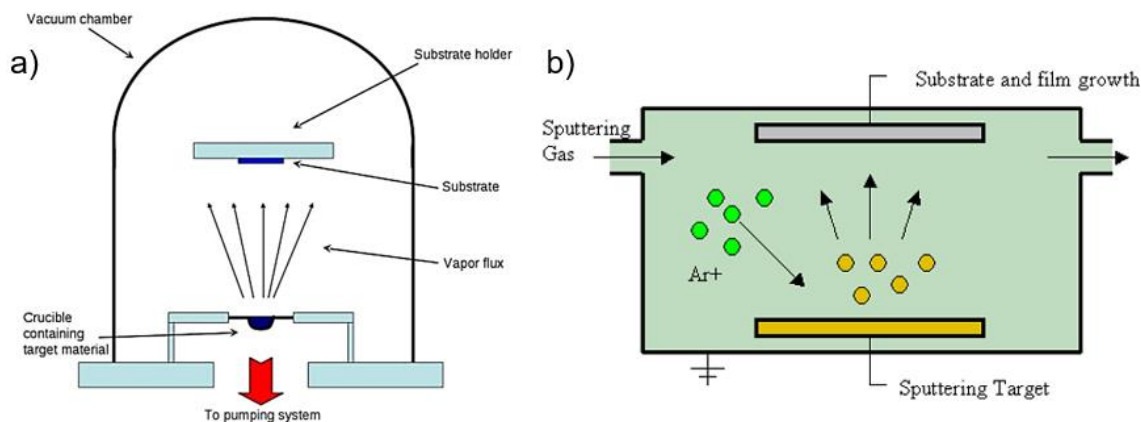


**Figure 3.1** Schematic of physical vapor deposition techniques configuration (a) Thermal evaporation. Reproduced with permission.<sup>[1]</sup> Copyright 2013, Elsevier Inc. (b) sputtering deposition.<sup>[2]</sup>

Thermal evaporation was devised by Faraday.<sup>[3]</sup> As shown in **Figure 3.1 a**, clusters of atoms or molecules are transferred to substrate in the form of a vapor flux from a target bulk materials that is placed in a metal crucible through heating process. The process is going under pressure below  $10^{-4}$  Torr at vacuum chamber. The heating temperature is around  $1500^{\circ}\text{C}$  and suitable for materials with melting point below it as target source. Besides crucible for placing the target materials, basket, boat, and wire are the other forms of heating surface for generating the vapor flux. The advantages of thermal evaporation are high deposition rate, low cost for large-scale deposition. However, the disadvantage is not suitable for fabricating thin film with multiple components because different components request different targets source that have different melting points.

Another PVD is sputtering as shown in **Figure 3.1 b**. The target material is bombarded by energetic ions (such as argon ions) that is generated in a glow-discharge plasma in front of the target material. The sputtering process differs from evaporation in the kinetic of particle emission, which transfers the atoms from target source by the collision based on momentum principle. The target materials can be single element, alloy, or compound.<sup>[4]</sup> The process performed in vacuum condition using either low-pressure plasma ( $< 5 \times 10^{-3}$  Torr) or high-pressure plasma ( $5 \times 10^{-3}$  Torr –  $30 \times 10^{-3}$  Torr).<sup>[5]</sup> During the bombardment process, secondary electrons are also generated and play an role in maintaining the plasma. The configurations that are widely used for plasma generation are direct current, radiofrequency, and magnetron assist. The plasma consists of electrons, ions, and neutral species, which functions as ac conductor. The ions in plasma can be accelerated at high energy to the cathode where target material is located at and bombard the atoms from cathode. Electrons with enough energy in the plasma move toward the anode and are collected.<sup>[6]</sup>

### 3.1.2 Electrochemical deposition

Electrochemical deposition is a method to coat conductive particle suspended in a fluid under the influence of an electric field between cathode and anode electrodes. Compared to the deposition such as thermal evaporation and sputtering, the electrochemical deposition is less expensive and more versatile for simultaneously coating large number of samples. The configuration of electrochemical deposition is call electrolytic cell consisting of two electrodes which is apart from each other and dipped into an electrolyte. The electrodes are connecting to a DC power supply that renders one electrode in negative charge (also called cathode) while the other electrode is in positive charge (also called anode). An electrolyte is an ionic solution comprising of cations and anions. Reduction process is happened in cathode where cations migrate toward to it and receive electrons to be chemically transformed to neutral elements/molecules, while oxidation process is happened in anode where anions move toward and release the electrons to it. These two processes happened in each half cell is called electrochemical reaction where electrons are transferring from anions to cation.<sup>[7]</sup>

In general, the electrolyte solution is aqueous. The salts, acids, and bases, represented by  $C_xA_y$ , dissolving into the solvent and dissociate into cations and anions which can be described in following equation



Where  $Z+$  and  $Z-$  are the ion charge numbers.

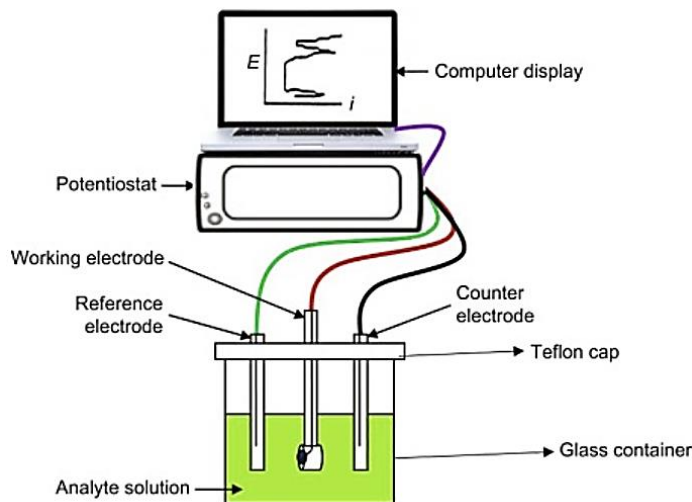


**Figure 3.2** Schematic illustration of three-electrode electrochemical cell system. Reproduced with permission.<sup>[8]</sup> Copyright 2018, Elsevier Ltd.

The most widely used electrochemical cell system is three-electrode configuration, which includes a working electrode, a reference electrode, and a counter electrode as shown in **Figure 3.2**. Working electrode is where the reaction take place when in contact with analyte solution and applying a certain potential. The electrons transfer between the working electrode and analyte solution and the current at the electrode will pass through the counter electrode for balance. The counter electrode is made of inert conducting materials such as platinum. Although no current pass through the reference electrode, the reference electrode is necessary and is known as reduction potential, which acts as a reference when measuring the working electrode potential. The standard hydrogen electrode (SHE), the calomel electrode and silver/silver chloride electrode are the most used reference electrode in the three-electrode system. The reference electrode is insulated from the analyte solution via an intermediate bridge to avoid contamination of analyte solution and it is placed as much close as possible to the working electrode to reduce any drop caused by cell resistance.<sup>[8]</sup>

Au plating solution is employed in this thesis. The most important gold plating chemical is highly toxic electrolyte, potassium gold cyanide  $K[Au(CN)_2]$ . When  $K[Au(CN)_2]$  dissolve in water and dissociates in  $K^+$  and  $[Au(CN)_2]^-$ . The  $[Au(CN)_2]^-$  initially move to anode and dissolve into  $Au^+$  and  $CN^-$  ions. Then,  $Au^+$  ions move back to the cathode and are neutralized and deposited on the cathode (working electrode).<sup>[9]</sup>

### 3.1.3 Photolithography

Photolithography is a process that transfer shapes or patterns from a template (mask) onto a substrate surface using light, which are widely used in micro manufacturing applications and semiconductor industry. In brief, photolithography can be deemed as printing with light to transfer a geometric pattern from a photomask to a photosensitive material. As shown in **Figure 3.3**, the light energy pass through a patterned mask and focused onto the photoresist, where chemical reaction take place, followed by development to create the desired pattern on the surface.

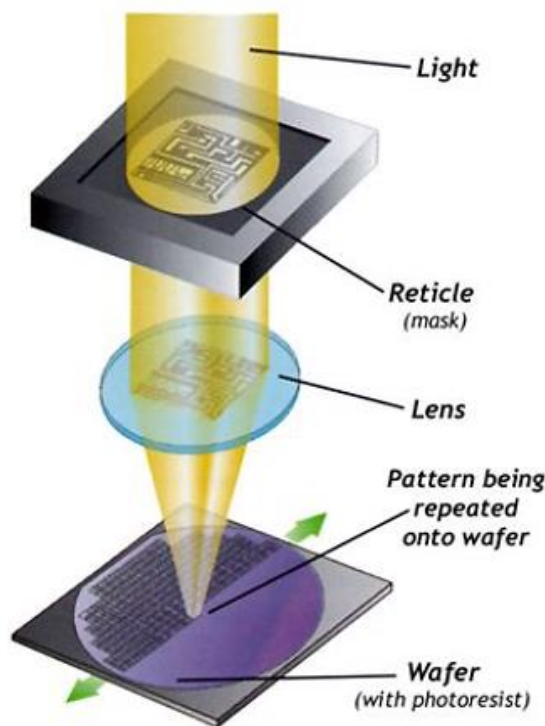


**Figure 3.3** Schematic illustration of photolithography configuration.<sup>[10]</sup>

The optical resolution of photolithograph is critically determining the smallest fabrication size of device. The most widely used light source is UV light. Other light source such as

electron beam or x-ray are also employed for better resolution. However, the wavelength of the light and capability of the lens are the bottleneck of achieving a very small feature with a good resolution. According to Abbe-Rayleigh criterion as follows:

$$d_{\min} = 0.61 \frac{\lambda}{n \sin \alpha}$$

Where  $d_{\min}$  is the minimal size of feature,  $\lambda$  is the wavelength of light source,  $n$  is the refraction index of the environment,  $\alpha$  is the aperture angle. Hence, to achieve a small structure with good resolution, a good numerical aperture (determine diffraction limit) and short wavelength must be employed.<sup>[11]</sup> Current state-of-the-art technique such as deep ultraviolet light with wavelength of 248 nm and 193 nm allow to obtain minimum size below 100 nm, and extreme ultraviolet with radiation of 13.5 nm has been developed.<sup>[12]</sup> Because of such a short wavelength of radiation cannot be diffracted by the lens of system and absorbed by bulk masks, the extreme ultraviolet need a transition from diffractive to fully reflective optics.<sup>[13]</sup>

The photolithography process includes wafer cleaning, photoresist spin-coating, soft backing, make alignment, exposure, photoresist developing, hard backing, etching and photoresist removal as shown in **Figure 3.4**.

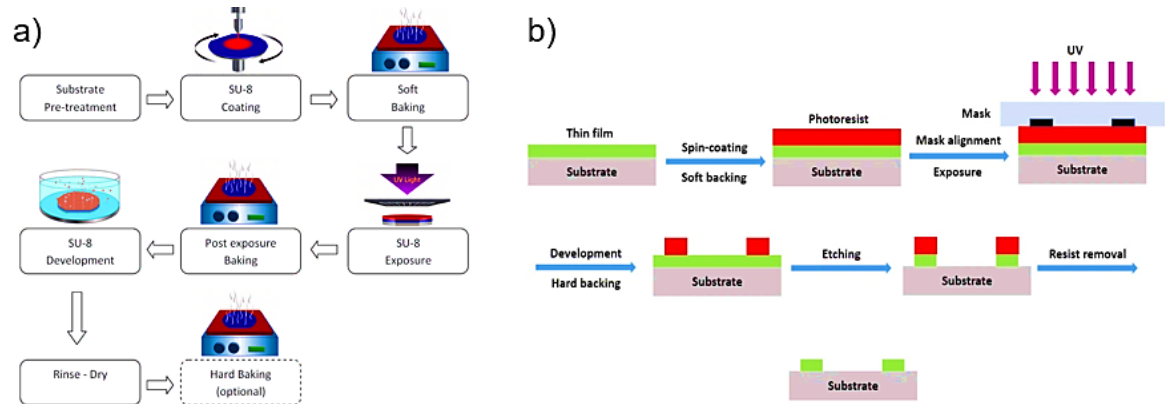


**Figure 3.4** photolithography procedures and steps (a) Experimental procedures, SU-8 is an epoxy-based negative photoresist.<sup>[14]</sup> (b) photolithographic steps.<sup>[15]</sup>

The substrate begins with cleaning to remove the surface contaminants using trichloroethylene, acetone, or methanol, then treated by liquid or gaseous to enhance adhesion of photoresist to the substrate. Next, photoresist spin on the substrate. After that, it will be pre-baked at ~100 °C on a hotplate to drive off the excessive photoresist solvent.

Then, the substrate with photoresist is aligned with patterned photomask and exposed to UV light to trigger the chemical reaction on the portion of exposed photoresist, followed by a post exposure baking to reduce destructive and constructive interference patterns of the incident light.<sup>[14]</sup> After that, photoresist developer is employed to wash away either the exposed or non-exposed portions which depend on the positive or negative photoresist. When a non-chemically amplified resist was used, the hard baking sometimes is performed for few minutes to consolidate the remaining the photoresist to make it more durable and protect the underlying layer in future procedures. Lastly, the substrate is etched physically or chemically. The area with remained photoresist is well-protected and kept while the rests are removing.<sup>[15]</sup>

#### 3.1.4 Electromechanical characterization

The electromechanical characterization system for the stretchable electronics in this thesis consist of Keithley 4200-Semiconductor characterization system (Keithley 4200-SCS) and mechanical tester. Keithley 4200-SCS is an analyzer to provide electrical characterization of materials, semiconductor devices. Mechanical tester (MTS Criterion Model 42) is to perform tension, compression, and flexure tests on stretchable electronics. The electrochemical characterization system setup and configuration is shown in **Figure 3.5**. The specimen (stretchable electronics) was clamped between upper and bottom grippers. At the same time, the stretchable electronics was connected to the Keithley 4200-SCS through the copper wire and liquid metal (eutectic CaIn). The electrical properties of stretchable electronics were recorded simultaneously as the crossheads move up and down. This setup is normally used for dynamic cycling test or to obtain relationship for stress and strain. A home-built mechanical tester is also used for static test in the thesis work. The working principle is similar but it is manually moving the crossheads instead of automation.

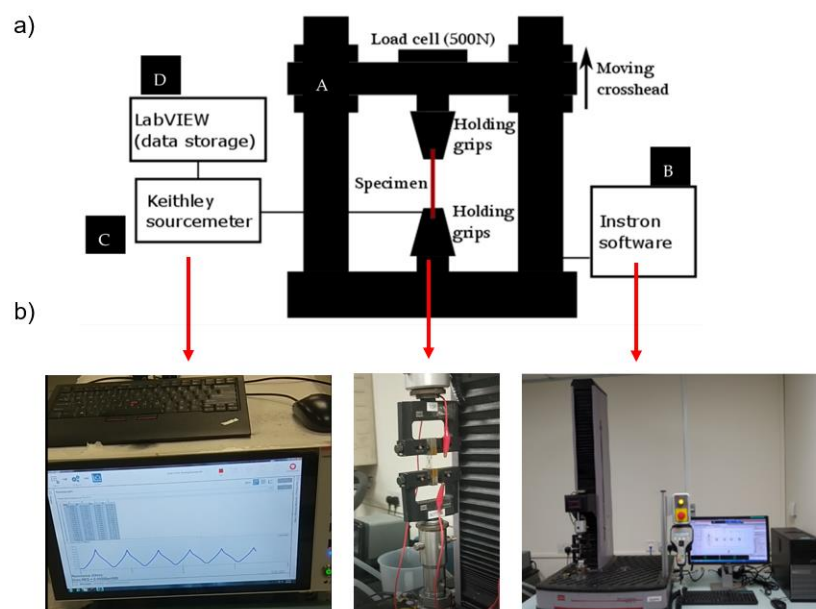


**Figure 3.5** The setup of electrochemical test. (a) configuration. Reproduced with permission.<sup>[16]</sup> Copyright 2018 by the authors. Licensee MDPI, Basel, Switzerland. Distributed under the terms and conditions of the Creative Commons Attribution (CC BY) license (<http://creativecommons.org/licenses/by/4.0/>). (b) equipment for each component.

The electrical connection is illustration in **Figure 3.6**. The liquid metal is placed on the sample to be tested and connect to extend Cu cables through the Cu wires. The extend Cu cables is connected to Keithley system and record the electrical data. The force driven to the gripper can be either manually and automatically as shown in **Figure 3.6 a** and **Figure 3.6 b**, respectively.

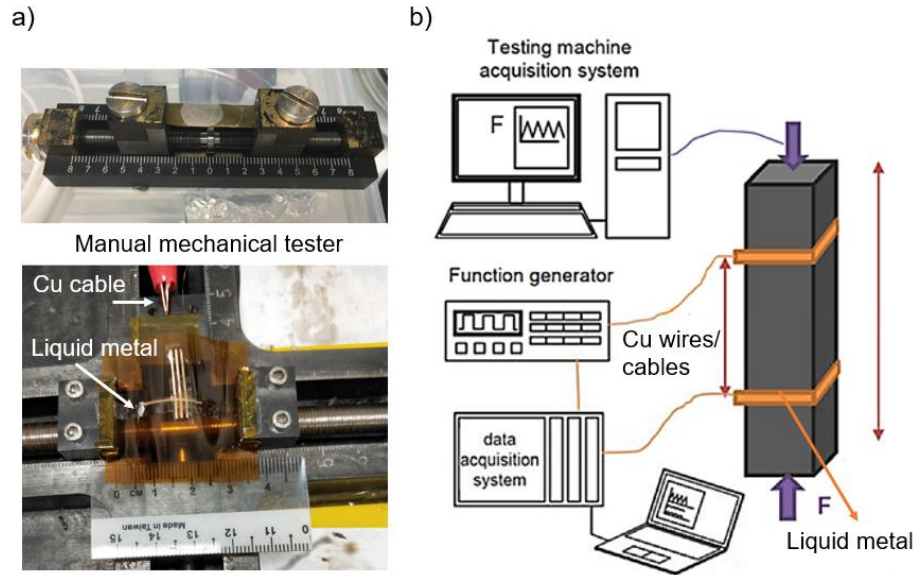


**Figure 3.6** The electrical connection for electromechanical test. (a) Manual mechanical tester (b) Automatic mechanical tester.

### 3.2 Rational selection for thickness measurement and simulation

#### 3.2.1 Thickness measurement

Thin film thickness on elastomer (PDMS) is measured by either direct or indirect methods. After comparing those method, indirect method was employed in this thesis. The techniques employed in the direct measure include AFM, SEM and FIB, which is directly measure the metallic thin film on PDMS. However, some problems encounters that affect the accuracy as shown in **Figure 3.7**. For example, using AFM to measure the metallic thin film on PDMS, the soft and uneven PDMS make measurement unstable and roughly. The tip may stick onto the PDMS and affect the accuracy.

	Methods		Reasons
Direct measurement	AFM (PDMS)	x	PDMS uneven & soft
	SEM (PDMS)	x	Poor adhesion and thin film delaminate from PDMS
	FIB (PDMS)	x	PDMS undergoes thermal expansion

Indirect measurement	AFM (Si/SiO <sub>2</sub> based)	√	Flat, stable, and accurate
----------------------	---------------------------------	---	----------------------------

**Figure 3.7** Comparison of methods for measuring the thickness of thin film on elastomer.

Second method is using SEM to measure the cross-section of metallic thin film on PDMS. To take a good cross-section image, the sample should have a sharp and flat edge. Cut the Au/PDMS in ambient condition will curve the edge as the PDMS deforms largely which impedes the flat view of cross-section and cannot measure the thickness accurately. Freezing Au/PDMS in liquid N<sub>2</sub> and cut sample in frozen state can give a sharp edge, however, due to the large thermal expansion mismatch between Au thin film and PDMS, Au thin film curved and delaminate from PDMS as shown in **Figure 3.8 (a-b)**. Using FIB-SEM technique to cut the sample, due to the high thermal energy, the PDMS expand and curve which affect the measurement of the thin film thickness (**Figure 3.8 c-d**). After trying the possible direct measurements, it seems no method suitable. The indirect measurement was conducted by measuring the thickness of deposited Au on the wafer. The fabrication process is in the same way of deposition Au on PDMS. By using AFM to measure the thickness of Au on wafer to indirectly indicate the thickness of Au on the PDMS.

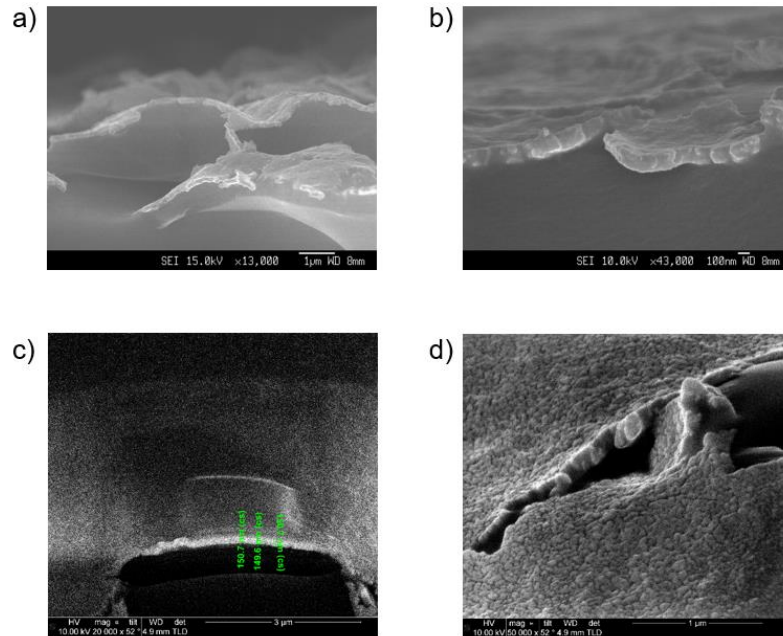


**Figure 3.8** Cross-section of Au thin film on PDMS under (a-b) SEM and (c-d) FIB-SEM.

As shown in **Figure 3.9**, measuring the Au thin film on wafer is much more stable and less fluctuation than measuring Au thin film on the PDMS. Thus, we choose indirect

measurement to quantify the thickness of Au on PDMS. In this thesis, five measurements are conducted at different locations on wafer within a defined region and take the average value as the final value.

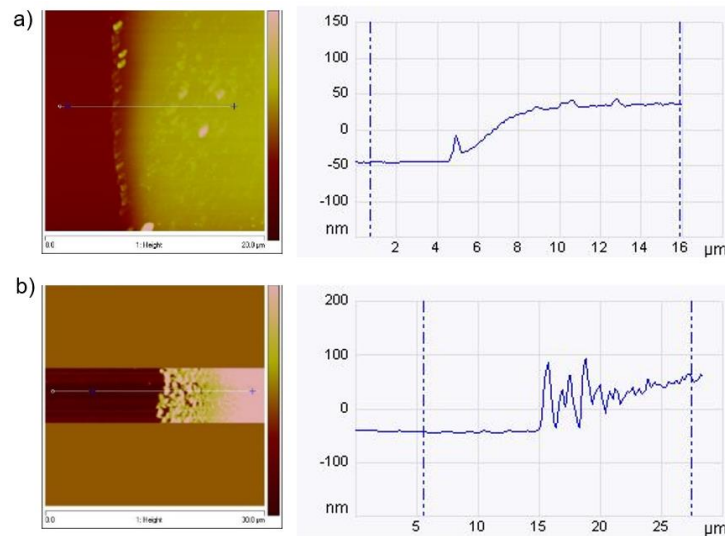


**Figure 3.9** Measuring the thickness of Au thin film on (a) wafer, and (b) PDMS

### 3.2.2 Finite Element Analysis (FEA) simulation

The finite element analysis (FEA) is a numerical method for solving engineering and mathematical physics problems, which include structural analysis, fluid flow, heat transfer, electromagnetic protentional and mass transport. Especially for problem involving complicated geometries, loading, material properties, it is difficult to do analysis experimentally. FEA is an acceptable solution by dividing the system into an equivalent system of small bodies or units (nodes), boundary line and surface. In FEA, it formulates equation for each finite element and combine them to obtain the solution of whole body. There are two types of approaches to describe the motion. One is Lagrangian, where a particle moves from one point to another point along its trajectory. The movement properties are determined by tracking the motion as a function of time. This can be imaging by sitting the boat and flow with river. Another one is Eulerian, where the variation is described within a fixed space as a function of time. The movement properties are determined by analyzing the behavior of the functions. This can be imaging by sitting on the bank of a river and watching the water flowing at a fixed location.

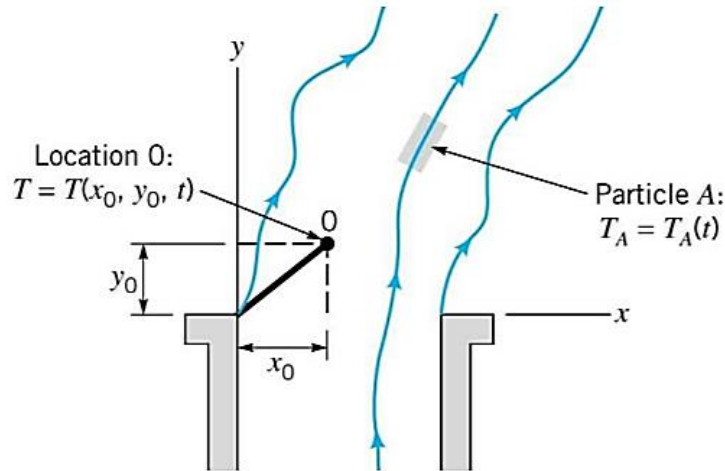


**Figure 3.10** Illustration of difference between (a) Eulerian and (b) Lagrangian.

Taking smoke going up a chimney as an example (**Figure 3.10**), a thermometer was attached to the top of chimney at point 0 and record  $T$  as a function of time. In Eulerian method, as different smoke particles pass through 0, the temperature change and gives  $T(x_0, y_0, z_0, t)$  method, more thermometers involved will give  $T(x, y, z, t)$ . The flow velocity can be described by a function  $u(x, t)$ , where  $x$  is position and  $t$  is time. However, in Lagrangian method, thermometer is attached to a particle A and move with particle. The initial temperature record as  $T_A$ . As the particle moves in the time of  $t$ , temperature become  $T_A(t)$ . All the particles in the time of  $t$  can be record if we know the position of every particle at the function of  $t$ . The flow velocity  $u$  can be described by a function  $X(x_0, t)$ , where  $x_0$  is position at initial time  $t_0$ , and it is a time-depend vector. So, the velocity of particle expressed in Eulerian can be translate into Lagrangian as follows<sup>[17]</sup>:

$$u(X(x_0, t), t) = \frac{\partial X}{\partial t}(x_0, t)$$

Generally, Eulerian approach is commonly used for fluid flow which has large deformation, whilst Lagrangian approach is used for rigid solids which has small deformation. CEL is hybrid method that combine Eulerian and Lagrangian method. In this thesis work, CEL method is employed as in our system as there are two types of materials that has large Young's modulus difference. One is elastomer that has large deformation under the force, and the other one is rigid metal with negligible deformation. So, it cannot be properly conducting simulation by using either Eulerian or Lagrangian method. CEL is an appreciate method that solve this problem. An Eulerian continuum model is used for elastomer and a

Lagrangian particle model is used for metal solid. Both models are applied to simulate the movement behavior of rigid solid in the elastomer under the puncturing force.

## References

- [1] R. J. Martín-Palma, A. Lakhtakia, in *Engineered Biomimicry*, (Eds: A. Lakhtakia, R. J. Martín-Palma), Elsevier, Boston 2013, 383.
- [2] "Sputter deposition", can be found under [https://en.wikipedia.org/wiki/Sputter\\_deposition](https://en.wikipedia.org/wiki/Sputter_deposition), **2020**.
- [3] M. Faraday, *Philos. Trans. R. Soc. of London* **1857**, 147, 145.
- [4] P. J. Kelly, R. D. Arnell, *Vacuum* **2000**, 56, 159.
- [5] Z. L. N. S. Wei Gao, *An Introduction to Electronic Materials for Engineers*, World Scientific Publishing Company, **2011**.
- [6] S. M. Rossmagel, *J. Vac. Sci. Technol. A* **2003**, 21, S74.
- [7] C. A. D. Rodriguez, G. Tremiliosi-Filho, in *Encyclopedia of Tribology*, (Eds: Q. J. Wang, Y.-W. Chung), Springer US, Boston, MA **2013**, 918.
- [8] P. S. Nnamchi, C. S. Obayi, in *Characterization of Nanomaterials*, (Eds: S. Mohan Bhagyaraj, O. S. Oluwafemi, N. Kalarikkal, S. Thomas), Woodhead Publishing, 2018, 103.
- [9] P. Wilkinson, *Gold Bulk* **1986**, 19, 3.
- [10] c. C. Yocca, M. Lora, J. Leonatti, "THE USE OF EUV LITHOGRAPHY IN CONSUMER MICROCHIP MANUFACTURING", **2017**.
- [11] F. Hubenthal, in *Comprehensive Nanoscience and Technology*, (Eds: D. L. Andrews, G. D. Scholes, G. P. Wiederrecht), Academic Press, Amsterdam **2011**, 375.
- [12] G. Tallents, E. Wagenaars, G. Pert, *Nat. Photonics*. **2010**, 4, 809.
- [13] M. Van Rossum, in *Encyclopedia of Condensed Matter Physics*, (Eds: F. Bassani, G. L. Liedl, P. Wyder), Elsevier, Oxford **2005**, 394.
- [14] "Photolithography", can be found under <http://toppicture.dx.am/?top=3&definitions=Photolithography>.
- [15] B. Mozooni, "Optical Lithography", can be found under <https://techomat.wordpress.com/2015/06/07/optical-lithography/>, **2015**.
- [16] M. Mosallaei, J. Jokinen, M. Kanerva, M. Mantysalo, *Micromachines (Basel)* **2018**, 9.

[17] "Lagrangian and Eulerian specification of the flow field", can be found under [https://en.wikipedia.org/wiki/Lagrangian\\_and\\_Eulerian\\_specification\\_of\\_the\\_flow\\_field](https://en.wikipedia.org/wiki/Lagrangian_and_Eulerian_specification_of_the_flow_field), **2020**.

## Chapter 4\*

### **Mechanically Adaptative Properties of Discrete Structure Based Devices on Elastic Substrate**

*Mechanical adaptation is a vital requirement for wearable electronics to ensure the electronics to accommodate with various deformations such as stretch, bend, twist and so forth, while keeps electrical functions of electronics during deformable conditions. This requirement is challenging especially for inorganic-based memristors. Because conventional inorganic-based memristors are manufacturing based on semiconductive materials, which is brittle and fragile under deformations. To solve this problem, we employ a discrete-structured active layer instead of traditional continuous bulky structure. This chapter demonstrates the mechanically adaptative properties of memristors can be achieved by this kind of heterogenous structure. The results show that the discrete structure endows memristors with excellent flexibility (half fold) and stretchability (40%) without losing electrical functions. Meanwhile, the underlying mechanism is elaborated by using FEA simulation.*

## 4.1 Introduction

Stretchable electronics have been drawn much attention for their wide applications in wearable devices,<sup>[1-2]</sup>electronics skin,<sup>[3-5]</sup> soft robotics<sup>[6-7]</sup> and so forth. To ensure good performance of stretchable devices, current researchers put large effort into protecting the electronics from electrical failure during various deformations such as stretch, bend, twist<sup>[8-9]</sup>. The two main strategies are involved including develop intrinsic materials properties and design exquisite geometrics. For intrinsic materials properties, researchers either choose materials that are naturally innate stretchable and flexible such as polymeric materials,<sup>[10-11]</sup> organic semiconductor,<sup>[12-14]</sup> graphene/CNT,<sup>[15-20]</sup> liquid metal,<sup>[21-22]</sup> or artificial engineering of the materials in molecular level.<sup>[23]</sup> As for geometrics design, researchers enhance mechanical stretchability or flexibility via some rational geometric designs such as buckles,<sup>[24-25]</sup> wavy patterns,<sup>[26]</sup> kirigami/origami/auxetic structure,<sup>[27-34]</sup> interlocking nanofibers.<sup>[9]</sup>

Amongst components in stretchable electronic system, stretchable memristors play a vital role in data processing, information storage, neuromorphic and in-memory computing.<sup>[35]</sup> Resistive switching random access memory (RRAMs) have been considered as a promising candidate to replace the present flash-based technology due to high performance and simple architecture with metal/insulator/metal (MIM) sandwich structure<sup>[36]</sup>. It can be modulated into high resistance state (HRS or off state) and low resistance state (LRS or on state) via external electrical stimuli. Generally, the insulator layer (active material) sandwiched between two metallic electrodes is transition metal oxide like  $\text{Al}_2\text{O}_3$ ,  $\text{HfO}_x$ ,  $\text{TiO}_2$ , and  $\text{TaO}_x$ .<sup>[37-40]</sup> However, they are a bulky continuous structure that is brittle and rigid and greatly hinder them from adapting to various mechanical deformations. When employing them on the elastic substrate for stretchable/flexible applications, they are easily broken into pieces under deformations. As shown in **Figure 4.1a**, when poking a bulky structure on elastic substrate, the continuous structure crack into pieces and destroy structural integrity totally, which threaten especially for memristor to store data safely. In contrast with bulky continuous structure, due to the space between discrete units that give more mobility for structure to acclimatize to stresses, discrete structure has more degree of freedom in accommodate with different shape and curve, which give more space to stretchability and flexibility. In analogy to cut a mango, the mesocarp is continuous

structure and exocarp is soft substrate. When we bend it, the continuous mesocarp was broken into two and damage its original continuity of structure. Replacing the continuous mesocarp with discrete mesocarp, the discrete mesocarp can keep its original structure without destruction under the bending condition (**Figure 4.1b**). Herein, we report a stretchable memristor based on a discrete structure design in active layer through current existing conventional semiconduction fabrication technologies.

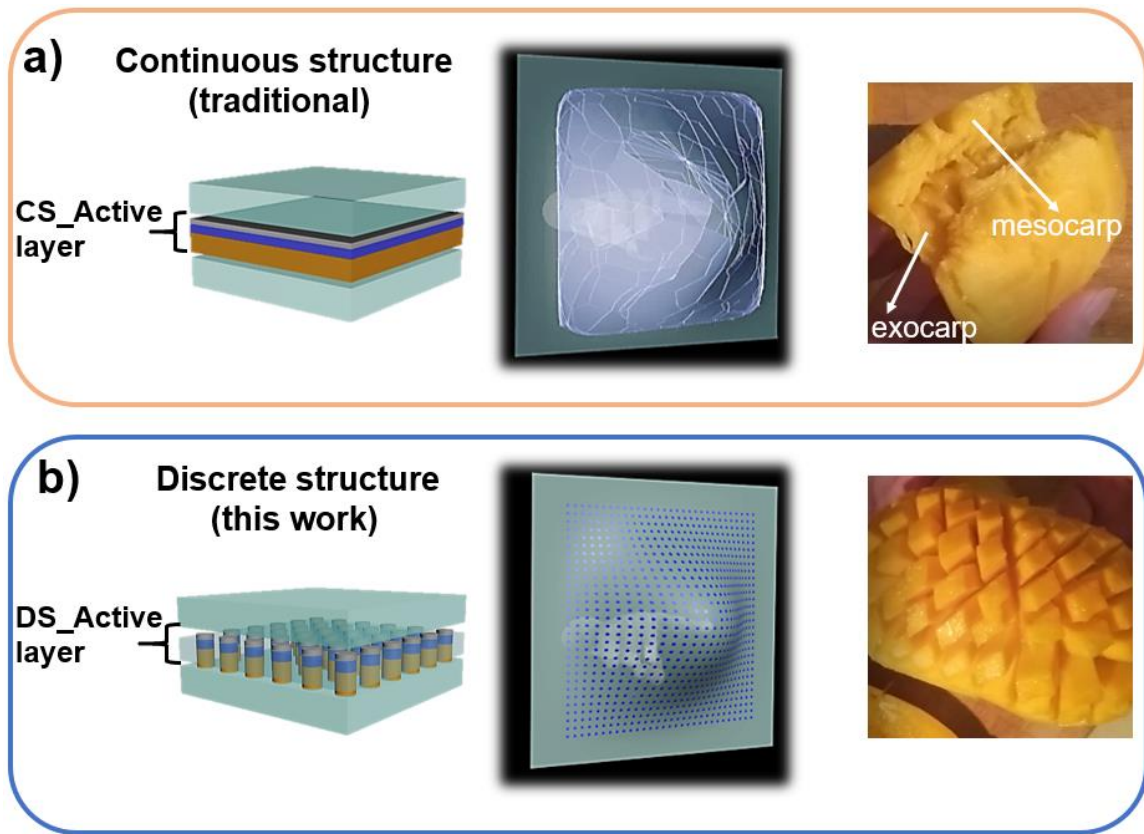


**Figure 4.1** Continuous structure (CS) v.s Discrete structure (DS) during mechanical deformation. (a) Scheme of traditional RRAM with continuous structure of active layer(left). Continuous structure on elastic substrate is brittle and easily crack under mechanical deformation(middle). In analogue to a bulky mango under bending, it is broken into two pieces and destroy the original continuous structure (right). (b) Scheme of RRAM with discrete structure of active layer(left). Discrete structure on elastic substrate is flexible to adapt to mechanical deformation(middle). In analogue to a discrete mango under bending, it remains original discrete structure without damage (right).

The rational design of stretchable discrete-structure memristor (DS-memristor) with crossbar configuration is schematic illustrated in **Figure 4.2 a**. The active layer is no longer

conventional bulky continuous structure, instead of consisting of number of discrete units of Ag/HfO<sub>2</sub>/Au sandwiched in between two Au strips electrodes on SEBS substrates. Ag side is attached to the top electrodes while Au side is attached with bottom electrodes. Both top and bottom electrodes cross each other perpendicularly. **Figure 4.2 b** is a focused ion beam scanning electron microscopy (FIB-SEM) image of discrete units of Ag/HfO<sub>2</sub>/Au on the Cu foil. The discrete units are uniformly distributed and keep distance away from each other. The size of discrete units and distance between each other can be modified during fabrication and FIB-image shows the diameter of 25μm and space distance around 30μm. SEM image of DS-memristor is shown in **Figure 4.2 c**. The discrete device units in between two Au electrode on SEBS substrates. The discrete units are wrapped by SEBS.

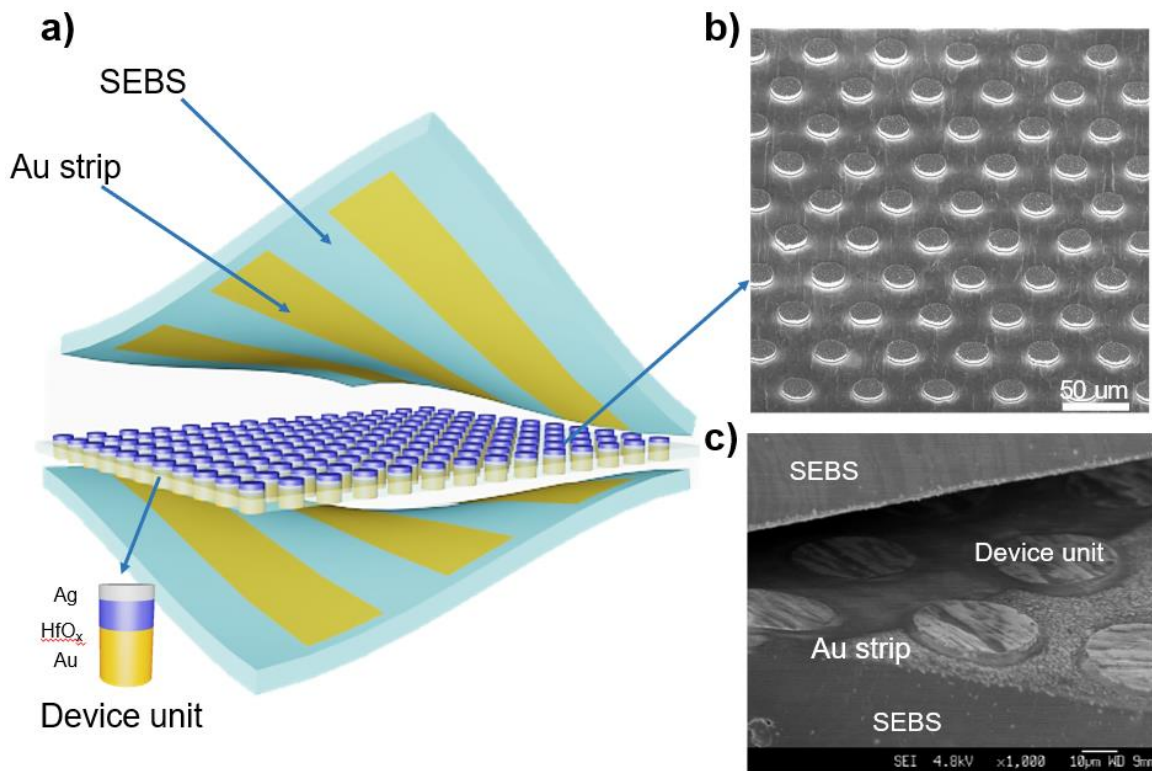


**Figure 4.2** (a) The schematic of a flexible discrete-structure memristor (DS-memristor) with crossbar configuration. (b) FIB-SEM image of discrete structure of active layer of Ag/HfO<sub>2</sub>/Au on Cu foil. (c) SEM of stretchable memristor with discrete units sandwiched between top and bottom Au electrodes on SEBS substrates.

From experimental results, this kind of structure ensure stretchable memristors with a good mechanical adaptative property whilst maintaining normal electrical functions such as data

writing, erasing, and reading. Especially, stretchable memristors based on discrete structure can be stretched to up to 40% and half-folded bending. Besides, the data stored in DS-memristor can be kept safety in both static state and dynamic cycling motions. Thus, the discrete structure is demonstrated as an effective strategy to enhance stretchability and flexibility of stretchable memristors and could be applied to other inorganic devices with similar structure.

## 4.2 Experimental methods

### 4.2.1 Fabrication of stretchable memristors

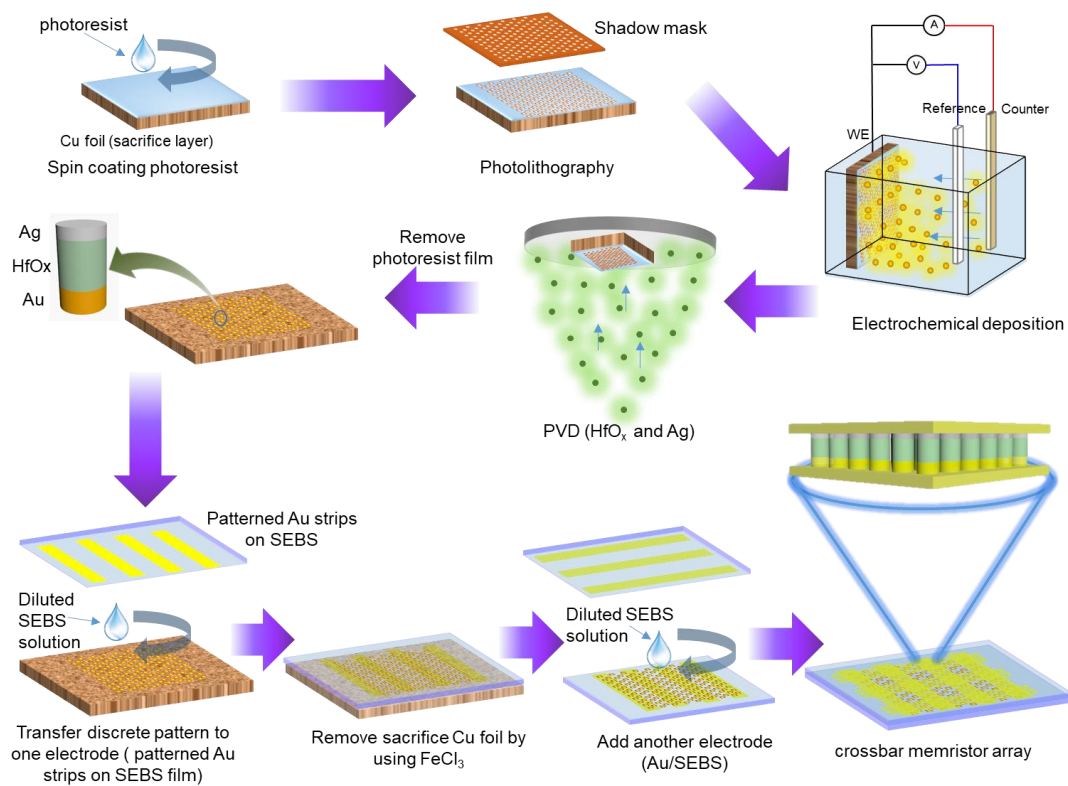


**Figure 4.3** Fabrication process of discrete structure based stretchable memristors.

*Fabrication of top/bottom electrodes:* SEBS substrate were prepared by dissolving in Toluene at concentration of 15% w/w and casting into clean glass slide, dried up in fume hood at room temperature for one night and formed a thin film with thickness of  $\approx 300$  nm.

Electrodes Au/SEBS were fabricated by thermally evaporating Au of the thickness of 60nm on the SEBS film with a shadow mask.

*Fabrication of discreted-structure memory device:* Firstly, photoresist (AZ4620) was spin-coated on Cu foil at speed of 2500rpm for 60s, then heated on hotplate at 100°C for 5mins, followed by photolithography with patterned photomask (expose to UV light for 3s) and dipped in the developer solution for 10s, washed by DI water and dried up by N<sub>2</sub>. Secondly, electrochemical synthesized Au inside the developed area of photoresist on Cu foil. 50% v/v of water/gold plating solution (Orotemp 24 RTU RACK; Technic Inc., Anaheim, CA) was used as electrolyte and deposited at a fix potential -950 mV for 1 h, then washed by DI water and dried up with N<sub>2</sub> for next step. After photolithography and electrochemical deposition, we need to fabricate oxide layer and Ag layer on Cu foil. Cu foil was deposited with HfO<sub>2</sub> via physical vapor deposition technique (PRO Line PVD 75, Kurt J. Lesker) at room temperature with a base pressure  $< 2 \times 10^{-5}$  torr. During the sputtering process, high purity Ar (99.999%) and O<sub>2</sub> (99.999%) with ratio of 10:1 (Ar/ O<sub>2</sub>) were introduced into the chamber with deposition power of 100 W under the operation pressure of 8 mTorr. The whole sputtering deposition last for 2000s with sample rotating speed at 10 rpm. Subsequently, a 20nm Ag film was evaporated using a tungsten boat (2.00'' Dia. x 0.125'' Thick 99.95%, Kurt J. Lesker) towards the Cu foil by using thermal evaporator (NANO 36, Kurt J. Lesker) under a vacuum pressure of  $< 1.0 \times 10^{-4}$  Pa. Next, using acetone to wash the remaining photoresist on Cu foil, left over discreted-structure on Cu foil and dried up. Finally, spin-coated diluted SEBS (SEBS : Toluene = 1:30 v/v) on Cu foil with discreted-structure at 5000 rpm and rapidly transferred Cu foil with discreted-structure to one Au/SEBS electrode and pressed slightly, dried up at 60 °C oven over night and then removed the Cu foil by using 1M FeCl<sub>3</sub>, the discreted-structure was successfully transferred into one Au/SEBS electrode. Spin-coating the Au/SEBS electrode of discreted-structure with diluted SEBS (SEBS : Toluene = 1:30 v/v) at 4000 rpm for 1s and then cover it with anther Au/SEBS electrode and slightly press it. The discreted-structure memory device was achieved.

The discrete units can be controlled through employing the difference size of the patterned photomask during photolithographic process, which range from 5  $\mu\text{m}$  to 40  $\mu\text{m}$  as shown in figure 4.4. The space distance between units range from 10  $\mu\text{m}$  to 50  $\mu\text{m}$ .

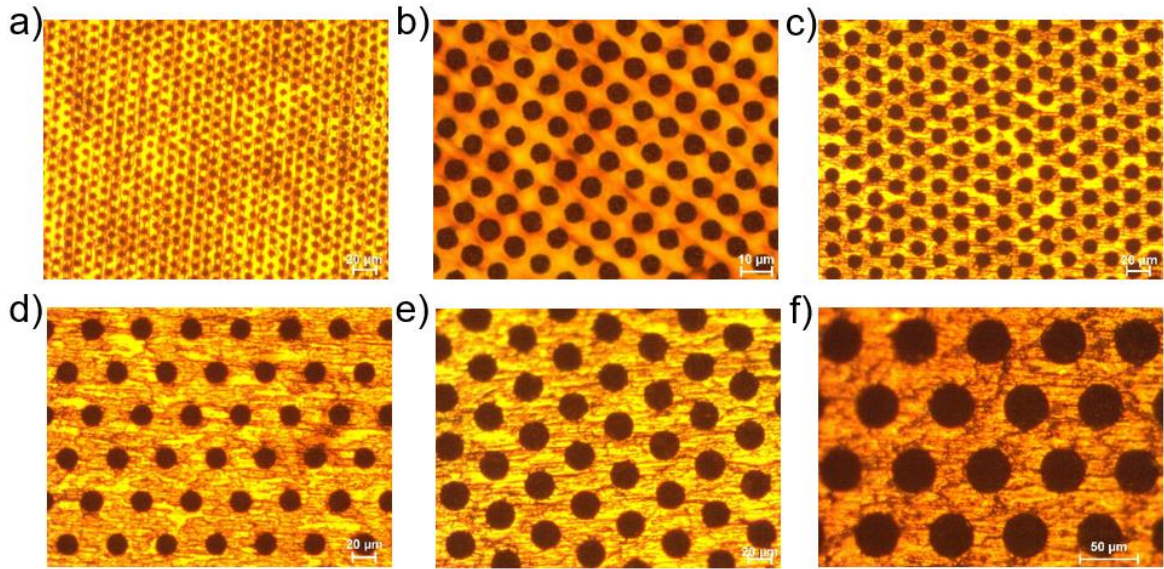


**Figure 4.4** The optical microscope images of discrete units with size (a) 5 $\mu\text{m}$ , (b) 7 $\mu\text{m}$ , (c) 15 $\mu\text{m}$ , (d) 20 $\mu\text{m}$ , (e) 25 $\mu\text{m}$ , and (f) 40 $\mu\text{m}$  on the Cu foil. The size of discrete units and the distance between each unit were tens of microns ranging from 10  $\mu\text{m}$ -50  $\mu\text{m}$ .

Device characterization and mechanical measurements: The current-voltage ( $I$ - $V$ ) characterization and resistance were obtained by a semiconductor parameter analyzer (Keithley 4200-SCS, Cleveland, OH, USA). The SEM image was collected using a Field-Emission SEM (JEOL, FESEM-7600F) and optical microscope (ZEISS). The cycling test of mechanical tension was performed by MTS Criterion Model 42 (Instron 5848) and bending test was carried out by a custom-made manual tensioner.

#### 4.2.2 Electrical characterization of DS-memristor

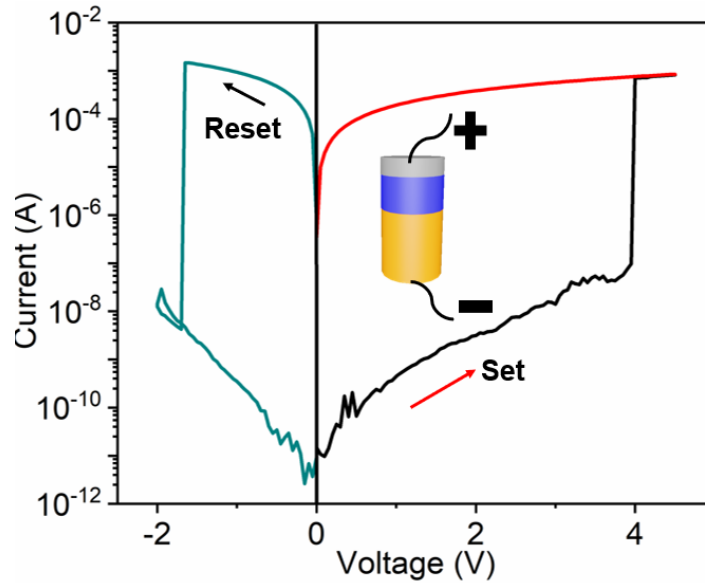


**Figure 4.5** A typical  $I$ - $V$  characterization of DS-memristor under a voltage sweeping mode at room temperature.

A voltage bias was applied to the top electrode which was contacted with Ag end of pillars, and the bottom electrode was grounded which was contacted with Au end of pillars. When started at zero bias and continuously increased the voltage, the current of DS-memristor gradually increased from  $10^{-11}$  to  $10^{-7}$  A. Until the voltage reached around 4 V, the current suddenly increased to the compliance limit by four orders of magnitude, indicating the memristor switched from HRS to LRS. The memristor remained in LRS during subsequent sweep from zero to positive voltage. When applied reverse bias from zero to negative about -2 V, the memristor switches back to HRS, indicating the nonvolatile resistive switching memristive behavior.

#### 4.2.3 Electrical characterization of electrode Au/SEBS

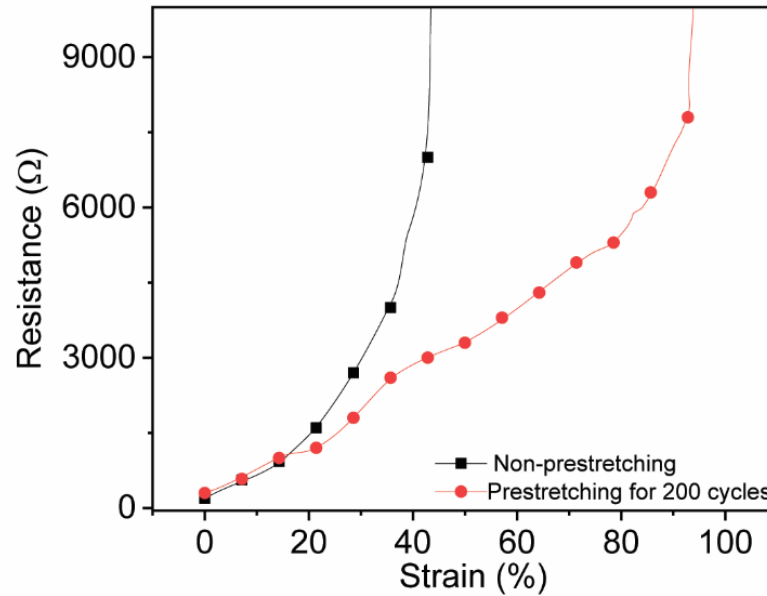


**Figure 4.6** Electrical and mechanical properties of top and bottom electrodes (Au/SEBS) with crossbar configuration. Black line is electrical performance of top and bottom electrodes without warm-up by stretching-releasing for 200 cycles before fabrication, while red line is electrical performance of top and bottom electrodes with warm-up by stretching-releasing for 200 cycles before fabricating in crossbar configuration. The resistance increase under strain is much slower for electrodes with warm-up for 200 times, indicating the stretchability of electrodes with warm-up are better than electrodes without warm-up.

Two Au/SEBS electrodes were fabricated in crossbar configuration. From **Figure 4.6**, the electrodes with warm-up have better stretchability before the resistance increase drastically than non-warm-up electrodes. For crack-based electrodes, crack generation and propagation are critical for forming a conductive path and hence affect electrical performance of electrodes. Before two electrodes being fabricated together, there has inner stress within thin film and substrate, which have negative influence on crack generation and propagation. The stretching-releasing process help to release stress concentration that is induced within the thin film during fabrication, which facilitate a steady crack generation and propagation and give rise to a more uniform conductive path for electrons to pass by. From substrate point of view, the warm-up process also assists in relieving the inner stress within the polymer molecular chains so that the stress applied to the thin film is uniform. These are the possible reasons for electrodes with warm-up have better stretchability than non-warm-up electrodes.

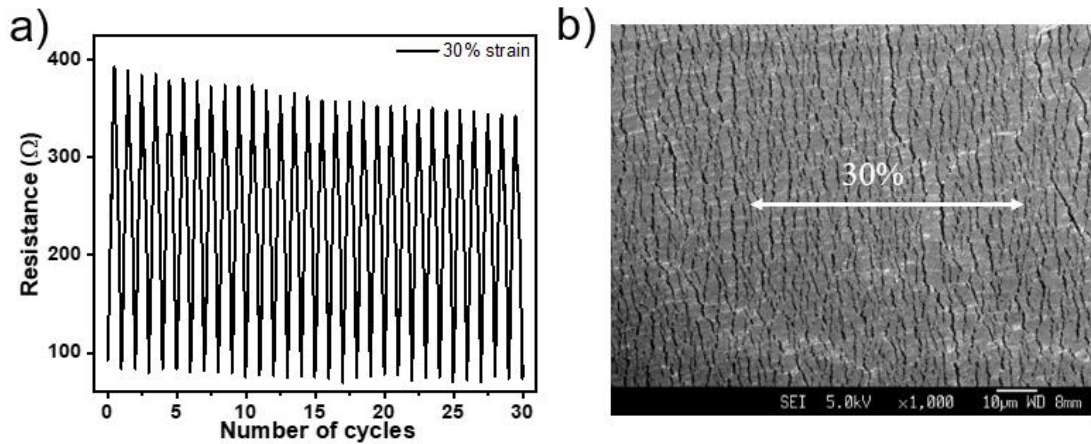


**Figure 4.7** The behavior of Au strip on SEBS under cycling stretching and crack morphology in Au electrode. (a) Cyclic electrical performance of electrode (Au on SEBS). (b) SEM image of microcracks on electrode (Au/SEBS) at 30% strain.

The stability of two electrodes Au/SEBS in crossbar configuration was performed under 30% strain for more than 100 consecutive loading and unloading cycles (**Figure 4.7 a**). The decline of resistance at the first tens of cycles due to the crack generation and propagation is not stable. And the SEM image (**Figure 4.7b**) shows the microcrack morphology under 30% strain. The crack within Au film open and close with mechanical loading and unloading is the reason why the resistance changes regularly and cyclically.

### 4.3 Principle Outcomes

This chapter mainly present the stretchability and flexibility of discrete structure based memristors, to prove the effectiveness of discrete structure on improving mechanical adaptation properties of stretchable memristors.

#### 4.3.1 Memristor flexibility

To compare the flexibility of the continuous structure memristor (CS-memristor) and the discrete structure memristor (DS-memristor) under bending condition. Both CS-memristor and DS-memristor were fabricated with the same materials Ag/HfO<sub>x</sub>/Au sandwiched between the top and the bottom Au electrodes. **Figure 4.8** and **Figure 4.8 d** are the schematic diagrams of CS-memristor and DS-memristor, respectively. From the photograph **Figure 4.8 b**, CS-memristor was broken into two parts when bend it, and

obvious cracks are observed in optical microscope (**Figure 4.8c**). This fracture seriously destroys the intact structure of CS-memristor and damage the device electrical functions. However, no fracture is found when bend DS-memristor under almost half folding (**Figure 4.8 e**), the structure of DS-memristor under optical images remain intact without damages as shown in **Figure 4.8 f**. This indicates that the discrete structure has advantage over continuous structure on against mechanical stress.

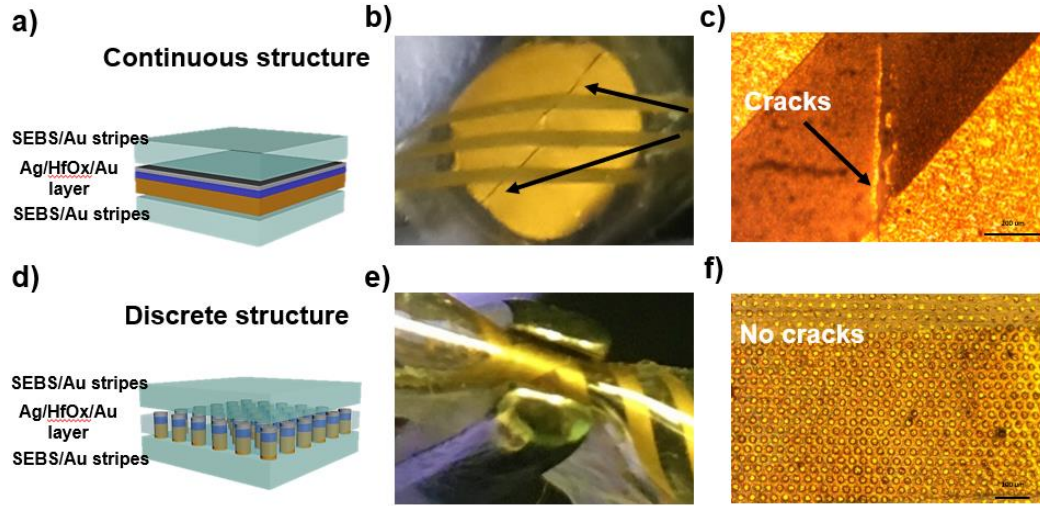


**Figure 4.8** Comparison of CS and DS based on flexibility. (a) Schematic of conventional memristor with continuous structure of active layer. (b) Photograph of continuous structure based memristor under bending condition and fracture. (c) Optical image of cracks in the continuous structure based memristor after bending. (d) Schematic of memristor with discrete structure of active layer. (e) Photograph of discrete structure based memristor under bending condition and no fracture. (c) Optical image of discrete structure based memristor after bending and structure is intact without cracks.

To investigate electrical behavior and the flexibility of DS-memristor. The  $I$ - $V$  characteristic of DS-memristors at different states, from flat to half fold showing that DS-memristors can work properly in terms of data writing and erasing under different bending radiuses (**Figure 4.9 a**). The repeatability of operation voltages for devices to set and reset under different bending radius were consistent and steadily, indicating the stability of device under various bending states (**Figure 4.9 b**). The data storage capability of DS-memristor under bending is shown in **Figure 4.9 c**. The resistance in both HRS and LRS is steady readout without abruptly changing at different bending conditions, suggesting that

data in devices are safely kept without loss. LRS slightly increases as the bending radius decreases due to the conductivity change of crack-based Au electrodes under mechanical force. The retention characteristics of both HRS and LRS under flat and bending conditions (photo inset is bending radius = 1.6 mm) were examined as shown in **Figure 4.9 d**. Resistance in HRS and LRS are well-separated at a readout voltage of 50 mV over 3600 s, and no noticeable resistance change for both non-bending and bending conditions, suggesting the great stability and reliability of DS-memristor in information storage under flexion.

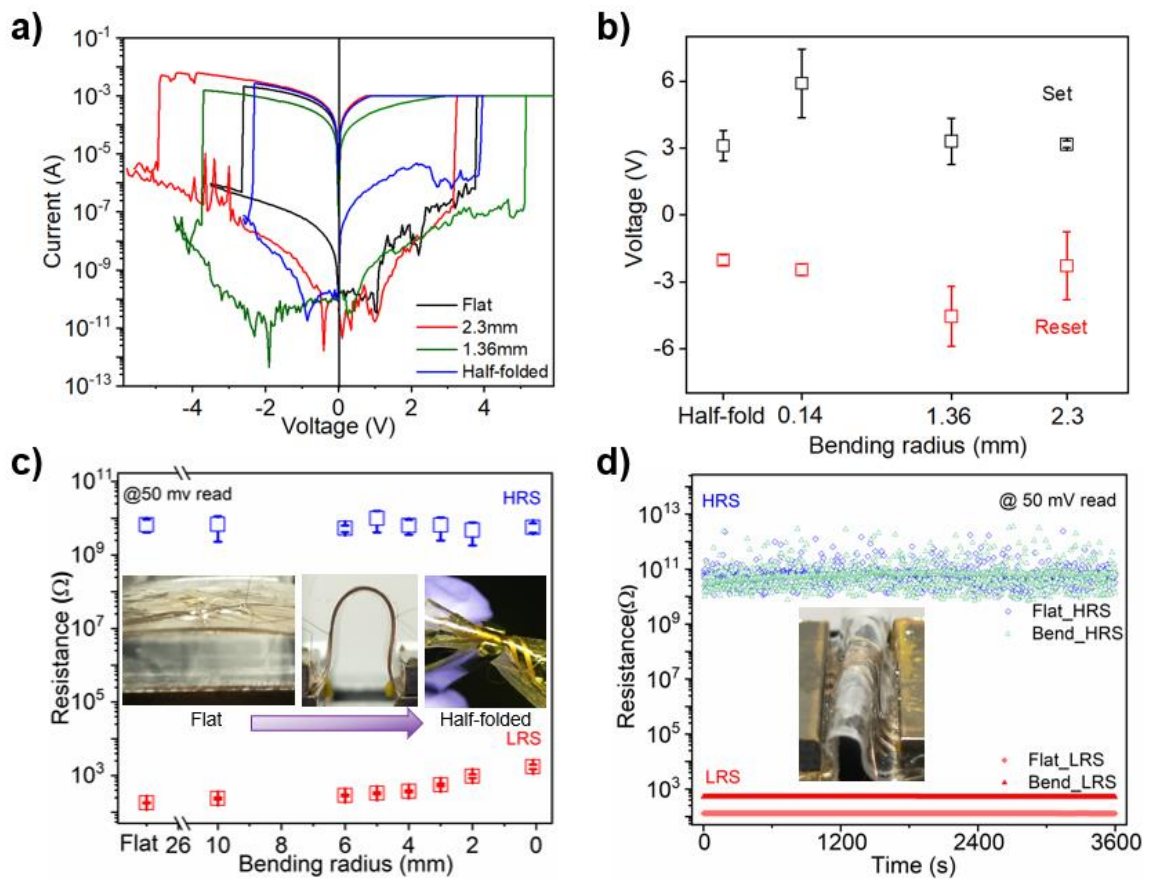


**Figure 4.9** Electrical performance of DS-memristor under flexion. (a) The  $I$ - $V$  characteristic of DS-memristor under different bending conditions. (b) Repeatability of set and reset voltages for DS-memristor under different bending conditions. (c) Two resistance state (HRS and LRS) under different bending radius from flat to half fold. (d) Retention characteristics of HRS and LRS under a continuous 50 mV readout voltage at flat and bending condition for 3600 s (bending radius = 1.6 mm).

### 4.3.2 Memristor stretchability

In addition to the flexibility, stretchability is another important mechanical adaptative property for wearable memristors. The  $I$ - $V$  characteristic of DS-memristor at various stretching states from 10% to 40% shows the devices can perform electrical functions of writing and erasing at different stretching states (**Figure 4.10 a**). The operation voltages for DS-memristors to set and reset are  $4 \pm 2$  V and  $-4 \pm 2$  V under different stretching conditions, indicating the performance of devices under stretching are stable and consistent (**Figure 4.10 b**). Meanwhile, the distribution of switching voltages for 10 devices indicate the good repeatability and consistency of device-to-device operation. The set voltage is  $3 \pm 1$  V and reset voltage is  $-3 \pm 1$  V (**Figure 4.10 c**).

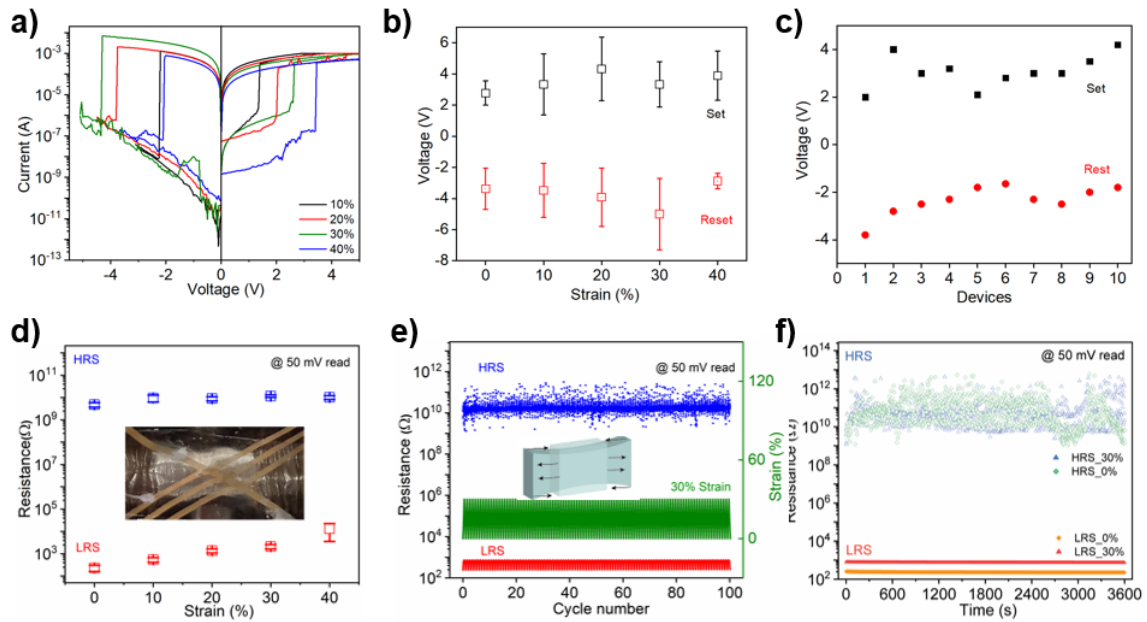


**Figure 4.10** Electrical performance of DS-memristor under tension. (a)  $I$ - $V$  characteristic of DS-memristor at various stretching states. (b) The operation voltages of device under different stretching. (c) Device to device distribution of operation voltages for setting and resetting. (d) Resistance reading for HRS and LRS at 50 mV readout voltage under different strains. (e) Two resistance states (HRS and LRS) under a continuous 50 mV readout voltage for 100 cycles of 30% stretch-release. (f) Retention characteristics of HRS and LRS under a continuous 50 mV readout voltage at strain of 0% and 30% for 3600 s.

The resistance at HRS and LRS under static stretching are well-separated manifests the DS-memristor excellent in storing information and can tolerate tensile force up to 40%

strain without data loss (**Figure 4.10 d**). Furthermore, the resistance of DS-memristor was evaluated at 50 mV simultaneously under dynamic motion by 30% strain loading and unloading for 100 cycles, both LRS and HRS are stable with a resistance OFF/ON ratio of  $10^7$ , indicating the information are stored robustly within the device under complex dynamic deformation (**Figure 4.10 e**). The resistance at LRS is varying with applied strain due to the resistance change of Au electrode on the SEBS substrate under various strain, which is consistent with electrodes of Au/SEBS under cyclic stretching-releasing in **Figure 4.7**. The retention characteristics of HRS and LRS at 0% and 30% strains in DS-memristor show no difference under a readout voltage of 50 mV, proving a good stability of DS-memristor under stretching condition over 3600 s (**Figure 4.10 f**).

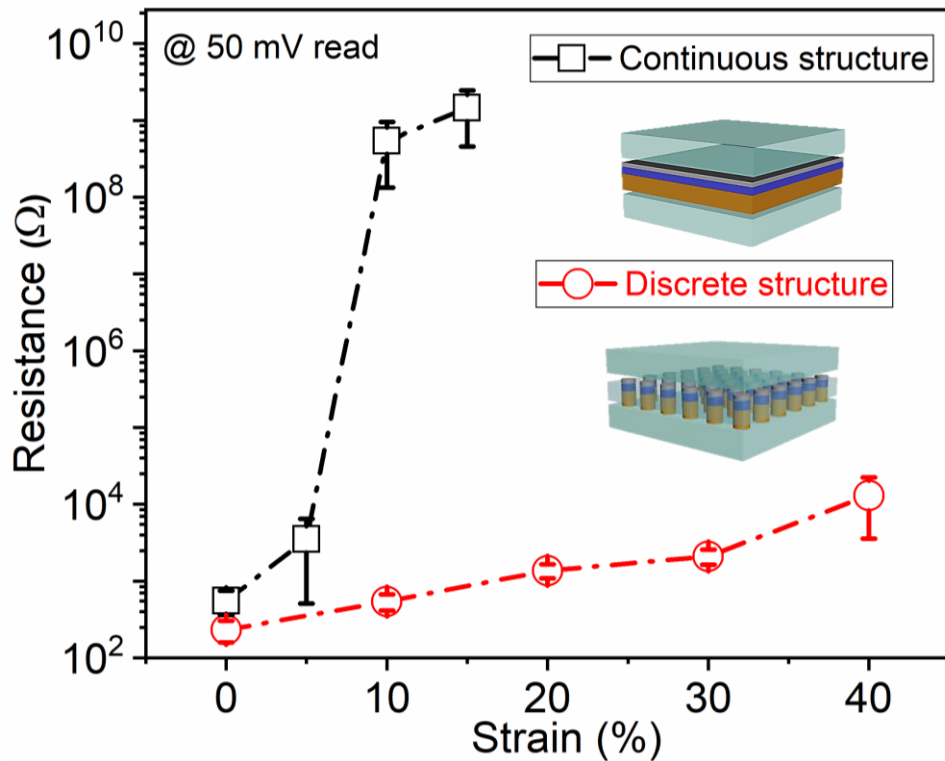


**Figure 4.11** The comparison of resistance at LRS in CS memristor and DS-memristor against applied strain.

In this work, we define the effective stretchability of the memristor as resistance value under stretching without changing more than 100 times as compared to original resistance  $R_0$  (namely,  $\Delta R < 100R_0$ ). Thus, the effective stretchability for CS-memristor is 10% as the resistance dramatically increases from  $10^3$  to  $10^9$  at the strain of 10%. However, the

effective stretchability of the DS-memristor is 40% as resistance increase much slower from  $10^3$  to  $10^4$  at the strain of 40%, indicating that the discrete structure has advantages on enhancing stretchability of memristor over continuous structure (**Figure 4.11**).

To investigate the underlying mechanism of stretchability enhancement by discrete structure. Finite element analysis (FEA) is employed to analyze the strain distribution of the continuous structure and the discrete structure on elastic substrate at 30% strain (**Figure 4.12**).

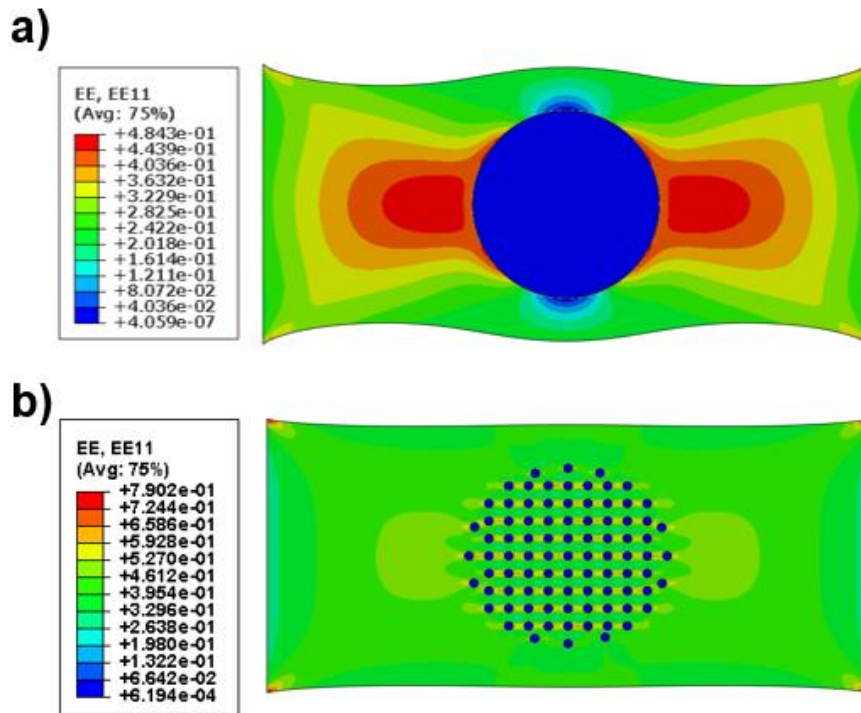


**Figure 4.12** Finite element simulations of strain distribution for (a) continuous structure, and (b) discrete structure on elastic substrate under 30% strains, respectively.

From FEA results, strain distribution for discrete structure on elastic substrate was much less concentrated than in that of the continuous structure, revealing the strain energy can be dissipated uniformly within discrete structure on elastomer. However, in the case of continuous structure, majority of strain energy is absorbed by the region of the elastomer in vicinity of the structure. That region that is absorbing large strain energy is the weakest area in entire system and more easily to reach the critical failure energy, leading to the integrity of device system rupture and electrical failure. This can explain why resistance

change largely and rapidly at LRS in CS-memristor at strain 10%, because large strain concentrate locally in the region of elastomer induces electrical failure of Au electrode and result in device failure. While the discrete structure can effectively alleviate locally strain energy concentration at the interface between device units and elastic substrate by uniformly distributing energy throughout the film, hence enhancing stretchability of memristor.

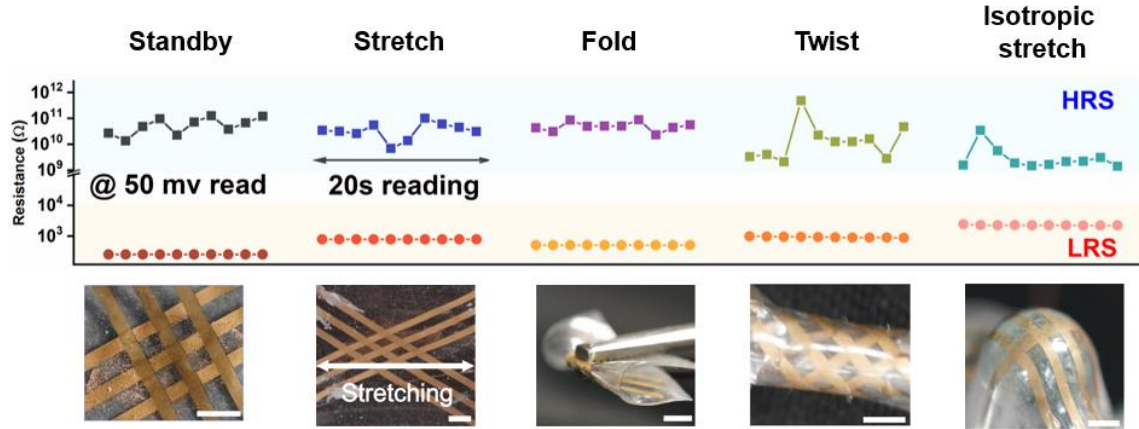


**Figure 4.13** HRS and LRS of DS-memristor under various mechanical deformations such as standby, stretching, half-folding, twisting, and isotropic stretching.

To demonstrate an overall mechanical adaptative property of DS-memristor, resistance of HRS and LRS are record at 50 mV for 20s under stretching, half-folding, twisting, and isotropic stretching (**Figure 4.13**). The HRS and LRS keep stable at resistance OFF/ON ratio of  $10^7$  for any mechanical deformations. Besides, the real-time reading of HRS and LRS under bending and twisting are shown in **Figure 4.14**, proving that the information in DS-memristor are robustly stored under various dynamic mechanical deformations. Some resistance fluctuation at LRS is attribute to the decrease conductivity of Au/SEBS electrodes during bending and twisting of device.

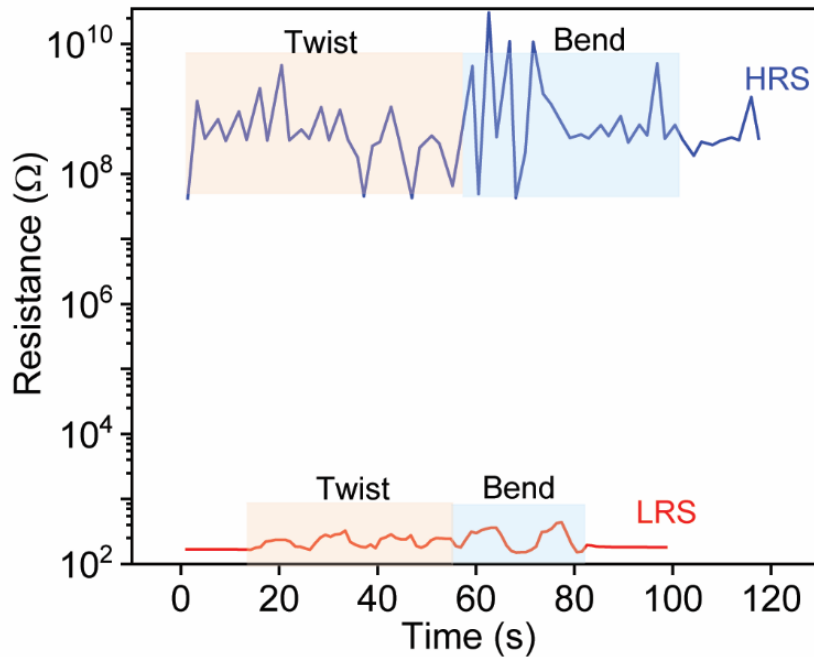


**Figure 4.14** Real-time reading of HRS and LRS in a DS-memristor under the twisting and bending deformations. Some fluctuation in LRS come from the Au electrode resistance during the twist and bend.

#### 4.4 Conclusion

In this chapter, we employed a discrete structure to confer memristors with outstanding mechanical adaptative properties. The conventional inorganic active layer of continuous bulky structure is brittle and rigid, which has limit stretchability of 10% and cannot tolerate with bending force. The discrete structure based memristors have excellent conformability for large mechanical deformations such as half-fold and large strain (~40%), while remaining electrical functions in terms of data writing, erasing, and storage no matter in a static state or dynamic movement. The discrete structure can significantly enhance stretchability and flexibility of memristors by effectively reducing strain concentration at the interface between the rigid active units and the soft substrate via dissipating strain energy uniformly throughout the film, and hence improving the mechanical adaptative properties of stretchable memristors. This strategy is compatible with current exiting semiconductor fabrication technologies and promising to apply it to other similar two terminal devices with similar structure for wearable devices applications.

## References

- [1] A. Nag, S. C. Mukhopadhyay, J. Kosel, *IEEE Sens. J.* **2017**, *17*, 3949.
- [2] T. Q. Trung, N.-E. Lee, *Adv. Mater.* **2016**, *28*, 4338.
- [3] A. Chortos, Z. Bao, *Mater. Today* **2014**, *17*, 321.
- [4] W. W. Lee, Y. J. Tan, H. Yao, S. Li, H. H. See, M. Hon, K. A. Ng, B. Xiong, J. S. Ho, B. C. K. Tee, *Sci. Robot.* **2019**, *4*, eaax2198.
- [5] Y. Liu, M. Pharr, G. A. Salvatore, *ACS Nano* **2017**, *11*, 9614.
- [6] M. Cianchetti, C. Laschi, A. Menciassi, P. Dario, *Nat. Rev. Mater.* **2018**, *3*, 143.
- [7] S. I. Rich, R. J. Wood, C. Majidi, *Nat. Electron.* **2018**, *1*, 102.
- [8] G. P. T. Choi, L. H. Dudte, L. Mahadevan, *Nat. Mater.* **2019**, *18*, 999.
- [9] C. Pang, G.-Y. Lee, T.-i. Kim, S. M. Kim, H. N. Kim, S.-H. Ahn, K.-Y. Suh, *Nat. Mater.* **2012**, *11*, 795.
- [10] M. Vosgueritchian, D. J. Lipomi, Z. Bao, *Adv. Funct. Mater.* **2012**, *22*, 421.
- [11] Y. Wang, C. Zhu, R. Pfattner, H. Yan, L. Jin, S. Chen, F. Molina-Lopez, F. Lissel, J. Liu, N. I. Rabiah, Z. Chen, J. W. Chung, C. Linder, M. F. Toney, B. Murmann, Z. Bao, *Sci. Adv.* **2017**, *3*, e1602076.
- [12] J. Y. Oh, D. Son, T. Katsumata, Y. Lee, Y. Kim, J. Lopez, H.-C. Wu, J. Kang, J. Park, X. Gu, J. Mun, N. G.-J. Wang, Y. Yin, W. Cai, Y. Yun, J. B. H. Tok, Z. Bao, *Sci. Adv.* **2019**, *5*, eaav3097.
- [13] G.-J. N. Wang, A. Gasperini, Z. Bao, *Adv. Electron. Mater.* **2018**, *4*.
- [14] J. Xu, S. Wang, G.-J. N. Wang, C. Zhu, S. Luo, L. Jin, X. Gu, S. Chen, V. R. Feig, J. W. F. To, S. Rondeau-Gagné, J. Park, B. C. Schroeder, C. Lu, J. Y. Oh, Y. Wang, Y.-H. Kim, H. Yan, R. Sinclair, D. Zhou, G. Xue, B. Murmann, C. Linder, W. Cai, J. B. H. Tok, J. W. Chung, Z. Bao, *Science* **2017**, *355*, 59.
- [15] J. Park, Y. Lee, J. Hong, M. Ha, Y.-D. Jung, H. Lim, S. Y. Kim, H. Ko, *ACS Nano* **2014**, *8*, 4689.
- [16] R. Rahimi, M. Ochoa, W. Yu, B. Ziaie, *ACS Appl. Mater. Interfaces* **2015**, *7*, 4463.
- [17] T. Yamada, Y. Hayamizu, Y. Yamamoto, Y. Yomogida, A. Izadi-Najafabadi, D. N. Futaba, K. Hata, *Nat. Nanotechnol.* **2011**, *6*, 296.
- [18] M. Hempel, D. Nezich, J. Kong, M. Hofmann, *Nano Lett.* **2012**, *12*, 5714.

- [19] X. Li, R. Zhang, W. Yu, K. Wang, J. Wei, D. Wu, A. Cao, Z. Li, Y. Cheng, Q. Zheng, R. S. Ruoff, H. Zhu, *Sci. Rep.* **2012**, 2, 870.
- [20] Y. Liu, D. Zhang, K. Wang, Y. Liu, Y. Shang, *Composites Part A: Appl. Sci. Manuf.* **2016**, 80, 95.
- [21] M. D. Bartlett, A. Fassler, N. Kazem, E. J. Markvicka, P. Mandal, C. Majidi, *Adv. Mater.* **2016**, 28, 3726.
- [22] M. D. Dickey, in *Stretchable Bioelectronics for Medical Devices and Systems*, (Eds: J. A. Rogers, R. Ghaffari, D.-H. Kim), Springer International Publishing, Cham **2016**, 3.
- [23] X. Yan, Z. Liu, Q. Zhang, J. Lopez, H. Wang, H. C. Wu, S. Niu, H. Yan, S. Wang, T. Lei, J. Li, D. Qi, P. Huang, J. Huang, Y. Zhang, Y. Wang, G. Li, J. B. Tok, X. Chen, Z. Bao, *J. Am. Chem. Soc.* **2018**, 140, 5280.
- [24] Y. Sun, W. M. Choi, H. Jiang, Y. Y. Huang, J. A. Rogers, *Nat. Nanotechnol.* **2006**, 1, 201.
- [25] Y. Zhang, S. Xu, H. Fu, J. Lee, J. Su, K. C. Hwang, J. A. Rogers, Y. Huang, *Soft Matter* **2013**, 9, 8062.
- [26] D. H. Kim, J. Xiao, J. Song, Y. Huang, J. A. Rogers, *Adv. Mater.* **2010**, 22, 2108.
- [27] K. Bertoldi, V. Vitelli, J. Christensen, M. van Hecke, *Nat. Rev. Mater.* **2017**, 2, 17066.
- [28] S. J. P. Callens, A. A. Zadpoor, *Mater. Today* **2018**, 21, 241.
- [29] L. Mahadevan, S. Rica, *Science* **2005**, 307, 1740.
- [30] M. Schenk, S. D. Guest, *PNAS* **2013**, 110, 3276.
- [31] Y. Tang, G. Lin, S. Yang, Y. K. Yi, R. D. Kamien, J. Yin, *Adv. Mater.* **2017**, 29, 1604262.
- [32] P. Won, J. J. Park, T. Lee, I. Ha, S. Han, M. Choi, J. Lee, S. Hong, K.-J. Cho, S. H. Ko, *Nano Lett.* **2019**, 19, 6087.
- [33] Y. Zhang, Z. Yan, K. Nan, D. Xiao, Y. Liu, H. Luan, H. Fu, X. Wang, Q. Yang, J. Wang, W. Ren, H. Si, F. Liu, L. Yang, H. Li, J. Wang, X. Guo, H. Luo, L. Wang, Y. Huang, J. A. Rogers, *PNAS* **2015**, 112, 11757.
- [34] Y. Jiang, Z. Liu, N. Matsuhisa, D. Qi, W. R. Leow, H. Yang, J. Yu, G. Chen, Y. Liu, C. Wan, Z. Liu, X. Chen, *Adv. Mater.* **2018**, 30, e1706589.
- [35] J. J. Yang, D. B. Strukov, D. R. Stewart, *Nat. Nanotechnol.* **2013**, 8, 13.

- [36] T.-C. Chang, K.-C. Chang, T.-M. Tsai, T.-J. Chu, S. M. Sze, *Mater. Today* **2016**, *19*, 254.
- [37] D.-H. Kwon, K. M. Kim, J. H. Jang, J. M. Jeon, M. H. Lee, G. H. Kim, X.-S. Li, G.-S. Park, B. Lee, S. Han, M. Kim, C. S. Hwang, *Nat.Nanotechnol.* **2010**, *5*, 148.
- [38] Y. Hou, U. Celano, L. Goux, L. Liu, A. Fantini, R. Degraeve, A. Youssef, Z. Xu, Y. Cheng, J. Kang, M. Jurczak, W. Vandervorst, *Appl. Phys. Lett.* **2016**, *108*.
- [39] Jyoti, R. Kaur, S. Singh, J. Sharma, S. K. Tripathi, *J. Electron. Mater.* **2019**, *48*, 5995.
- [40] J. Shang, W. Xue, Z. Ji, G. Liu, X. Niu, X. Yi, L. Pan, Q. Zhan, X. H. Xu, R. W. Li, *Nanoscale* **2017**, *9*, 7037.

## Chapter 5\*

### **Mechanical Damages Endurance of Discrete Structure Based Devices on Elastic Substrate**

*Stretchable electronics in applications request them to keep electrical properties under complex situations which consist of mechanical deformations and mechanical damages from environment. Large research works emphasis on mechanical deformation adaptation, however, rarely focus on devices tolerating with mechanical damages. The previous chapter has demonstrated that discrete structure based memristors excel in accommodating to mechanical deformations. This chapter mainly present the how this discrete structure imparts the mechanical damages endurance to stretchable memristors. The results show that discrete structure based memristor can work properly under the cut and puncture damages without losing memristor functions. Even in an extreme condition such as consecutive 100 times of punctures or fully cut of a working cell, stretchable memristor can retain normal electrical functions. Lastly, the discrete structure based memristor was punctured with spine of cactus as a demonstration for a real-world application.*

## 5.1 Introduction

In the era of big data, high velocity and huge volume of data are generated from mobile individuals and subjects, which bring pressure to the center servers in cloud. The edge computing becomes an emerging technology to reduce workload in cloud by dealing with real-time data locally at edge devices.<sup>[1-2]</sup> Wearable devices and skin electronics are the most promising candidates for edge devices as they are compact and portable, which provide instantaneous point of care monitoring for healthcare and diagnosis,<sup>[3-5]</sup> continuous motion detection<sup>[6-8]</sup> and is a flexible platform for Internet of Things (IoTs).<sup>[9-12]</sup> Currently, numerous researches emphasis on improving the stretchability and flexibility of wearable devices to make it adaptable to mechanical deformation,<sup>[13-21]</sup> rare attention has been paid on devices endurance against mechanical damages.<sup>[22-26]</sup> However, wearable devices in practical are facing to a dynamic environment that consists of not only complex mechanical forces but also uncertainties such as extreme temperature, moisture attacks, or accidentally mechanical damages. Thereinto, mechanical damages are the most happened and unforeseen in applications. For instance, wearable devices may suffer accidental scratch or cut in outdoor activities. Soft robots designed for executing tasks in extreme environments require to tolerate unexpected damages such as piercing or puncture from sharp objects. For wearable electronics, stretchable memristor is an indispensable component for data processing and storage. Thus, to develop a wearable memristor that is mechanically conformable and mechanical damage durable is vital and desirable to apply it in real-world situation.

The most common architecture of traditional memristors are metal/insulator/metal (MIM) sandwich structure.<sup>[27-29]</sup> The insulator between two metal electrodes is the active layer involving a semiconductive material with a block of continuous structure that is much fragile and vulnerable to mechanical deformation and damages. The fracture easily happened in the continuous structure under mechanical deformation or damages, result in device functional failure and data loss, which is devastating destroy for memristor in application. Therefore, it is challenge to develop memristors to maintain a good electrical performance under various physical deformations for wearable applications and mechanical damage endurance against attacks from environment.

In chapter 4, the discrete structure based stretchable memristor (DS-memristor) have been demonstrated that can function well under various mechanical deformation. Based on this discrete structure design, it has been further investigated and proved as an effective strategy for the DS-memristors to tolerate mechanical damages such as puncture and cut, which is quite significant for wearable memristors to be applied in an extreme condition or harsh environment.

## 5.2 Principal outcomes

### 5.2.1 Mechanical damages endurance of elastic substrate

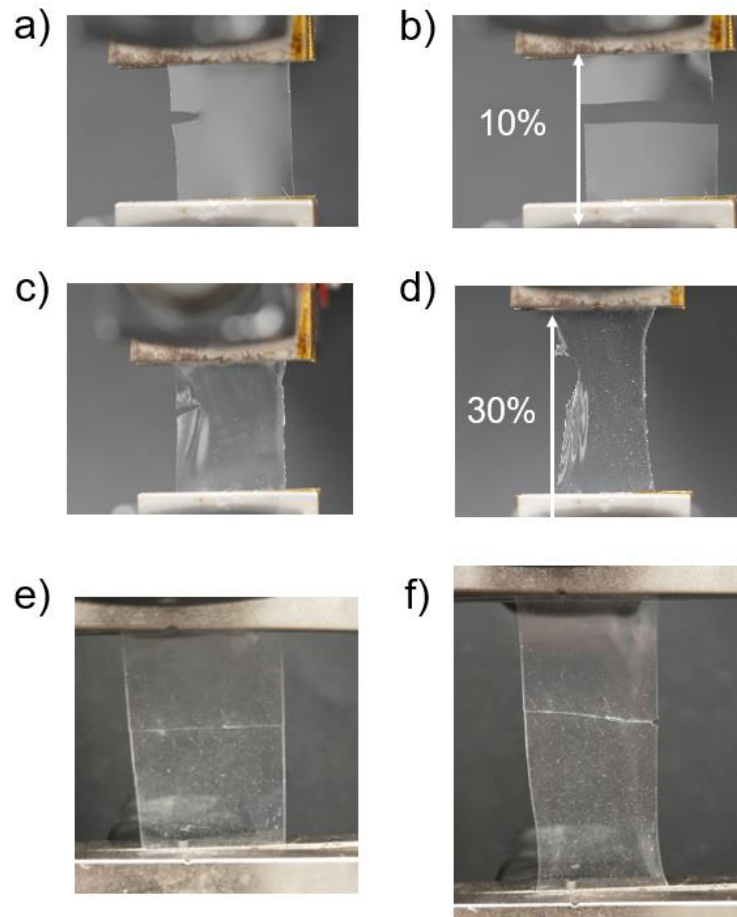


**Figure 5.1** Comparison of mechanical behaviors of PDMS and SEBS under cut damage. (a) PDMS substrate with an induced notch. (b) PDMS substrate with a notch can only be stretched to 10% and rupture. (c) SEBS substrate with an induced notch. (d) SEBS with a notch can be stretched to 30% without rupture. (e) SEBS film is fully cut and healed at initial state (0% strain). (f) SEBS after self-healing can be stretched to 40% without break.

PDMS is one of most popular substrates to be used in flexile electronics. However, PDMS is a notch-sensitive polymer that forms sharp tip at the notch and easily rupture when there is a notch with it<sup>[22, 30]</sup> (**Figure 5.1 b**). Thus, PDMS is not a good substrate in our system for memristors with mechanical damage endurance. In contrast, SEBS is fracture-toughness in nature and a notch-insensitive polymer. The notch in SEBS is blunted (**Figure 5.1 d**) that greatly reduce the strain concentration on the notch tip, retard the crack propagation and avoid the substrate rupture.<sup>[31-33]</sup> Besides, SEBS<sup>[34-36]</sup> has certain autonomous self-healing property that can be healed from fully cut and remains the stretchability up to 70%.

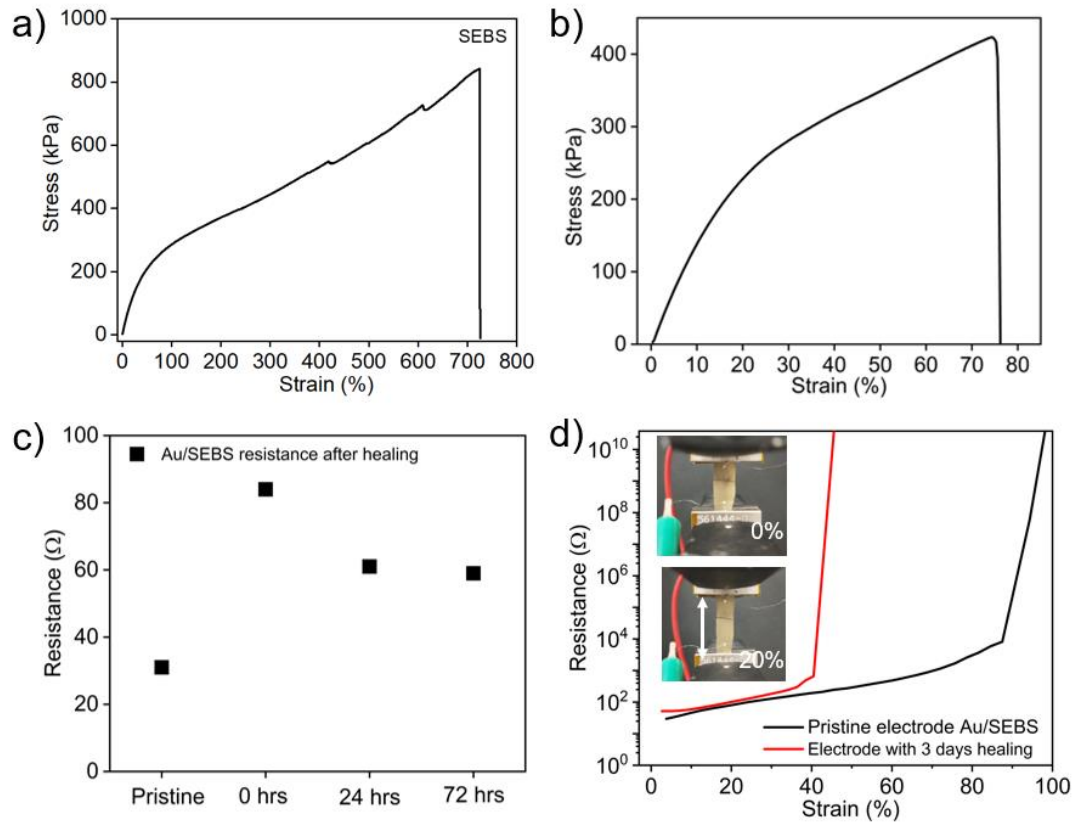


**Figure 5.2** Mechanical property of SEBS and electromechanical properties of Au/SEBS electrode without fully cut and fully cut with self-healing. (a) Stress-strain curve of SEBS film with large stretchability of >700%. (b) stress-strain curve for SEBS after self-healing from fully cut, the stretchability after self-healing remain as large as 70%. (c) Resistance of electrode Au/SEBS before cut and after cut, and healing for 3 days. (d) electromechanical properties of electrode Au/SEBS before cut and after cut with 3 days healing.

To investigate the SEBS self-healing property, we cut the SEBS fully and allow it to heal for one night. SEBS film before cut can be stretched more than 700% (**Figure 5.2 a**). After fully cut and heal, SEBS film can be stretched up to 70% (**Figure 5.2 b**). The electrode was fabricated by depositing Au on the SEBS and can be stretched to 80% (**Figure 5.2 c**). A fully cut was made on the electrode, and the two cut pieces were physically in contact with a good alignment. The conductive network was able to reconnected and gradually decrease over time to reach stable after 3 days, suggesting that the reconstruction of Au thin film due to the autonomous self-repair capability of SEBS.<sup>[37]</sup> The electrode was able to recover 40% of stretchability after 3 days of self-healing, which was reflected by the recovery of electrical performance (**Figure 5.2 d**). Because of fracture-toughness and self-healing properties, SEBS is suitable for our memristor system for mechanical damage endurance.

### 5.2.2 Puncture endurance of stretchable memristors

In real-world situation, devices in service are often attacked by mechanical damages from the environment, such as unexpected cut damage, or encounter extreme condition with sharp objects. To compare the mechanical damage behavior difference between the continuous structure discrete structure, both CS-memristor and DS-memristor were fabricated in same condition with same materials and punctured with a sharp insulative pin. The schematic diagram in **Figure 5.3(a)** shows the active layer in CS-memristor is broken and forming large cracks. The optical microscopic image of the real sample in **Figure 5.3 (b)**, CS-memristor after puncture and removing pin, a large hole was apparently left behind with cracks around it, indicating that the continuous structure is serious destroy by pin puncture. In the case of DS-memristor, the schematic diagram in **Figure 5.3 (c)** conceptual describe that the discrete units right round the pin have mobility to move or rotate so that it escapes from penetration. This phenomenon is likely happened in small wood cubes floating in liquid and being poked by a stick. The wood cubes float away from stick. The optical microscopic image of DS-memristor after the puncture is shown in **Figure 5.3 (d)**. A scar (dark area) was left on the SEBS surface. When zoom in the view, the discrete units remain intact with no noticeable cracks, indicating that discrete structure are undamaged after pin puncture (**Figure 5.3 e**).

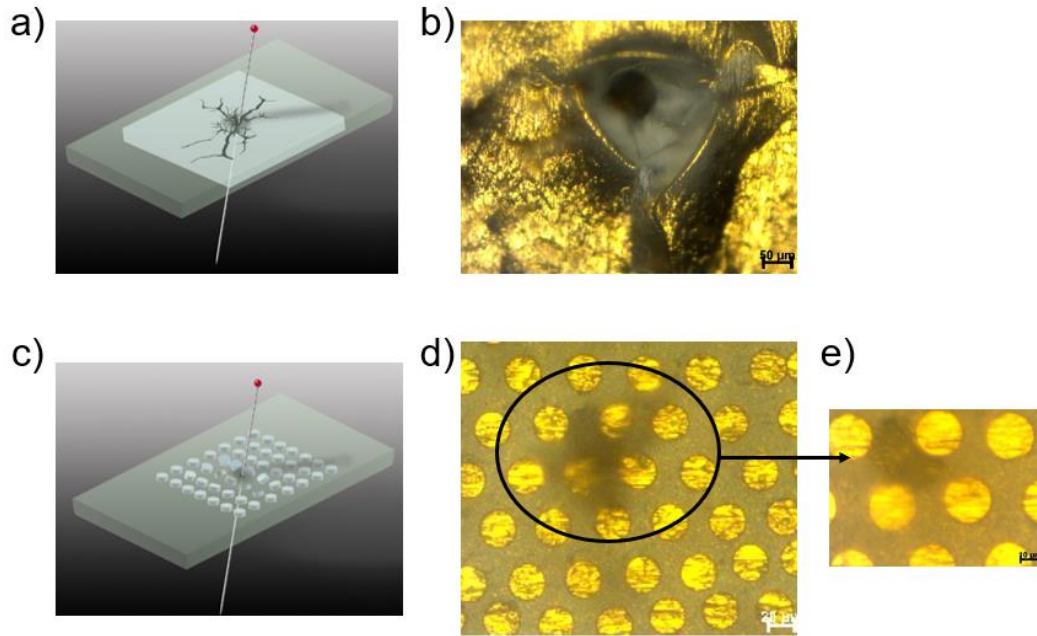


**Figure 5.3** Schematic of continuous structure (a) and discrete structure (c) under puncture damage. Optical microscope images for devices with continuous structure(b) and discrete structure(d) after puncture with pin removal. (e) Magnification image of discrete units around the pin scar are intact without a good condition.

Further investigation is conducted to see the electrical performance of CS-memristor and DS-memristor after pin puncture. The  $I$ - $V$  curve of CS-memristor and DS-memristor further proves that structure destruction directly threatens the memristor electrical function. CS-memristor after puncture is completely losing functions of data writing and erasing (**Figure 5.4 b**). DS-memristor after the puncture in **Figure 5.4 (a)** shows the device functions as normal. The set and reset voltage for DS-memristor before piercing is 4 V and -4 V, respectively. After puncturing, the set and reset voltage is 3 V and -7.8V, respectively.

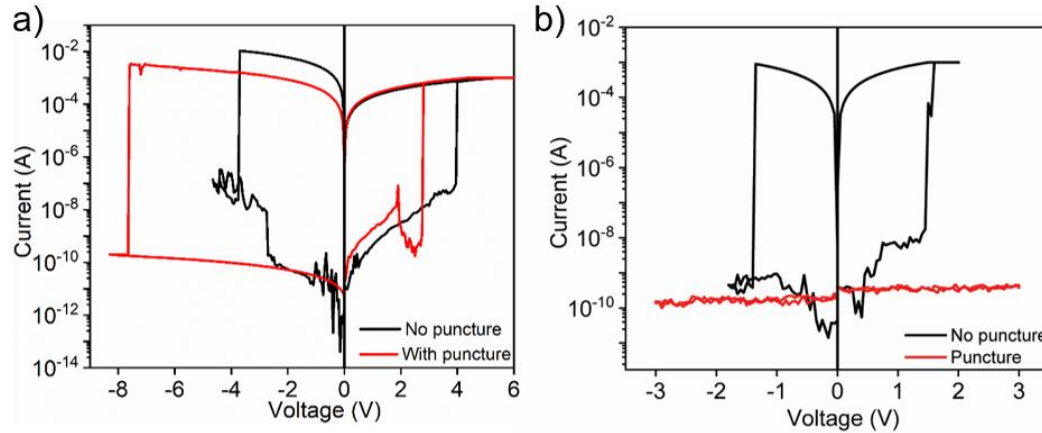


**Figure 5.4** Comparison of I-V characteristics for discrete structure based memristor and continuous structure based memristor before and after pin puncture. (a) The I-V curve of DS-memristor before and after puncture. (b) The I-V curve of CS-memristor before and after puncture.

Moreover, the electrical performance and the stretchability of DS-memristor was examined under the puncture condition. The resistance at HRS and LRS for the DS-memristor with a working cell punctured by pin was measured under uni-axial strain as shown in **Figure 5.5 (a)**. The effective stretchability of the DS-memristor with pin puncture is 40%. No decline in the electrical performance and stretchability as compared to non-punctured DS-memristor which has been discussed in chapter 4 (**Figure 4.10 d**), showing that puncturing does not affect the electrical and mechanical performance of the device. Furthermore, reading of HRS and LRS for pin-punctured DS-memristor was continuously recording at a dynamic motion by consecutive 30% stretching-releasing for 100 cycles (**Figure 5.5 b**), no abrupt change were detected suggest that information is stable kept within pin-punctured working cell of DS-memristor.

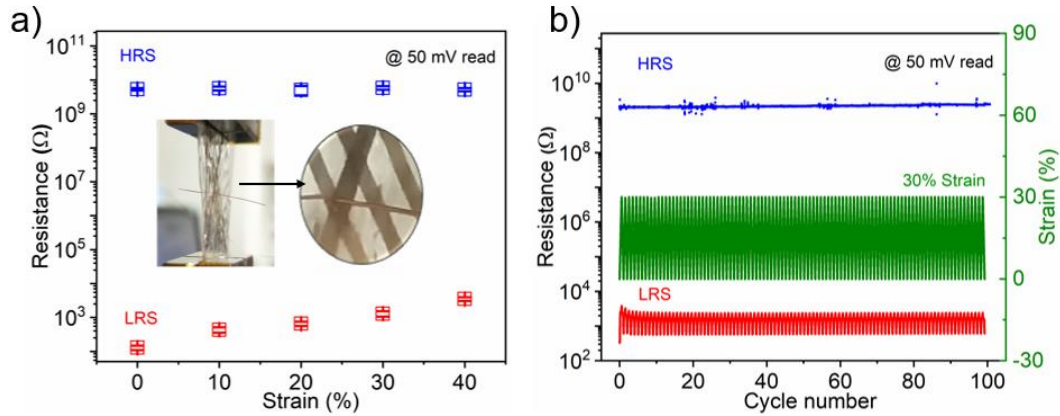


**Figure 5.5** Electrical performance of DS-memristor with pin puncture at static and dynamic conditions. (a) Resistance state of DS-memristor versus strain. (b) Resistance state of DS-memristor under 50 mV readout voltage for 1000 cycles of stretching-releasing.

Next, we further exam the electrical performance of DS-memristor at an extreme damage condition. A working cell of DS-memristor was punctured consecutively by an insulative pin as shown in **Figure 5.6 (a)**. The HRS and LRS were recorded after every 5 punctures. From the reading in HRS and LRS, there no abnormal and abrupt change showing no information loss in device during puncture process. The  $I$ - $V$  curve of pin-punctured DS-memristor at 25 times, 50 times and 100 times proves that device maintains a good memory functions of information writing and erasing (**Figure 5.6 b**). The device surface is full of pin scars after being punctured by 50 times and 100 times are shown in optical images in **Figure 5.6 c** and **Figure 5.6 d**, respectively.

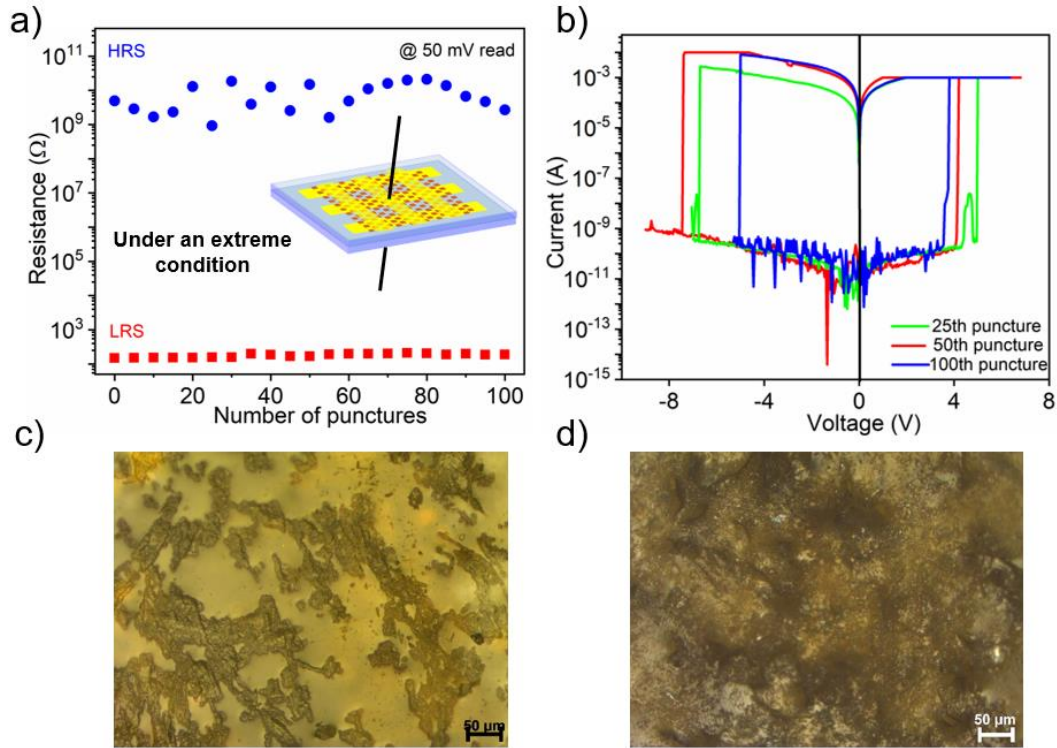


**Figure 5.6** Electrical performance of DS-memristor at extreme puncture damage condition. (a) The reading of HRS and LRS in DS-memristor with consecutive punctures up to 100 times. (b) The I-V curve of DS-memristor after undergoing 25th, 50th, and 100th puncture. (c-d) The optical images of DS-memristor after being punctured 50 and 100 times.

To understand the underlying mechanism of discrete structure contributing to puncture damage endurance. The FEA simulation was conducted to analyze the displacement of discrete units during puncture process. We set up model based on the real sample size with diameter of 25  $\mu\text{m}$  and space distance of 35  $\mu\text{m}$ . The pin has a sharp tip (tip angle is 20 degree) and body diameter of pin is 120  $\mu\text{m}$ , which is much larger than the diameter of discrete units (**Figure 5.7**). In virtue of coupled Eulerian-Lagrangian technique (CEL), the displacement of the discrete units was simulated and providing insights into their kinematic behaviors during the puncture, revealing discrete units evasive action from the sharp pin.

As shown in **Figure 5.7**, a rectangular region of  $6D \times 3\sqrt{3}D$  (720  $\mu\text{m} \times 623.5 \mu\text{m}$ ) is simulated, where  $D = 120 \mu\text{m}$  is the diameter of the pin. The thickness  $T$  of the SEBS substrate is 702  $\mu\text{m}$ . A hexagonally arranged array of Au pillars with diameter  $d$ , thickness  $t$  and centre to centre distance  $l$  of 25  $\mu\text{m}$ , 5  $\mu\text{m}$  and 60  $\mu\text{m}$  are placed on the middle plane of the substrate. A Eulerian space of 720  $\mu\text{m} \times 623.5 \mu\text{m} \times 1400 \mu\text{m}$  is built to accommodate

the large deformation of the substrate during the puncture. The pin is simulated as a rigid cylindrical shell with the tip cut by a plane whose normal vector forms a 60-degree angle between the axial direction.

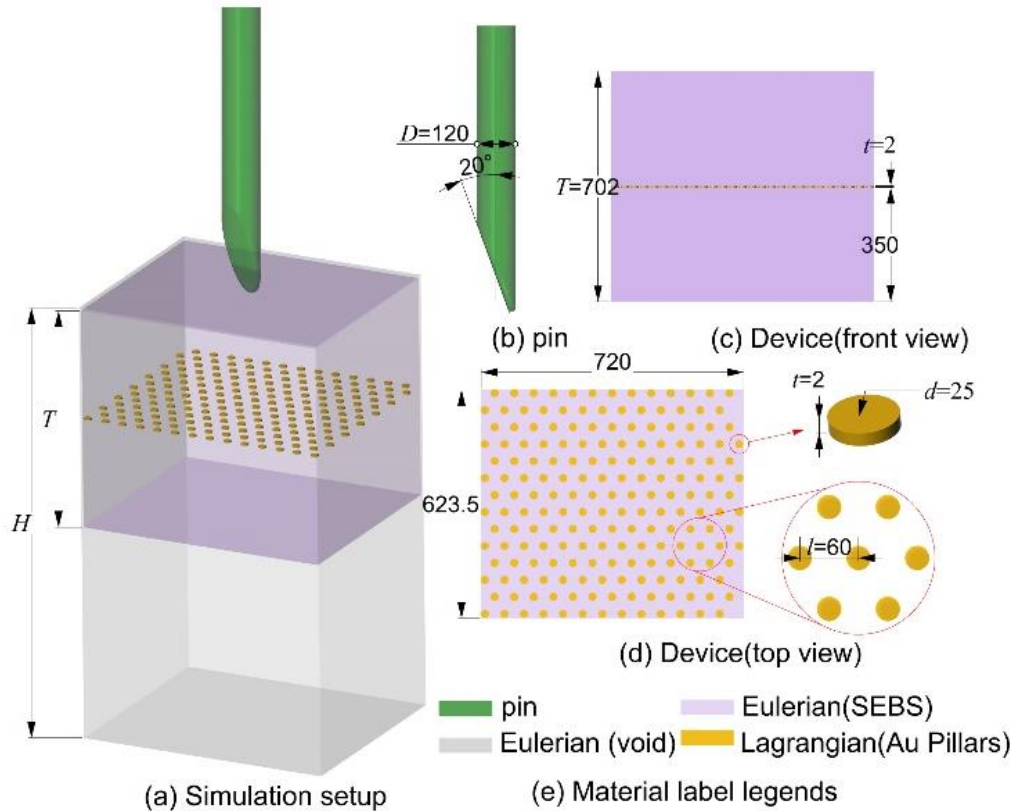


**Figure 5.7** Schematic of the model setup for the FEA simulation. (a) The model setup. (b) Dimension of the pin. (c) Front view of the device. (d) Top view of the device, insets of the dimension of the Au pillar and the hexagonal arrangement. (e) The legends that indicate the material in the model.

In this FEA simulation, the Au pillars were modelled as linear elastic material with Lagrangian formulation with parameters  $\rho_{Au} = 19.32 \text{ g/cm}^3$ ,  $E = 79 \text{ GPa}$ ,  $\nu = 0.42$ . The large strain nonlinear behaviour of SEBS was modelled as hyperelastic material by two term Mooney-Rivlin Model, with  $C_{10} = 337.8 \text{ kPa}$ ,  $C_{01} = 83.4 \text{ kPa}$ ,  $D_1 = 9.6e - 6 \text{ kPa}^{-1}$ . The density of SEBS was set as  $\rho_{SEBS} = 1.3 \text{ g/cm}^3$ . The pin was simulated as rigid shell. The boundary conditions are set as fixed in all direction on the four lateral planes of the model, and a gradually increased smooth downward velocity for the pin with the final displacement on Z direction of 1400  $\mu\text{m}$  within 0.1s and an average velocity of

0.14m/s. From the FEA simulation result, the motion of the Au units during the puncture shows an escape behaviour of those units. The Au units that are “floating” in the SEBS substrate “flow” accordingly to the deformation of the SEBS, which effectively eliminates most of the direct contact between the pillars and pin.

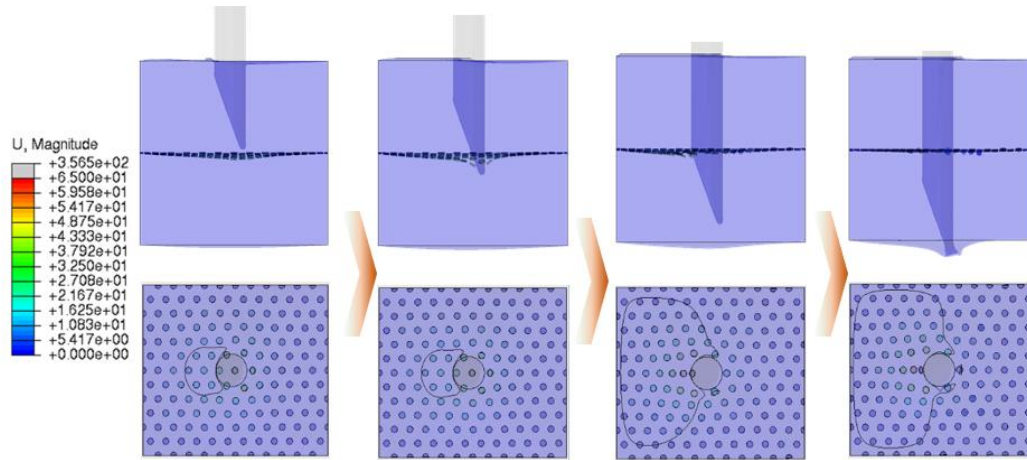


**Figure 5.8** Finite element analysis simulations of displacement of discrete structure units during the whole pin puncture process.

FEA simulations as shown in **Figure 5.8** give us further insight into the processes of how the discrete units escape sharp pin from initial state to the end. The four FEA results at the top are the front views of the pin that start at four different states, from approaching position until passing through the units. The four simulation results at the bottom are top view accordingly. The escape behavior of discrete units ascribes the large Young’s modulus difference between discrete units and substrate. The pillars consist of major Au ( $\sim 2\mu\text{m}$ ) and minor  $\text{HfO}_2/\text{Ag}$  ( $\sim 20\text{nm}$ ). Taking the Young’s modulus of pillars as Au (50-78GPa), and SEBS is a highly viscoelastic polymer with Young’s modulus of 0.1Mpa. As pillars are embedded into SEBS, the pillars are well-protected by the surrounding SEBS in the case of the puncture. From the FEA simulation results, the pillars in vicinity of the pin tip have some mobility to move away and self-spin that are artful escape from the puncture. This is explaining the reason why the discrete units around the pin hole keep intact from the puncture.

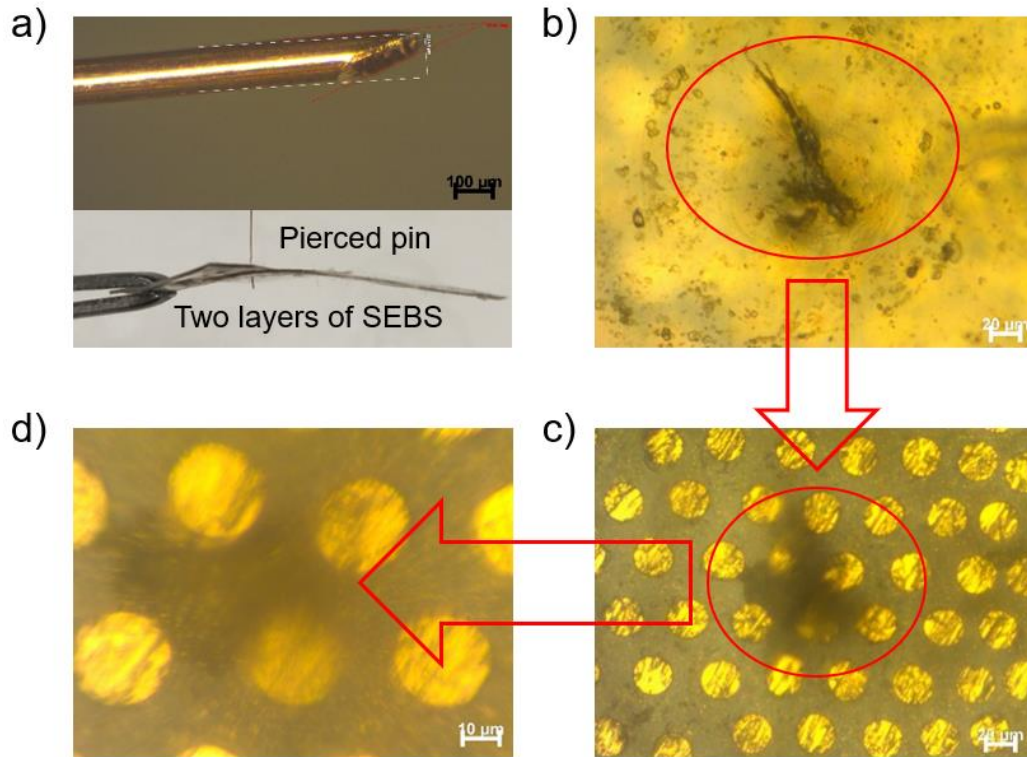


**Figure 5.9** Optical image of pin and discrete units after puncture. (a) Optical images of pin with a sharp tip and photos of cross-view of punctured DS-memristor. (b) The surface of memristor with a pin scar after pin puncture and removal. (c) The optical image of discrete units after puncture. The dark area is where pin had been punctured. (d) Magnification of optical image of discrete units around the pin scar.

After underlying the evasive behavior of discrete structure under pin puncture by FEA simulation. The optical images were taken to further verify the condition of discrete units after pin puncture. Because the pin diameter is  $120\ \mu\text{m}$  and discrete units is  $25\ \mu\text{m}$ , the area of being punctured by pin should cover several discrete units. If there is no movement on the discrete units during puncture, the units' structure should be damage by the pin. From optical images in **Figure 5.9 (c)**, the discrete units around pin scar have blur shape. After zoom in the image in **Figure 5.9 (d)**, the edge of discrete units is clear and undamaged. The blur view in the images due to uneven of surface caused by SEBS large deformation after puncture. This further proves that discrete units float with SEBS deformation and hence escape from piercing.

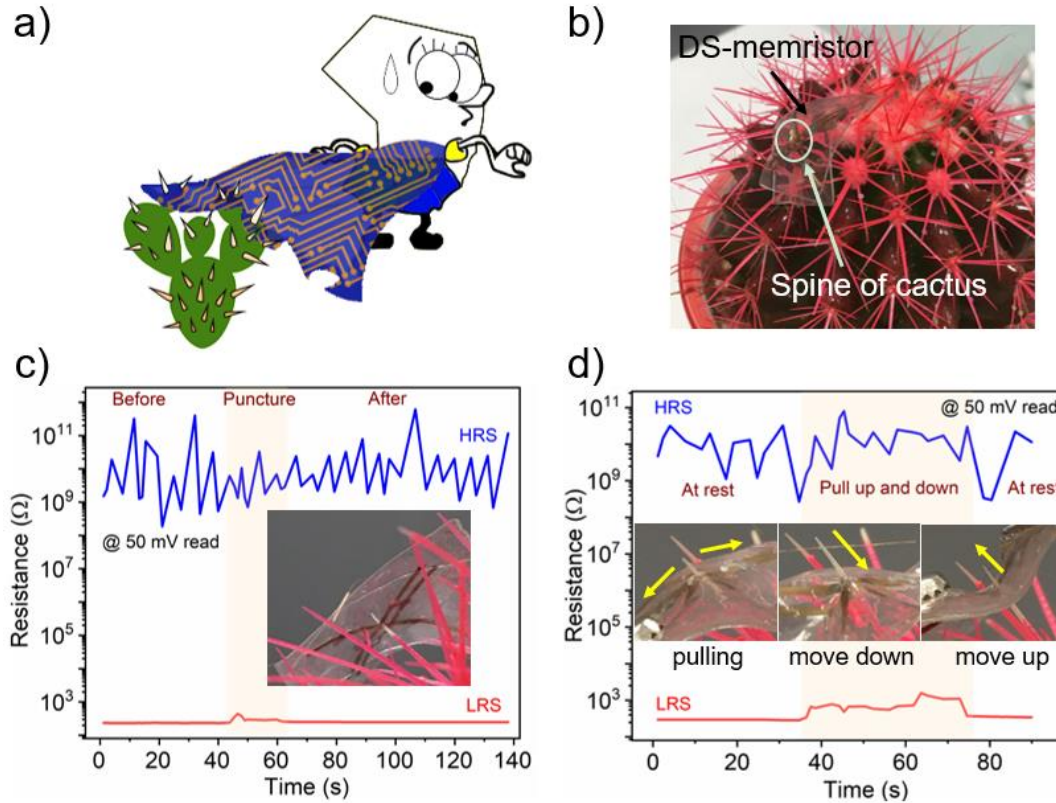


**Figure 5.10** Demonstration of DS-memristor performance in real application. (a) Schematic scenario of wearable device encounter puncture by sharp thorn in wild. (b) A working cell of DS-memristor is punctured by a sharp spine of cactus. (c) Real-time resistance record of HRS and LRS when DS-memristor is punctured with sharp spine of cactus. (d) Real-time resistance record of HRS and LRS after DS-memristor being punctured and drag device up and down along the spine of cactus.

One possible scenario for wearable devices suffering from scratch or puncture easily is outdoor activities (**Figure 5.10 a**). To demonstrate the DS-memristor performance in the wild, we employed a sharp spine of the cactus as a proof-of-concept (**Figure 5.10 b**). We punctured a working cell of DS-memristor with a sharp spine of the cactus and record the resistance simultaneously during whole puncture process. The real-time resistance reading of HRS and LRS are stable without abrupt changes, indicating information is store robustly during the puncture. Furthermore, we involved a dynamic motion by pulling the DS-memristor up and down along the spine of the cactus, the resistance reading has no abrupt change except for small fluctuation in LRS, which is caused by the conductivity change of Au electrode during the pulling, which is consistent with result in chapter 4 (**Figure 4.7**).

The demo strongly proves that the DS-memristor has ability to store information robustly under puncture damage in a dynamic harsh environment for real application.

### 5.2.3 Tear endurance of stretchable memristors

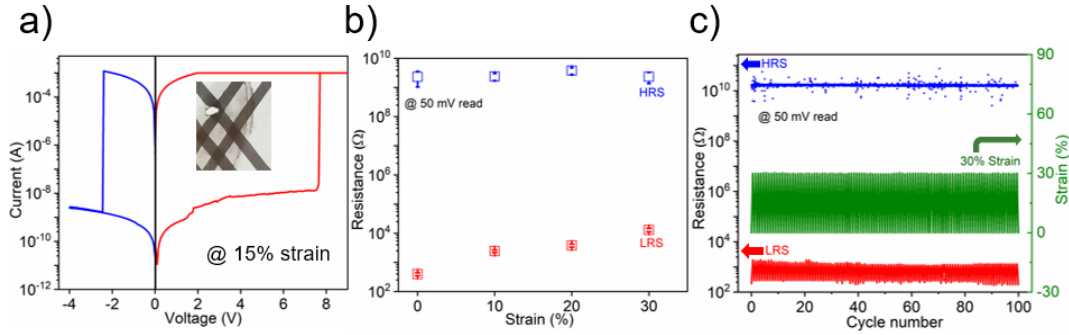


**Figure 5.11** Electrical performance of DS-memristor under tear damage. (a) I-V curve of DS-memristor with a work cell half-cut in diagonal. (b) The reading of HRS and LRS in DS-memristor with a working cell half cut in diagonal versus strain. (c) The reading of HRS and LRS in DS-memristor with a working cell half cut in diagonal under 50 mV readout voltage at dynamic condition.

To further explore the ability of DS-memristor against tear mechanical damage, we carried out tear damage by half-diagonal cut a working cell of device. The tearing damage is introduced into a working cell of DS-memristor respect to crossbar configuration, I-V characteristics shows the device under tear damage remains writing and erasing functions at the strain of 15% with a set voltage of 8V and reset voltage of -2V (**Figure 5.11 a**). The stretchability of DS-memristor under tear damage in static state maintains at 30% whereas the resistance in LRS changes from  $\sim 10^2$  to  $\sim 10^4$  (**Figure 5.11 b**). There is a slightly decreasing in stretchability as compare to non-tear DS-memristor with stretchability of 40%. Despite tear damage, the HRS and LRS are well-separated and keep stable under continuous readout voltage of 50 mV for 100 cycles of 30% loading and unloading (**Figure 5.11 c**), indicating discrete structure has advantage in resisting to tear damage because of the same evasive manner of units to sharp edge.

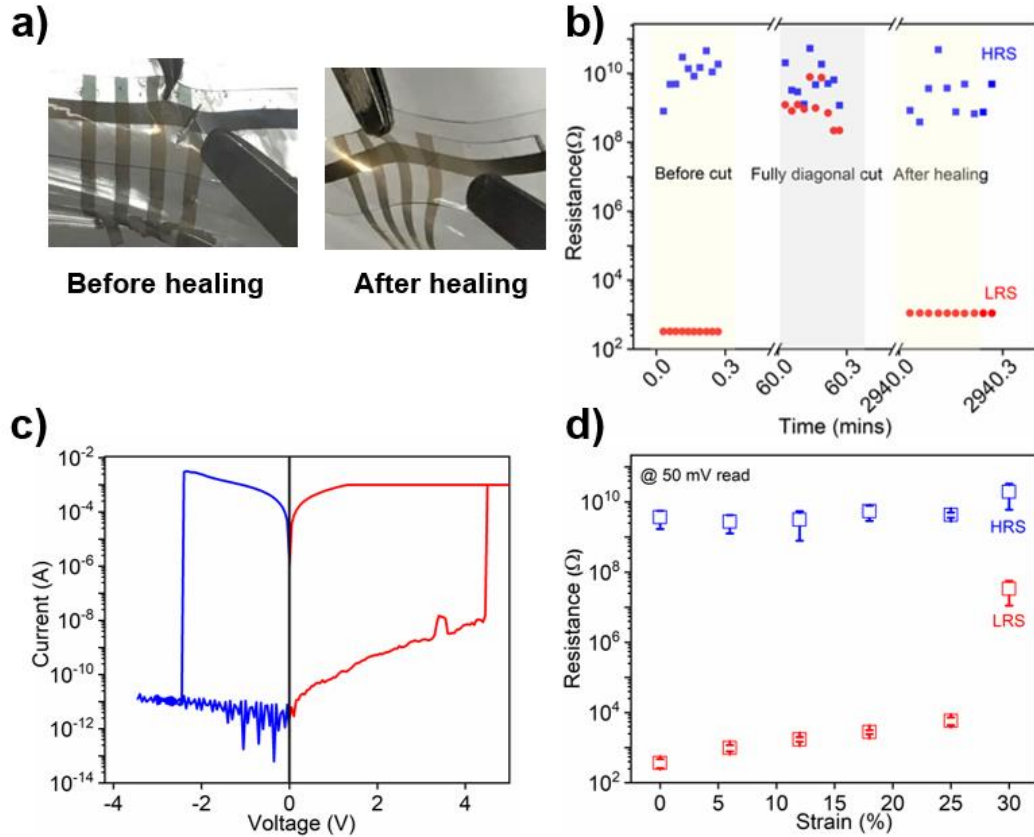


**Figure 5.12** Electrical performance of DS-memristor after self-healing under extreme tear damage. (a) Photos of DS-memristor with fully diagonal cut and after self-healing. (b) HRS and LRS of DS-memristor before fully cut diagonally, being fully cut diagonally and after self-healing. (c) I-V curve of self-healed DS-memristor after fully cut diagonally. (d) Resistance at HRS and LRS after self-healed DS-memristor versus strain.

Furthermore, to exam the endurance of DS-memristor to extreme tear damage, a fully diagonal cutting was applied in the working area of device. As SEBS is a highly viscoelastic at room temperature that exhibits minor autonomous intrinsic self-healing property due to the mobile chain diffusion<sup>[34-36]</sup>. Photographs in **Figure 5.12 a** shows a working cell of device being fully diagonal cut (left) and after self-healing (right). The electrical characteristics for both HRS and LRS is shown in **Figure 5.12 b**. After fully diagonal cut, the resistance in LRS has a dramatically increase from  $10^2$  to  $10^9$ . After healing at room temperature, the resistance of LRS come back to  $10^3$ . The abrupt change of resistance in LRS is caused by fully diagonal cut that break electrons path in electrodes of Au/SEBS. After healing, the resistance at LRS is recovered indicating electrode

Au/SEBS are healed and information in devices without the loss. Meanwhile, we tested the I-V curve for self-healed DS-memristor, the set and reset voltage after self-healing is 4 V and -2.5V, indicating the self-healed DS-memristor after fully diagonal cut remains electrical functions of data writing and erasing (**Figure 5.12 c**). The resistance at HRS for self-healed DS-memristor keep stable without resistance switching, and LRS has slightly increase until 25%, indicating the effective stretchability of self-healed DS-memristor is 25% (**Figure 5.12 d**).

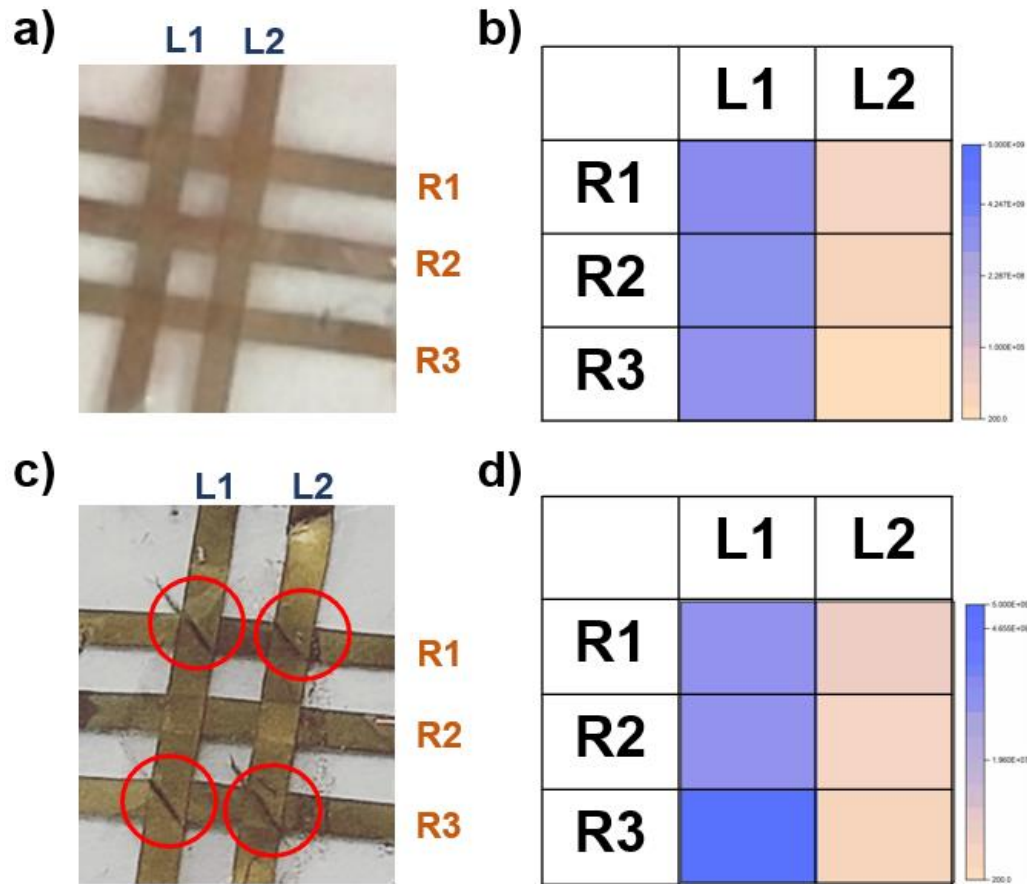


**Figure 5.13** Information storage for self-healed 3 x 2 array DS-memristor after 4 working cells with fully diagonal cut. Photographs of a 3 x2 crossbar flexible discrete structure memristor array (a) before and (c) after fully diagonal cut, and its corresponding color map of readout resistance in DS-memristor (b) before fully diagonal cut and (d) after healing.

As a demonstration, we fabricated a 3x2 crossbar memristor (**Figure 5.13 a**), in which devices in first bit line on the left stored 1(HRS) and 0 (LRS) stored in second bit line on the right as shown in color map of readout resistance (**Figure 5.13 b**). We applied 4 fully

diagonal cut at each corner of working cell (**Figure 5.13 c**), allow it to heal and measure the resistance as shown in color map (**Figure 5.13 d**). The resistance for self-healed DS-memristor in first bit line and second bit line is consistent with the readout before cut, proving that information in 3x2 crossbar memristor are stored without loss and device was successfully recovered from cut. To sum up, the discrete structure design makes stretchable memristor possible to against puncture and tear damages even in an extreme condition.

### 5.3 Conclusion

In this chapter, we further demonstrated the discrete structure coupled with a self-healing elastomer endows stretchable memristors with excellent mechanical endurance against puncture and tear damages. Even at extreme situations such as consecutive puncture a DS-memristor up to 100 times or fully cut along the diagonal of the working cell, the memristors still remain resistive switching and storage properties in terms of information writing, erasing and storage under tear damage. The underlying mechanism of mechanical damages endurance comes from an evasive behavior of discrete units in elastic substrate due to the large Young's modulus difference between them, which allow the discrete units to move away or self-spin when encounter sharp object. The information stored in DS-memristor was remained when puncturing by spine of cactus and dragging it along the spine, demonstrating the possible practical application of DS-memristor in real-world environment. This work is significant for wearable electronics as it paves a new path for making stretchable electronics against mechanical damages, which explore more opportunity for applying stretchable electronics in a harsh condition.

### References

- [1] O. Krestinskaya, A. P. James, L. O. Chua, *IEEE Trans. Neural Netw. Learn. Syst.* **2020**, *31*, 4.
- [2] Y. Yang, *Nat. Electron.* **2019**, *2*, 4.
- [3] H. U. Chung, B. H. Kim, J. Y. Lee, J. Lee, Z. Xie, E. M. Ibler, K. Lee, A. Banks, J. Y. Jeong, J. Kim, C. Ogle, D. Grande, Y. Yu, H. Jang, P. Assem, D. Ryu, J. W. Kwak, M. Namkoong, J. B. Park, Y. Lee, D. H. Kim, A. Ryu, J. Jeong, K. You, B. Ji, Z. Liu, Q. Huo,

- X. Feng, Y. Deng, Y. Xu, K. I. Jang, J. Kim, Y. Zhang, R. Ghaffari, C. M. Rand, M. Schau, A. Hamvas, D. E. Weese-Mayer, Y. Huang, S. M. Lee, C. H. Lee, N. R. Shanbhag, A. S. Paller, S. Xu, J. A. Rogers, *Science* **2019**, 363.
- [4] K. Lee, X. Ni, J. Y. Lee, H. Arafa, D. J. Pe, S. Xu, R. Avila, M. Irie, J. H. Lee, R. L. Easterlin, D. H. Kim, H. U. Chung, O. O. Olabisi, S. Getaneh, E. Chung, M. Hill, J. Bell, H. Jang, C. Liu, J. B. Park, J. Kim, S. B. Kim, S. Mehta, M. Pharr, A. Tzavelis, J. T. Reeder, I. Huang, Y. Deng, Z. Xie, C. R. Davies, Y. Huang, J. A. Rogers, *Nat. Biomed. Eng.* **2020**, 4, 148.
- [5] M. Ha, S. Lim, H. Ko, *J. Mater. Chem.B* **2018**, 6, 4043.
- [6] H. Bai, S. Li, J. Barreiros, Y. Tu, C. R. Pollock, R. F. Shepherd, *Science* **2020**, 370, 848.
- [7] H. Jeon, S. K. Hong, M. S. Kim, S. J. Cho, G. Lim, *ACS Appl. Mater. Interfaces* **2017**, 9, 41712.
- [8] C.-Z. Hang, X.-F. Zhao, S.-Y. Xi, Y.-H. Shang, K.-P. Yuan, F. Yang, Q.-G. Wang, J.-C. Wang, D. W. Zhang, H.-L. Lu, *Nano Energy* **2020**, 76, 105064.
- [9] J.-C. Ni, C.-S. Yang, J.-K. Huang, L. C. Shiu, *Procedia Comput. Sci.* **2019**, 154, 161.
- [10] G. Yang, M. Jiang, W. Ouyang, G. Ji, H. Xie, A. M. Rahmani, P. Liljeberg, H. Tenhunen, *IEEE J. Biomed. Health Inform.* **2018**, 22, 1711.
- [11] T. Nguyen Gia, V. K. Sarker, I. Tcareenko, A. M. Rahmani, T. Westerlund, P. Liljeberg, H. Tenhunen, *Microprocessors Microsy.* **2018**, 56, 34.
- [12] Q. Shi, B. Dong, T. He, Z. Sun, J. Zhu, Z. Zhang, C. Lee, *InfoMat* **2020**, 2, 1131.
- [13] Y. Wang, J. Wang, S. Cao, D. Kong, *J. Mater. Chem. C* **2019**, 7, 9748.
- [14] H.-J. Kim, K. Sim, A. Thukral, C. Yu, *Sci. Adv.* **2017**, 3, e1701114.
- [15] G. Shi, Z. Zhao, J.-H. Pai, I. Lee, L. Zhang, C. Stevenson, K. Ishara, R. Zhang, H. Zhu, J. Ma, *Adv. Funct. Mater.* **2016**, 26, 7614.
- [16] M. S. Lee, K. Lee, S. Y. Kim, H. Lee, J. Park, K. H. Choi, H. K. Kim, D. G. Kim, D. Y. Lee, S. Nam, J. U. Park, *Nano Lett.* **2013**, 13, 2814.
- [17] F. Xu, Y. Zhu, *Adv. Mater.* **2012**, 24, 5117.
- [18] Z. Liu, D. Qi, G. Hu, H. Wang, Y. Jiang, G. Chen, Y. Luo, X. J. Loh, B. Liedberg, X. Chen, *Adv. Mater.* **2018**, 30.

- [19] Y. Jiang, Z. Liu, N. Matsuhisa, D. Qi, W. R. Leow, H. Yang, J. Yu, G. Chen, Y. Liu, C. Wan, Z. Liu, X. Chen, *Adv. Mater.* **2018**, *30*, e1706589.
- [20] D. Qi, Z. Liu, M. Yu, Y. Liu, Y. Tang, J. Lv, Y. Li, J. Wei, B. Liedberg, Z. Yu, X. Chen, *Adv. Mater.* **2015**, *27*, 3145.
- [21] Z. Liu, D. Qi, P. Guo, Y. Liu, B. Zhu, H. Yang, Y. Liu, B. Li, C. Zhang, J. Yu, B. Liedberg, X. Chen, *Adv. Mater.* **2015**, *27*, 6230.
- [22] X. Yan, Z. Liu, Q. Zhang, J. Lopez, H. Wang, H. C. Wu, S. Niu, H. Yan, S. Wang, T. Lei, J. Li, D. Qi, P. Huang, J. Huang, Y. Zhang, Y. Wang, G. Li, J. B. Tok, X. Chen, Z. Bao, *J. Am. Chem. Soc.* **2018**, *140*, 5280.
- [23] J. Xu, S. Wang, G.-J. N. Wang, C. Zhu, S. Luo, L. Jin, X. Gu, S. Chen, V. R. Feig, J. W. F. To, S. Rondeau-Gagné, J. Park, B. C. Schroeder, C. Lu, J. Y. Oh, Y. Wang, Y.-H. Kim, H. Yan, R. Sinclair, D. Zhou, G. Xue, B. Murmann, C. Linder, W. Cai, J. B. H. Tok, J. W. Chung, Z. Bao, *Science* **2017**, *355*, 59.
- [24] E. W. Hawkes, L. H. Blumenschein, J. D. Greer, A. M. Okamura, *Sci. Robot.* **2017**, *2*, eaan3028.
- [25] Y. Hao, Z. Gong, Z. Xie, S. Guan, X. Yang, Z. Ren, T. Wang, L. Wen, "Universal soft pneumatic robotic gripper with variable effective length", presented at *2016 35th CCC*, 27-29 July **2016**, 2016.
- [26] R. F. S. Michael T. Tolley, Bobak Mosadegh, Kevin C. Galloway, Michael Wehner, Michael Karpelson, Robert J. Wood, and George M. Whitesides, *Soft Robot.* **2014**, *1*, 213.
- [27] C. Ma, Z. Luo, W. Huang, L. Zhao, Q. Chen, Y. Lin, X. Liu, Z. Chen, C. Liu, H. Sun, X. Jin, Y. Yin, X. Li, *Nat. Commun.* **2020**, *11*, 1439.
- [28] Jyoti, R. Kaur, S. Singh, J. Sharma, S. K. Tripathi, *J. Electron. Mater.* **2019**, *48*, 5995.
- [29] T.-C. Chang, K.-C. Chang, T.-M. Tsai, T.-J. Chu, S. M. Sze, *Mater. Today* **2016**, *19*, 254.
- [30] Z. Wang, C. Xiang, X. Yao, P. Le Floch, J. Mendez, Z. Suo, *Proc. Natl. Acad. Sci. U S A* **2019**, *116*, 5967.
- [31] C. Li, H. Yang, Z. Suo, J. Tang, *J. Mech. Phys. Solids.* **2020**, *134*.
- [32] J. Y. Sun, X. Zhao, W. R. Illeperuma, O. Chaudhuri, K. H. Oh, D. J. Mooney, J. J. Vlassak, Z. Suo, *Nature* **2012**, *489*, 133.

- [33] C. Xiang, Z. Wang, C. Yang, X. Yao, Y. Wang, Z. Suo, *Mater. Today* **2020**, 34, 7.
- [34] Z. X. Zhang, X. R. Dai, L. Zou, S. B. Wen, T. K. Sinha, H. Li, *Express Polym. Lett.* **2019**, 13, 948.
- [35] R. J. Varley, D. A. Craze, A. P. Mouritz, C. H. Wang, *Macromol. Mater. Eng.* **2013**, 298, 1232.
- [36] A. Nellesen, A. M. Schmidt, J. Bertling, M. von Tapavicza, in *Des. Nat. V*, **2010**, 431.
- [37] D. Son, J. Kang, O. Vardoulis, Y. Kim, N. Matsuhisa, J. Y. Oh, J. W. F. To, J. Mun, T. Katsumata, Y. Liu, A. F. McGuire, M. Krasen, F. Molina-Lopez, J. Ham, U. Kraft, Y. Lee, Y. Yun, J. B. H. Tok, Z. Bao, *Nat. Nanotechnol.* **2018**, 13, 1057.

## Chapter 6\*

### **Mechanical Behaviors and Electrical Properties of Thickness-gradient Structure based Thin Films on Elastic Substrate**

*The conductive thin film on elastic substrate is a very common architecture for stretchable electrodes and strain sensors in wearable electronics. In general, the film on elastic substrate is in the form of homogeneity rather than heterogeneity. This work studies how heterogenous thin film influence the mechanical behaviors and its electrical properties of stretchable electronics by employing a gradient-structure thin film with gradually change in thickness (called thickness-gradient structure) on elastomers. The results showed that strain distribution in thickness-gradient structure affect cracks morphologies and hence the electromechanical properties of stretchable electronics. Besides, the anisotropic electrical property was observed and depended on variation of thickness-gradient. Lastly, the work demonstrates that high sensitivity of strain sensors ( $GF \sim 1665$  at large strain  $\sim 30\%$ ) can be realized by this thickness-gradient structure.*

## 6.1 Introduction

The development of digital communication technologies spurs explosive growth of electronic devices for cyber-physical system (CPS),<sup>[1-2]</sup> internet of things (IoTs)<sup>[3-8]</sup> and edging computing<sup>[8-9]</sup>. Conventional electronics are silicon-based semiconductor devices that is too rigid and brittle to be applied to curvilinear surface or soft deformation scenarios, such as human tissues and joints. Wearable electronics are emerging in the past decade and rapid developed recently due to compact and versatile in size, flexible and comfortable to fit with various topologies and geometries, which promote real-time monitoring for medical diagnostics and therapies<sup>[10-12]</sup> and continuously detection for motions<sup>[13-15]</sup>.

Generally, the wearable electronics consist of two components, one is active materials/elements that provide electrical performance or functional properties, another is elastic substrate that enable the active materials/elements to deformable and conformable with it under mechanical forces such as stretch, bend, twist, shear and so on. The nanomaterials, in forms of metal nanoparticles, nanowire and nano mesh, or CNTs, graphene and polymer nanofibers on elastomer, is the most common architecture being employed for stretchable electrodes and strain sensors in wearable electronics.<sup>[16-25]</sup> Among those conductive active materials, metallic thin films have been widely adopted and study due to the ease of fabrication and compatible with commercial technique for mass production. Currently, tremendous research have investigated the electrical and mechanical properties of thin film on elastomer based on a homogeneous layer with relatively uniform composition and microstructure<sup>[15, 17, 19, 26]</sup>, the electrical and mechanical properties of a heterogeneous layer of thin film on elastomer are rarely explored.<sup>[27-28]</sup> With respect to heterogeneities, nature offers a rich source of paradigms in microstructure and chemical components such as seashells, bone, and teeth that possess impressive mechanical properties and functions which cannot be achievable by homogeneity.<sup>[29-34]</sup> For example, bamboo (*Bambusa*) has a graded structure in longitudinal profile that can withstand extreme wind loads.<sup>[35-36]</sup> Thus, this work is going to discover the mechanical behaviors and electrical properties of heterogenous thin film on elastomer for potential wearable applications.

Thickness-gradient structure is a kind of heterogenous structure, which the thickness of thin film is gradually changing without abrupt changes. As thickness is a factor to determine the

crack morphologies and hence affect the conductivity of crack-based stretchable strain sensors and electrodes.<sup>[17, 19]</sup> Researcher had been fabricated high sensitivity of stretchable strain sensors by using this kind of heterogenous structure. However, the fabrication of thickness-gradient structure is a self-assemble coffee-ring process and the change of thickness-gradient cannot be control manually, so the sensitivity of strain sensors drops quickly at different stretching ranges.<sup>[27]</sup> Therefore, to investigate the effect of thickness-gradient thin film on electrical and mechanical properties in a quantitatively way, a thickness-gradient thin films were fabricated by thermal evaporation deposition at different angles. The results show that the variation of thickness-gradient can be tuned by adjusting the tilted deposition angles, and the electrical properties of thin film not only depends on the thickness gradient variation, but also relies on the direction of mechanical forces applied with respect to the direction of thickness gradient variation. Besides, the anisotropic electrical property was observed on this thickness-gradient thin film structure and model was proposed to elaborate this phenomenon. Lastly, a high sensitivity of strain sensors of GF~1665 at large strain ~30% can be realized by this heterogenous structure.

## 6.2 Experimental methods

### 6.2.1 Fabrication of thickness-gradient thin film on elastic substrate

Stretchable strain sensor substrate preparation: the PDMS (Sylgard 184, Dow corning, USA) of prepolymer base and cross-linking curing agent were prepared and fully mixed at a weight ratio of 10:1. In order to obtain bubble free samples, mixed uncured PDMS (10:1) were defoamed by centrifugal machine at rotational speed of 8000 rpm for 5mins. And then, defoamed PDMS (10:1) was spin-coated at 600 rpm for 60s on a piece of fluorinated silicon wafer. After spin coating, curing the PDMS in the oven 60°C for 3 days. At last, cutting PDMS into desired sizes and peel off the PDMS from fluorinated silicon wafer and transfer them on the glasses and applied O<sub>2</sub> plasma treatment at pressure 0.5mbar with 30% power for 0.5 min before Au evaporation deposition.

Silicon wafer fluorinated treatment: Silicon wafer was washing by using acetone, ethanol and DI water and using N<sub>2</sub> to dry up. Then placed the washed silicon wafer in a clean petridish. Then applying O<sub>2</sub> plasma treatment (power 70%, 0.5mbar) for 3mins. Taking 2ul

1H, 1H, 2H, 2H perfluoro-octyl-trichlorosilane by a pipette and dropped inside the glass petridish around the cleaned wafer and covered it by another glass petridish, then placed the whole petridish on a hot plate at temperature 160°C for 3hrs. After this hydrophobization treatment, washed the fluorinated wafer by DI water.

Templates of PDMS holder for Au evaporation deposition: glass templates with angles of  $\theta = 15^\circ, 30^\circ, 45^\circ, 60^\circ, 75^\circ$  for tilted angles deposition. The glass templates with various angles were hand-made by using two pieces of glass slides with size of 3.5 cm x 3.5 cm and sticking together with high temperature tape. Hand-made glass templates are arranged in a circle with radius of 7cm from the center of thermal evaporator substrate holder as shown in **Figure 6.1**.

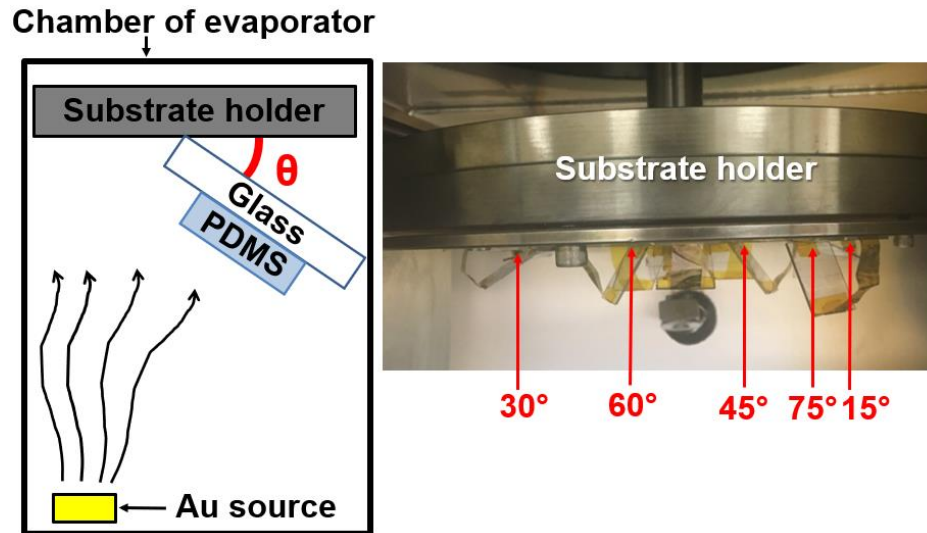


**Figure 6.1** Set-up configuration of thermal evaporation and location of sample template holders. (Schematic on the left and photograph on the right)

### 6.2.2 Thickness-gradient quantification

To quantify the relationship between the thickness gradient variation according to the deposition tilted angles. AFM was used to quantify the thickness of Au on the silicon wafer that were deposited at the same condition as PDMS substrate did to indirectly measure the thickness of Au thin film on PDMS. The silicon wafer slides were placed on the glass template at the same location and with same size as shown in below **Figure 6.2 (a-b)**.

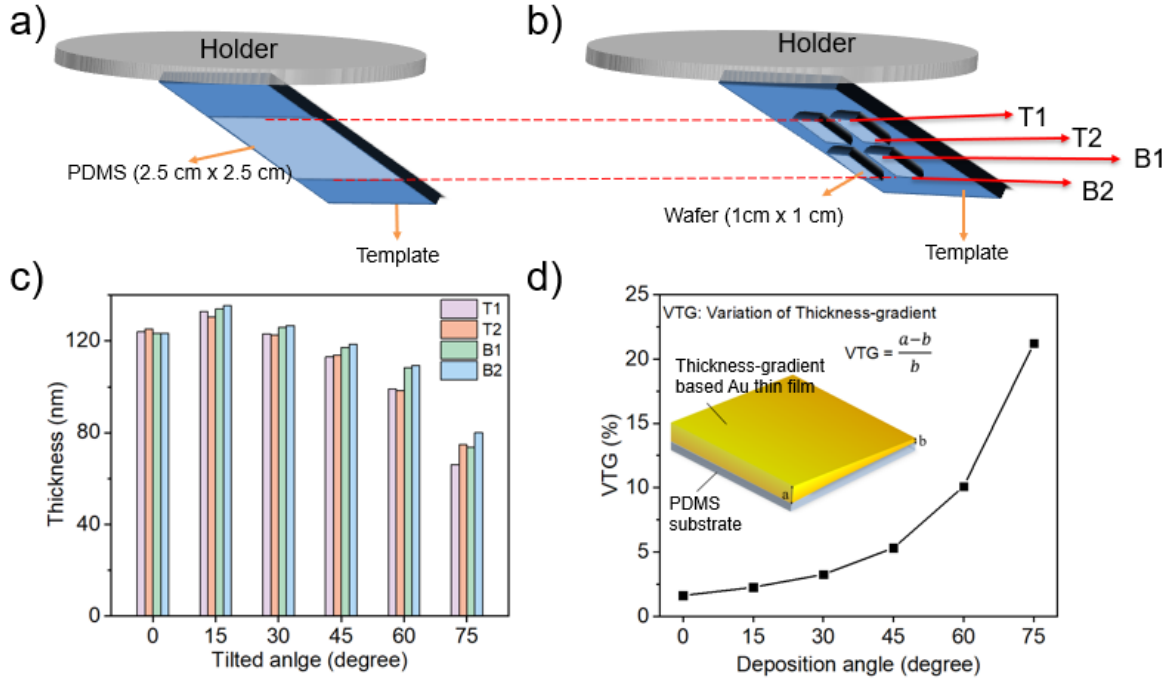


**Figure 6.2** Thickness gradient variation quantification. (a-b) PDMS with size of 2.5 cm x 2.5 cm on the glass template (b) Small pieces of silicon wafer with size of 1 cm x 1 cm on the glass template and aligned with position of PDMS horizontally. (c) Average thickness of gold film on silicon wafer at the portion of T1, T2, B1 and B2. (d) Relationship of the thickness-gradient variation with respect to the deposition angles.

PDMS with size of 2.5 cm x 2.5 cm on the glass and silicon wafers with 1 cm x 1cm were installed on the deposition holder at different deposition angles and are aligned as shown in Figure 6.2 **Figure 6.2**. Silicon wafer on the top portion is divided into two sections marked as T1 and T2, and the silicon wafer on the bottom portion divided into two sections marked as B1 and B2. The thickness of these four sections (T1, T2, B1 and B2) are measure under AFM later. The variation of thickness-gradient (VTG) is calculated based on following equation, whereas b is the average thickness of B1 and B2, the a is average thickness of T1 and T2.

$$\text{Variation of Thickness-gradient} = \frac{a-b}{b}$$

From the **Figure 6.2 (c)**, at the low title angle (<15 deg), Au film on the top and bottom has no much different, the variation of thickness-gradient is not obvious at this condition. At the titled angle between 15 degree to 75 degree, the bottom part of Au film is thicker

than top part of Au thin film. And the thickness-gradient variation increases as tilted angle increases (**Figure 6.2 d**).

The thickness-gradient Au film can be formed on tilted angle deposition because the bottom part is closer to the Au source as compared the top part. The Au particles reach the bottom part and nucleate firstly, and top part nucleate later. The nuclei on the bottom region are larger due to more time to grow than nuclei on the top, because of the Ostwald ripening, large ones tend to grow while small ones shrink, bottom region have more chance to grow more nuclei and less time to reach the critical size and form the film than the top region. Another possible reason is the energized Au particles on the top trend to diffuse to the bottom region due to gravitational force. The average of thickness decrease as the tilted angle increase is because the larger the tilted angle is, the less contact area for Au particles to attach to the surface of substrate.

### 6.3 Principle Outcomes

#### 6.3.1 Mechanical direction effect on electrical properties

The electrical properties of thickness-gradient thin film on elastomer not only depend on thickness gradient variation, but also the direction of stress applied to the film. There are two directions to be identified and investigated in the experiment. We define the direction of applied strain perpendicular to the direction of thickness gradient variation as transverse direction, while the applied strain parallel to the direction of thickness gradient variation as longitudinal direction as shown in **Figure 6.3** (a) and (c). From FEA simulation results, there is no stress distribution across the film in transverse direction, while stress distribute across the film in the longitudinal direction.

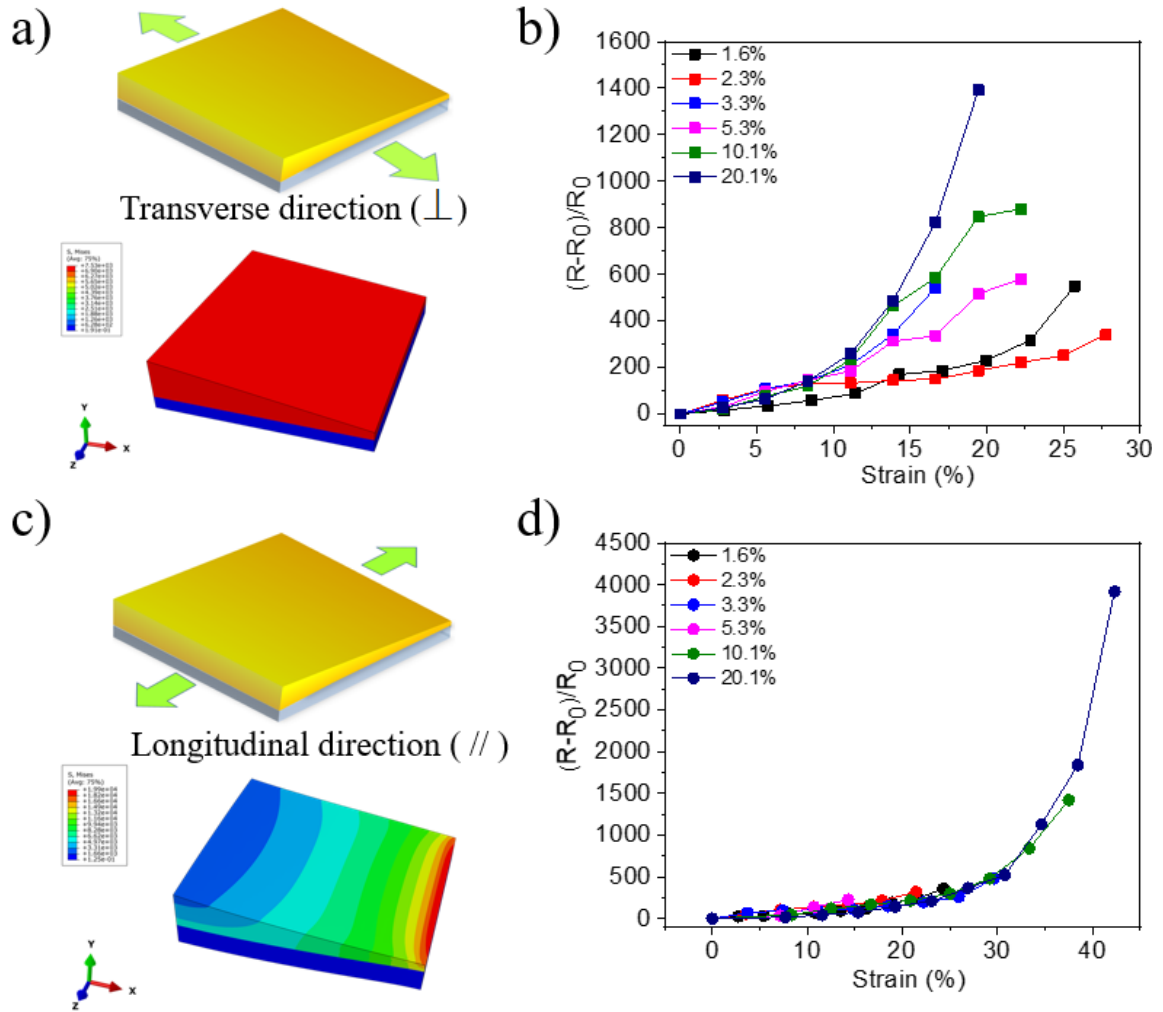


**Figure 6.3** Electrical and mechanical properties of thickness-gradient gold film on elastic. (a) FEA result for transverse direction. (b) Relative resistance change of thickness-gradient gold thin film versus applied strain at transverse direction. (c) FEA result for longitudinal direction. (d) Relative resistance change of thickness-gradient gold thin film versus applied strain at longitudinal direction.

The electrical and mechanical properties were investigated by applying tensile stress with respect to the direction of thickness change. For thickness-gradient Au/PDMS at transverse direction, the relative resistance change is significantly affected by the thickness-gradient variation. The larger the thickness-gradient variation is, the higher the relative resistance change is. In other words, the low thickness-gradient variation has low relative resistance change and large electrical stretchability, which is more suitable for being used as stretchable electrode, while large thickness-gradient variation has higher sensitivity and is suitable for being used as stretchable strain sensors. In contrast, for thickness-gradient

Au/PDMS at longitudinal direction, the relative resistance change is not affected by thickness gradient variation. However, the electrical stretchability is affected by the thickness gradient variation. That is, larger the thickness gradient variation is, larger the electrical stretchability is, but no sensitivity difference. This can be concluded that the mechanical behavior and electrical property of thickness-gradient Au/PDMS are affected by both thickness-gradient variation and direction of mechanical stress.

### 6.3.2 Electrically anisotropic property of thickness-gradient Au / PDMS

The comparison of mechanical and electrical properties for thickness-gradient Au/PDMS at transverse and longitudinal direction is shown in **Figure 6.4**. For the flat Au thin film on PDMS (**Figure 6.4 a**), the relative resistance change versus strain is similar at transverse and longitudinal directions. As the thickness-gradient variation increase, the difference of relative resistance also increases at transverse and longitudinal direction (**Figure 6.4 b-f**), especially for Au/PDMS with thickness-gradient variation of 10.1% and 20.1%, which exhibit an obvious anisotropic property in relative resistance change. The relative resistance change of thickness-gradient Au/PDMS in longitudinal direction is much slower than transverse direction, indicating the thickness-gradient Au/PDMS tend to be more stretchable in longitudinal direction than transverse direction, however, the sensitivity in transverse direction is higher than longitudinal direction. As mentioned earlier in Figure 6.3, FEA results shows that the thickness-gradient Au/PDMS in longitudinal direction has stress distribution while no stress distribution in transverse direction. Therefore, it can be inferred that the stress distribution is the vital parameter that affect the electrical stretchability and sensitivity. To understand the underlying reason how the stress distribution plays a role in the performance of thickness-gradient Au/PDMS, cracks morphologies are taken by confocal microscopy as shown in **Figure 6.5**.

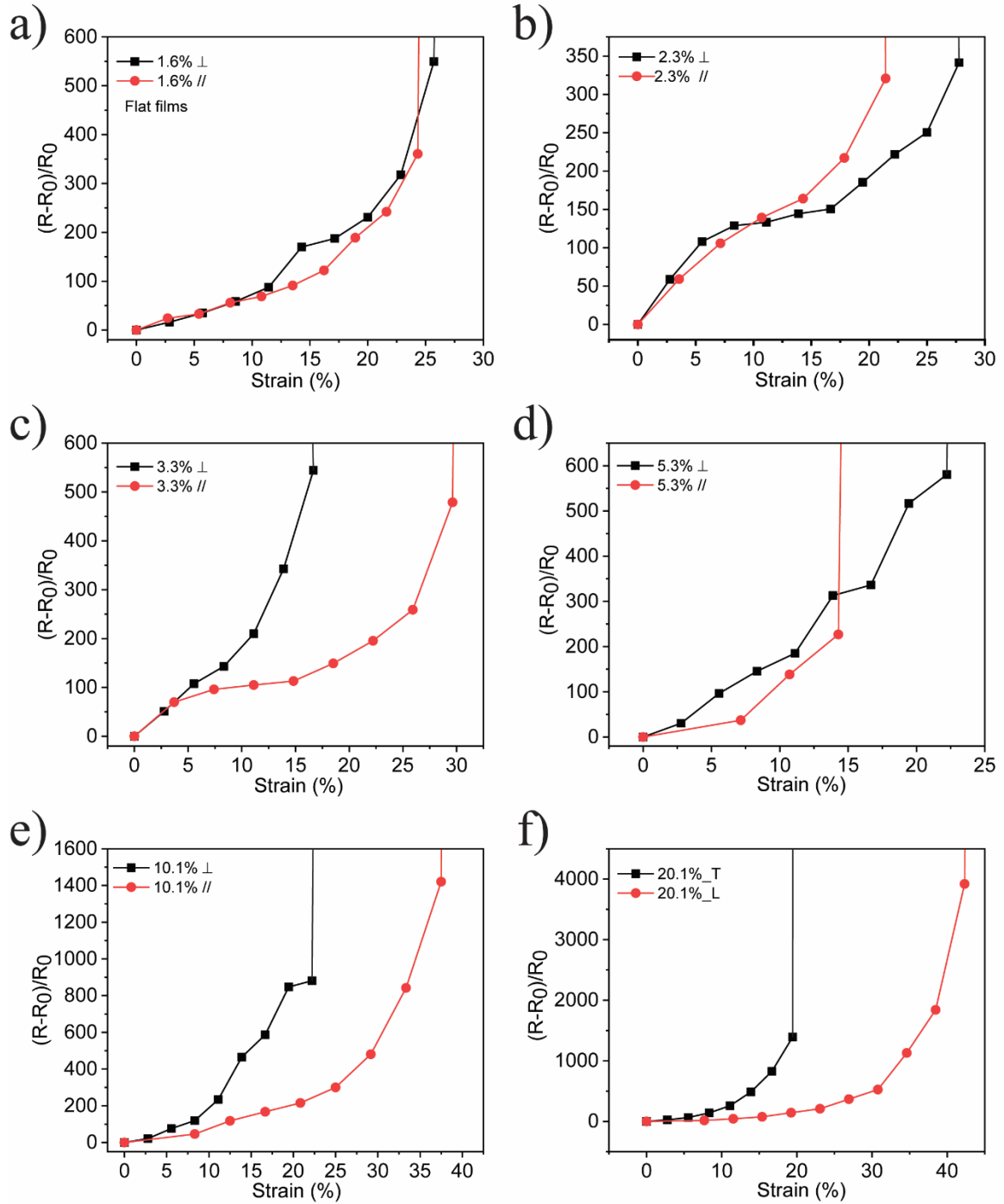


**Figure 6.4** Anisotropic property of gradient-thickness Au/PDMS versus strain at transverse and longitudinal direction. Relative resistance change of (a) flat Au/PDMS, and thickness-gradient Au/PDMS with variation of (b) 2.3%, (c) 3.3%, (d) 5.3%, (e) 10.1%, (f) 20.1%.

As the electrically anisotropic property is obvious for thickness-gradient Au/PDMS with variation of 10.1% and 20.1%. The crack morphologies for thickness-gradient Au/PDMS with variation of 10.1% and 20.1% at transverse and longitudinal direction are taken as shown in **Figure 6.5**. From confocal microscopic images, the crack at transverse direction are straight (**Figure 6.5 a-b**) while cracks at longitudinal direction are zigzagged (**Figure 6.5 c-d**), which can be inferred that propagation of cracks across the Au film at longitudinal direction are more difficult compared to transverse direction, meaning the cracks under same strain are easily run through the film at transverse direction and reach critical strain earlier than longitudinal direction. This is also consistent with electrical property that sensitivity at transverse direction is higher, while electrical stretchability is larger at longitudinal direction.

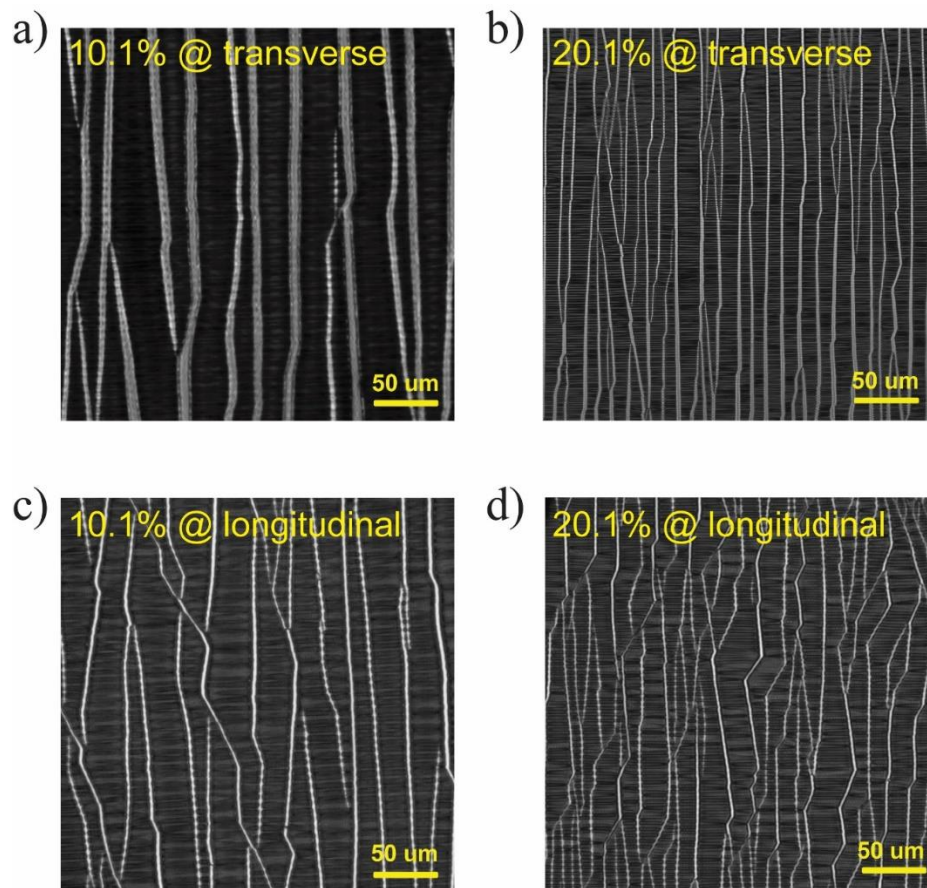


**Figure 6.5** Confocal microscopic images of crack morphologies of thickness-gradient Au/PDMS at transverse and longitudinal direction. Au/PDMS with VTG of 10.1% at (a) transverse direction and (c) longitudinal direction. Au/PDMS with VTG of 20.1% at (b) transverse direction and (d) longitudinal direction.

Crack morphology is vital sign to indicate the conductivity of metallic thin film, which has been widely studies such as density, depth, width, length.<sup>[17, 19, 26, 37]</sup> At transverse direction, since crack propagate in straight manner, the crack run across thin film and easily retard the electron pathway and cause electrically break down, indicating conductivity of thin film is change rapidly and high sensitivity. However, at longitudinal direction, since crack propagate in zigzagged manner, meaning more energy are required for crack to run across the thin film, indicating the conductivity of thin film change slow but large electrical stretchability. That is, at a certain strain, it may critical for cracks at transverse direction as straight cracks have cut off the movement pathway of electrons (**Figure 6.6 a**), but not a problem for cracks at longitudinal direction because the cracks propagated in zigzagged manner delay the critical point to reach unless more strain energy are applied to make cracks throughout the film (**Figure 6.6 b**).

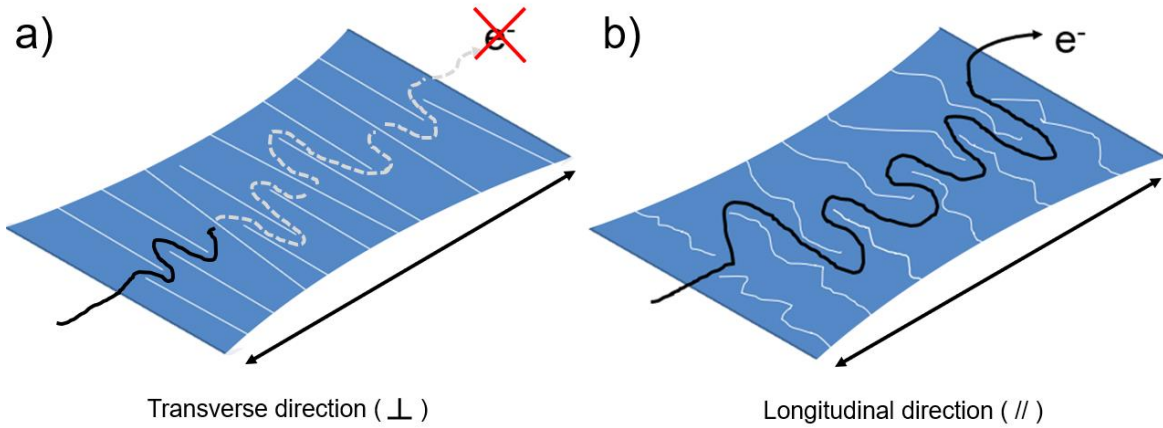


**Figure 6.6** Schematic illustration of effect of crack propagation on relative resistance change. (a) At transverse direction, crack propagate at straight manner. (b) At longitudinal direction, crack propagated at zigzagged manner.

Without stress distribution in transverse direction, the cracks propagate straightly and smoothly within the Au film. With stress distribution involved in longitudinal direction, cracks propagate tortuously and zigzag. Therefore, we believe that stress distribution of thickness-gradient Au/PDSM play a role in tuning the crack propagation manners.

Next, we want to establish models to describe the electrically anisotropic property of thickness-gradient Au/PDMS in transverse and longitudinal directions. Theoretically,

tensile stress is proportional to strain by the modulus of Young's modulus as shown in formula below

$$\sigma = E \cdot \varepsilon \quad \text{eq (1)}$$

Since

$$\sigma = \frac{F}{A} = \frac{F}{w \cdot h} \quad \text{eq (2)}$$

From equation (1) and (2):

$$F = (w \cdot h)(E \cdot \varepsilon) \quad \text{eq (3)}$$

Where  $w$  is the width of thin film,  $h$  is height of thin film, and  $E$  is Young's modulus of conductive material, they are constant in our thickness-gradient system. Thus, the product of  $w$ ,  $h$ ,  $E$  can be replaced by a constant  $K$ , and equation (3) can be expressed as

$$F = K \cdot \varepsilon \quad \text{eq (4)}$$

The equation (4) is also Hooke's law for linear spring, so we can employ spring model in our system as shown in Figure 6.7.

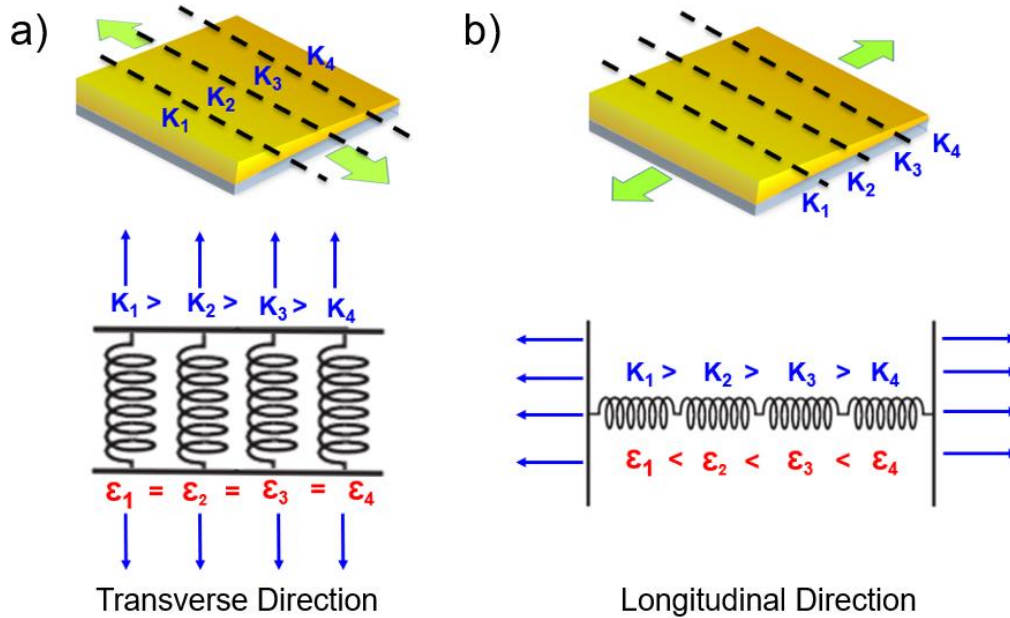


**Figure 6.7** Spring models involved into thickness-gradient thin film on elastomers. (a) Thickness-gradient Au/PDMS in transverse direction can be described by springs in parallel. (b) Thickness-gradient Au/PDMS in longitudinal direction can be described by springs in series.

The critical stretchability of strain sensors defines as the strain where electrical performance is maintained, which depends on the thickness of conductive films. The thickness-gradient Au/PDMS is discretized into small individual parts. In transverse direction as shown in Figure 6.7 **Figure 6.7 (a)**, the height of thickness is changing and perpendicular to the direction of applied stress, which can be regarded as the springs with different coefficient  $K_1$ ,  $K_2$ ,  $K_3$ , and  $K_4$  in parallel. In this case, the extension of each spring is same, indicating the strain of each divided part is same. Similarly, in longitudinal direction as shown in **Figure 6.7 (b)**, the height of thickness is changing along with direction of applied stress, which can be deemed as springs with different coefficient  $K$  in series. And in this case, the extension of spring is different, indicating the strain for divided parts is varying under stretching.

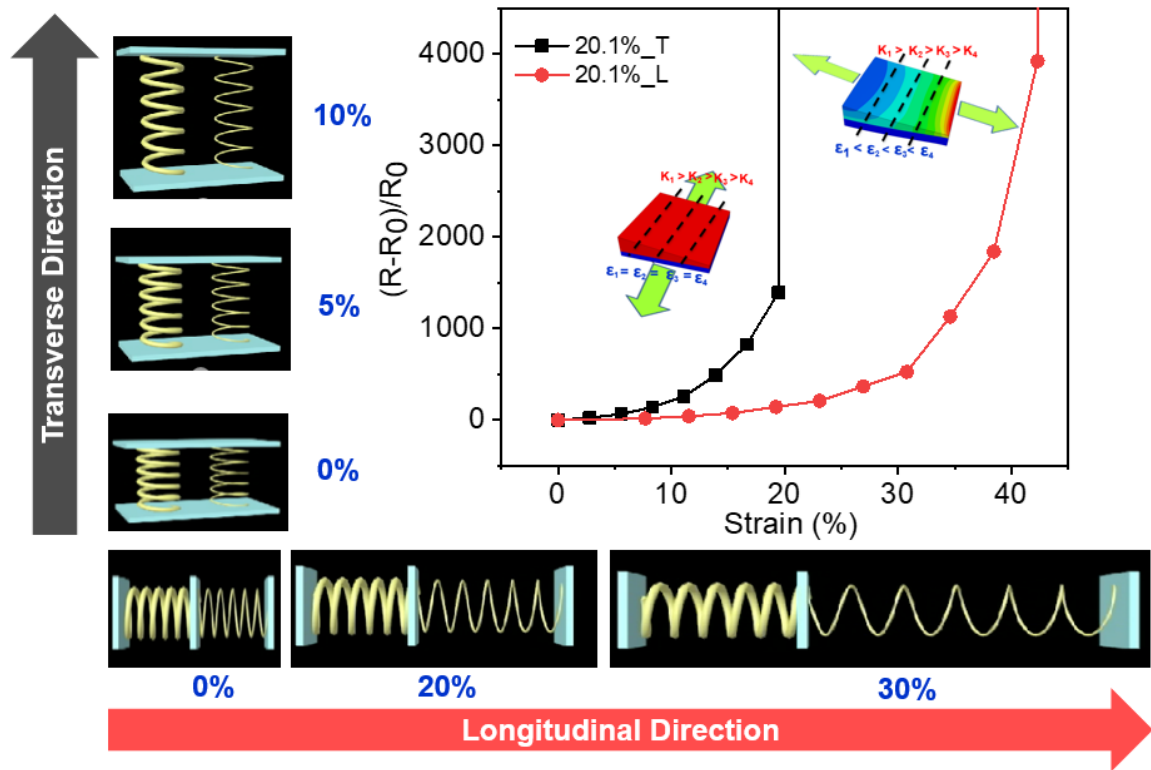


**Figure 6.8** Illustration of electrically anisotropic property of thickness-gradient Au/PDMS based on spring models.

We use spring models to elaborate the electrically anisotropic property of thickness-gradient Au/PDMS. From equation 4, coefficient  $K = w \cdot h \cdot E$ , where  $w$  and  $E$  is constant, so  $K$  is proportional to the thickness of thin film. As thinner thin film forms large cracks

and thinner film forms small cracks,<sup>[17]</sup> the higher coefficient  $K$  means larger change of relative resistance. Therefore, coefficient  $K$  in spring model determines the electrical property of conductive film in thickness-gradient system.

Taking Au/PDMS with thickness-gradient variation of 20.1% as an example in **Figure 6.8**, at smaller strain less than 5%, the relative resistance change for transverse direction and longitudinal direction is similar. At large extension of 20%, thickness-gradient Au/PDMS in transverse direction has larger relative resistance change than longitudinal direction. Because based on model of springs in parallel, the parts with large coefficient  $K$  and small  $K$  are under same strain, large  $K$  determines the electrical property of Au thin film, hence large relative resistance change. In contrast, for the longitudinal direction with springs in series model, the strain for every small individual part is different. The part with small coefficient  $K$  takes most of the strain energy by elongating more and less strain energy is loading on the parts with large coefficient  $K$ , so the relative resistance change is relatively small at the 20% elongation. Until it further extends to a critical strain, where strain energy cannot be totally consumed by parts with small  $K$ , large  $K$  parts start to involve into extension to share excessive strain energy, the change of relative resistance begins to increase dramatically at strain of 30%. That's the reason why thickness-gradient Au/PDMS in transverse direction has high sensitivity and reach critical strain earlier, while thickness-gradient Au/PDMS in longitudinal direction is more electrically stretchable.

According to our investigation on the mechanical behavior and electrical properties of thickness-gradient Au/PDMS, the thickness-gradient Au/PDMS with variation of 20.1% in transverse direction is more sensitive and suitable for being used as stretchable strain sensors. After optimization of fabrication condition, a highly sensitivity of stretchable strain sensors with  $GF=1665$  at strain  $\varepsilon=30$  is achieved, which is much better than others (**Figure 6.9 c**). The stability of performance was also evaluated under more than 150 cycles of 30% stretching and releasing (**Figure 6.9 b**). Taking SEM images of crack morphologies at three regions of various thickness (**Figure 6.9 a**), the width of cracks in thick region ( $K1$ ) are large while small in thin region ( $K3$ ), which is consistent with our model that thick region has larger coefficient  $K$  and thin region has small coefficient  $K$ .

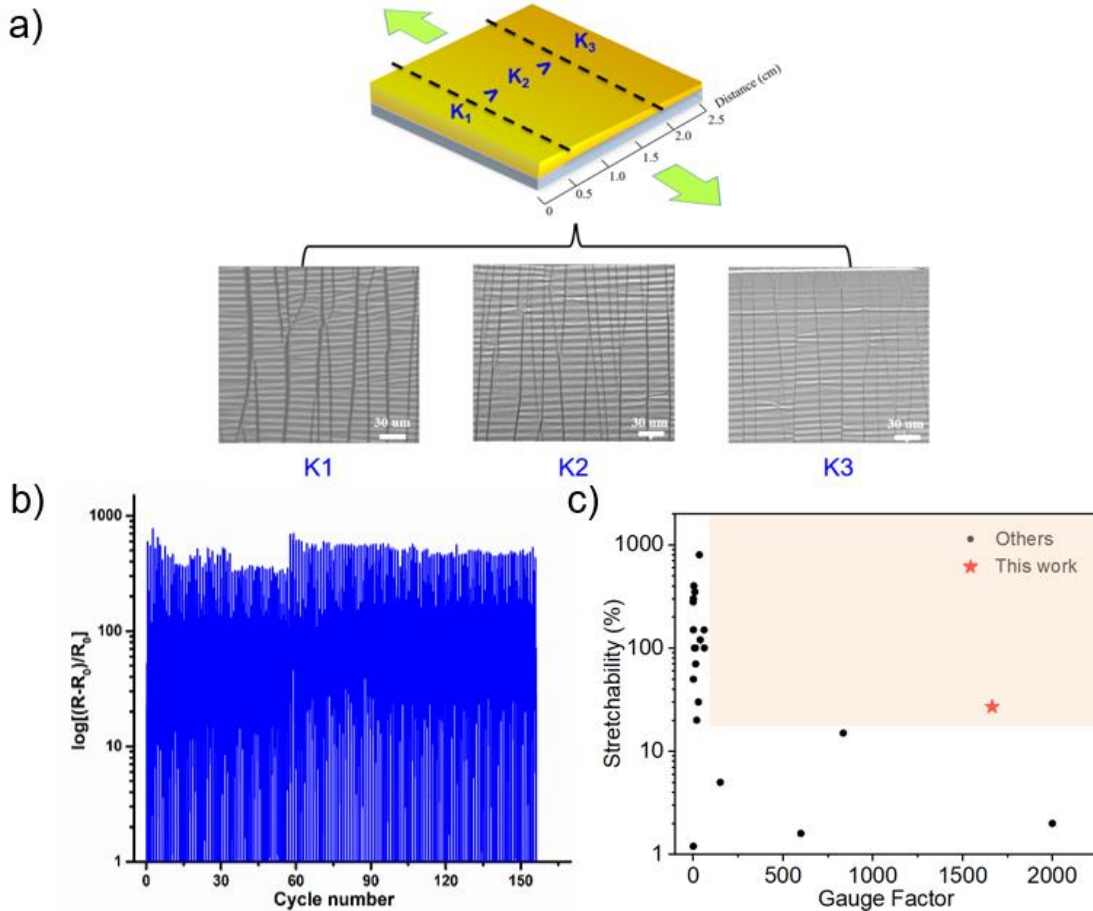


**Figure 6.9** Crack morphologies and electrical performance of stretchable strain sensors with thickness-gradient variation of 20.1%. (a) SEM images of cracks at regions with different coefficient  $K$ . (b) Cycling electrical performance test (c) Comparison of performance of stretchable strain sensors with others.

## 6.4 Conclusion

This work study the mechanical behavior and electrical properties of heterogeneous thin film on elastomers, which is different from conventional fabrication of homogeneous thin film on elastomers for cracked-based stretchable electrodes and strain sensors. Unlike the traditional flat thin film on elastomer, thickness-gradient thin films on PDMS were fabricated by using thermal evaporation on the PDSM. The variation of thickness-gradient can be adjustable by tuning the tilted deposition angles. Results shows that the mechanical and electrical properties of thickness-gradient Au thin film on elastomers depends on both thickness-gradient variation and direction of tensile force. Besides, the electrically anisotropic property of thickness-gradient Au/PDMS was influenced by thickness-gradient

variation and was caused by strain distribution that affects cracks propagation manners. Meanwhile, spring models are proposed to elaborate the electrically anisotropic property. Lastly as a demonstration, a highly sensitivity of thickness-gradient strain sensor with  $GF=1665$  at strain  $\varepsilon=30$  is achieved, which open a new direction of employing heterogenous structure on elastomers and discover more special properties for stretchable electrodes and strain sensors applications.

## References

- [1] S. Ali, S. B. Qaisar, H. Saeed, M. F. Khan, M. Naeem, A. Anpalagan, *Sensors* **2015**, *15*, 7172.
- [2] L. Gürgen, O. N. Günalp, Y. Benazzouz, M. Gallissot, *2013 DATE* **2013**, 1149.
- [3] P. Kumari, M. López-Benítez, G. M. Lee, T. Kim, A. S. Minhas, "Wearable Internet of Things - from human activity tracking to clinical integration", presented at *2017 39th Annual International Conference of the IEEE EMBC*, 11-15 July **2017**, 2017.
- [4] S. Li, B. Zhang, P. Fei, P. M. Shakeel, R. D. J. Samuel, *Aggress. Violent Behav.* **2020**, 101541.
- [5] G. Manogaran, P. M. Shakeel, H. Fouad, Y. Nam, S. Baskar, N. Chilamkurti, R. Sundarasekar, *Sensors* **2019**, *19*, 3030.
- [6] J.-C. Ni, C.-S. Yang, J.-K. Huang, L. C. Shiu, *Procedia Comput. Sci.* **2019**, *154*, 161.
- [7] G. Yang, M. Jiang, W. Ouyang, G. Ji, H. Xie, A. M. Rahmani, P. Liljeberg, H. Tenhunen, *IEEE J. Biomed. Health Inform* **2018**, *22*, 1711.
- [8] Y. Yang, *Nat. Electron.* **2019**, *2*, 4.
- [9] O. Krestinskaya, A. P. James, L. O. Chua, *IEEE Trans. Neural. Netw. Learn. Syst.* **2020**, *31*, 4.
- [10] H. U. Chung, B. H. Kim, J. Y. Lee, J. Lee, Z. Xie, E. M. Ibler, K. Lee, A. Banks, J. Y. Jeong, J. Kim, C. Ogle, D. Grande, Y. Yu, H. Jang, P. Assem, D. Ryu, J. W. Kwak, M. Namkoong, J. B. Park, Y. Lee, D. H. Kim, A. Ryu, J. Jeong, K. You, B. Ji, Z. Liu, Q. Huo, X. Feng, Y. Deng, Y. Xu, K. I. Jang, J. Kim, Y. Zhang, R. Ghaffari, C. M. Rand, M. Schau, A. Hamvas, D. E. Weese-Mayer, Y. Huang, S. M. Lee, C. H. Lee, N. R. Shanbhag, A. S. Paller, S. Xu, J. A. Rogers, *Science* **2019**, 363.

- [11] D. H. Kim, N. Lu, R. Ma, Y. S. Kim, R. H. Kim, S. Wang, J. Wu, S. M. Won, H. Tao, A. Islam, K. J. Yu, T. I. Kim, R. Chowdhury, M. Ying, L. Xu, M. Li, H. J. Chung, H. Keum, M. McCormick, P. Liu, Y. W. Zhang, F. G. Omenetto, Y. Huang, T. Coleman, J. A. Rogers, *Science* **2011**, 333, 838.
- [12] K. Lee, X. Ni, J. Y. Lee, H. Arafa, D. J. Pe, S. Xu, R. Avila, M. Irie, J. H. Lee, R. L. Easterlin, D. H. Kim, H. U. Chung, O. O. Olabisi, S. Getaneh, E. Chung, M. Hill, J. Bell, H. Jang, C. Liu, J. B. Park, J. Kim, S. B. Kim, S. Mehta, M. Pharr, A. Tzavelis, J. T. Reeder, I. Huang, Y. Deng, Z. Xie, C. R. Davies, Y. Huang, J. A. Rogers, *Nat. Biomed. Eng.* **2020**, 4, 148.
- [13] D. Son, J. Lee, S. Qiao, R. Ghaffari, J. Kim, J. E. Lee, C. Song, S. J. Kim, D. J. Lee, S. W. Jun, S. Yang, M. Park, J. Shin, K. Do, M. Lee, K. Kang, C. S. Hwang, N. Lu, T. Hyeon, D. H. Kim, *Nat. Nanotechnol.* **2014**, 9, 397.
- [14] C.-Z. Hang, X.-F. Zhao, S.-Y. Xi, Y.-H. Shang, K.-P. Yuan, F. Yang, Q.-G. Wang, J.-C. Wang, D. W. Zhang, H.-L. Lu, *Nano Energy* **2020**, 76, 105064.
- [15] J. Lee, S. Kim, J. Lee, D. Yang, B. C. Park, S. Ryu, I. Park, *Nanoscale* **2014**, 6, 11932.
- [16] Y. Wang, J. Wang, S. Cao, D. Kong, *J. Mater. Chem. C* **2019**, 7, 9748.
- [17] T. Sakorikar, M. K. Kavitha, P. Vayalamkuzhi, M. Jaiswal, *Sci.Rep.* **2017**, 7, 2598.
- [18] T. Lee, Y. W. Choi, G. Lee, S. M. Kim, D. Kang, M. Choi, *RSC Adv.* **2017**, 7, 34810.
- [19] H. Jeon, S. K. Hong, M. S. Kim, S. J. Cho, G. Lim, *ACS Appl. Mater. Interfaces* **2017**, 9, 41712.
- [20] G. Shi, Z. Zhao, J.-H. Pai, I. Lee, L. Zhang, C. Stevenson, K. Ishara, R. Zhang, H. Zhu, J. Ma, *Adv. Funct. Mater.* **2016**, 26, 7614.
- [21] S. Dai, Q. Li, G. Liu, H. Yang, Y. Yang, D. Zhao, W. Wang, M. Qiu, *Appl. Phys. Lett.* **2016**, 108, 121103.
- [22] I. K. Moon, J. I. Kim, H. Lee, K. Hur, W. C. Kim, H. Lee, *Sci. Rep.* **2013**, 3, 1112.
- [23] M. S. Lee, K. Lee, S. Y. Kim, H. Lee, J. Park, K. H. Choi, H. K. Kim, D. G. Kim, D. Y. Lee, S. Nam, J. U. Park, *Nano Lett.* **2013**, 13, 2814.
- [24] H. Guo, N. Lin, Y. Chen, Z. Wang, Q. Xie, T. Zheng, N. Gao, S. Li, J. Kang, D. Cai, D.-L. Peng, *Sci. Rep.* **2013**, 3, 2323.
- [25] F. Xu, Y. Zhu, *Adv. Mater.* **2012**, 24, 5117.

- [26] D. Kang, P. V. Pikhitsa, Y. W. Choi, C. Lee, S. S. Shin, L. Piao, B. Park, K. Y. Suh, T. I. Kim, M. Choi, *Nature* **2014**, 516, 222.
- [27] Z. Liu, D. Qi, P. Guo, Y. Liu, B. Zhu, H. Yang, Y. Liu, B. Li, C. Zhang, J. Yu, B. Liedberg, X. Chen, *Adv. Mater.* **2015**, 27, 6230.
- [28] Y. Lee, J. Myoung, S. Cho, J. Park, J. Kim, H. Lee, Y. Lee, S. Lee, C. Baig, H. Ko, *ACS Nano* **2020**.
- [29] Z. Liu, M. A. Meyers, Z. Zhang, R. O. Ritchie, *Prog. Mater. Sci.* **2017**, 88, 467.
- [30] J. Wang, Q. Cheng, Z. Tang, *Chem. Soc. Rev.* **2012**, 41, 1111.
- [31] Y. L. Chan, A. H. W. Ngan, N. M. King, *J. Mech. Behav. Biomed. Mater.* **2011**, 4, 785.
- [32] V. Imbeni, J. J. Kruzic, G. W. Marshall, S. J. Marshall, R. O. Ritchie, *Nat. Mater.* **2005**, 4, 229.
- [33] H. H. Lu, S. Thomopoulos, *Annu. Rev. Biomed. Eng.* **2013**, 15, 201.
- [34] L. Smith, Y. Xia, L. M. Galatz, G. M. Genin, S. Thomopoulos, *Connect Tissue Res.* **2012**, 53, 95.
- [35] S. Sutnaun, S. Srisuwan, P. Jindasai, B. Cherdchim, N. Matan, B. Kyokong, *WJST* **2011**, 2, 81.
- [36] A. Ray, S. Das, S. Mondal, P. Ramachandrarao, *J. Mater. Sci.* **2004**, 39, 1055.
- [37] Y. Jiang, Z. Liu, N. Matsuhisa, D. Qi, W. R. Leow, H. Yang, J. Yu, G. Chen, Y. Liu, C. Wan, Z. Liu, X. Chen, *Adv. Mater.* **2018**, 30, e1706589.

## Chapter 7

### Conclusions and recommendations

*This chapter consist of two main parts. The first part is summarized the works that have been done in this thesis, including the structure designs, properties study and device fabrication. The second part is the future works that are recommended to be further explore based on the current works, which can be either in theoretical study or system integration for applications such as motion detection, human-machine interface, and healthcare management system.*

## 7.1 Conclusions

In this thesis, two types of heterogeneity design have been involved in stretchable electronics. One is discrete structure with abrupt variation of Young's modulus, which is combination of the hardness and the softness and applying in active layer of the stretchable memristor. This heterogeneous design demonstrates to be able to effectively facilitate the strain energy and alleviate the strain concentration and hence enhance the mechanical adaptability of stretchable memristor (40% stretchability and half fold flexibility). Moreover, the rigid functional materials wrapped by soft polymer matrix is protected from mechanical damages such as puncture and cut. Confront with mechanical damages, the soft materials act as a cushion to dissipate large strain energy by deformation, which cause the embedded rigid parts flow with it and exhibit an evasive behavior. Thus, being protected memristor active materials from puncture and cut damages. A series of results have showed that stretchable memristor performs as normal under various deformations, and functions well after being underwent serious mechanical damages, indicating this heterogenous structure successfully endow inorganic-based memristor with not only stretchable, flexible, but also mechanical damage durable, which has not been achieved before in the field of the stretchable memristor. This heterogenous structure could be a universal approach for other devices with similar two-terminal sandwich configuration and pave a way for stretchable devices to explore possibility of applications in extreme and harsh environment.

Another type of heterogeneity design is a gradient structure with continuous variation of thickness and employing it in the metallic thin film on the elastomer. It was found that the electrical properties depend on the direction of applying force. Namely, the force applied perpendicular (denoted as transverse direction) or parallel (denoted as longitudinal direction) to the variation direction of thickness-gradient will give an anisotropic electrical property. The larger the variation of thickness, the larger anisotropic electrical property can be obtained. Having investigated the underlying mechanism of anisotropic electrical property, the crack morphologies are difference in these two scenarios due to the strain distribution. In transverse direction, strain is uniform across the sample and the cracks are straight, which gives rise to a larger sensitivity. However, in the longitudinal direction, there is strain distribution which causes cracks propagate in zigzag manner that give rise

to a gradual resistance change but more stretchability. These two scenarios can be described by spring models. In this thesis, the force applied perpendicular to the variation direction of thickness-gradient was investigated and a highly sensitivity stretchable strain sensors with sensitivity of  $\sim 1665$  at large strain  $\sim 30\%$  was obtained. This heterogeneous structure offers a strategy to tune the electrical properties of strain sensors by using strain distribution caused by thickness variation. The method is easy and compatible with commercial technique for large scale fabrication. Meanwhile, most strain sensors are fabricated based on the uniform 2D thin film on elastomer. This work involved the factor of height and discover the anisotropic electrical property that has not been discussed in the field of strain sensor. The current work is preliminary results. There is a large space for more theoretical study and practical applications that will discuss later.

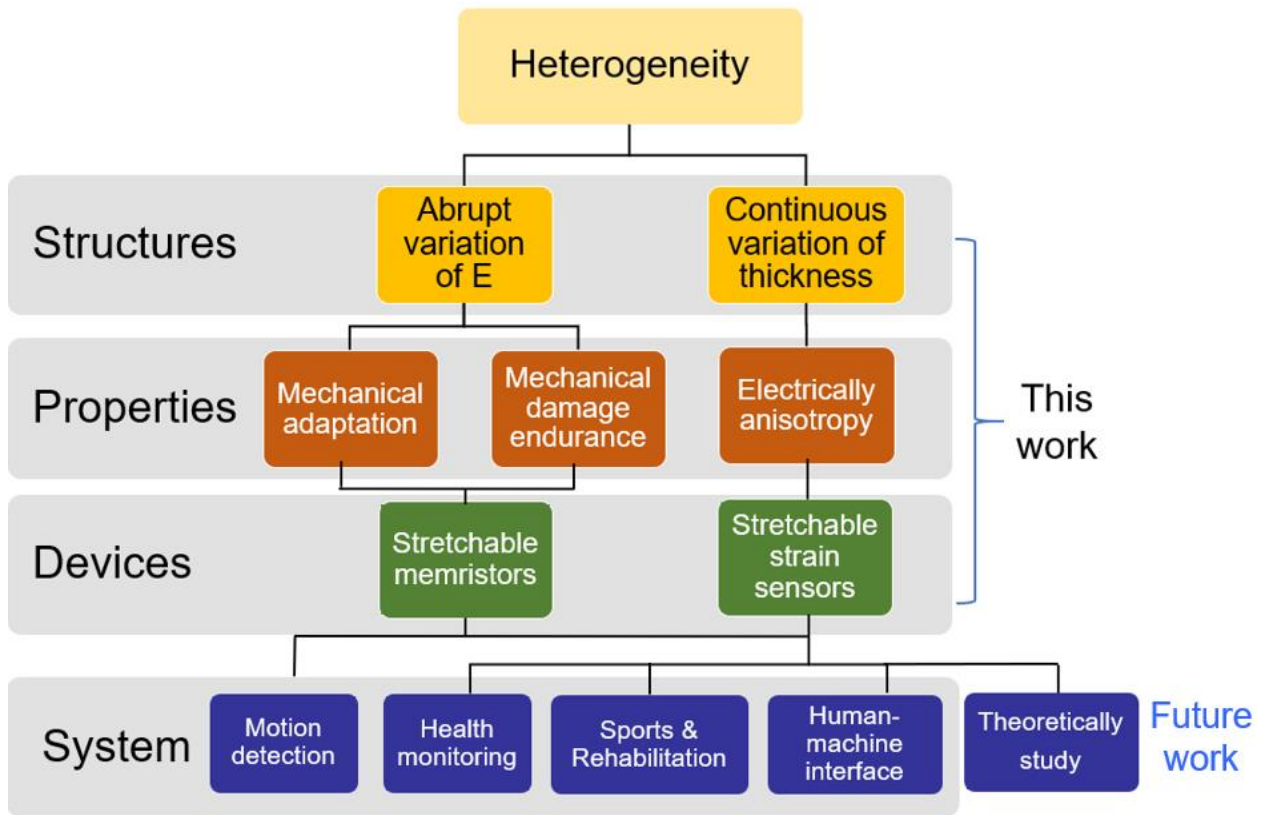


**Figure 7.1** The frame of this thesis.

The overall frame of this thesis is illustrated in **Figure 7.1**. The works have been done including structure design, properties discovery and device fabrication. There are more works going to complete in future, which include the theoretical study of anisotropic

electrical property, applications of stretchable strain sensors and stretchable memristors, and build an integrated wearable system for motion detection.

## 7.2 Future work recommendations

### 7.2.1 Theoretical study of anisotropic electrical property

One further research direction can be theoretical study of anisotropic electrical property caused by the thickness-gradient structure. The preliminary result shows that the anisotropic electrical property proportional depends on the variation of thickness-gradient. Currently, the variation of thickness-gradient is only up to 20%, more experiments can be done to increase the variation of thickness-gradient and study the relationship between electrical property and stress as shown in **Figure 7.2**.

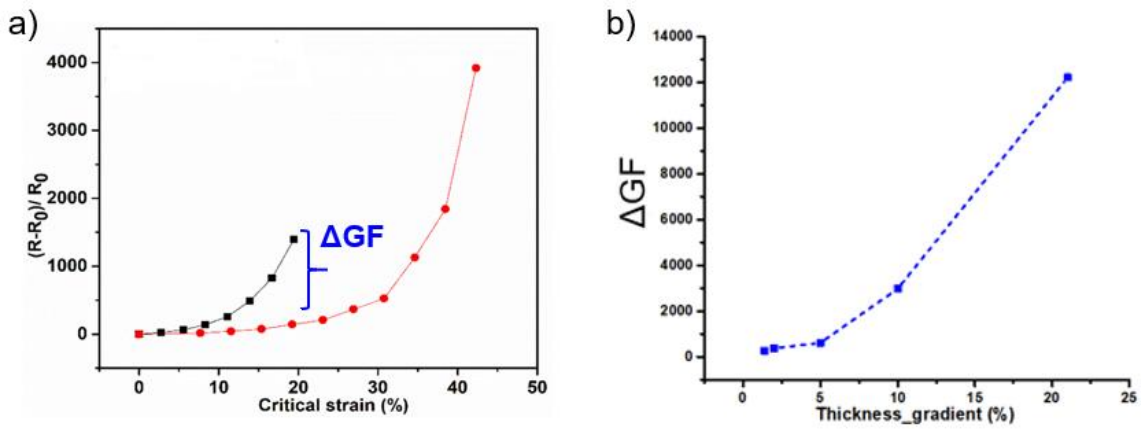


**Figure 7.2** Recommendation for theoretical study of thickness-gradient stretchable strain sensors (a) Anisotropic property (b) Relationship between sensitivity difference (gauge factor difference in transverse and longitudinal direction) and variation of thickness-gradient.

The anisotropic property of thickness-gradient structure can be defined as the difference of sensitivity difference ( $\Delta GF$ ) between GF in transverse direction (force applied in perpendicular to the variation of thickness-gradient) and longitudinal direction (force applied in parallel to the variation of thickness-gradient). The equation can be expressed as follows:

$$\Delta GF = | GF_{\perp} - GF_{\parallel} |$$

Where  $GF_{\parallel}$  is gauge factor (sensitivity) where stress is parallel to the variation of the thickness-gradient.  $GF_{\perp}$  is gauge factor where stress is perpendicular to the variation of the thickness-gradient.

The electrical property and stress relationship (stress-resistive) relationship:

$$\Delta GF = C \cdot \sigma$$

Where  $C$  is a parameter that determined by the variation of thickness-gradient.  $\sigma$  is stress.

Generally, the electrical property of thin film on elastomer is based on 2D manner. The electrical property of thin film on elastomer can be tuned by a 3D manner through the change of height of thickness. This theoretical study can give a guide on how the surface strain distribution affect the electrical property by using tuning the height of thickness in a quantitatively way which provide a fundamental knowledge in the field of stretchable strain sensors.

### 7.2.2 Applications of stretchable strain sensors

- **Health monitoring for caring either elderly or individuals**

As people is living longer than before, the population is aging globally. The high quality and efficient medicine treatment and healthcare are needed to improve personal life. Intelligent biomedical clothes and wearable ambulatory health monitoring system enable to provide continuously point-of-care monitoring with cost-efficient access to the best care and illness prevention. This early and instantaneously detection can limit the acute event people to take care of themselves at anywhere he goes. As for healthy people, the wearable techniques can help them to develop a healthier lifestyle and improve personal fitness.

Besides, due to the pandemic Covid-19, it has accelerated and prompted an explosion of interest of the wearable technology for health monitoring. Wearable sensors are used in textiles for clothing and efforts has been made to gear towards preventing the spread of virus and predicting the possible infection. Wearable sensors can also potentially

assist in providing real-time remote monitoring, symptom prediction and contact tracing for infected patients or self-quarantined individuals.<sup>[1-2]</sup>

Data can be collected by wearable devices from human body through the blood pressure,<sup>[3]</sup> oxygen saturation,<sup>[4]</sup> pulse,<sup>[5-6]</sup> breath,<sup>[7-9]</sup> heart-beat,<sup>[7, 10]</sup> body temperature<sup>[11-12]</sup> and movement.<sup>[13-14]</sup> Stretchable strain sensors play a vital role in detecting the strain on skin, ankles, wrist, joints, and pulse. For respiratory disease, respiratory biomarkers such as cough frequency, intensity, sound, respiratory rate can be measured by wearable strain sensor from the thorax and throat that give professional clinicians information and help doctors to screening and pre-diagnosis.<sup>[15]</sup>

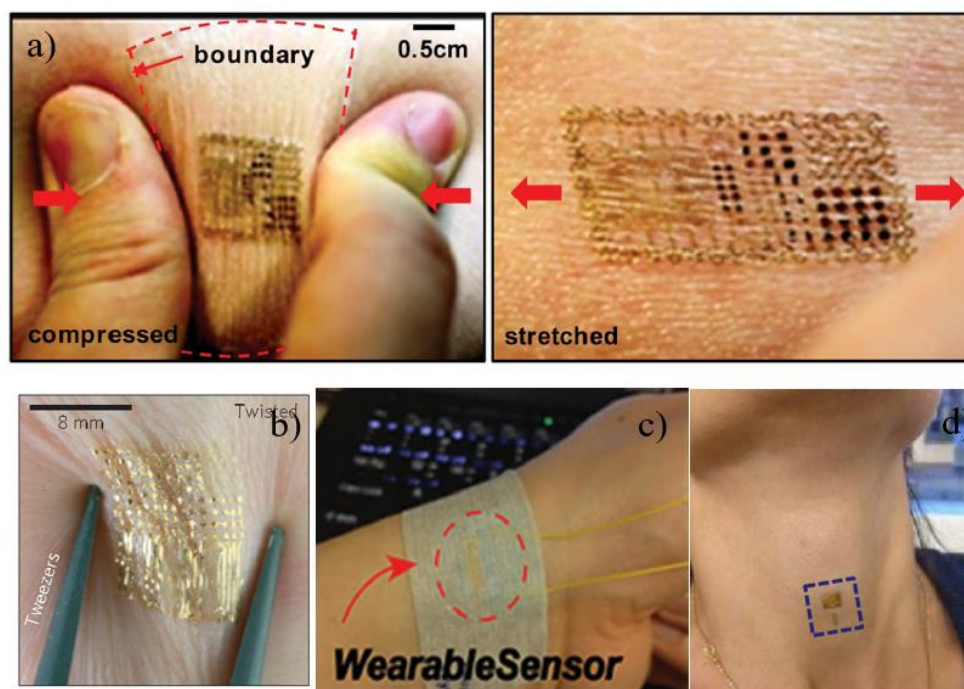


**Figure 7.3** Applications of stretchable strain sensors in healthcare monitoring. (a) Integrating multifunctional sensor for temperature, strain and electrophysiological detection. Reproduced with permission.<sup>[16]</sup> Copyright 2016, American Chemical Society. (b) Skin-like wearable temperature sensors and heaters. Reproduced with permission.<sup>[11]</sup> Copyright 2013, Macmillan Publishers Limited. (c) Pulse-detectable pressure sensor. Reproduced with permission.<sup>[6]</sup> Copyright 2014, Wiley-VCH. (d) Blood pressure measured from neck. Reproduced with permission.<sup>[17]</sup> Copyright 2014, Macmillan Publishers Limited.

- **Sports and rehabilitation**

Cardiovascular strain is calculated from heart rate (HR) and heart rate variability (HRV). Viral illness increases physiological stress on the body which can be indicated by increasing of HR. An elevation in HR can be detected hours or days before the onset of symptoms in many cases of viral infection.<sup>[18]</sup> HRV provide insight into overall individual health and stress. HRV decrease significantly indicate inadequate recovery and increased physiological stress.<sup>[19]</sup>

In the context of athletic training, cardiovascular strain has been collected and studied to adjust the workload of athletes and prevent over-training.<sup>[20-21]</sup> Besides, people usually get injuries because of improper exercise. Lateral collateral ligament (LCL) is usually happened on people with regular exercise or overtraining. Ligaments that connect the bottom of the femur and top of fibula in the knees are commonly injured due to direct force trauma to the inside of knee, resulting in pressure on the outside of the knee and cause the LCL stretchy or tear. Using wearable strain sensors can monitor the work-out position and prevent the injuries and over-training. Strain sensors was mounted in the kneepad to minimize the knee ligament injury by preventing the excessive Varus stress and hyperextension. It also can be used as a wearable technique to facilitate rehabilitation for post-event patients to recovery.

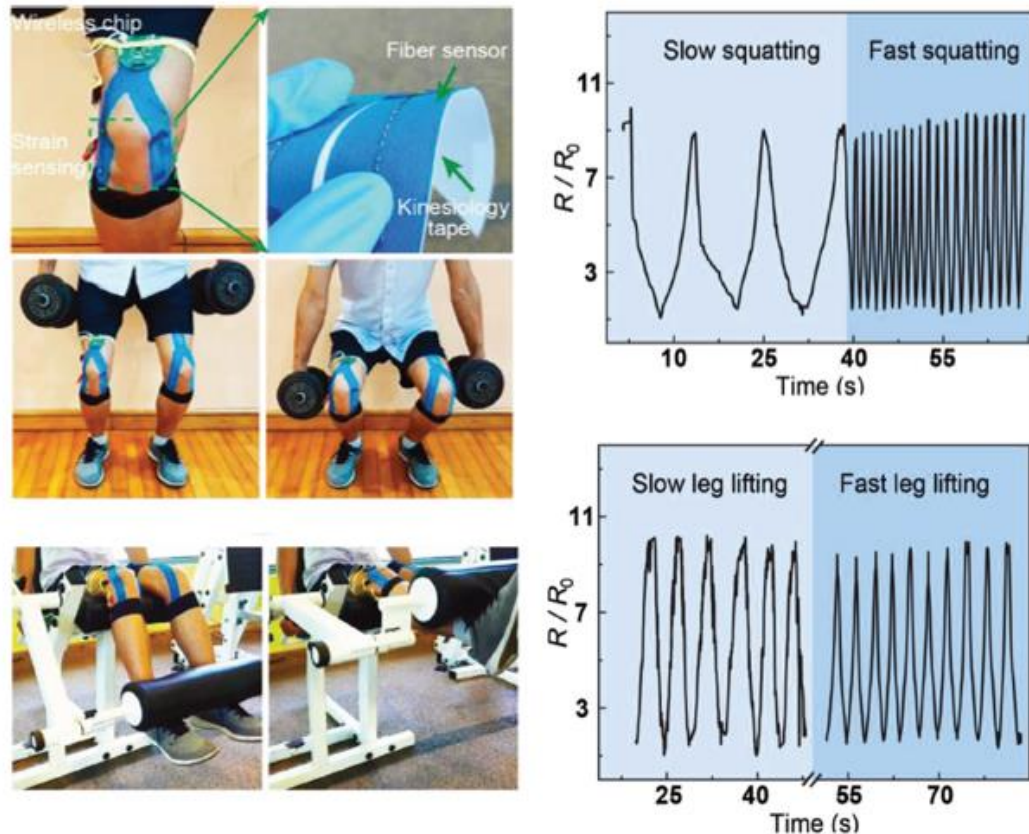


**Figure 7.4** Stretchable strain sensor adhesive to kinesiology tape and mount on the knees for sport monitoring. Reproduced with permission.<sup>[22]</sup> Copyright 2017, Wiley-VCH.

- **Human-machine interface (HMI)**

Human-machine interface offers window for users to communicate with equipment, robots, and virtual world. Conventional HMIs are keyboard, mouse, and touchpad. Currently, more entertainment and a feeling of realistic interaction are involved between users and machines to enhance the engagement. In addition to vision and voice recognition that capture motion, body gestures are also employed for a high precision and multiple degree of freedom (DOF) control.<sup>[23]</sup> Thus, stretchable strain sensors are employed to fabricated textile-based or glove-based human-machine interactions. With the aid of face, body, or hand gestures, the subtle emotions and detailed motions can be captured for the collection of comprehensive information. A visual and somatosensory system that converges vision and hand gesture has been developed to enhance the accuracy of recognition in human-machine interaction as show in **Figure 7.5**.

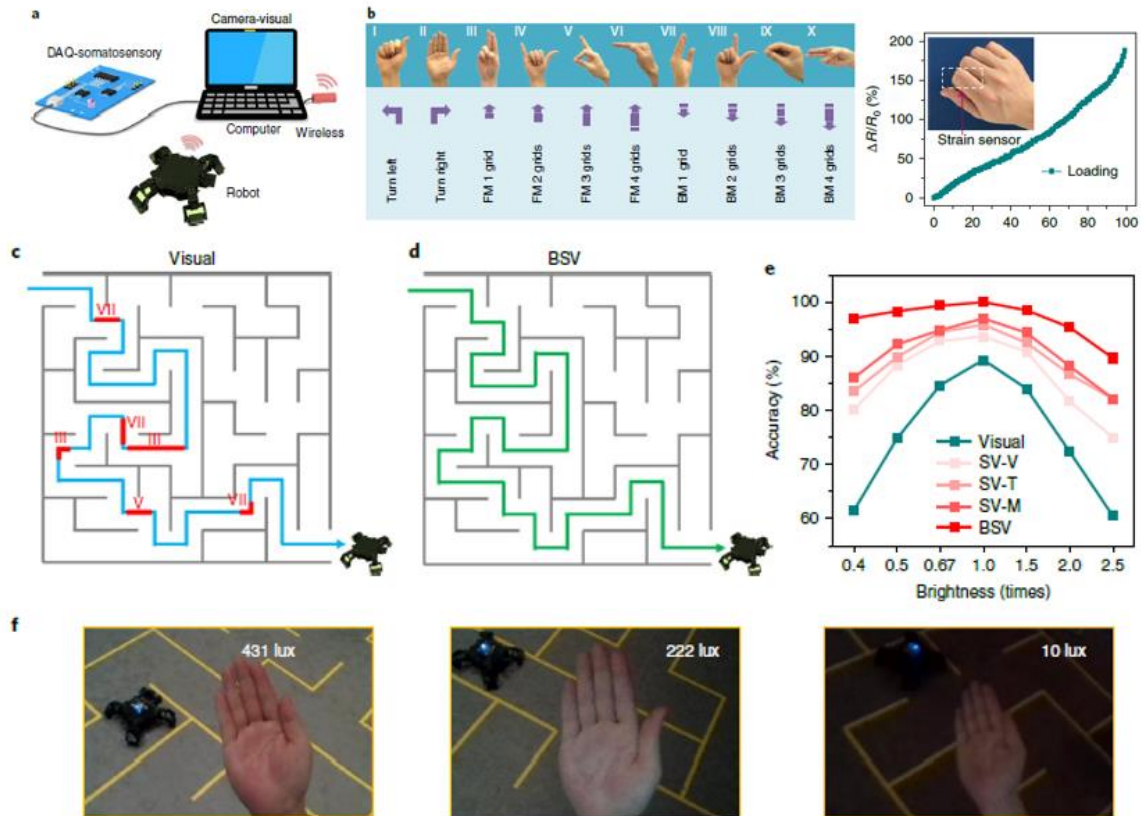


**Figure 7.5** HMI application. A Somatosensory vision system associated with learning architecture to control a robot that can implement the accurate recognition under conditions such as in the dark, over-exposed illumination and a complex noise background. Reproduced with permission.<sup>[24]</sup> Copyright 2020, the Author(s), under exclusive licence to Springer Nature Limited.

The somatosensory vision system associated with learning architecture can perform a high accurate (100%) recognition by integrating visual data from camera and somatosensory data from skin-like stretchable strain sensors. Unlike the conventional human-machine interface which relies on visual images/videos to recognize the motions, the recognition accuracy is limited by the quality of images that are affected by the environmental condition such as varying lights or complex background. This multimodal fusion system combine both visual data and sensory data overcome this limitation, which can achieve 100% accuracy at normal light and maintain high accuracy (>96.7%) in non-ideal conditions such as in dark, over-exposed illumination and complex background with noises. This work is a good example to show that stretchable strain sensors is promising in human-machine interaction applications.<sup>[24]</sup>

### 7.3.3 Wearable system

- **Integrated wearable system**

An integrated wearable motion detection system was fabricated by integrating of stretchable memristor and stretchable strain sensor was mounted on the elbow to detect the flexion as shown in **Figure 7.6**.

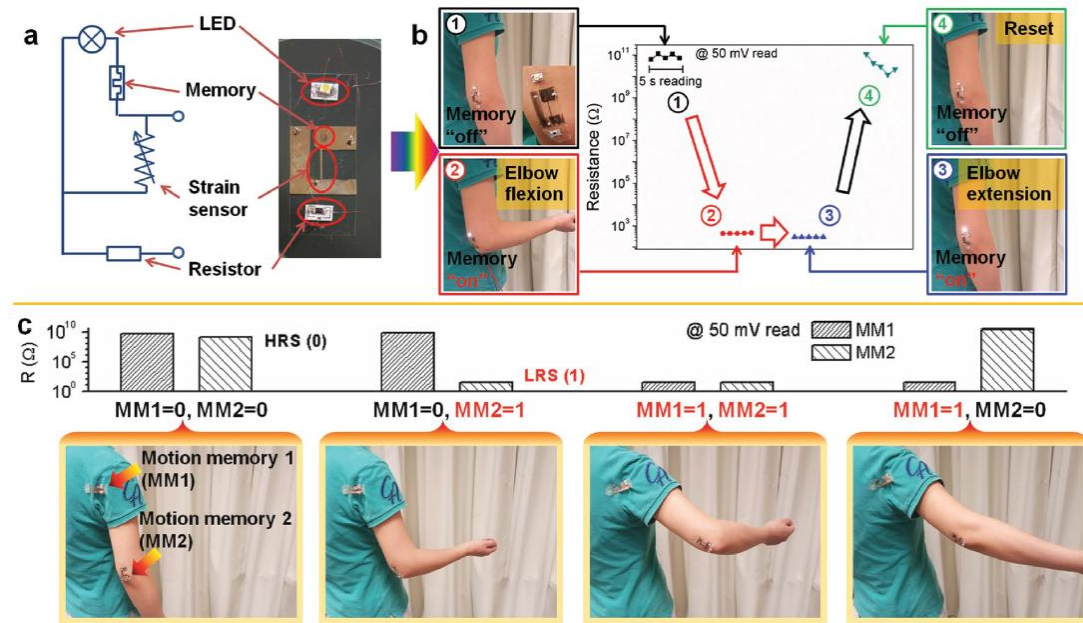


**Figure 7.6** A wearable motion memory system with detection unit (stretchable strain sensor) and storage unit (stretchable memristor) for human motion monitoring. Reproduced with permission.

[25] Copyright 2017, Wiley-VCH.

In response to the elbow flexion, the elongation of stretchable strain sensor will trigger the stretchable memristor switch between On and Off state, the information of motion had been stored in the memristor. The motion information can be record and read through the different resistance level of each motion detection system. A multiple such kind of motion detection systems can be mounted on the different joints of human and cooperate each other to record the information of complex motions, which show potential application in mimic the biological actuation.<sup>[25]</sup>

- **Leveraging big data and artificial intelligence in health management**

An intelligent healthcare system can be established by leveraging big data, IoTs and artificial intelligent. Wearable techniques provide continuous monitoring platform to collect biophysiological signals from the patients or individuals, which is fundamental part in this intelligent healthcare system for diagnosis analysis, prediction, and treatment. Wearable sensors are responsible for performing the data-collection in terms of physiological and physical parameters, such as heart rate, blood pressure, glucose level, position, etc. The collective data can send to established edge devices such as PC, mobiles for data processing, analysis and even for pre-recognition and prediction through the deep machine learning. The data then upload to the cloud serve through the wireless or internet communication and transmit to the professional medical access point or hospital for analysis and diagnosis. The medical system gather various techniques and provide a platform for each technique to cooperate with each other, which allows doctors to give professional medical assistants remotely regardless of distance and help patients to get a faster and immediate medical access that save time, especially perfect for emergency and poverty regions with resource shortage. Meanwhile, wearable sensors offer a real-time monitoring for patients required intensive care and customized personal care for training and rehabilitation.

Although we are still in infant stage for this system, the rapid development of wearable devices, communication and information technologies, and artificial intelligent promote us gear towards to this goal and will be come true near future. The works in this thesis mainly contribute in the field of wearable devices on the stretchable memristor for data processing and storage and stretchable strain sensors for data detection and collection. Making stretchable devices to be able work properly and keep its functions under a dynamic and unconstrained environment consisting of various forces and accidents is challenge. This work develops a memristor that can work at various deformations and protect data from loss when encountering mechanical damages which is significant to move wearable electronics a step forward to real application and explore possibility in harsh condition. The highly stretchable strain sensor is promising to apply on body for motion detection that can be used to prevent athletes from overtraining, rehabilitation, and human-machine interaction for entertainment.

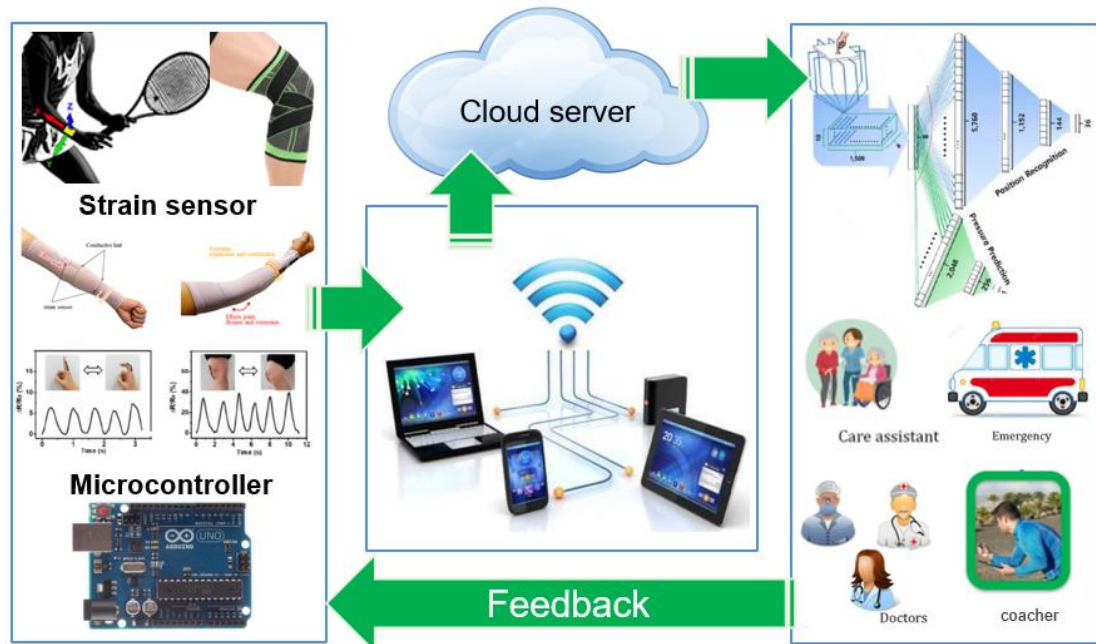


**Figure 7.7** Schematic illustration of wearable device play a role in leveraging big data in health management. Reproduced / modified from references [26-29]. Copyright 2015, Wiley-VCH; Copyright 2014, IEEE; Copyright 2017, the Author(s), licensed under a Creative Commons Attribution 4.0 International License (<http://creativecommons.org/licenses/by/4.0/>); Copyright 2017, IEEE.

There is a huge space to discover and a multi-discipline collaboration is required for us to implement it. Fortunately, some research groups are on the way to this direction and achieve incredible results on it.<sup>[30-31]</sup> This chapter will wrap up by challenges come with hopes, aim for higher and down to earth.

## References

- [1] C. P. Adans-Dester, S. Bamberg, F. P. Bertacchi, B. Caulfield, K. Chappie, D. Demarchi, M. K. Erb, J. Estrada, E. E. Fabara, M. Freni, K. E. Friedl, R. Ghaffari, G. Gill, M. S. Greenberg, R. W. Hoyt, E. Jovanov, C. M. Kanzler, D. Katabi, M. Kernan, C. Kigin, S. I. Lee, S. Leonhardt, N. H. Lovell, J. Mantilla, T. H. McCoy, N. M. Luo, G. A. Miller, J. Moore, D. O'Keeffe, J. Palmer, F. Parisi, S. Patel, J. Po, B. L. Pugliese, T. Quatieri, T. Rahman, N. Ramasarma, J. A. Rogers, G. U. Ruiz-Esparza, S. Sapienza, G. Schiurring, L. Schwamm, H. Shafiee, S. Kelly Silacci, N. M. Sims, T. Talkar, W. J. Tharion, J. A. Toombs,

- C. Uschnig, G. P. Vergara-Diaz, P. Wacnik, M. D. Wang, J. Welch, L. Williamson, R. Zafonte, A. Zai, Y.-T. Zhang, G. J. Tearney, R. Ahmad, D. R. Walt, P. Bonato, *IEEE Open J. Eng. Med. Biology* **2020**, *1*, 243.
- [2] M. M. Islam, S. Mahmud, L. J. Muhammad, M. R. Islam, S. Nooruddin, S. I. Ayon, *SN Comput. Sci.* **2020**, *1*, 320.
- [3] P. B. a. M. Zens, *Biomed. Microdevices* **2012**, *14*, 573.
- [4] M. M. Rodgers, V. M. Pai, R. S. Conroy, *IEEE Sens. J.* **2015**, *15*, 3119.
- [5] Y. Jiang, Z. Liu, N. Matsuhisa, D. Qi, W. R. Leow, H. Yang, J. Yu, G. Chen, Y. Liu, C. Wan, Z. Liu, X. Chen, *Adv. Mater.* **2018**, *30*, e1706589.
- [6] C. Pang, J. H. Koo, A. Nguyen, J. M. Caves, M. G. Kim, A. Chortos, K. Kim, P. J. Wang, J. B. Tok, Z. Bao, *Adv. Mater.* **2015**, *27*, 634.
- [7] Y. Wang, L. Wang, T. Yang, X. Li, X. Zang, M. Zhu, K. Wang, D. Wu, H. Zhu, *Adv. Funct. Mater.* **2014**, *24*, 4666.
- [8] S. Duan, K. Yang, Z. Wang, M. Chen, L. Zhang, H. Zhang, C. Li, *ACS Appl. Mater. Interfaces* **2016**, *8*, 2187.
- [9] T. Yamada, Y. Hayamizu, Y. Yamamoto, Y. Yomogida, A. Izadi-Najafabadi, D. N. Futaba, K. Hata, *Nat. Nanotechnol.* **2011**, *6*, 296.
- [10] C. Pang, G. Y. Lee, T. I. Kim, S. M. Kim, H. N. Kim, S. H. Ahn, K. Y. Suh, *Nat. Mater.* **2012**, *11*, 795.
- [11] R. C. Webb, A. P. Bonifas, A. Behnaz, Y. Zhang, K. J. Yu, H. Cheng, M. Shi, Z. Bian, Z. Liu, Y. S. Kim, W. H. Yeo, J. S. Park, J. Song, Y. Li, Y. Huang, A. M. Gorbach, J. A. Rogers, *Nat. Mater.* **2013**, *12*, 938.
- [12] S. Harada, K. Kanao, Y. Yamamoto, T. Arie, S. Akita, K. Takei, *ACS Nano* **2014**, *8*, 12851.
- [13] N. Lu, C. Lu, S. Yang, J. Rogers, *Adv. Funct. Mater.* **2012**, *22*, 4044.
- [14] D.-H. Kim, N. Lu, R. Ma, Y.-S. Kim, R.-H. Kim, S. Wang, J. Wu, S. M. Won, H. Tao, A. Islam, K. J. Yu, T.-i. Kim, R. Chowdhury, M. Ying, L. Xu, M. Li, H.-J. Chung, H. Keum, M. McCormick, P. Liu, Y.-W. Zhang, F. G. Omenetto, Y. Huang, T. Coleman, J. A. Rogers, *Science*. **2011**, *333*, 838.
- [15] H. Jeong, J. A. Rogers, S. Xu, *Sci. Adv.* **2020**, *6*.

- [16] M. Amjadi, M. Turan, C. P. Clementson, M. Sitti, *ACS Appl. Mater. Interfaces* **2016**, 8, 5618.
- [17] C. Dagdeviren, Y. Su, P. Joe, R. Yona, Y. Liu, Y.-S. Kim, Y. Huang, A. R. Damadoran, J. Xia, L. W. Martin, Y. Huang, J. A. Rogers, *Nat. Commun.* **2014**, 5.
- [18] X. Li, J. Dunn, D. Salins, G. Zhou, W. Zhou, S. M. Schüssler-Fiorenza Rose, D. Perelman, E. Colbert, R. Runge, S. Rego, R. Sonecha, S. Datta, T. McLaughlin, M. P. Snyder, *PLOS Biology* **2017**, 15, e2001402.
- [19] D. R. Seshadri, E. V. Davies, E. R. Harlow, J. J. Hsu, S. C. Knighton, T. A. Walker, J. E. Voos, C. K. Drummond, *Frontiers in Digital Health* **2020**, 2.
- [20] D. R. Seshadri, C. Drummond, J. Craker, J. R. Rowbottom, J. E. Voos, *IEEE Pulse* **2017**, 8, 38.
- [21] D. R. Seshadri, R. T. Li, J. E. Voos, J. R. Rowbottom, C. M. Alfes, C. A. Zorman, C. K. Drummond, *npj Digit. Med.* **2019**, 2, 72.
- [22] Z. Liu, D. Qi, G. Hu, H. Wang, Y. Jiang, G. Chen, Y. Luo, X. J. Loh, B. Liedberg, X. Chen, *Adv. Mater.* **2018**, 30.
- [23] M. Zhu, Z. Sun, Z. Zhang, Q. Shi, T. He, H. Liu, T. Chen, C. Lee, *Sci. Adv.* **2020**, 6, eaaz8693.
- [24] M. Wang, Z. Yan, T. Wang, P. Cai, S. Gao, Y. Zeng, C. Wan, H. Wang, L. Pan, J. Yu, S. Pan, K. He, J. Lu, X. Chen, *Nat. Electron.* **2020**.
- [25] Y. Liu, Z. Liu, B. Zhu, J. Yu, K. He, W. R. Leow, M. Wang, B. K. Chandran, D. Qi, H. Wang, G. Chen, C. Xu, X. Chen, *Adv. Mater.* **2017**, 29.
- [26] S. Gong, D. T. H. Lai, B. Su, K. J. Si, Z. Ma, L. W. Yap, P. Guo, W. Cheng, *Adv. Electron. Mater.* **2015**, 1, 1400063.
- [27] A. Lanata, G. Valenza, M. Nardelli, C. Gentili, E. P. Scilingo, *IEEE J. Biomed. Health Inform.* **2015**, 19, 132.
- [28] K. S. Sohn, J. Chung, M. Y. Cho, S. Timilsina, W. B. Park, M. Pyo, N. Shin, K. Sohn, J. S. Kim, *Sci. Rep.* **2017**, 7, 11061.
- [29] M. Kos, I. Kramberger, *IEEE Access.* **2017**, 1.
- [30] H. U. Chung, B. H. Kim, J. Y. Lee, J. Lee, Z. Xie, E. M. Ibler, K. Lee, A. Banks, J. Y. Jeong, J. Kim, C. Ogle, D. Grande, Y. Yu, H. Jang, P. Assem, D. Ryu, J. W. Kwak, M. Namkoong, J. B. Park, Y. Lee, D. H. Kim, A. Ryu, J. Jeong, K. You, B. Ji, Z. Liu, Q. Huo,

X. Feng, Y. Deng, Y. Xu, K. I. Jang, J. Kim, Y. Zhang, R. Ghaffari, C. M. Rand, M. Schau, A. Hamvas, D. E. Weese-Mayer, Y. Huang, S. M. Lee, C. H. Lee, N. R. Shanbhag, A. S. Paller, S. Xu, J. A. Rogers, *Science* **2019**, 363.

[31] K. Lee, X. Ni, J. Y. Lee, H. Arafa, D. J. Pe, S. Xu, R. Avila, M. Irie, J. H. Lee, R. L. Easterlin, D. H. Kim, H. U. Chung, O. O. Olabisi, S. Getaneh, E. Chung, M. Hill, J. Bell, H. Jang, C. Liu, J. B. Park, J. Kim, S. B. Kim, S. Mehta, M. Pharr, A. Tzavelis, J. T. Reeder, I. Huang, Y. Deng, Z. Xie, C. R. Davies, Y. Huang, J. A. Rogers, *Nat. Biomed. Eng.* **2020**, 4, 148.